Interactions between sedimentation and deformation in deepwater fold and thrust belts

Ian Richard Clark

ProQuest LLC
789 East Eisenhower Parkway
P.O. Box 1346
Ann Arbor, MI 48106-1346

DECLARATION

This work has not previously been accepted in substance for any degree and is not concurrently submitted in candidature for any degree.

Signed ..... (candidate) Date 03/03/2010

STATEMENT 1

This thesis is being submitted in partial fulfillment of the requirements for the degree of PhD.

Signed ..... (candidate) Date 03/03/2010

STATEMENT 2

This thesis is the result of my own independent work/investigation, except where otherwise stated. Other sources are acknowledged by explicit references.

Signed ..... (candidate) Date 03/03/2010

STATEMENT 3

I hereby give consent for my thesis, if accepted, to be available for photocopying and for inter-library loan, and for the title and summary to be made available to outside organisations.

Signed ..... (candidate) Date 03/03/2010

STATEMENT 4:

I hereby give consent for my thesis, if accepted, to be available for photocopying and for inter-library loans after expiry of a bar on access previously approved by the Graduate Development Committee.

Signed ..... (candidate) Date 03/03/2010

Acknowledgements

First and foremost, I would like to thank my project supervisor, Joe Cartwright, for giving me the opportunity to carry out this work, and especially for giving me the academic freedom to pursue my own interests over the course of the PhD. I am also indebted to all of the helpful people at Shell for giving me the chance to undertake several work placements in Houston, and I have learnt a great deal from each and every one of those visits.

Thanks also to all of the people in the 3D Lab, past and present, who have always provided much needed help and support throughout my years as a PhD student.

Last but not least, thanks also to my friends and family their constant support, and for never failing to give me encouragement throughout all of my time spent in Cardiff.

CONTENTS

CHAPTER 5

CHAPTER 6

CHAPTER 7

List of Figures

ABSTRACT

The progress of modern hydrocarbon exploration into increasingly deepwater settings has led to a renewed interest in deepwater fold and thrust belts. Deepwater fold and thrust belts often form as a result thin-skinned compression above a ductile substrate, such as overpressured shale or salt. The compression driving deformation in these settings accommodates up-dip extension due to gravitational collapse of passive margin deltaic systems. Deformation in these settings is accompanied by a range of coeval sedimentary processes which interact with the deforming seafloor topography both at large scales to form kilometre-thick growth sequences, and at smaller scales involving individual flow events. Thus, in order to fully understand how these systems evolve, it is necessary to link structural and sedimentary processes when developing conceptual models which may then be applied to predicting facies distributions in these settings.

Imaging of deepwater fold and thrust belts using three-dimensional (3D) seismic data permits detailed investigations to be carried out into the development of, and interactions between, features such as folds, growth sequences and submarine channel levee systems. Although such data has already been used to advance our understanding of many deepwater depositional systems, it has not been fully utilised to study the interactions between deformation and sedimentation in these settings.

The aim of this study is to utilise 3D seismic data volumes from the Eastern Nile Foldbelt and the deepwater western Niger Delta to study the interactions between sedimentation and deformation, and to extract some general principles which can be applied to other deepwater fold and thrust belts. The scale of investigation ranges from growth sequences - which are up to two kilometres thick, to more detailed interactions between smaller scale (c. 500m in width) submarine channel levee systems and fold growth.

For the first time, a coherent set of end-member interactions between submarine channel systems and evolving seafloor structures is presented. These interactions form a descriptive framework and serve as a basis for comparing submarine channel responses to deformation from various deepwater fold and thrust belt settings. Transitions between these interactions is controlled by factors such as relative timing and rates of deformation compared to sedimentation, and recognition of these interactions allows more accurate inferences to be made regarding the evolution of seafloor relief during folding. The interactions between submarine channel development and folding also depends on the fold structural style which is critical in controlling the nature of localised accommodation space adjacent to the fold.

Changes in accommodation space associated with folding can result in dramatic spatial variations in channel morphology over less than a hundred metres.

This study also documents the strong control on growth sequence development and internal architecture as a result of variations in structural style along strike. Relationships such as overlap and onlap can be used to predict submarine channel responses to folding, given a knowledge of the fold structural style. The internal architecture of growth sequences is also dependant on compensational stacking relationships, and the case study from the Niger Delta shows an important example of how mass transport deposits play a key role in filling local accommodation space and influencing subsequent sedimentation pathways.

The results presented in this thesis demonstrate that 3D seismic data can be a powerful tool in our understanding of deepwater fold and thrust belt systems, and that linking structural and stratigraphic investigations can provide new insights into the interactions between deformation and sedimentation.

Chapter 1

CHAPTER 1

INTRODUCTION

1.1 Rationale

Deepwater fold and thrust belts can occur in water depths of up to 3000m, and are becoming increasingly important, but high risk, settings for modern hydrocarbon exploration. These are geological settings where deformational processes can exert a powerful control on sediment distribution and also on sedimentary processes. Therefore, understanding the detailed interactions between deformation and sedimentation in such settings provides a link between the disciplines of structural geology and sedimentology, and such knowledge can be applied to better understand and predict reservoir occurrence (or lack of) in such settings. From a scientific perspective, these settings provide ideal natural laboratories for the study of a wide variety of structural and sedimentological processes. Deepwater fold and thrust belts occur in areas of tectonic compression, with the main driving processes being:

1 Thick skinned plate collision processes involving subduction, examples include the Barbados Accretionary Prism (Westbrook et al., 1988); the Makran Accretionary Prism (Kukowski et al., 2001), the Nankai Trough (Moore et al., 1990) and the Mediterranean Ridge (Chaumillon and Mascle, 1997).
2 Thin skinned, gravitational collapse of large deltaic sediment wedges deposited on passive margins. These form the systems studied in this thesis. Examples include the Niger Delta (e.g. Doust and Omatsola, 1990; Morley and Guerin, 1996; Billotti and Shaw, 2005), the Gulf of Mexico (e.g. Wu et al., 1990; Peel et al., 1995; Trudgill et al., 1995) and the Angolan Margin (Brun and Fort, 2004).

In addition, some deepwater fold belts may form as a result of a combination of the above processes, one example being the NW Borneo fold belt (Hesse et al., 2009).

The seafloor bathymetry of many deepwater fold belts is characterised by numerous folds which form above upwards propagating blind thrusts (e.g Demyttenaere et al., 2000; Huyghe et al., 2004; Heinio and Davies, 2006). The structural styles and mechanisms of formation of these folds have been extensively documented in the literature, primarily by using two-dimensional models and reconstructions based on natural examples from both seismic profiles (e.g. Shaw and Suppe, 1994; Rowan, 1997; Masaferro et al., 1999; Mitra, 2002) and outcrop analogues (e.g. Poblet and Hardy, 1995; Poblet et al., 1998; Ford et al., 1997). Coeval sedimentation

during fold uplift results in the formation of geometrically distinctive sedimentary packages adjacent to the fold limbs termed growth sequences (e.g. Suppe et al., 1992; Burbank and Verges, 1994). Growth sequences provide a sedimentary record of the relative rates of uplift and also the sedimentary responses to emerging fold relief (e.g. Burbank et al., 1996). In deep water fold and thrust belts, the preservation potential of growth sequences is much greater than their subaerial counterparts exposed at outcrop, and this allows detailed studies using 3D seismic data to be undertaken. Relatively few studies take into account the three-dimensional spatial and temporal evolution of multiple fold structures and their associated growth sequences in these settings (Salvini and Storti, 2002; Higgins et al., 2007; Morley, 2009). One of the aims of this thesis is to study the three dimensional development of growth sequences from a stratigraphic, rather than structural perspective in an attempt to gain new insights into the interactions between sedimentation and deformation during fold uplift.

Sedimentation in many deepwater fold belts is driven by gravity current processes – such as channel levee systems formed by the passage of successive turbidity currents over time (see recent review by Wynn et al., 2007), and also large scale, catastrophic mass wasting events (e.g. Frey Martinez et al., 2005; Gee et al., 2007). At a smaller scale, individual folds can also be affected by mass wasting from the fold limbs, and by erosion due to turbidity currents (Heinio and Davies, 2006). Submarine channel levee systems are now extensively documented in the literature, but relatively few studies focus on the link between channel development and deformation in structurally active settings (Huyghe et al., 2000; Ferry et al., 2005; Gee and Gawthorpe, 2006). This is despite a generally good understanding of the way in which flow character and deposition from turbidity currents varies in response to bathymetric features (Alexander and Morris 1994; Bursik and Woods 2000; Kneller et al., 1995; Lamb et al., 2005; Toniolo et al., 2006). Since submarine channels form key conduits for sedimentation in many deepwater fold belts, another primary aim of this thesis is to examine how these systems evolve in active deformational settings.

1.2 Overview of sedimentation and tectonics in deepwater fold belts

Deformation in deepwater fold and thrust belts results in a complex seafloor bathymetry which controls the distribution of sediments via the slope gradient, and also by variations in accommodation space (e.g. Demyttenaere et al., 2000; Smith et al., 2004; Gee and Gawthorpe, 2006). This section begins with a summary of current, large scale conceptual models for sedimentation in these settings (1.2.1). This is followed by a brief overview of growth sequences. Growth sequences are sedimentary packages which form coevally with fold growth and are critical in terms of recording sediment-structure interactions over time (1.2.2). The final section (1.2.3) summarises recent work on submarine channel systems with a focus on the interactions between channel development and underlying deformation.

1.2.1 Models of sedimentation on complex slopes in deepwater settings

Clastic sedimentation and submarine fan development in deep water environments can occur in water depths of over 5000m (e.g. Babonneau et al., 2002). Accommodation space is a key control on submarine fan architecture, especially in structurally active settings (e.g. Prather, 2003). In deepwater environments, accommodation space is best defined in a similar manner to that used for subaerial fluvial systems, where the magnitude of accommodation space is given by the difference between the depositional profile (in this case the slope) and a hypothetical equilibrium profile (Fig. 1.1, see also Mackin, 1948). The equilibrium profile represents a hypothetical surface along which neither erosion or deposition occurs (Mackin, 1948; Pirmez et al., 2000; Kneller, 2003;). For a submarine channel system, the shape of the equilibrium profile is generally thought to be concave upwards (Fig.1.1), and limited at its uppermost and lowermost points by the head of the submarine feeder canyon and by the channel-lobe transition respectively (Pirmez et al., 2000; Kneller, 2003). Base level for deepwater environments can be described as the point at which channelised flows become unconfined when they reach the basin floor (i.e. the channel-lobe transition – Kneller, 2003).

Modifications to the shape of the depositional surface due to deformation can cause variations in accommodation space and slope gradient leading to zones of enhanced erosion and deposition (e.g. Pirmez et al., 2000; Ferry et al., 2005; Smith, 2004). This is discussed in more detail in Chapter 6, section 6.2.3. Additionally, external controls also affect the overall shape of the equilibrium profile itself, such as sea level changes and variations in sediment supply character (Ross et al., 1994; Kneller 2003). Current conceptual models for the filling of structurally created accommodation space in deepwater settings can be summarised in terms of

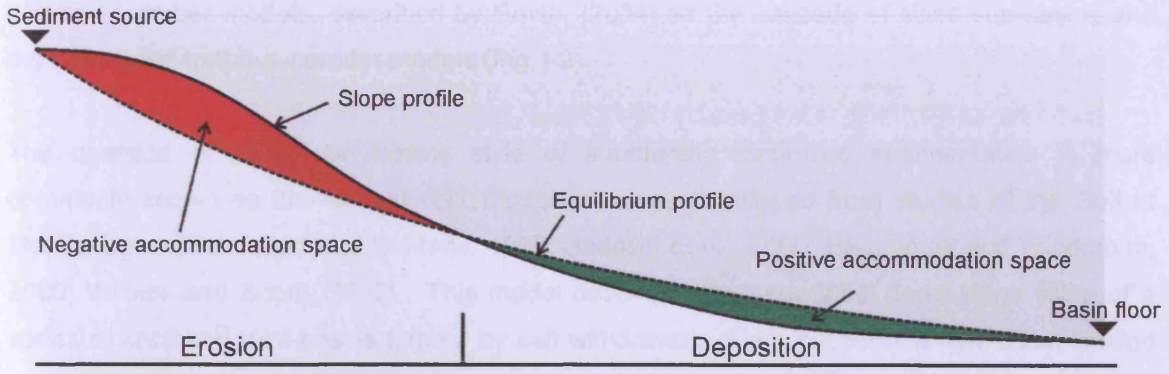

Figure 1.1: Summary of the equilibrium profile concept applied to deepwater sedimentary systems. Accommodation space in such settings is given by the difference between the depositional surface and a notional equilibrium profile. Modified from Kneller 2003.

two end-member models, described by Smith, (2004) as the cascade of silled sub-basins and the connected tortuous corridor models (Fig 1.2).

The cascade of silled sub basins style of structurally controlled sedimentation is more commonly known as the 'fill and spill' model, and was developed from studies of the Gulf of Mexico slope (Satterfield and Behrens, 1990; Badalini et al., 2000; Beaubouef and Friedmann, 2000; Winker and Booth, 2000). This model describes the sequential down-slope filling of a series of enclosed mini-basins formed by salt withdrawal. Each successive mini-basin is filled up to its spill point, after which bypass occurs resulting in filling of the next basin down-slope (Fig 1.2). Erosion tends to focus at the spill points as the bypassing flows adjust to the local change in base level in order to reach the next mini-basin lower on the slope (Beauboeuf and Friedmann, 2000). The end result is a series of basin fills whose age progressively decreases in the down-slope direction (Fig 1.2). Each basin is linked by channels which bypass basins further upslope and incise the spill points between each basin.

The connected tortuous corridor model of structurally controlled slope sedimentation (Fig 1.2) involves a flow path that is not broken into separate mini-basins, but instead follows a tortuous route which is heavily influenced by the surrounding bathymetric relief (Smith, 2004). Examples of tortuous flow pathways on the present day seafloor of the Eastern Mediterranean can clearly be seen in Chapter 3 (Fig. 3.1). The down-slope flow pathway can be influenced by several types of deformation, some examples are:

1. Folds detached within salt or shale: These often form stepped slopes where sediment pathways are guided around the edges of multiple fold structures according to the overall down-slope gradient. Examples include the shale-detached folds offshore NW Borneo (Demyttenaere et al., 2000; Morley, 2009), the Niger Delta fold belt (Pirmez et al., 2000; Hooper et al., 2002; Heinio and Davies, 2006)
2. Extensional faulting which guides flow pathways around the lateral terminations. An example of this is documented by Ferry et al., (2005) from offshore Angola.
3. Salt diapirism which guides sedimentation into the zones of withdrawal around growing diapirs. This is documented by Gee and Gawthorpe, (2006), from the Angolan slope.

Areas of increased erosion and deposition along the connected tortuous corridor are controlled by variations in the underlying slope gradient, such as where flow paths cross extensional faults or folds (Demytteneare et al., 2000; Huyghe et al., 2004; Ferry et al., 2005). In contrast to the fill and spill model, the age of deposits does not systematically young down-slope, but will be affected by channel avulsions (Fig1.2). Of these two models for slope sedimentation in structurally complex settings, the connected tortuous corridor model seems more appropriate to

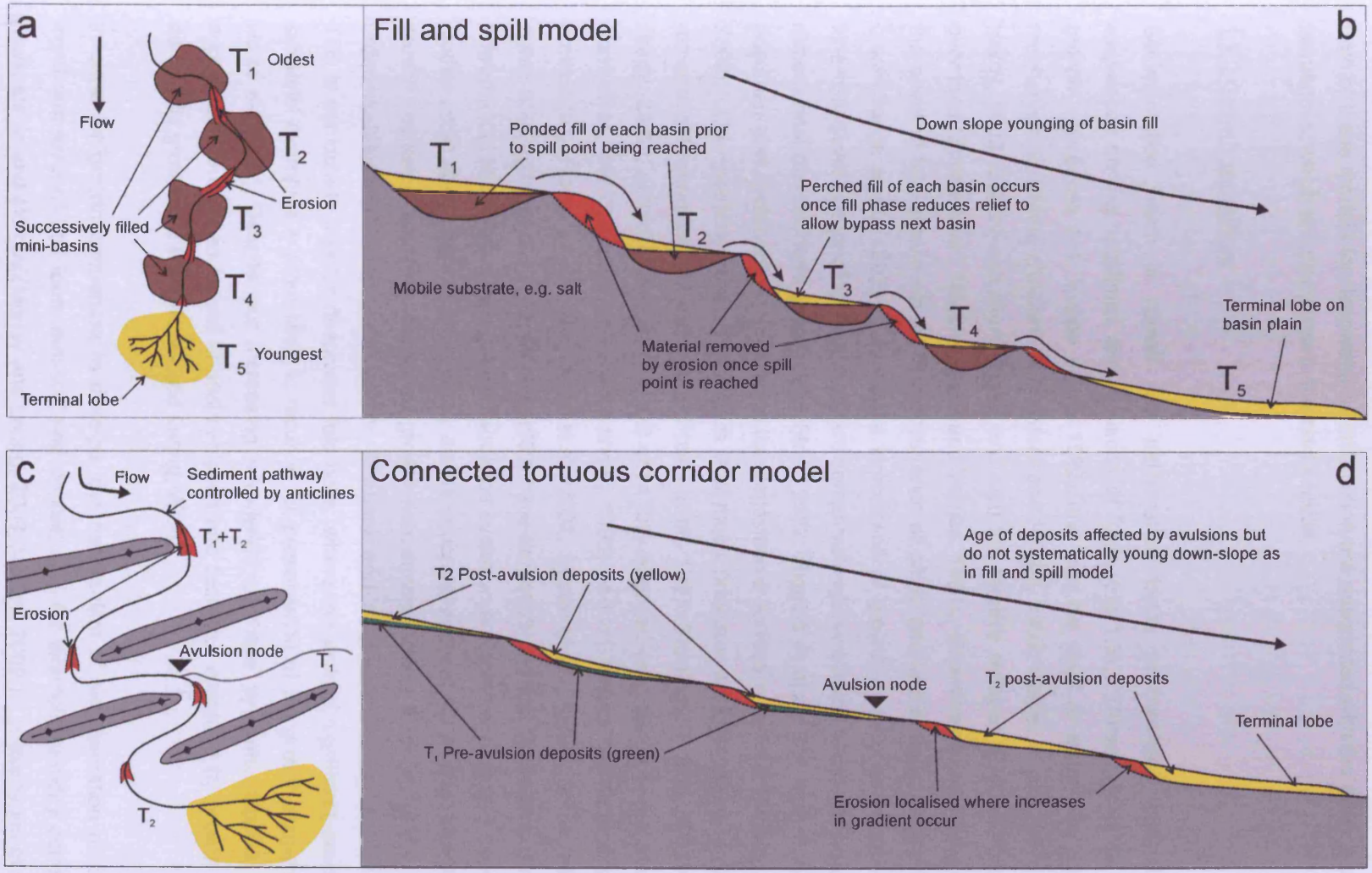

Figure 1.2: Summary of the fill and spill and connected tortuous corridoor models for sedimentation in structurally complex seafloor settings. The fill and spill model (**a** and **b**) applies to confined mini-basins where each basin is sequentially filled in a down-slope direction. The connected tortuous corridoor model (**c** and **d**) applies to slopes where flows are not confined, but guided by bathymetric features which obstruct flow. See text for details.

the deepwater fold belts which are the structural setting of the systems analysed in this thesis. Both of these models for deepwater sedimentation are associated with the deposition of growth sequences, which are discussed in the next section.

1.2.2 Growth sequences

Sedimentation which is coeval with deformation forms geometrically distinctive growth sequences on the backlimbs and forelimbs of folds (Fig 1.3). These packages are termed growth sequences (c.f. Suppe et al., 1992) and can be used to determine the kinematic mechanism of folding (Rowan, 1997; Storti and Poblet, 1997; Poblet et al., 1997; Bernal and Hardy, 2002; Salvini and Storti, 2002) and also the relative rates of uplift and sedimentation over time (Suppe et al., 1992; Burbank and Verges, 1994). Growth sequences can also record the onset of fold growth via the first occurrence of onlap and/or thinning onto the fold limb or crest (Suppe et al., 1992). Despite the importance of growth sequences in constraining the kinematics and history of folding, there are comparatively few studies which consider their three dimensional development (Salvini and Storti, 2002; Higgins et al., 2009) and even less which document the evolution of fold relief at the depositional surface over time (Morley and Leong, 2008). One possible reason for this is that much previous work is based largely on two-dimensional numerical modelling (e.g. Poblet et al., 1997; Storti and Poblet, 1997; Bernal and Hardy, 2002), outcrop data, which is not often fully exposed (e.g. Burbank and Verges, 1994; Ford et al., 1997; Zapata and Allmendinger, 1996) and on limited two-dimensional seismic profiles (e.g. Rowan, 1997; Masaferro et al., 2002; Suppe et al., 2002). Some recent studies however (Higgins et al., 2009; Morley, 2009) have demonstrated that 3D seismic data can be a powerful tool in characterising growth sequence evolution and fold development over time. The studies listed above tend to focus purely on the structural aspects of fold evolution derived from growth sequence analysis. However, growth sequences provide a record of the interactions between deformation and sedimentation (Burbank and Verges, 1994; Burbank et al., 1996). This is particularly true for deepwater fold belts, where the lack of significant erosion seen in subaerial examples is more likely to result in full preservation of the growth sequence in deep water settings. Despite our increasing knowledge of these systems, studies which fully appreciate the detailed record of sedimentation and tectonics recorded by growth sequences during fold growth are few (Morley and Leong, 2008).

In order for growth sequences to develop, the mechanism of sedimentation must involve a significant level of bed load transport and deposition – for example turbidity currents, debris flows, slides and slumps (Morley and Leong, 2008; Morley, 2009;). These types of flows show a response to the structurally induced bathymetry and will pond within bathymetric low points

and become diverted around positive fold relief (e.g. Demytteneare et al., 2000; Huyghe et al., 2004). However, in deep water environments hemipelagic and pelagic sedimentation can form drape-like packages of uniform thickness across the fold crest (Chapter 4 – Fig. 4.5). These result in a different stratal geometry compared to that observed for growth sequences, especially if the fold limbs are not steep enough to induce mass wasting. This creates an important pitfall when interpreting the correct timing of the onset of fold growth (Cartwright 1992). This is discussed in more detail in Chapter 2 under section 2.2 – seismic interpretation methods.

The key characteristic of a growth sequence associated with folding is a bed geometry showing expansion and divergence away from the fold crest (Fig 1.3). This has been recognised from studies at outcrop scale (e.g. Riba, 1976) but is most clearly seen on seismic profiles (Rowan et al., 1997; Suppe et al., 2002; Masaferro et al., 2002; Briggs et al., 2006). The geometry of the stratal boundaries within the growth sequence will vary according to the relative rates of uplift and sedimentation (Fig 1.3, see also Burbank and Verges, 1994). The use of the term 'relative' reflects the fact that, where age calibrations are unavailable it can be difficult to separate whether sedimentation rate or uplift rate is the key controlling factor in controlling growth sequence deposition. Another potential pitfall is caused by interpreting narrow stratigraphic intervals, where spatial variations can occur due to distance from the sediment source – see Chapter 5 – Fig. 5.14) High relative rates of uplift versus sedimentation result in an onlapping and offlapping stratal geometry within growth sequences (Fig 1.3). The onlap and offlap termination points mark the positive relief against which deposition from the flows whose deposits comprise the growth sequence terminate against. These points form key markers in interpreting palaeo-seafloor relief during fold growth and coeval sedimentation. If the relative rate of uplift is low compared to sedimentation rates then sedimentary packages will show thinning but otherwise continuous stratal geometries across the fold crest (Fig 1.3). This stratigraphic relationship implies that no positive relief develops at the depositional surface during folding, and that sedimentation completely heals over the growing fold (Burbank and Verges, 1994).

Within deepwater fold belts, an important sedimentary component of many growth sequences are submarine channel levee systems. Hemipelagic and mass transport deposits can also form important components of growth sequences, with the proportion of each being dependent on the local geological setting (e.g. Morley and Leong, 2008, see also Chapter 4). The deposits from submarine channel systems form important hydrocarbon reservoirs in these settings however (e.g. Clemenceau et al., 2000; Fonnesu, 2000; Abreau et al 2003; Mayall et al., 2006), and they are described in the next section.

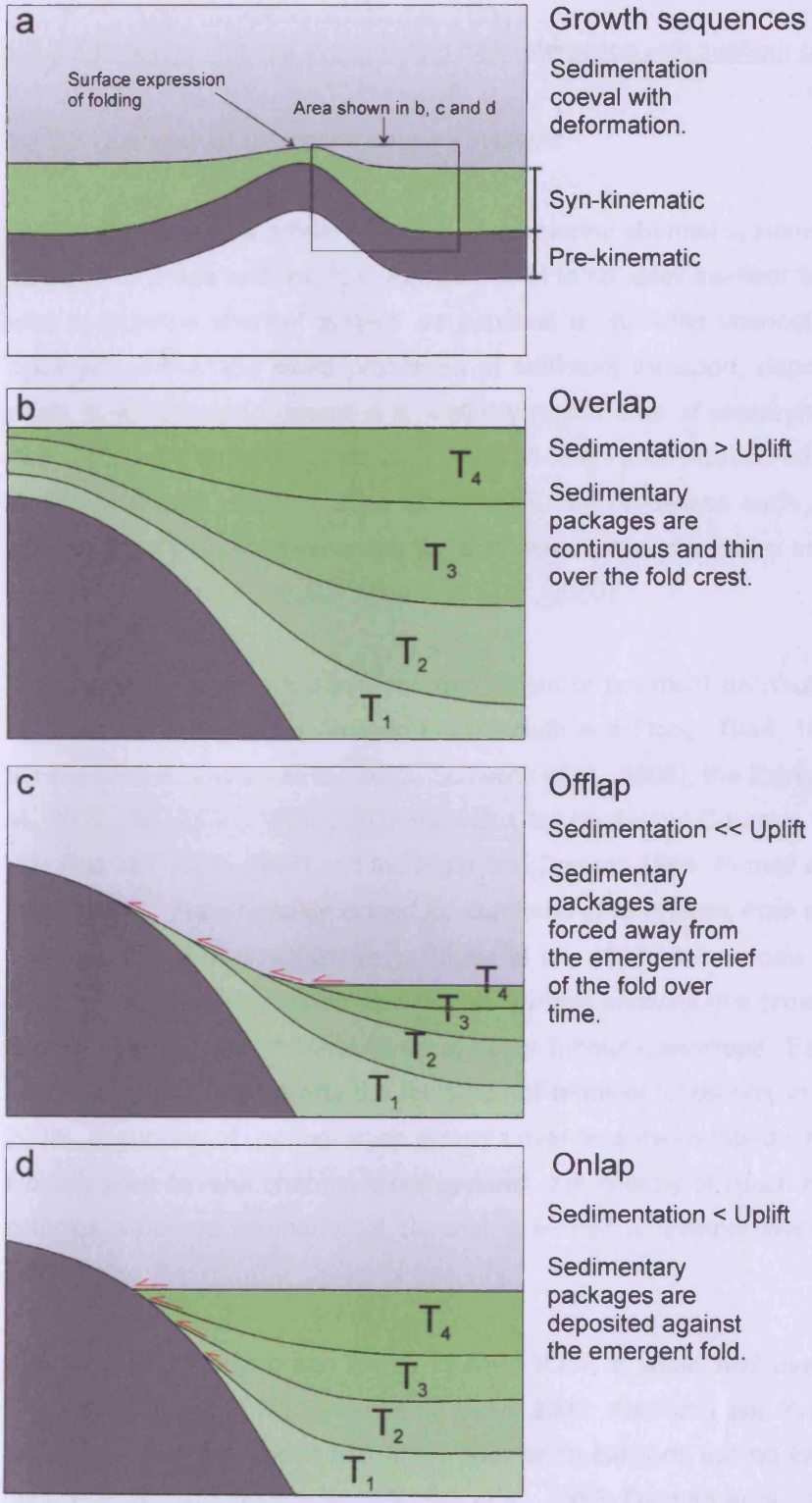

Figure 1.3: Definitions of growth sequence geometry used in this thesis, adapted from Burbank and Verges 1994. Overlap (**b**), offlap (**c**) and onlap (**d**) indivually represent differring relative rates of uplift versus sedimentation during folding.

1.2.3 Submarine channel systems and their interaction with seafloor deformation

1.2.3.1 Overview of submarine channel systems:

This section presents a brief overview of submarine channel systems with an emphasis on the response of these systems to deformation and to complex seafloor bathymetry. The use of the term 'submarine channel system' as opposed to 'turbidite channel' throughout this thesis is deliberate in that the exact processes of sediment transport, deposition and flow behaviour within these channel systems is a relatively recent area of research (e.g. Corney et al., 2006; Keevil et al., 2006; Imran et al., 2007; Peakall et al., 2007; Straub et al., 2008). The use of this term also reflects recent studies which show that processes such as hyperpycnal flows may also be an important mechanism for sedimentation and erosion in submarine channels and canyons (Flood et al., 2009; Khriponouff et al., 2009).

Submarine channels are a primary mechanism of sediment distribution in many deep sea fan systems, for example the Amazon fan (Damuth and Flood, 1984, 1985; Damuth et al., 1988), the Bengal fan (Curray et al., 2003, Schwenk et al., 2005), the Zaire/Congo fan (Babonneau et al., 2002; Droz et al., 1996, 2003), the Indus fan (Kolla and Coumes 1987; Deptuck et al., 2003; Von Rad and Tahir, 1997) and the Niger fan (Damuth 1994; Pirmez et al., 2000; Deptuck et al., 2003; 2007). They typically extend for hundreds of kilometres from the shoreline and persist in water depths of over 4000m (e.g. Hagen et al., 1994; Babonneau et al., 2002; Jegou et al., 2008). The submarine channel system as a whole consists of a proximal canyon which feeds a number of individual channel levee systems further downslope. Each channel levee system ends on the basin plain with the formation of terminal lobes (Wynn et al., 2002; Jegou et al., 2008). Avulsions of channel levee systems over time mean that a single submarine canyon will typically feed several channel levee systems, the entirety of which is termed a channel levee-complex, whereas an individual channel is termed a channel levee system (Deptuck et al., 2003).

The submarine canyon can be up to over 10km in width and over 1km in depth (Fig. 1.4; Babonneau et al., 2002; Pirmez and Imran, 2003; Antobreh and Krastel, 2006). Present day highstand conditions mean that many submarine canyons are no longer directly connected to their original fluvial source (e.g. Bouma et al., 1985; Damuth et al., 1988). Notable exceptions to this include the Montery Canyon (e.g. Smith et al., 2007) and the Zaire Canyon (Heezen et al., 1964; Khripounoff et al., 2003) and also the Var Canyon (Khripounoff et al., 2009). Submarine canyon morphology is often characterised by multiple scarps due to sidewall

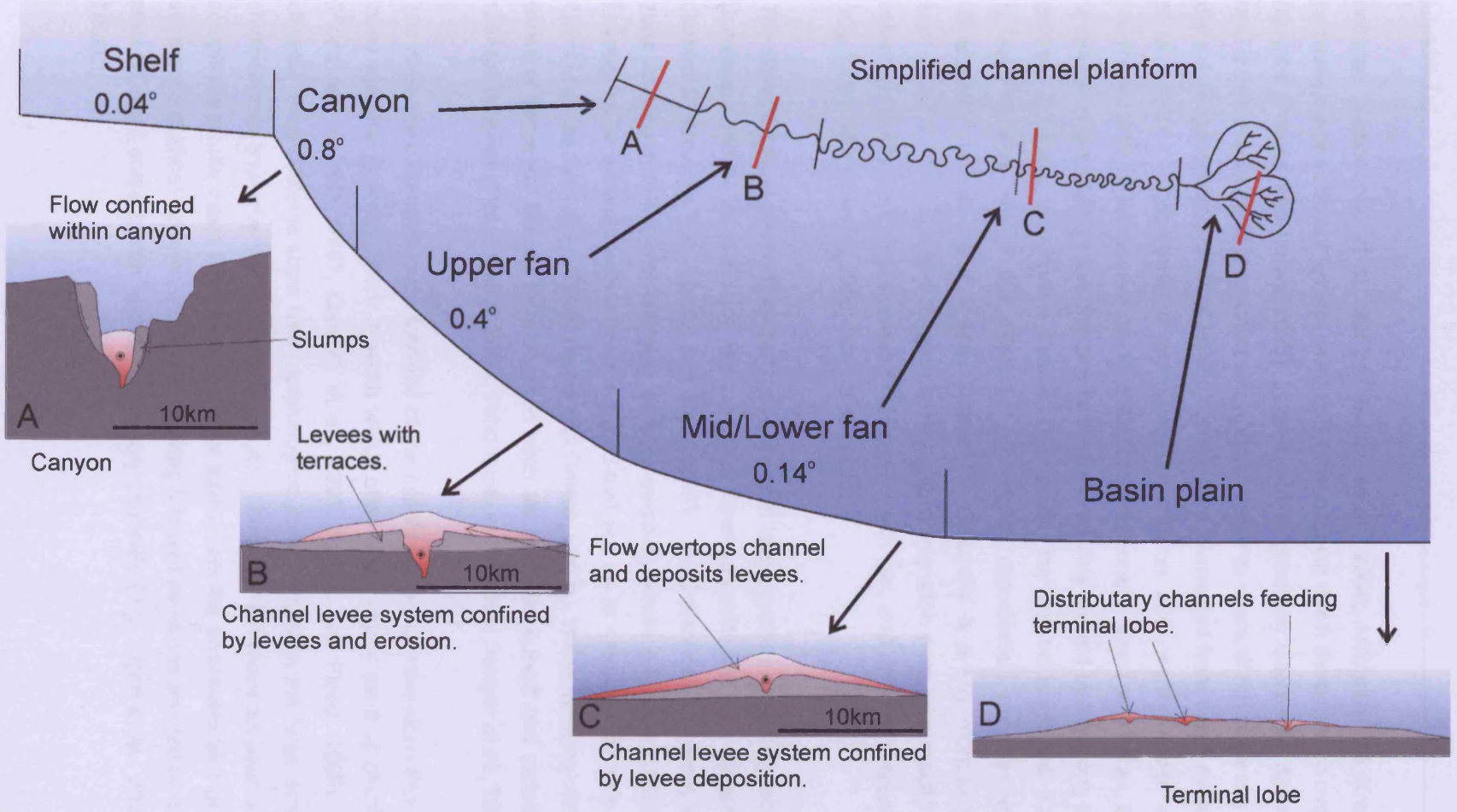

Figure 1.4: Overview of submarine channel systems and their down-slope variation in morphology. The overall scale and architectural complexity of the submarine channel decreases downslope due to progressive loss of flow volume (depicted by the red shaded areas) both down slope and over time. The profiles A to D show general cross sections of the channel levee system at each point along the slope. *Slope values from Pirmez and Imran 2003, channel cross sectional profiles modified from Babonneau et al 2002.*

collapse (Babonneau et al., 2002; Popescu et al., 2004; Antobreh and Krastel, 2006) and canyons are of sufficient vertical relief that flows passing down them cannot overtop the canyon margins (Pirmez and Imran, 2003). Canyon relief gradually decreases down-slope (Fig.1.4) until a transitional zone is reached where flows begin to overspill the sidewalls and deposit the classic wedge shaped channel levees commonly documented from these systems (e.g. Skene et al., 2002). This transition zone between canyon and channel levee system is often associated with an increase in the sinuosity of the channel (Pirmez and Imran, 2003). Sinuosity is defined as the straight line distance between two points divided by the along channel distance between the same two points – a value of 1 indicates the channel is straight. Channel sinuosity is used a measure of the effects of underlying deformation on channel levee system development in this thesis – see Chapter 3. Sinuosity is a key morphological feature of submarine channel systems as progressive lateral migration over time results in deposition of extensive, sand-rich lateral accretion packages which can, and do form hydrocarbon reservoirs (e.g. Mayall and Stewart, 2000; Abreau et al 2003).

The down-slope transition from canyon to channel levee system is typically accompanied by a decrease in the depth of erosion into the pre-channel substrate and an increase in height of the channel levees (Fig. 1.4; Pirmez and Imran, 2003). Avulsions can frequently occur within this zone and form radial, fore-stepping or back-stepping avulsion patterns (Kolla, 2007). The channel levee systems within this zone (mid-fan) are up to 4km in width with a relief of over 100m (e.g. Deptuck et al., 2003; Heinio and Davies, 2007). These systems often show multiple levels of terraces, formed by processes such as meander cut-off and incision, and also by sidewall collapse (Posamentier, 2003; Babonneau et al., 2004; Sawyer et al., 2007).

The large scale channel levee systems of the middle fan pass down-slope into smaller channel levee systems typically 500m in width which often show highly sinuous planform geometries (Flood and Damuth, 1987; Damuth et al., 1995; Pirmez and Flood, 1995). These smaller channel levee systems show less morphological complexity than the large scale (km in width) channel levee systems further up dip (Fig 1.4). The lower fan channels pass into terminal lobe complexes on the basin floor, these terminal lobes mark the basinward limit of deposition from submarine channel systems with lobes showing frequent avulsions and fed by compensationally stacked small scale (c.10m width) distributary channels (e.g. Wynn et al., 2002; Jegou et al., 2008).

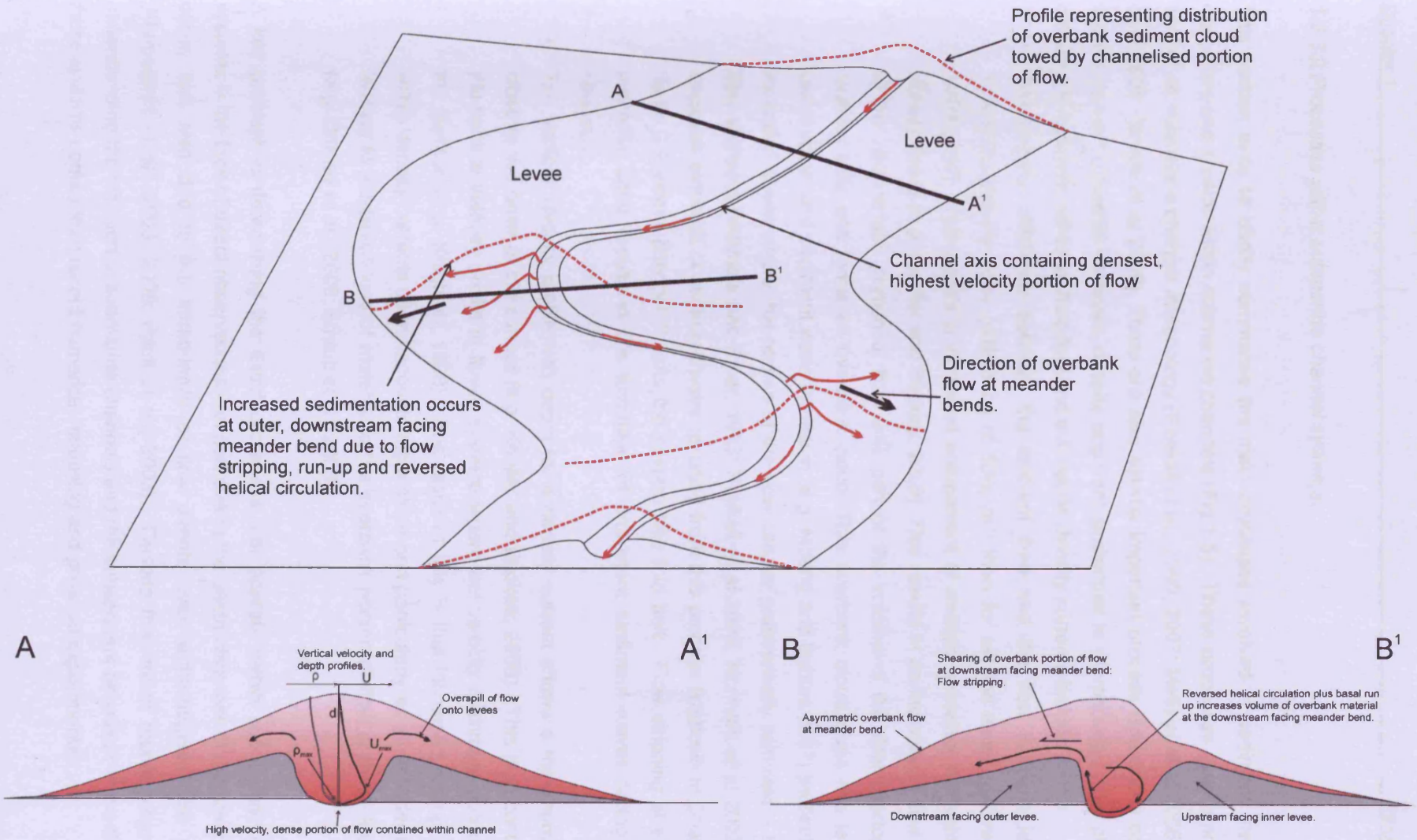

Figure 1.5: Summary of the key flow processes operating within submarine channel systems. Key processes include a portion of the flow which exists as an overbank cloud outside of the main channel. Other processes include flow stripping and reversed helical circulation (relative to subaerial channels) at meander bends. See text for details.

1.2.3.2 Processes within submarine channel systems:

This section aims to briefly summarise the main processes involved in sediment transport, deposition and erosion within submarine channels (Fig 1.5). These processes exert a powerful control on submarine channel morphology (Peakall et al., 2000; 2007; Metivier et al 2005; Kane et al 2008; Straub et al 2008). There are also several important process differences between submarine and subaerial channels, despite apparent similarities in morphology. Key physical differences between subaerial fluid flow and submarine density currents include:

- The density difference between the ambient fluid and the flow is much less for submarine density flows (difference of 50kg m^3) than for air and water (difference of 1000kg m^3). This results in increased entrainment of ambient seawater into submarine density flows (e.g. Kneller and Buckee, 2000). This results in an increase in flow height of the channelised portion of flow until part of the volume of the flow overtops the channel axis and forms an overbank cloud. This overbank cloud gives rise to levee construction and sediment wave formation (e.g. Mohrig and Buttles 2007) particularly at meander bends where this portion of the flow can be preferentially removed – termed flow stripping (Normark and Piper, 1983; Peakall et al 2000; Normark et al 2002). An excellent example of sediment wave resulting from this process is shown in Chapter 3, figure 3.1 where channel C exits the eastern Nile fold belt: Flow stripping at a sharp meander bend results in the formation of prominent sediment waves facing down stream.
- The vertical velocity profile with depth for a density current shows a maximum value close to the base of the current (e.g. Kneller and Buckee, 2000). This is in contrast to the vertical velocity profile in fluvial systems where the velocity maximum occurs near the surface (e.g. Knighton, 1998). The result of this is that increased run-up occurs within density currents upon encountering a slope and particularly as at meander bends, leading to increased loss of material to the overbank portion of flow at these locations (e.g. Corney et al., 2006; Straub et al., 2008).

A key problem in determining the exact processes that operate within submarine channel systems is the lack of direct observations – in part due to the destructiveness of the flows which occur, and also due to the infrequency of flow events over anthropogenic time scales (Khripounoff et al., 2003, 2009; Paull et al., 2003). Despite this, much recent progress in understanding the initiation of submarine channels and the subsequent behaviour of the flows in these systems comes from recent numerical modelling and physical experiments.

The inception of submarine channels from an initial flow spreading laterally downslope is still a relatively poorly understood process (Imran et al., 1998; Metivier et al., 2005; Yu et al., 2006). A key factor which appears to be responsible for the process of channel initiation is the difference between erosion and deposition rates across a spreading turbidity current (Imran et al 1998). Another necessary condition is the presence of a thin initial flow that incompletely covers the surface over which it is flowing, this results in the formation of flow lanes within the spreading flow with zones of increased deposition in between (Yu et al., 2006). This process then appears to generate a positive feedback where increasing deposition acts to separate and confine flow over time and establish a channel planform (Yu et al., 2006).

The flow processes operating within submarine channels are now better understood, with recent studies focussing on flow behaviour at channel bends associated with sinuous submarine channels (Corney et al., 2006; Keevil et al., 2006; 2007; Peakall et al., 2007; Kane et al., 2008). Interestingly, modelling of flows within sinuous submarine channels has shown that the direction of helical circulation at bends in submarine channel systems is reversed compared to subaerial channel systems (Fig. 1.5; Corney et al., 2006). This results in basal flow directed towards the outer bank of a meander (Fig. 1.5). Basal flow towards the outer bank, combined with inertial runup (Straub et al., 2008) and overbank shearing (flow stripping – Keevil et al., 2007) results in significantly increased super-elevation of the flow surface and increased over-spilling of material onto the outer bank at meander bends (Straub et al., 2008). An important implication of this process is that a significant proportion of the coarse grained basal flow portion can become deposited outside of the channel axis entirely (Straub et al., 2008). The commonly observed fields of sediment waves which occur on the down-stream facing outer banks of meanders in highly sinuous submarine channels appear to support these processes (Fig. 1.5; see also Normark et al., 2002; Posamentier, 2003).

1.2.3.3 Response of submarine channels to deformation:

Relatively few studies focus on the interactions between submarine channel systems and deformation (Huyghe et al., 2004; Ferry et al., 2005; Gee and Gawthorpe, 2006; Heinio and Davies, 2007). This is despite the common occurrence of submarine channels within actively deforming deepwater settings (e.g. Hagen et al., 1994; Laursen and Normark, 2002; Broucke et al., 2004; Alonso and Ercilla, 2003; Fildani and Normark, 2004; Adeogba et al., 2005; Cross et al., 2009). Studies of submarine channels from Nigeria, the Amazon Fan, Gulf of Mexico and the Rhone fan indicate that these systems tend to adjust to a concave upwards equilibrium profile over time, despite the influence of deformation on slope profiles (Pirmez et al., 2000). In an analogous manner to fluvial systems, the planform response of submarine channel systems

to underlying deformation and changes in slope can be explained in terms of the channel system adjusting to reach a hypothetical equilibrium slope for a given set of flow parameters (Fig 1.6; Ferry et al., 2005).

The morphological response of submarine channel systems to deformation is similar to that observed for fluvial systems (e.g. Ouchi, 1985). An increase in slope, caused for example by underlying folding or faulting can result in a decrease in channel sinuosity as the channel decreases the length of the reach to match the equilibrium slope (Fig 1.6; Ferry et al., 2005). The decrease in sinuosity will often be associated with an increase in the level of erosion over the particular channel segment – this is most often expressed as a decreased width:depth ratio, with the channel becoming narrower and deeper and increasingly V-shaped in cross section (Ferry et al., 2005). The increase in erosion may be associated with decreased levee deposition due to increased confinement of the flow by the more deeply incised channel, with the maximum erosion localised at the point where the slope value increases. This was observed by Ferry et al., 2005 and also from studies from the Gulf of Mexico at the spill points between mini-basins (e.g. Beauboeuf and Friedmann, 2000). A decrease in sinuosity and increase in erosion due to underlying uplift may also be associated with the formation of knick-points which then propagate upstream and incise into previous channel deposits, resulting in the formation of terraces (Heinio and Davies, 2007). Knick-point formation and their upstream propagation may be one of the mechanisms by which submarine channels attempt to re-gain equilibrium where deformation of the underlying slope occurs.

Decreases in the underlying slope gradient lead to an increase in submarine channel sinuosity as the channel system lengthens in order to adjust its local slope to match equilibrium slope conditions (Fig 1.6; see also Ferry et al., 2005). An increase in sinuosity is accompanied by aggradation of the channel axis as well as lateral migration. Increases in submarine channel sinuosity related to an underlying decrease in slope values have been documented from the hanging walls of normal faults offshore Angola by Ferry et al., (2005). Gee and Gawthorpe, (2006) also observed localised sinuosity increases within a circular depression surrounding a salt diapir, again from the Angolan Margin.

Understanding the response in submarine channel development to deformation of the underlying slope is critical in order to predict, for example, localised areas of increased sinuosity and erosion in structurally active deepwater settings. Areas of increased sinuosity can potentially lead to laterally extensive, sand rich lateral accretion deposits (e.g. Abreu et al., 2003), whereas localised zones of erosion can lead to loss of reservoir connectivity and cannibalisation of previously deposited channel axis deposits (e.g. Heinio and Davies., 2007).

Many of studies listed above tend to focus on the response of the channel axis, however the channel levees also form an important component of the system as the height of the channel levees acts to confine flow within the channel axis. Variations in channel levee thickness and extent was documented in response to relief created by salt withdrawal from offshore Angola by Gee and Gawthorpe, (2006), and this suggests that mapping levee extent could provide a useful tool when interpreting channel systems in areas affected by deformation. Although many studies have collected measurements of channel morphometric parameters (e.g. Pirmez and Imran, 2003; Huyghe et al., 2004; Ferry et al., 2005), the potential use of these parameters as detailed indicators of channel responses to deformation remains to be addressed. There is also a lack of a coherent descriptive framework with which to describe submarine channel-structure interactions, particularly given that a wide range of possible interactions and timing relationships relative to deformation exist. A detailed knowledge of how submarine channels interact with deforming structures would aid our conceptual models of how these channel systems develop over time, and hopefully be of use in the interpretation of these systems based on 3D seismic data.

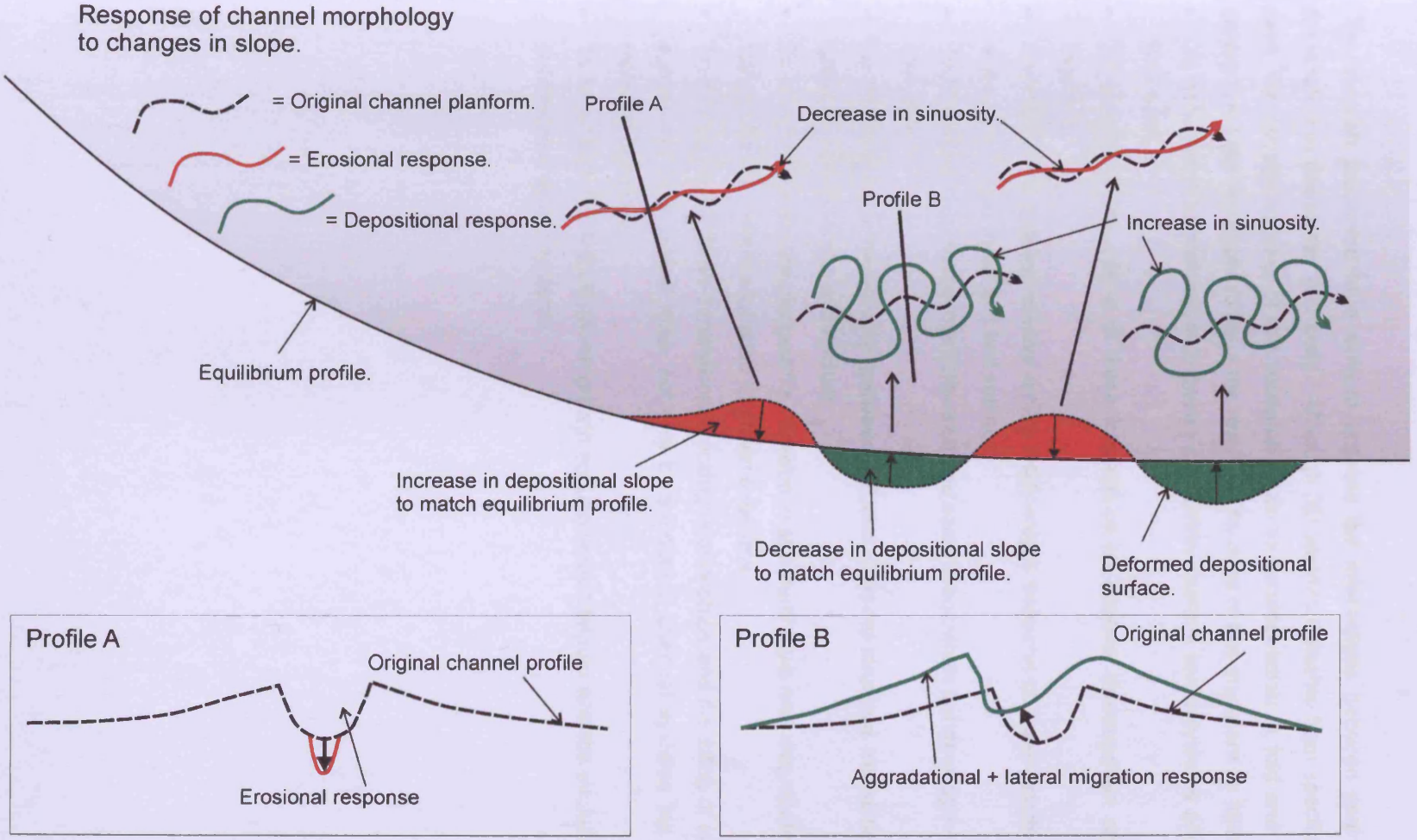

Figure 1.6: Response of submarine channel systems to variations in seafloor slope caused by deformation. Changes in the depositional slope result in channel re-adjustment in order to reach the equilibrium slope profile. Re-adjustment of the channel can involve a change in sinuosity as shown by the planform responses on the main part of the figure. Profiles A and B show the effect of re-adjustment on the cross sectional morphology of the channel.

1.3 Aims of study

The research presented here aims to address the interactions between sedimentation and deformation in deepwater fold belts. Although 3D seismic datasets from specific localities are used, the underlying aims of this research relate to sedimentation in fold and thrust belts in general, as does the applicability of the results. The aims of this study are as follows:

- To document the interactions between submarine channel levee systems and evolving fold structures.
- To investigate the effects of these interactions on channel development and morphology over time.
- Investigate the detailed relative timing relationships between channel-structure interactions and uplift in deep water fold belt settings.
- To investigate how these interactions can be used to constrain the development of fold relief over time.
- To document the relationship between detailed channel-structure interactions and larger scale growth sequence architecture.
- To Investigate how the along-strike variation in structural style and magnitude of uplift along folds relates to growth sequence evolution over time.
- To investigate the three dimensional stacking relationships and the filling of accommodation space over time around folds, not only by submarine channel systems but also by mass transport deposits.
- To investigate the links between growth sequence architecture and the evolution of submarine channel systems

Chapter 2

CHAPTER 2

METHODS

The results presented in this thesis are derived from the interpretation of 3D seismic data volumes. This type of data has contributed greatly to our understanding of many aspects of geology, particularly so in terms of deepwater sedimentary systems (e.g. Posamentier and Kolla 2003). The aim of this chapter is to give a brief overview of 3D seismic data and then to introduce the main interpretive methods used to derive the results presented in this thesis.

2.1 3D seismic data

The marine 3D seismic data volumes used in this thesis are typically acquired using an airgun seismic energy source, a series of geophones then detect the reflected energy of compressive (P) waves from physical boundaries within the earth (Sheriff and Geldart, 1995; Kearey et al., 2002; Hart, 1999). The strength of the seismic reflection from an interface is dependant on the acoustic impedance, z, where $z = \rho v$ where ρ is the density of the rock unit and v is the p-wave velocity. At geological boundaries between rocks of different lithologies – for example a shale layer above a sandstone layer, the contrast in physical properties (namely density) of the two rock units results in a strong acoustic impedance contrast giving a strong reflection. Seismic surveys also record the time taken for the p-wave to travel to and from the acoustic impedance contrast and as such the vertical scale in many seismic sections is given in two-way travel time (TwT).

Seismic data is displayed usually displayed in such a way that an increase in acoustic impedance corresponds with a peak in a seismic wavelet (Fig 2.1). This is termed 'SEG (Society of Exploration Geophysicists) normal polarity', this convention also applies to all of the data used in this thesis. The data used here is zero-phase (Fig 2.1), so called because the displayed wavelet is symmetrical with the peak corresponding to the zone of maximum energy (e.g. Brown, 1999). There are several advantages to using zero-phase data, namely that the zero phase wavelet shape reduces uncertainty when associating waveforms with subsurface interfaces and also that a horizon tracked along the centre of the wavelet coincides with the subsurface boundary causing the reflection.

The resolution of 3D seismic data varies with depth both vertically and horizontally, and generally decreases with depth. Despite the excellent three dimensional coverage which

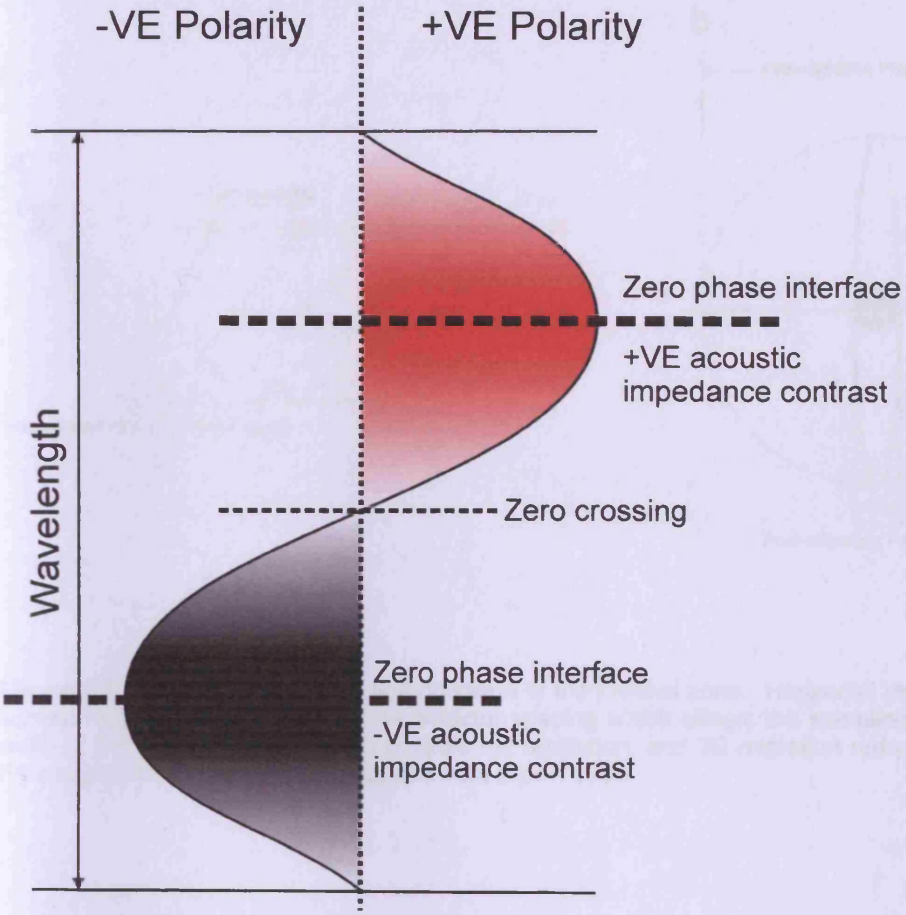

Figure 2.1: Seismic wave illustrating the conventions of polarity and phase used in this thesis. *Adapted from Hart 1999.*

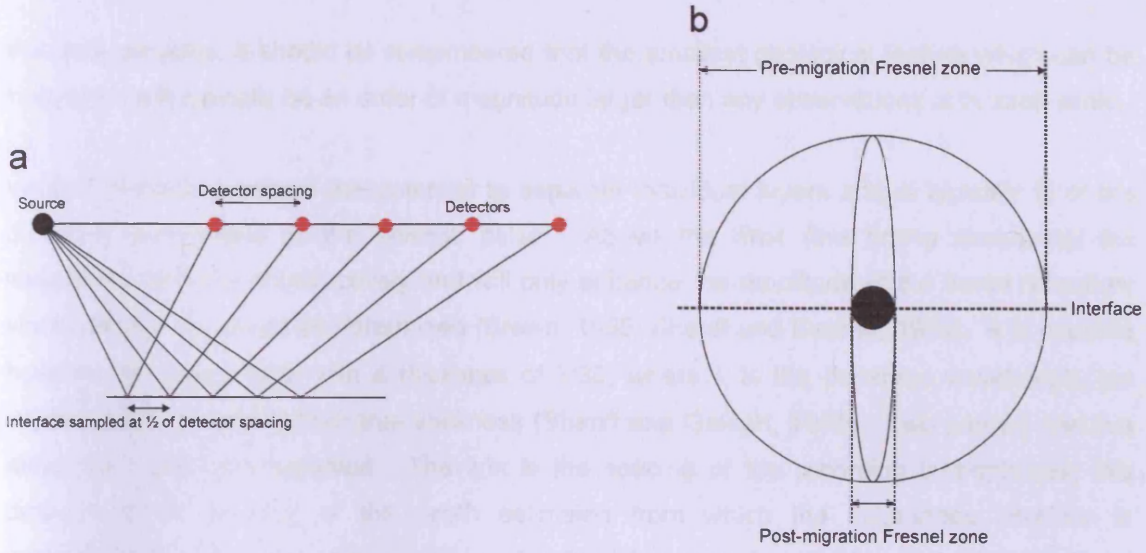

Figure 2.2: Horizontal resolution and definition of the Fresnel zone. Horizontal resolution in seismic surveys is determined in part by the detector spacing which affects the sampling interval (**a**). The width of the Fresnel zone (**b**) also controls the resolution, and 3D migration reduces the size of the Fresnel zone to a small sphere. *Adapted from Brown 1999.*

this data provides, it should be remembered that the smallest geological feature which can be imaged on will typically be an order of magnitude larger than any observations at outcrop scale.

Vertical resolution defines the potential to separate individual layers and is typically ¼ of the dominant wavelength of the seismic pulse. Above this limit (the tuning thickness), the waveforms interfere constructively and will only enhance the amplitude of the tuned reflection, whose thickness cannot be determined (Brown, 1999; Sheriff and Geldart, 1995). It is possible however, to detect beds with a thickness of $\lambda/30$, where λ is the dominant wavelength, but impossible to determine their true thickness (Sheriff and Geldart, 1995). Two primary controls affect the horizontal resolution. The first is the spacing of the recording hydrophones; this determines the spacing of the depth estimates from which the subsurface interface is reconstructed. The horizontal sampling of a flat lying seismic reflection is typically half the detector spacing (Fig 2.2; Kearey et al 2002). The second factor is the width of the Fresnel zone, which is defined by the energy returned to the detector within half a wavelength of the initial reflected arrival. Within this zone the reflected waves interfere constructively to give the reflected signal (Kearey et al 2002). Both vertical and horizontal resolution decrease with depth due to loss of higher frequencies via elastic absorption, and due to increasing compaction of sediments. This increases the velocity further, thus lowering the dominant frequency.

Before seismic data can be interpreted, it is filtered to increase the signal to noise ratio and remove unwanted frequencies to improve vertical and horizontal resolution (Kearey et al 2002; Sheriff and Geldart 1995). Data migration is then performed involving a number of processes including correcting the positions of reflections from dipping surfaces and focussing the energy spread over the Fresnel zone (Fig 2.2) to improve resolution (e.g. Brown 1999; Kearey et al 2002). Another purpose of migration is to collapse diffraction patterns caused by discontinuities whose radius of curvature is shorter than the wavelength of the incident rays. Offsets of stratal boundaries at faults can commonly cause diffraction patterns which unless removed can make fault interpretation difficult (e.g. Brown 1999).

The two datasets used in this thesis each have differing resolutions and acquisition parameters, and this information is given in the relevant chapters.

2.2 Interpretation of 3D seismic data

The results presented throughout this thesis are derived from from mapping of 3D seismic data volumes using Schlumberger Geoframe software. Mapping is the basic process by which three-dimensional surfaces of both structural and stratigraphic features are created. These surfaces

can then be used to derive additional seismic attributes, further aiding interpretation. Mapping is carried out by tracking the horizon of interest by hand on a series of lines orientated perpendicular to one another, typically in the original survey in-line and cross-line directions. In some complex areas, arbitrary lines are also picked but this is generally rare as these lines are difficult to subsequently correct. Spacing of the initial grid is of the same order of magnitude as the scale of the geological features of interest. The resulting grid then forms the seed points for automated tracking algorithms which interpolate the remaining data. The autotracking process can be controlled via a series of parameters to optimise the final map, for example the time search window can be narrowed in areas where reflections have similar amplitudes to avoid the autotracked horizon jumping up or down to another horizon.

Once mapping is complete, a number of attributes can then be derived to aid further interpretation. The seismic attributes used throughout this thesis are described below:

- Dip: Dip attribute maps show the derivative of the surface which reveals changes in gradient. Dip attribute maps are excellent indicators of surface morphology and variations in slope (see Fig. 3.1, Chapter 3). Due to the increased visibility of surface features on dip maps, they also enable more accurate measurements of morphology to be taken – for example the channel sinuosity measurements in Chapter 3.
- Amplitude: Seismic amplitude is measured at the crest of the reflection and when displayed in map form enables facies variations to be observed. An example is figure 4.8 in Chapter 4, which shows bright, high amplitude sheet like bodies inferred to represent coarser grained material relative to the surroundings. The amplitude observed for a horizon commonly varies laterally due to changes in the acoustic impedance caused by varying lithologies along the horizon. Amplitude maps are also useful for detecting faults, and a good example of this is seen on the top salt horizon for the Messinian from the Levant Basin in Chapter 3 (Fig 3.4).
- RMS Amplitude: RMS (root mean square) amplitude squares amplitude values over a specified time window and then averages the results. As RMS involves the squaring of amplitude values, high amplitudes will tend to become more noticeable on the final map (e.g. Brown, 2005). RMS amplitude can be used where the mapped horizon is of too poor quality to make horizon amplitude useful. Care must be taken when interpreting these maps however as the RMS window can cross stratigraphic and time boundaries, particularly if the time window is large and this can introduce unwanted values into the final map. For an example of this, see Chapter 5, Fig. 5.12, where the RMS amplitude map detects two small channel systems above the interval of interest, and care must be

taken not to interpret these channels as avulsions, as they are stratigraphically higher than the main channel system shown in this figure.

- Semblance: Semblance is an attribute calculated by comparing adjacent waveforms within a specified time window and returning a value which represents the similarity of the waveforms (see also Brown, 1999). Semblance is particularly useful for identifying discontinuous features in map view such as faults. Semblance can also prove useful for identifying stratigraphic features such as the basal scours on the lower surfaces of mass transport complexes – am example of this is shown in Chapter 4 (figure 4.8 and 4.11).

Isochron maps showing the time thickness between two horizons are used extensively throughout this thesis. In the context of growth sequences, isochron maps, combined with analysis of seismic sections, can provide important information about where uplift is concentrated. Isochron maps can also be used to make measurements of fold growth where overlapping growth sequences occur (see Chapter 5, figures 8 and 9). Isochron maps of channel levee systems are used extensively in chapter 3 to reveal the depositional pattern of the channel levee system as a whole and to assess channel development in areas of complex seafloor bathymetry, figure 8 from Chapter 3 presents a good example of how using these detailed isochron maps can reveal how channel levee systems respond to underlying deformation.

2.2.1 Potential sources of error

Velocity pull-ups and push-downs result from localised increases or decreases in the interval velocities of lithological units and can be caused by lateral facies variations. This effect introduces a potential source of error in measurements of submarine channel depth and erosional depth where the coarse grained channel fill is thick enough to create a local velocity pull-up. The fill of the channel systems studied in Chapter 3 are typically 50m in thickness, and this does not appear to result in large scale pull-ups compared to much larger channel levee systems with fill thicknesses of over 300m (e.g. Deptuck et al., 2007).

Lateral velocity contrasts due to the increase in vertical thickness across thrust faults can also result in pull-up and disruptions of reflections in the footwall block (e.g. Trinchero, 2000). This 'fault shadow' effect can lead to misinterpretation of structural styles and is relevant when only time-migrated data (as is used in this thesis) is being considered. In many cases where pull-ups and push-downs are observed in association with thrust faulting, evidence such as the occurrence of infilled footwall and hangingwall basins supports the interpretation that these

depressions are real geological features and not artefacts caused by velocity variations across thrust faults (see Chapter 3).

The presence of shallow gas within the subsurface can introduce variations in velocity throughout the seismic section, and the presence of a shallow gas hydrate layer is imaged within the Nigeria dataset, as well as being recognised from other areas of the Niger Delta (e.g. Hovland et al., 1997). This layer however does not seriously compromise the quality of the underlying data, and was not found to affect mapping significantly enough to alter the results shown in Chapter 4.

2.3 Quantitative measurements derived from seismic data

In order to support the data obtained from mapping, quantitative measurements were obtained of channel morphometric parameters (see Chapter 3, section 3.2) and of fold crestal relief and growth ratio (see Chapter 5, section 5.4). The details of how these measurements were undertaken are given in the relevant chapters. These measurements were all taken from seismic sections and dip attribute maps and are accurate to 1ms TwT and 10m respectively, these values representing the real dimensions of the on-screen cursor which forms the point from which the measurements were made. When measuring from seismic profiles (for example, channel depth – see Chapter 3, Fig. 3.9), all measurements are taken between zero crossings (Fig. 2.1) on seismic profiles. The reason for this is that the zero crossing can often be unambiguously identified on seismic profiles and this provides a consistent method for taking morphometric measurements.

To convert measurements to depth values, an average interval velocity of $2000ms^{-1}$ was assumed. However in the shallow (e.g. first 300m) part of the subsurface, the true interval velocity could be substantially lower – $1750ms^{-1}$, for example (see Deptuck et al., 2007). In the case of a shallowly buried channel fill which was 150ms in thickness, the difference in interval velocities leads to a thickness difference of c.19m. This affects the magnitude of the channel erosional depth profiles shown in Chapter 3, but not the interpretation of these profiles regarding timing of deformation.

Chapter 3

This chapter has been published as 'Interactions between submarine channel systems and deformation in deepwater fold belts: Examples from the Levant Basin, Eastern Mediterranean sea.' in the journal Marine and Petroleum Geology, 2009, v.26, p1465-1482.

The work presented in this chapter is that of the lead author (IRC), editorial support was provided by the project supervisor, JAC in accordance with a normal thesis chapter.

CHAPTER 3

INTERACTIONS BETWEEN SUBMARINE CHANNEL SYSTEMS AND DEFORMATION IN DEEPWATER FOLD BELTS: EXAMPLES FROM THE LEVANT BASIN, EASTERN MEDITERRANEAN SEA.

3.1 Abstract

Submarine channel levee systems form important hydrocarbon reservoirs in many deep marine settings and are often deposited within a structurally active setting. This study focuses on recent submarine channels that developed within a deepwater fold and thrust belt setting from the Levant Basin, eastern Mediterranean Sea. Compressional deformation within the study area is driven by the up-dip collapse of the Nile cone above the ductile Messinian Evaporites. Structures such as folds and strike slip faults exert a strong control on channel location and development over time. From this study four end member submarine channel-structure interactions can be defined: Confinement, diversion, deflection and blocking. Each of these channel-structure interactions results in a distinct submarine channel morphology and pattern of development compared to unconfined channel levee systems. Each interaction can also be used to assess timing relationships between submarine channel development and deformation.

3.2 Introduction

Submarine channel systems are key architectural elements of submarine fans associated with many of the world's major river systems (Lopez et al. 2001; McHargue and Webb 1986; Schwenk 2005). Many of these settings are affected by thin-skinned gravitational collapse, and are characterised by coeval sedimentation and deformation. Submarine channel systems are commonly described from such settings, examples include the Niger Delta (Deptuck et al. 2003; Adeogba et al. 2005; Heinio and Davies 2007), the Gulf of Mexico (Posamentier 2003; Pickering et al. 1986) the Nile Delta (Deptuck et al. 2003;2007, Heinio and Davies 2007), Brunei (Demyttenaere 2000) and Offshore West Africa (Gee and Gawthorpe 2006; Abreu et al. 2003). Submarine channels are also recognised from accretionary prisms located at subduction zones, examples include the Barbados Accretionary Prism (Huyghe et al. 2004), The Kuril Arc (Noda et al. 2008), the Central Chile Forearc (Hagen et al. 1996) and the Nankai Trough (Soh and Tokuyama 2002).

The use of 3D seismic data has contributed greatly to our understanding of submarine channels, particularly with regards to their architecture and temporal evolution (Deptuck et al. 2003; 2007; Posamentier 2003). However, the number of studies which address the interactions between submarine channel development and deformation is relatively few and

tend to focus only on a particular aspect of channel evolution, such as the channel axis. These studies have shown, for example, that increases in slope gradient caused by structural highs result in increased submarine channel incision, with channel down-cutting being localised where the gradient increase is highest (Huyghe et al. 2004; Ferry et al. 2005; Gee and Gawthorpe 2006). Studies have also shown that submarine channel sinuosity is a key factor in the development of potentially sand-rich lateral accretion packages (Abreu et al. 2003). In structurally complex slope settings, submarine channel sinuosity can vary according to changes in gradient. Higher sinuosity channel reaches tend to be localised where the underlying slope gradient decreases (Ferry et al. 2005; Gee and Gawthorpe 2006).

This study uses a 3D seismic data volume to document the interactions between submarine channel levee systems and deformation within a deepwater compressional province. The term 'interaction' is here used to represent the end result of submarine channel development under the influence of a structurally deformed seafloor. The aim is to investigate in detail how submarine channels respond to structurally modified slopes, with examples from the Levant Basin, Eastern Mediterranean. Compressional deformation results in folding and faulting, with the resulting topography causing obstructions to the down-slope flow pathways of recent (Pleistocene-Holocene) submarine channels. Based on our mapping, four end-member interactions between submarine channels and deformation can be defined – confinement, diversion, deflection and blocking. Although this study uses examples only from the Levant Basin, we have observed that these four types of interaction are common wherever submarine channels occur in structurally active deepwater settings, many of which are also areas of current hydrocarbon exploration, such as the deepwater Gulf of Mexico and deepwater Nigeria.

3.2.1 Geological Setting

The Levant Basin is located in the Eastern Mediterranean Sea and is bounded to the east by the passive continental margin of Israel, Lebanon and Syria, to the south by the north-easternern lobe of the Nile Deep Sea Fan, to the west by Eratosthenes seamount and to the north by the subduction zone and transform fault of the Cyprus Arc (Fig. 3.1, Ben-Avraham et al. 1988; Ben-Avraham et al. 1995; Vidal et al. 2000). Formation of the Levant Basin and the adjacent margin is related to a sequence of rifting events occurring from Early Permian to Middle Jurassic times associated with the initial break-up of Pangaea (Garfunkel, 1998). Final continental break-up and the initiation of ocean spreading occurred at the end of Mid Jurassic times (Garfunkel and Derin 1984). Compression in the Late Cretaceous and the development of the Syrian Arc Foldbelt and resulted in a series of NE-SW orientated folds along the Levant

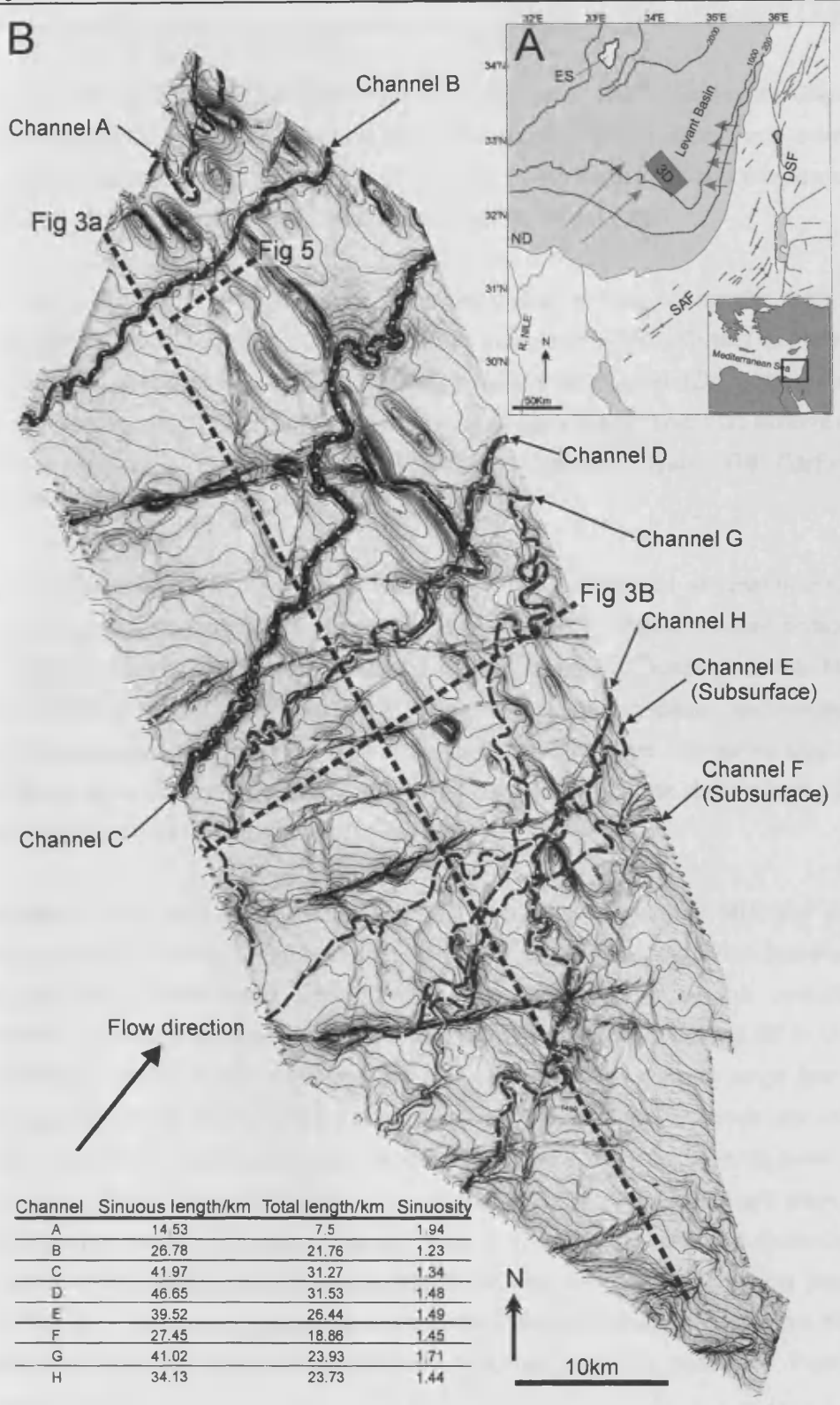

Channel	Sinuous length/km	Total length/km	Sinuosity
A	14.53	7.5	1.94
B	26.78	21.76	1.23
C	41.97	31.27	1.34
D	46.65	31.53	1.48
E	39.52	26.44	1.49
F	27.45	18.86	1.45
G	41.02	23.93	1.71
H	34.13	23.73	1.44

Figure 3.1: **3.1a** shows a location map of the 3D seismic survey used in this study. DSF = Dead Sea Fault System, SAF = Syrian Arc Fold Belt, ES = Eratosthenes Seamount, ND = Nile Delta. Arrows indicate direction of salt flow from the Nile Delta and Levant Margin. Adapted from Vidal et al. 2000, with salt movement direction from Netzeband et al. 2006. **3.1b** shows a dip attribute map of the seabed over the 3D survey area. This map is draped with time contours (Interval = 10ms TWT). The map shows channel levee systems A, B and C which are described in this study. Several other channel levee systems are present and some key characteristics of these are summarised in the inset table.

Margin (Eyal 1996; Buchbinder and Zilberman 1977; Garfunkel 1998). During the Oligocene, a system of submarine canyons developed along the Levant Margin. Headward extension of these canyons occurred throughout the Miocene due to intermittent uplift and emergence of the Levant Margin (Druckman et al. 1995; Buchbinder and Zilberman 1997).

Towards the end of the Miocene (5.9 Ma), narrowing of the connection between the Mediterranean Sea and the Atlantic Ocean led to the Messinian Salinity Crisis (Hsu et al. 1978). This resulted in a sea level fall of 800-1300m in the Mediterranean Sea (Druckman et al. 1995) and the deposition of a thick evaporitic sequence up to 2km thick. This was accompanied by erosion along the marginal areas of the Levant Basin (Cita and Ryan 1978; Garfunkel and Almagor 1987).

During Pliocene times, the Levant Basin was subjected to increased sedimentation, derived from the Nile Delta to the south west (Mart and Ben-Gai 1982). The increased sedimentation rate was accompanied by increased basin subsidence due to loading of the Messinian sequence (Tibor et al. 1992; Ben-Gai et al. 2005). In the Levant Basin, sedimentation was predominantly sourced by submarine channels. The source of these submarine channels was the Nile Delta, as is apparent from their north-east orientation and the down slope gradient in relation to the Nile Delta to the south-west (Fig. 3.1).

The 3D seismic data used in this study covers an area of approximately 1400 km^2 (Fig. 3.1). This survey covers a portion of the distal, north-eastern area of the Nile Deep Sea Fan, which extends into the Levant Basin and provides a detailed record of the post-Messinian sedimentation. Average seafloor gradients in the study area vary between 0.38° in the down-slope direction and 0.02° in the cross slope direction. Water depths typically range from 1000 to 1350 meters below sea level across the survey area. Submarine channels are ubiquitous throughout the post-Messinian sequence, typically consisting of single, channel levee systems which are rarely erosionally confined (Fig. 3.1). In comparison to the larger scale slope system, the submarine channels in this study area are most likely within the middle to lower fan region (c.f. Babboneau. et al. 2002). The most recent of these channels are visible on the present day seafloor (Fig. 3.1). Submarine channels are common features associated with the Nile Delta and subsurface examples have been previously described from the deepwater Western Nile (Samuel et al. 2003).

3.3 Dataset and Methodology

The 3D seismic dataset used in this study was acquired in 2000 by BG Group and partners. The data were migrated with a single pass 3D post-stack time migration to generate a 12.5 m by 12.5m grid with a 1ms sampling interval. The seismic data are processed to near zero phase and is displayed using SEG normal polarity, with an increase in acoustic impedance being represented by a positive amplitude (red) on seismic sections. The Plio-Pleistocene sedimentary section overlying the Messinian evaporites has a dominant frequency of 50Hz, with the estimated vertical and lateral resolution for this interval being 10 and 40m, respectively. This was determined using an average interval velocity of 2000 ms^{-1} derived from velocity checkshot data (Frey Martinez et al. 2005). The Messinian evaporites are characterised by a lower dominant frequency of 30 Hz, although the frequency within the Messinian sequence is variable and results in changes in vertical resolution within this unit (Bertoni and Cartwright 2006).

The channel levee systems in this study were characterised qualitatively using isochron maps of channel intervals. Using these, the thickness and areal extent of the channel levees and channel axis can be assessed and compared to the surrounding structures. The base of the levee package in such maps is defined as the surface against which the internal levee reflections downlap. The base of the channel is defined as the lowermost erosive surface associated with incision into the pre-channel sequence (Fig. 3.2, Deptuck et al. 2003; Mayall et al. 2006).

In order to quantitatively characterise the submarine channels in this study, the following morphometric parameters were measured (Fig. 3.2):

- Channel thalweg depth: Depth from modern sea level to the floor of the channel.
- Channel erosional depth: Maximum depth of incision into the pre-channel sequence.
- Width:Depth ratio: Channel width measured horizontally between levee crests and channel depth measured vertically from the levee crest to the channel floor.
- Sinuosity: Sinuosity is defined as the along-channel distance divided by the straight-line distance between the same two points along any particular reach of a channel (Fig. 3.2). Sinuosity was measured at 1km intervals along each channel segment as this adequately captures the sinuosity variations where typical meander widths are of the order of 500-1000m.

Each parameter (except sinuosity) was measured at 200m intervals along the sinuous length of each channel segment, using seismic profiles orientated perpendicular to the path of the channel axis at each measurement point. This interval was chosen as significant changes in

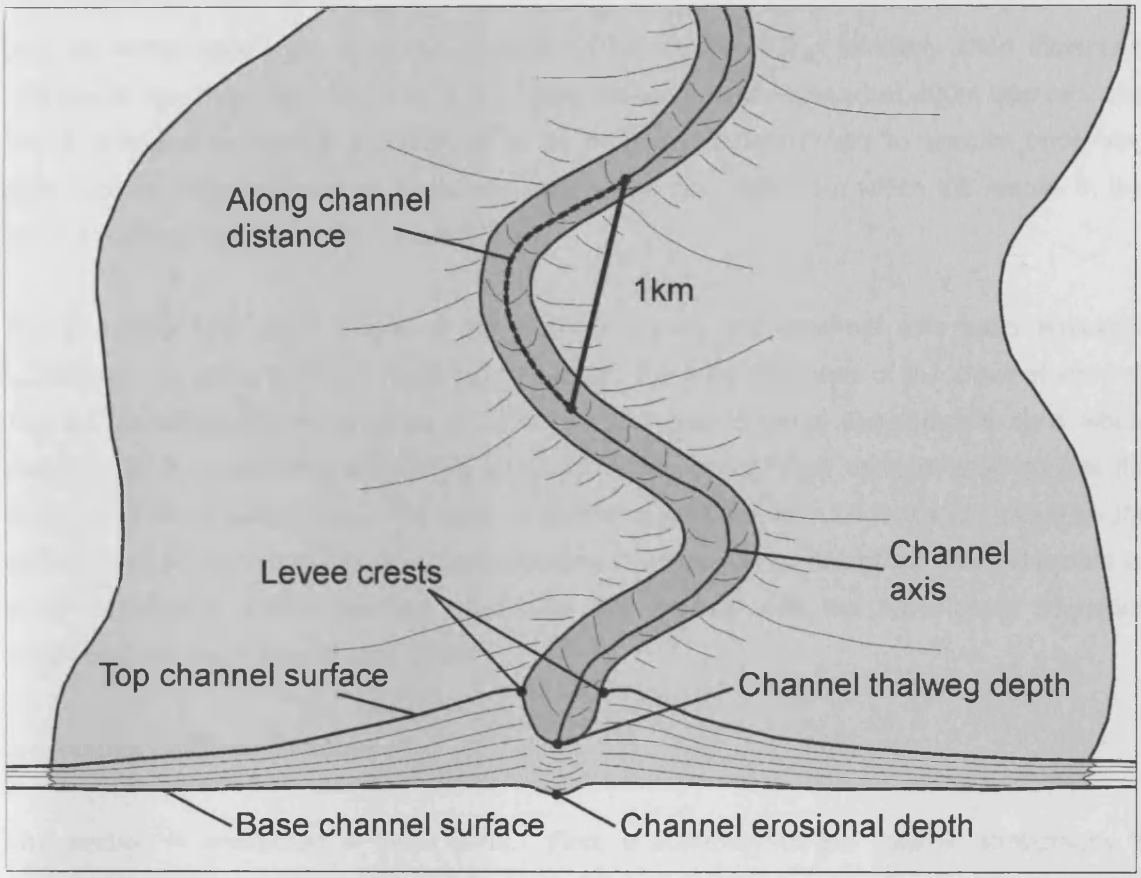

Figure 3.2: Block diagram summarising the methodology and terminology used to characterise the channel levee systems in this study. Channel isochron maps were calculated between the top and base channel surfaces to reveal the thickness and extent of the channel levees. Other parameters measured were channel sinuosity (window length = 1km), channel thalweg and erosional depth and also channel width (between levee crests).

channel morphology were observed to occur at the seafloor over relatively short distances, typically of less than 1km (e.g. Fig. 3.1). Using measurements spaced at 200m intervals also allows changes in channel morphology to be more accurately linked to specific underlying deformational features such as faults and folds. The raw data from which the results in this study are presented are given in Appendix A1.

The thickness and areal extent of the channel levees and channel axis were assessed qualitatively by using isochron maps which capture the time thickness of the channel interval. The aim of producing these maps is to understand how channel development as a whole responds to the underlying structurally controlled slope, rather than concentrating on just the response of the channel axis. The base of the levee package in such maps is defined as the surface against which the internal levee reflections downlap. The base of the channel is defined as the lowermost erosive surface associated with incision into the pre-channel sequence (Deptuck et al. 2003; Mayall et al. 2006).

3.4 Results and Observations

This section is presented in three parts. First, a summary of the seismic stratigraphy is presented in order to set the channel levee systems in their correct stratigraphic context. The second section describes the effects of Post-Messinian deformation which controls slope morphology. The third section describes three submarine channel systems in detail and their relationship with the surrounding deformation.

3.4.1 Seismic stratigraphy

This study focuses on the Post-Messinian, Plio-Pleistocene sedimentary section in the Levant Basin (Fig. 3.3). Recent studies in this area have focussed on either the Messinian sequence (e.g. Bertoni and Cartwright 2005; 2006; 2007; Gradmann et al. 2005), or the marginal areas of the Levant Basin (eg Frey-Martinez et al. 2005). Chronostratigraphic and lithological data for the post-Messinian sedimentary cover are based on unpublished reports from nearby wells (Frey-Martinez et al. 2005) as there are no published well calibrations within the area covered by the 3D seismic survey.

Previous work in this area (Bertoni and Cartwright 2005; 2006; 2007) studied the Messinian interval in detail, with the Pliocene-Quaternary overburden being assigned to a single unit. This study subdivides the post-Messinian sedimentary section further into three sub-units, with each

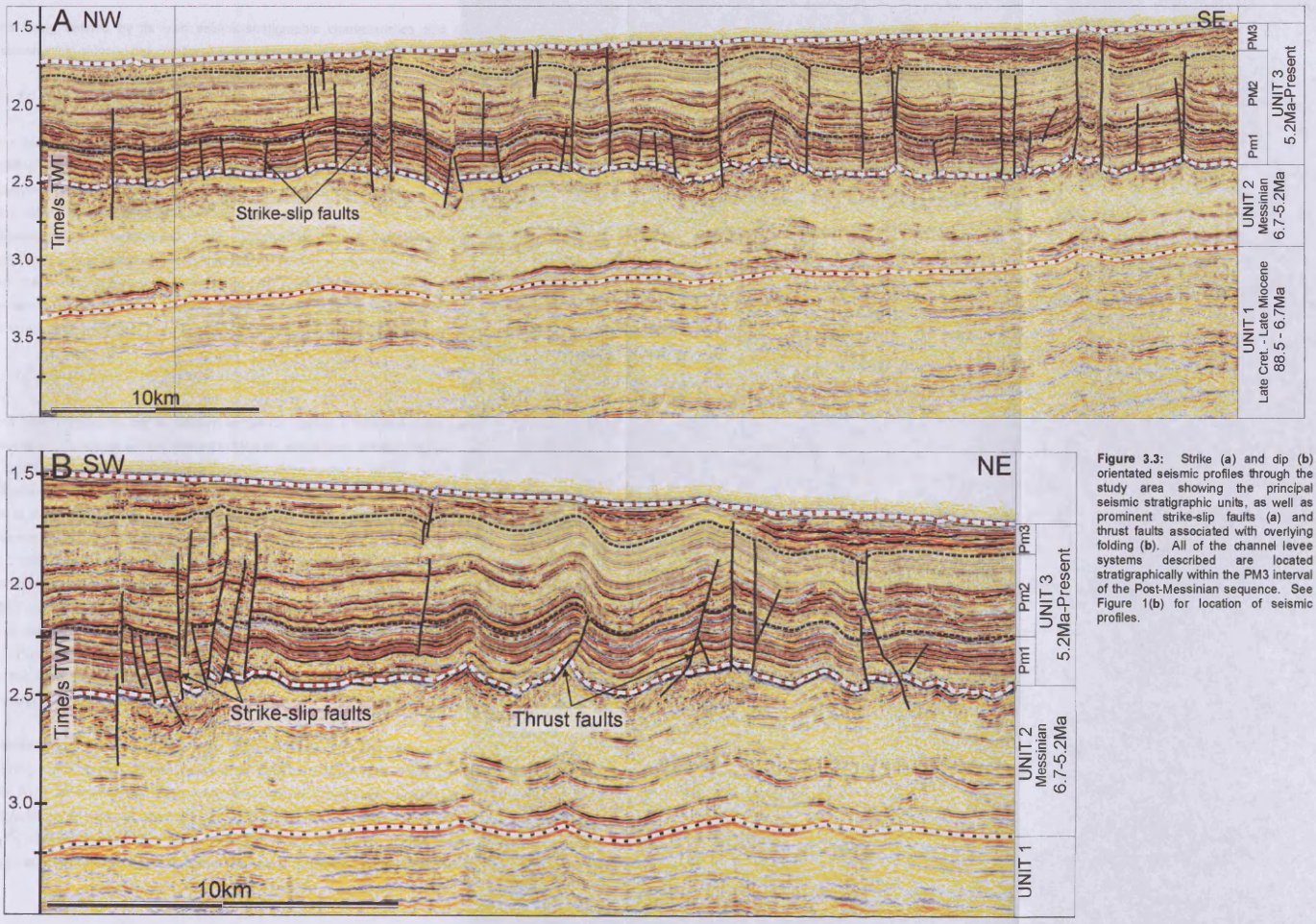

Figure 3.3: Strike (**a**) and dip (**b**) orientated seismic profiles through the study area showing the principal seismic stratigraphic units, as well as prominent strike-slip faults (**a**) and thrust faults associated with overlying folding (**b**). All of the channel levee systems described are located stratigraphically within the PM3 interval of the Post-Messinian sequence. See Figure 1(**b**) for location of seismic profiles.

unit being defined by its own seismic-stratigraphic characteristics and relationship to the extensive thin-skinned deformation affecting this area (see section 3.4.2).

3.4.1.1 Post-Messinian Unit 1 (PM1)

Unit PM1 is composed of locally continuous, high amplitude and parallel reflections, although continuity over the scale of the survey area is poor. Channels up to 500m wide, are commonly observed within this unit. These channels pre-date deformation and now provide useful kinematic markers for post-Messinian faulting (Fig. 3.4). Localised thickness changes associated with these channels result in localised downlap and apparent onlap surfaces within unit PM1. These local thickness variations are related to deposition from the channels, and are not the result of syn-sedimentary structural growth. Aside from the localised thickness variations associated with channel deposition, unit PM1 does not show any syn-kinematic sedimentation and this unit is assumed to pre-date salt related deformation in this area.

3.4.1.2 Post-Messinian Unit 2 (PM2)

Unit PM2 consists of low to medium amplitude, mainly continuous reflections, with localised packages of lower amplitude, chaotic reflections which pass laterally into more continuous units (Fig. 3.5). Unit PM2 contains several channel levee systems, which are larger and much more apparent on seismic sections that those described from within unit PM1. These channels are up to 2km wide, and show clear, wedge shaped levee deposits which taper away from the channel axis. The fill of the channel complexes within unit PM2 shows a variable seismic character (Fig. 3.5), with some channels having a high amplitude fill of discontinuous reflections and others having a low amplitude, seismically transparent fill. High amplitude channel fills are often associated with development of mounds above the channel axis that may be due to differential compaction of the sand-rich channel fill and the adjacent mud rich levee deposits (c.f. Posamentier 2003). The channel levee complexes are separated vertically by intervals of parallel reflections of constant thickness (Fig. 3.5). These intervals likely represent periods of channel abandonment in this area.

Unit PM2 displays internal thickness variations related to channel levee complexes where thinning of the channel levees occurs away from the channel axis. This thinning is associated with local downlap of the levee reflections onto the pre-channel surface as well as downlap within the levee packages themselves (Fig. 3.5). Where subsequent folding has occurred, tilting of the channel levees in the vicinity of the fold limbs can appear similar to onlap onto the fold crest, and failure to recognise this can result in a misleading interpretation of structural timing.

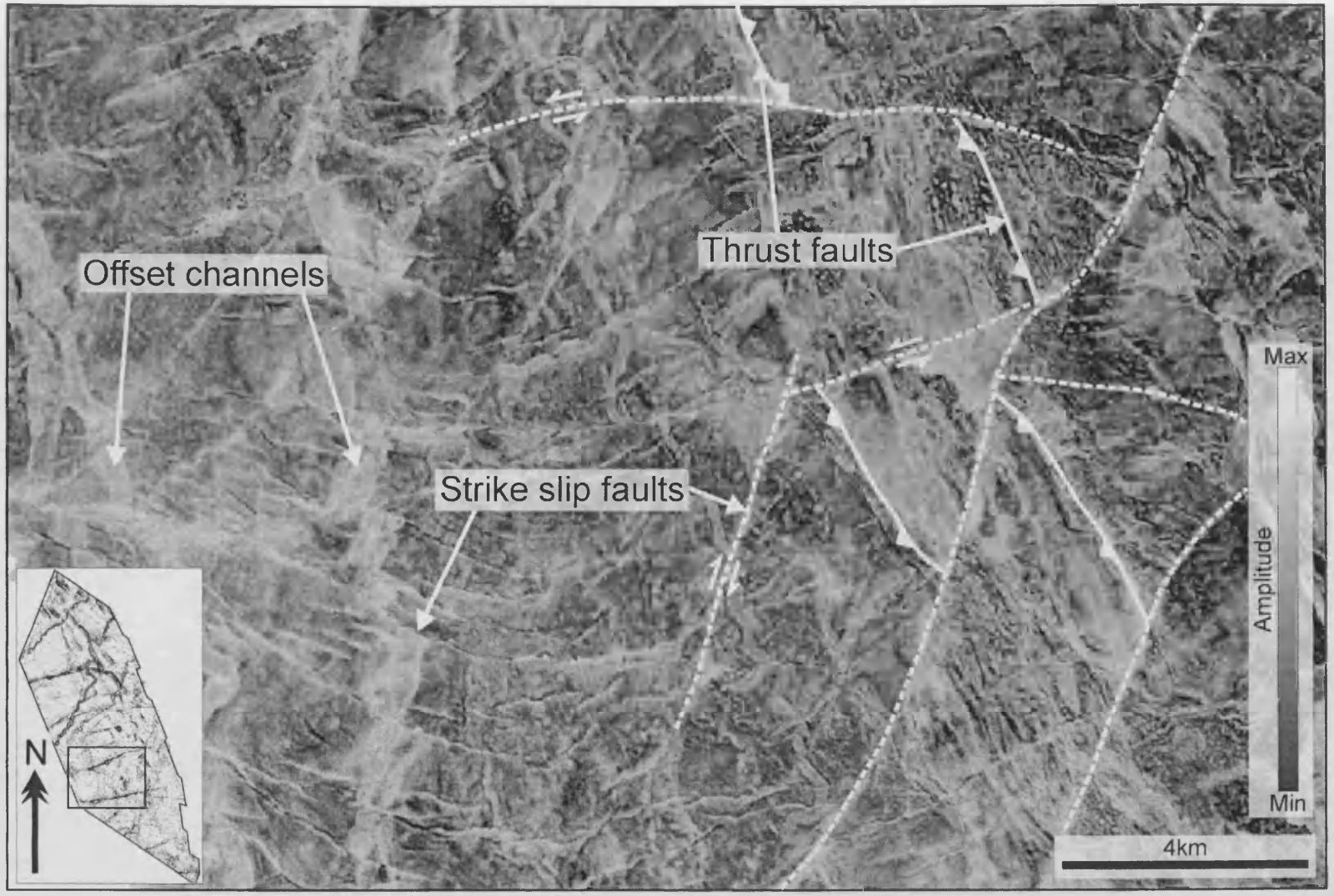

Figure 3.4: Amplitude map of the top Messinian horizon (Top unit 2 in Figures **3.3a** and **3.3a**). This image shows the strike-slip faulting and thrusting which affects the Post Messinian sequence. Channels provide useful markers for assessing the sense of offset of the strike slip fault systems which characterise this study area.

Figure 3.5: Representative seismic profile through the PM2 interval showing channel levee systems with both high and low amplitude fill characteristics. These channel systems are separated by packages of disturbed or parallel low amplitude reflections of uniform thickness.

True syn-kinematic intervals within unit PM2 are associated with expansion into the hangingwall and footwall synclines of thrust-related folds, and weakly developed onlap onto the fold limbs. These syn-kinematic intervals are not synchronous across the study area, but the largest, most continuous fold structures appear to have been the earliest to have been initiated. Within unit PM2, growth packages are separated by intervals of parallel reflections of constant thickness, indicating that even after the onset of deformation, the growth of the thrust folds was episodic throughout the deposition of unit PM2.

3.4.1.3 Post-Messinian Unit 3 (PM3):

Unit PM3 comprises mainly continuous medium to high amplitude reflections associated with the development of multiple channel levee complexes, the most recent of which are clearly visible on the present day seafloor (Fig. 3.1b). This unit thickens towards the south east of the study area, and in many places the thickness is strongly controlled by post-Messinian deformation (Fig. 3.6). Unit PM3 shows the greatest amount of thickening and growth into the hangingwall and footwall synclines associated with thrust related folds. Packages within PM3 thin onto the crests of these folds with internal reflections showing onlap against the fold limbs in the typical manner of syn-kinematic packages associated with growth folds (Burbank et al. 1996; Salvini and Storti 2002). The amount of growth into the fold limbs is greater than that seen in PM2, and suggests that the rate of structural growth relative to the rate of deposition was greater during the deposition of PM3 compared to the deposition of PM2.

The internal architecture of unit PM3 consists of multiple, vertically stacked channel levee systems (Fig. 3.3a). The flow direction of the channels is from the south west to the north-east and the channels are assumed to have been sourced from the Damietta branch of the Nile (Loncke et al. 2002) based on the direction of the maximum slope gradient and the position and orientation of the channels. In contrast, the architecture of the growth sequence presented in Chapter 4 consists of a significant proportion of other depositional elements, such as mass transport deposits (MTDs) and hemipelagic drape deposits.

The submarine channels developed within unit PM3 are all considered to be dominantly aggradational rather than erosional. The channel axis in these channels exhibits an aggradational geometry over the time period of channel deposition, with the channel axis being confined between the aggradational levee packages and not by incision into the underlying sequences (Fig. 3.2).

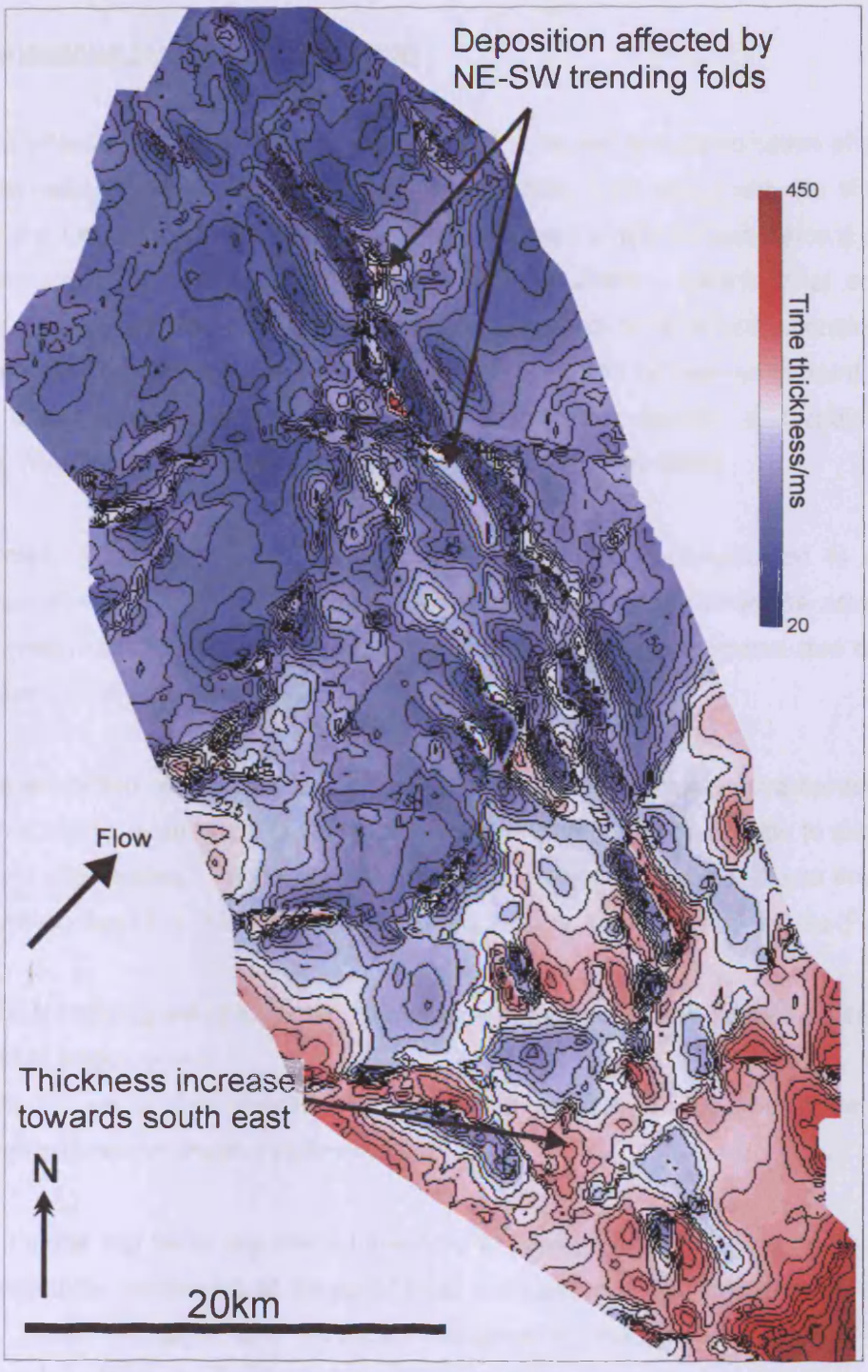

Figure 3.6: Isochron map of the PM3 interval, calculated between the seabed and base PM3 surfaces shown on Figures **3a** and **3b**. Contour interval is 25ms TWT. The isochron map shows a general increase in thickness towards the south east of the study area as well as the strong control on sediment distribution by north-east south-west trending folds.

3.4.2 Post-Messinian thin skinned deformation

Deformation affecting the post-Messinian overburden is related to a combination of gravitational collapse and subsequent basinward spreading of the Nile Cone along with the tilting induced collapse of the Levant Margin above the ductile Messinian evaporitic sequence (Loncke et al. 2006; Gradmann et al. 2005; Cartwright and Jackson 2008). Gravitational collapse and subsequent spreading of large prograding deltaic wedges results in linked extensional (up-dip) and compressional (down-dip) domains (Rowan et al. 2002 and references therein). Radial and concentric faults can also form as a result of perimeter extension and radial spreading respectively (Gaullier and Vendeville 2005; Cobbold and Szatmari 1991).

Post-Messinian deformation within the Levant Basin is further complicated to the east of Eratosthenes Seamount. This feature acts as a buttress to the basinwards advance of the Messinian evaporites, resulting in changes in orientation of the extensional and contractional structures (Loncke et al. 2006).

A conjugate set of thin skinned strike slip faults affect the post-Messinian overburden (Fig. 3.7). Many, but not all of the strike slip faults propagated upwards during deposition to reach the level of the present day seabed. These strike slip faults can be traced downwards to the uppermost Messinian evaporites (Fig. 3.3). The strike slip faults show two dominant trends (Figs. 3.1 and 3.7):

1. An E-W trending set of strike slip faults which are visible on the present seabed, showing sinistral displacement.
2. A NE-SW set of dextral strike slip faults which are largely obscured on the seabed by recent submarine channel sedimentation.

Both sets of strike slip faults are characterised by the development of small scale pop-up and pull-apart structures developed at zones of local transpression and transtension respectively (Fig. 3.7). These structures form significant bathymetric obstacles and obstruct the flow of recent submarine channels. Typical values of vertical relief shown by these pop-up structures is 90m, with the pull-aparts forming depressions up to 60m deep.

Thrust faults, detaching within the uppermost post-Messinian sequence, ramp upwards through the post-Messinian overburden with individual faults reaching as high as the base of unit PM3 (Fig. 3.3b). The dominant vergance of these thrusts is towards the north-east. The thrust faults are associated with overlying folds which vary in style along the strike of the thrust. At the lateral tips of individual thrusts, the fold style is commonly that of a symmetrical detachment fold

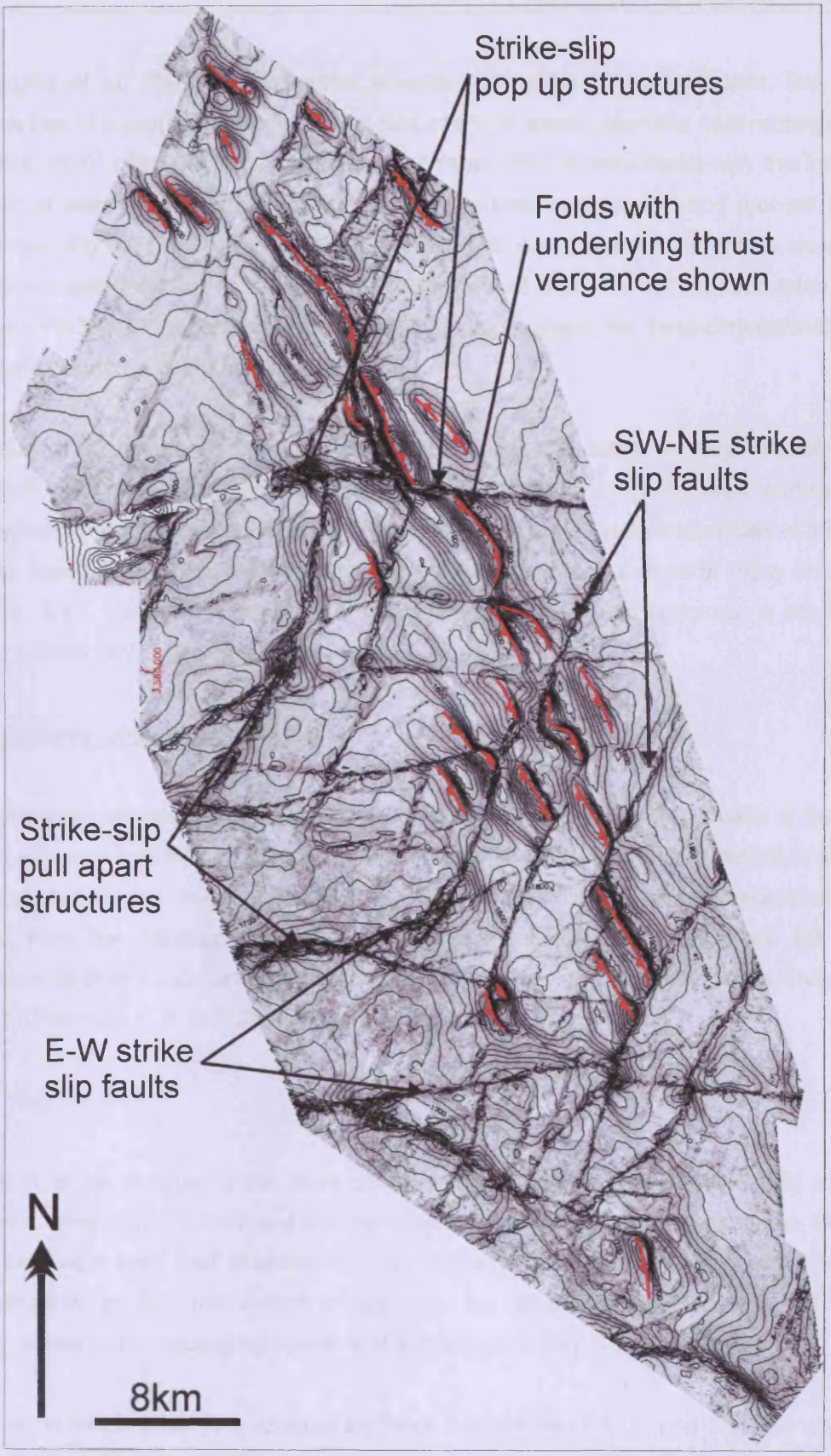

Figure 3.7: Dip attribute map of the base PM3 surface shown in Figure 3.3, overlaid with time contours spaced at 20ms TWT intervals. This surface represents the deformation which affects submarine channel development in this area. A prominent conjugate strike slip fault system is present at this level, as is a north-west south-east trending fold belt (underlying thrust vergance indicated). These folds are associated with depressions in the hanging walls and footwalls which combine with the relief of the fold crest to affect sedimentation within the PM3 interval.

(c.f. Higgins et al. 2007). Along strike towards the centre of many thrusts, the fold style becomes that of a transported detachment fold, many of which resemble fault propagation folds (e.g. Mitra 1990; Mitra 2002). Development of these folds is associated with the formation of depressions within the hangingwall and footwall, termed hangingwall and footwall synclines, respectively (Fig. 3.3b). The overall trend of the thrusts and the resultant folds is along a north-west, south-east orientation, perpendicular to the flow of the most recent submarine channels within unit PM3 (Fig. 3.1). Chapter 5 documents in more detail the three-dimensional evolution of the folds within the Gal C survey area.

The onset of thrust-related folding is dated here using the earliest onlap relationships and occurrence of stratal thinning onto the fold crests. Throughout the study area, earliest initiation of folding occurs within the middle of the PM2 interval, but observed occurrences of this are rare (2 folds), however the PM3 interval forms the primary growth sequence of many thrust-related folds (Fig. 3.3). Variation in the onset of folding between individual structures is constrained to within a c.50ms TWT interval of the top PM2 horizon.

3.4.4 Submarine channel case studies

Nine submarine channel levee systems were mapped in detail in to provide a database of channel structure interactions (Fig. 3.1). The channel levee systems are orientated south-west north-east, and all are developed within the PM3 interval. Three channel levee systems were selected from the database as being representative examples showing the full range of interactions between submarine channels and deformation in this area. These channel levee systems (Channels A, B and C) are described individually below.

3.4.4.1 Channel A

Channel A is the shortest of the three channel segments and crosses the study area in the north-west, where the PM3 interval is at its thinnest limit. This channel segment is 14.53 km in length, but has a high total sinuosity of 1.94. Although the length of this channel segment is short compared to the other described channels, the development of this channel system is strongly related to the underlying structurally formed slope (Fig. 3.8).

Development of Channel A is affected by three folds (termed 1, 2, and 3 in the downstream direction) orientated perpendicular to the channel flow direction (Fig. 3.8). The isochron map for this system shows that the thickest and most laterally extensive part of the channel-levee system occurs upstream of Fold 3 (Fig. 3.8). Within this area Channel A displays prominent

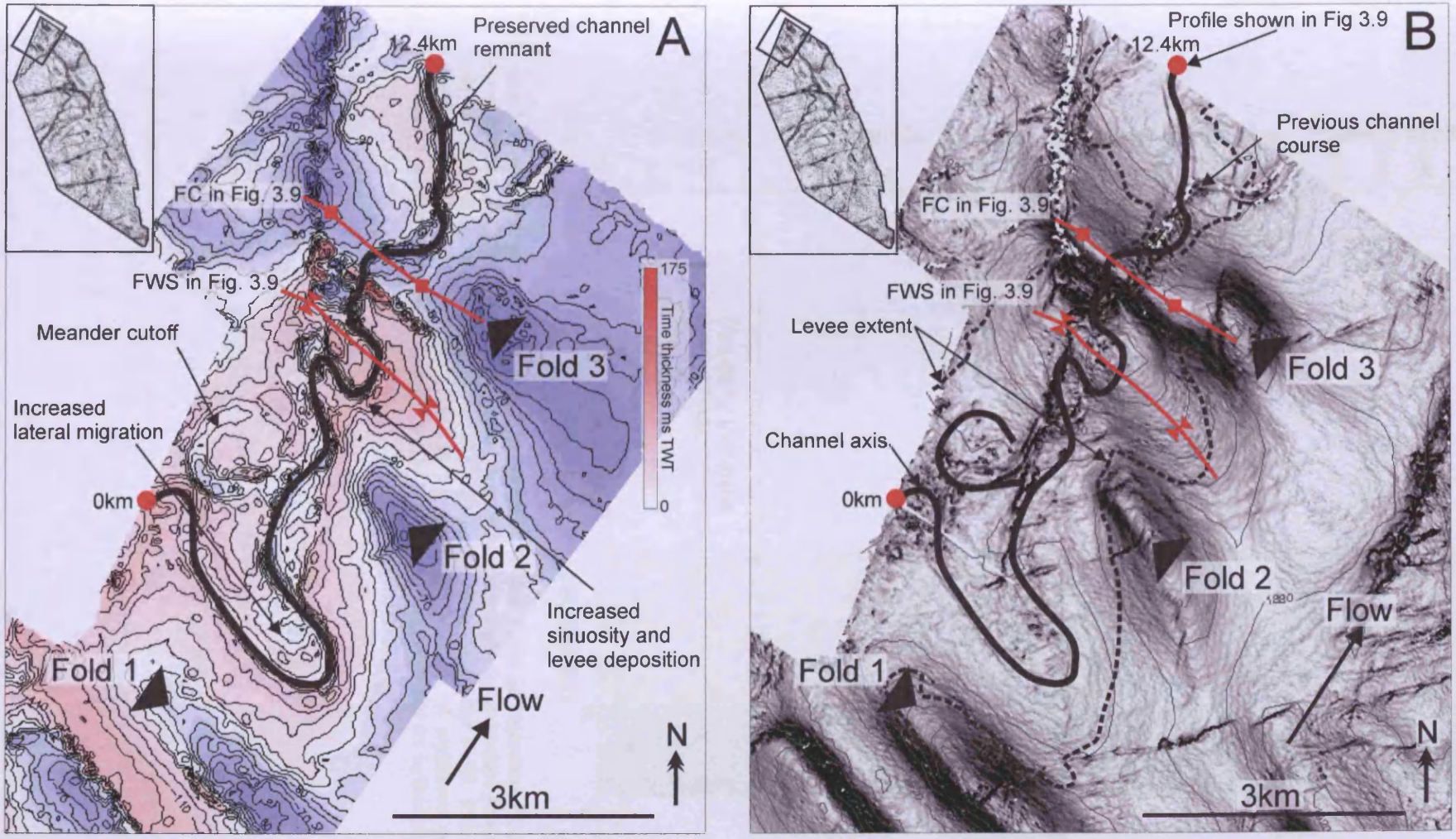

Figure 3.8: **3.8a**: Isochron map of Channel A (contour interval = 10ms TWT). This map reveals the strong control on channel development by the surrounding structures. Increased lateral migration is observed between Folds 1 and 2, with these folds also controlling channel levee distribution. The channel levee system shows a strong increase in thickness upstream of Fold 3 which blocks this channel resulting in a preserved channel remnant downstream of the fold. **3.8b**: Dip attribute map with overlayed time depth contours (20ms TWT interval). Also indicated on this map is the axis of channel A and also the levee extent taken from the isochron. This map shows increased sinuosity and levee deposition in the footwall of Fold 3, as well as revealing the structural control on levee distribution.

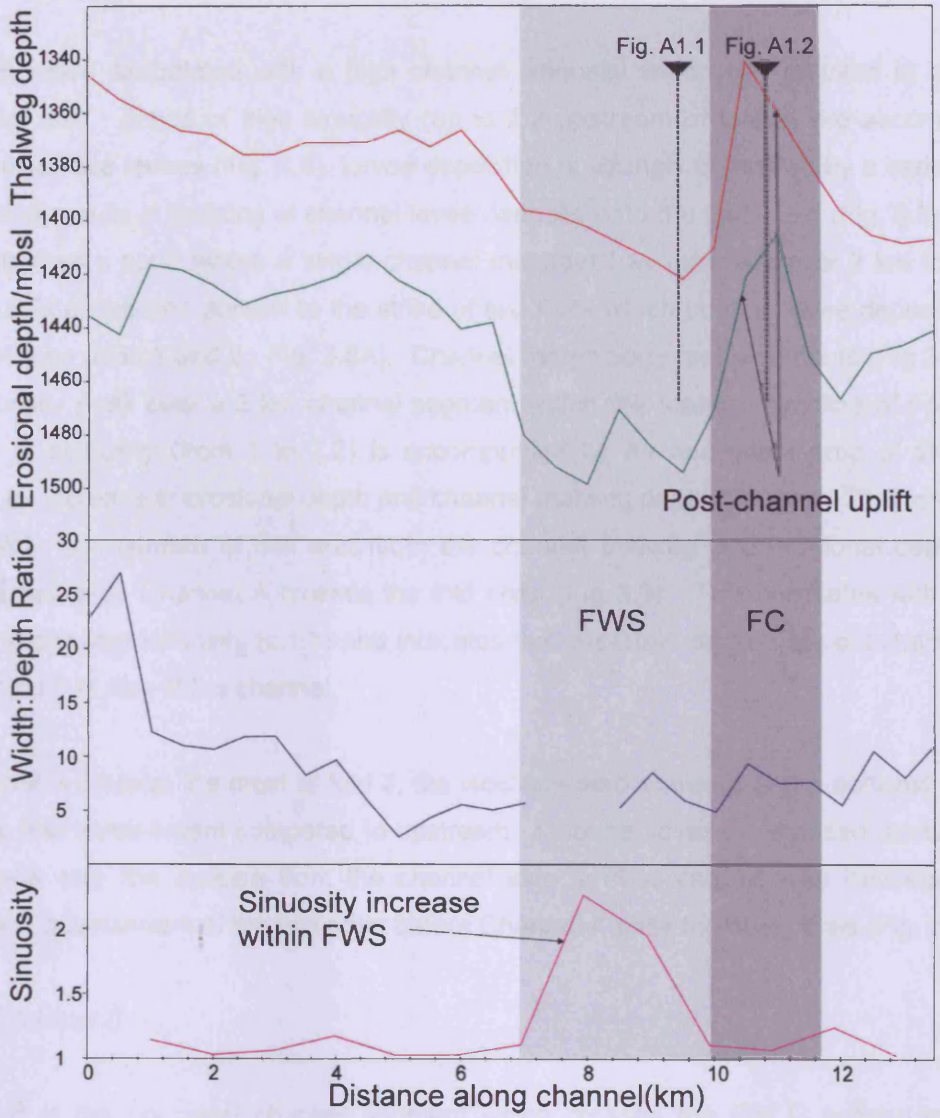

Figure 3.9: Morphology measurements for channel A. FWS = foot-wall syncline, FC = fold crest. This channel system was affected by post-channel uplift which results in the increased thalweg and erosional depth over the fold crest. Also note the increase in sinuosity within the FWS, this can be observed qualitatively on Figure 3.8. Figs. A1.1 and 1.2 show the location of additional seismic profiles in appendix A1 taken perpendicular to the channel axis orientation. See text for further details.

lateral migration associated with a high channel sinuosity which has resulted in a meander cutoff (Fig. 3.8). Zones of high sinuosity (up to 2.2 upstream of fold 3) are accompanied by laterally extensive levees (Fig. 3.8). Levee deposition is strongly controlled by a series of folds, whose relief results in thinning of channel-levee deposits onto the fold limbs (Fig. 3.8). Channel A also displays a zone where a single channel meander has migrated over 2 km towards the south east in a direction parallel to the strike of two folds which confine levee deposition in this area (Between folds 1 and 2 - Fig. 3.8A). Channel morphology measurements (Fig 3.9) show a high sinuosity peak over a 3 km channel segment within the footwall syncline of Fold 3. This increase in sinuosity (from 1 to 2.2) is accompanied by an equivalent area of this channel showing an increase in erosional depth and channel thalweg depth (30m and 20m respectively). Immediately downstream of this area both the channel thalweg and erosional depth show a sharp decrease as Channel A crosses the fold crest (Fig 3.9). This correlates with a zone of decreased channel sinuosity (c.1.1) and indicates that a certain degree of post-channel folding has affected this part of the channel.

As Channel A crosses the crest of fold 3, the isochron map shows a sharp contrast in channel thickness and levee extent compared to upstream. Channel levees are absent across the fold crest where only the incision from the channel axis is observed. Levee development only occurs 2km downstream of the fold crest before Channel A exits the study area (Fig. 3.8a).

3.4.4.2 Channel B:

Channel B is the youngest channel segment which crosses the Gal C survey area and is located in the north of the dataset where unit PM3 is relatively thin. This channel segment is 26.78km in length, with an average sinuosity of 1.23. The channel is typically 340m wide and 19m deep. Channel B is affected by two folds, termed 1 and 2 orientated perpendicular to the channel flow direction (Folds 1 and 2-Fig 3.10). However, channel B only exhibits a change in course in response to Fold 2 (Fig 3.10).

The isochron map for this channel interval shows two distinct regions, corresponding to the presence or absence of underlying deformation (Fig. 3.10). The initial 16.5km of this channel segment is unaffected by underlying deformation. This results in an approximately symmetrical distribution of levees either side of the channel axis (Fig. 3.10) with localised zones of increased levee thickness concentrated around channel meanders (Fig. 3.10). Before Channel A reaches the fold belt, it is affected by two strike slip faults which cross the channel at 15km and 16.5km (Fig 3.10). These strike slip faults have little effect on channel levee distribution. They do not

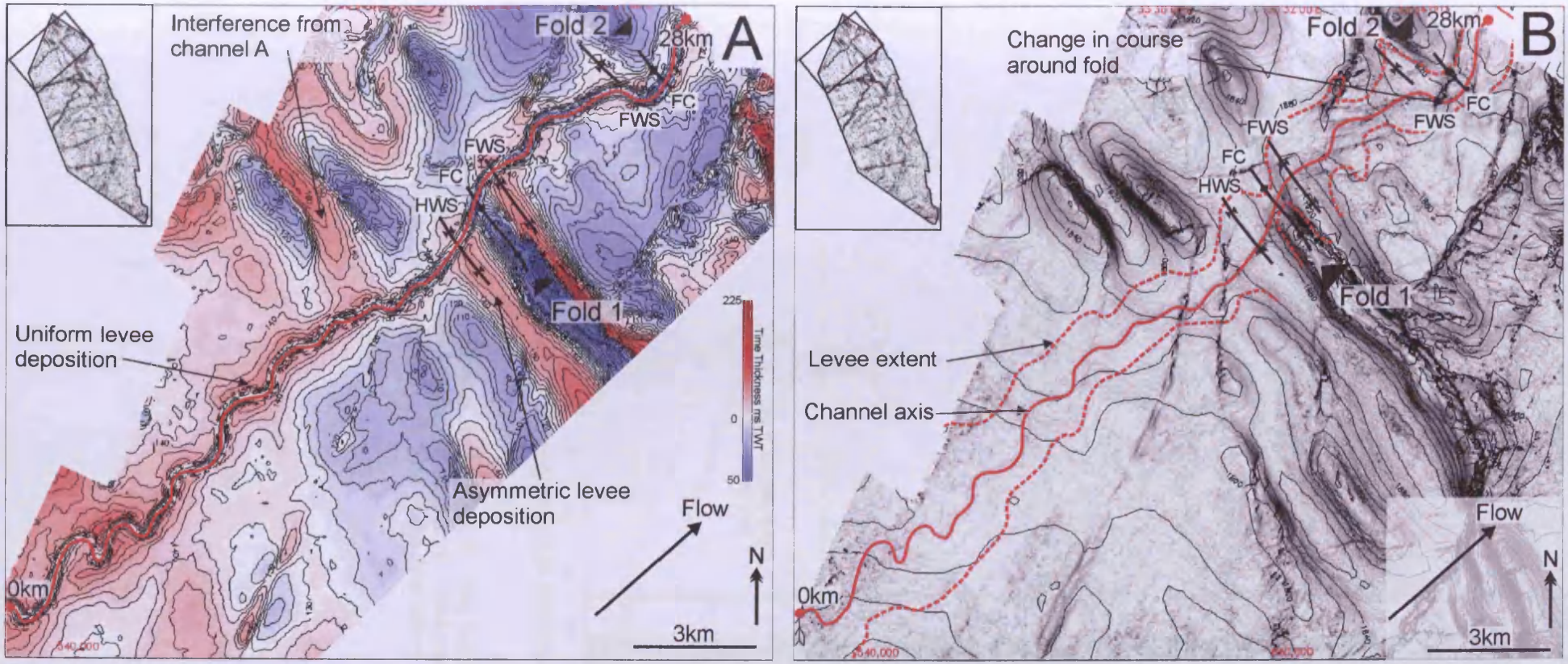

Figure 3.10: **10a**: Isochron map of the Channel B interval. Two zones of channel development can be identified from this map. Before channel B reaches the fold belt (Folds 1 and 2), levee distribution is approximately uniform on either side of the channel axis. In this area, variations in levee thickness and distribution are related to areas of increased sinuosity. This is in contrast to the asymmetric levee deposition seen as channel B crosses Fold 1 and also where channel B is diverted by Fold 2. **10b**: A dip attribute map of the base PM3 surface overlayed with time contours (Interval = 20ms TWT). The channel axis and levee extent are indicated. Note that where no underlying deformation affects this channel system, levee distribution is uniform about the channel axis, underlying structures induce the deposition of asymmetric levees. The exact levee extent within the hangingwall and footwall synclines of Fold 1 are untraceable due to interleaving of the levees of channel B with those of channel C to the south east.

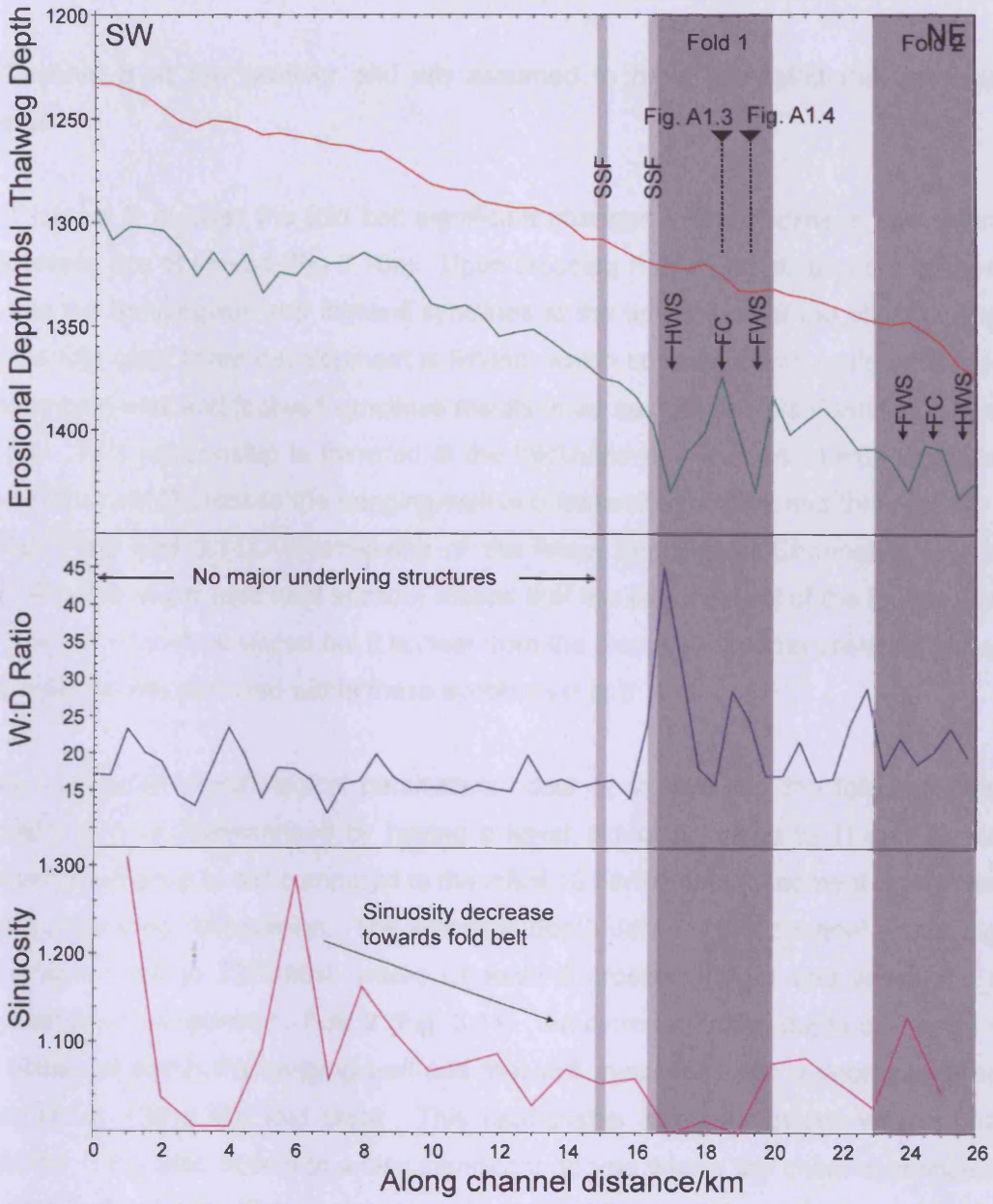

Figure 3.11: Morphology measurements for Channel B. See text for details. SSF = strike slip fault, HWS = hangingwall syncline, FWS = footwall syncline, FC = fold crest. Figs A1.3 and A1.4 correspond to additional seismic profiles in appendix A1, with profile orientation being perpendicular to the channel axis.

offset Channel B at the seafloor and are assumed to have pre-dated the development of Channel B.

Where Channel B crosses the fold belt significant changes in the thickness and extent of the channel levees are observed (Fig 3.10a). Upon crossing Fold 1, ponding of the levee deposits occurs into the hangingwall and footwall synclines to the south east of the channel (Fig. 3.10). Across the fold crest levee development is limited, which combined with preferential deposition into the hanging-wall and footwall synclines results in an asymmetric planform levee distribution (Fig. 3.10). This relationship is mirrored in the thickness of the channel axis deposits, which thicken as Channel B crosses the hanging-wall and footwall synclines and thins across the fold crest (Fig 3.10a and 3.11). Interleaving of the levee deposits of Channel B with those of Channel C to the south (see next section) means that the exact extent of the levees associated with Channel B cannot be traced but it is clear from the isopach map that preferential deposition of levee material has occurred within these synclines (Fig 3.10).

Changes in channel morphological parameters occur upon crossing the fold belt. Within this zone, Channel B is characterised by having a lower sinuosity (close to 1) and an increased width to depth ratio (up to 45) compared to the initial 16.5km channel segment where there is no significant underlying deformation. The erosional depth data for this channel shows significant variation (from 1425 to 1370mbsl) where Channel B crosses Fold 1 and where the channel course changes in response to Fold 2 (Fig. 3.11). An increase in the depth of erosion of up to 30m is observed within the hanging-wall and foot-wall synclines, with a decrease in erosional depth occurring above the fold crest. This relationship is most obvious where Channel B crosses Fold 1, but also occurs to a less significant degree where the channel changes course around Fold 2 (Fig. 3.11). The erosional depth profile of Channel B as it crosses the two folds is mirrored to a much lesser degree in the channel thalweg depth profile (Fig. 3.11). Upwards perturbations in the channel depth profile occur above the underlying points of decreased erosional depth.

3.4.4.3 Channel C:

Channel C crosses the study area to the south east of Channel B, this channel segment is 41.97 km in length with a sinuosity of 1.34. The average width and depth for this channel segment is 490m and 26.7m respectively. The overall flow direction of this channel segment is perpendicular to the strike of the fold belt, which significantly affects channel morphology and the development of this channel levee system.

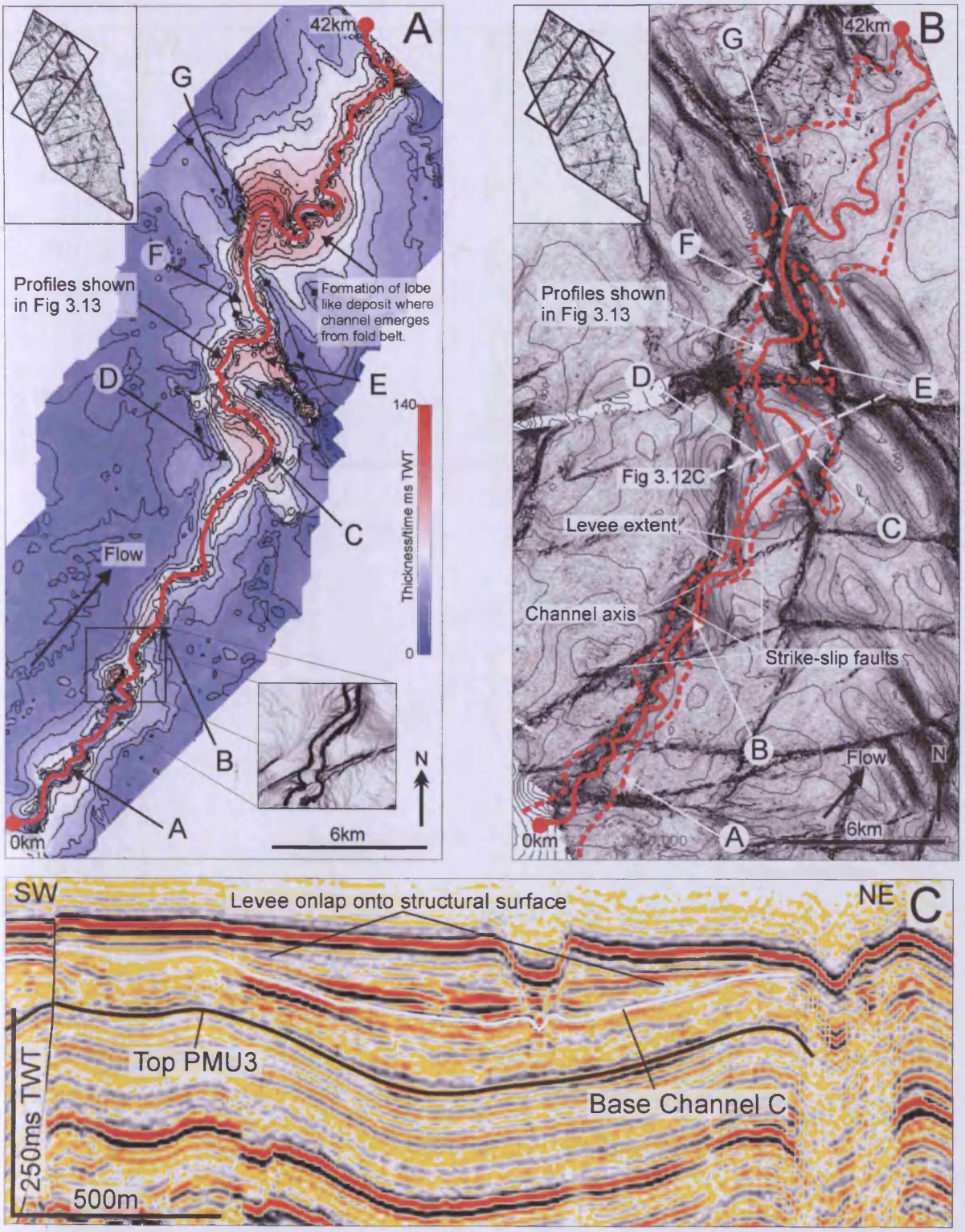

Figure 3.12: **3.12a**: Isochron map of Channel C, contoured at an interval of 20ms TWT. Inset map shows the seafloor in the vicinity of several recently active strike slip faults which now offset the floor of Channel C. **12b** Dip attribute map of the base PM3 surface overlayed with time contours spaced at 20ms TWT. The outline of the levee extent of Channel C and the channel axis are indicated. Points A to G are described in section 3.3.2. **12c**: Seismic line illustrating confinement of Channel C, note the levee onlap onto the pre-channel fold induced topography.

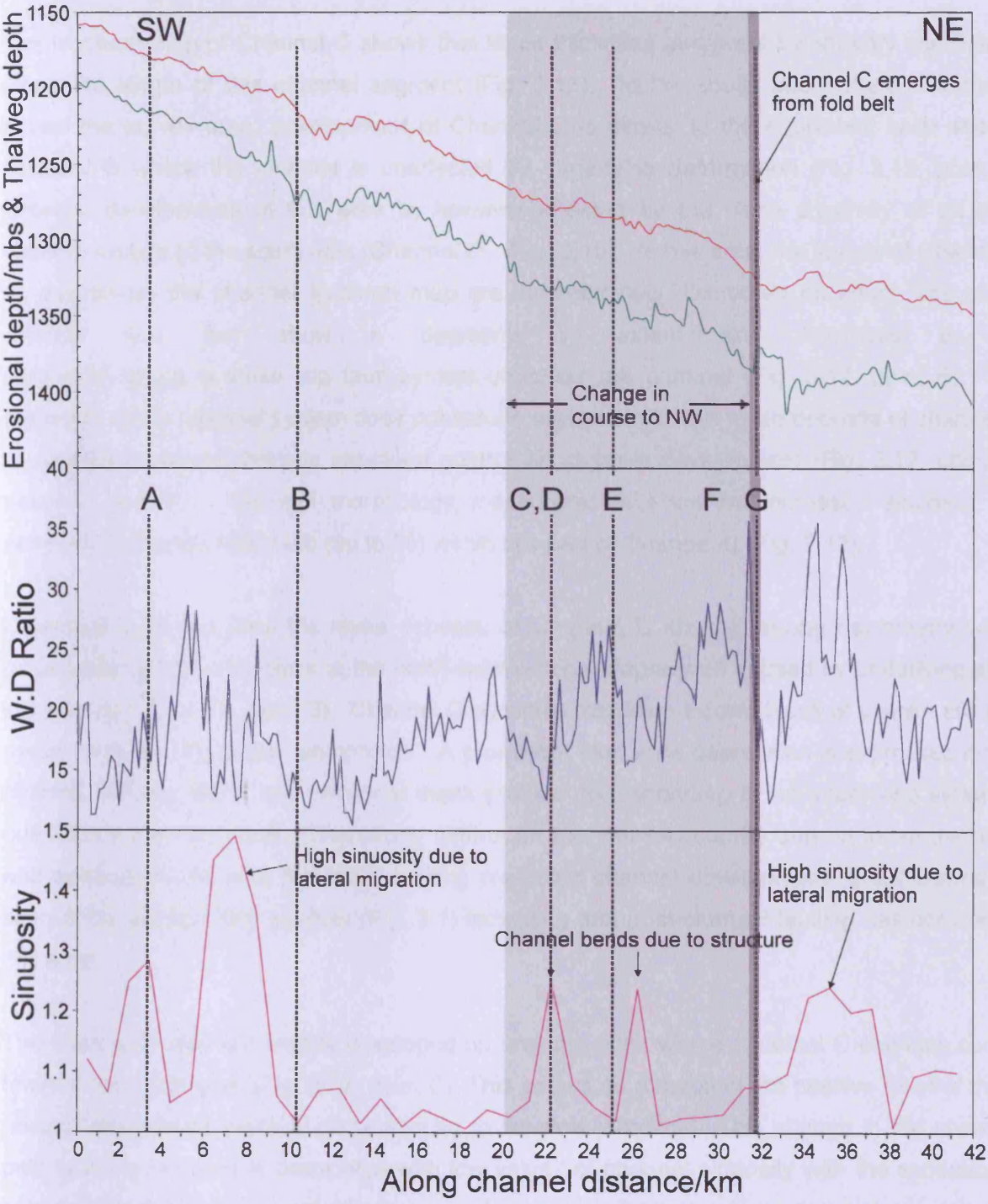

Figure 3.13: Channel morphology measurements for Channel C. The area where this channel is affected by the fold belt is highlighted. Points A to F correspond to specific features described in the text and referred to in the previous figure (3.12). See text for details.

The isochron map of Channel C shows that levee thickness and areal extent vary significantly along the length of this channel segment (Fig. 3.12). In the south west, where Channel C enters the survey area, development of Channel C is similar to the equivalent zone seen in Channel B where the channel is unaffected by underlying deformation (Fig. 3.12, point A). Channel development in this area is, however affected by the close proximity of an older channel system to the south east (Channel D – Fig. 3.1b). In this area, the levees of Channel C as imaged on the channel isochron map are symmetrically distributed on either side of the channel axis but show a decrease in extent and thickness to the north-east where a strike slip fault system underlies the channel (Fig. 3.12, point B). The presence of this channel system does not induce asymmetry in the levee deposits of channel C, in contrast to where there is structural control on channel development (Fig. 3.12, compare points A and E). Channel morphology measurements show an increased sinuosity and generally increased W:D ratio (up to 30) within this part of Channel C (Fig. 3.13).

Downstream of this area the levee deposits of Channel C show a strong asymmetry where preferential deposition occurs to the north-west within a depression caused by underlying strike slip faulting (Fig. 3.12, point B). Channel C occupies the down-thrown block of a strike slip fault system with an extensional component. A prominent 4km wide depression is expressed on the channel thalweg depth and erosional depth profiles corresponding to an underlying strike-slip pull apart zone (Fig 3.13). The strong control on the channel course and on levee thickness and distribution indicates that initial faulting pre-dated channel development. Fault scarps are seen at the present day seafloor (Fig. 3.1) indicating that post-channel faulting has occurred in this area.

The channel levees are weakly developed up until the point where Channel C changes course towards the north-west (Fig. 3.12, point C). This occurs as a result of the positive relief of thrust related folds whose strike is perpendicular to the flow direction. This change in the channels path to the north-west is associated with low values of channel sinuosity with the exception of two prominent peaks, representing sharp changes in channel course and not true sinuous meander bends formed by lateral migration of the channel axis (Fig. 3.13). The channel depth profile throughout this area is highly variable and this is most likely due to small amounts of post-channel deformation (mainly folding) causing perturbations to the profile. The levees of Channel C are strongly developed (thick and laterally extensive) within this area but show an asymmetric distribution (Fig. 3.12, points D and E, also Fig. 3.12c). Initially, the left hand (SW) levee is more strongly developed (Fig. 3.12, point D) until Channel C crosses a strike slip fault, after which the right hand (NE) levee is strongly developed (Fig. 3.12, point E) with its

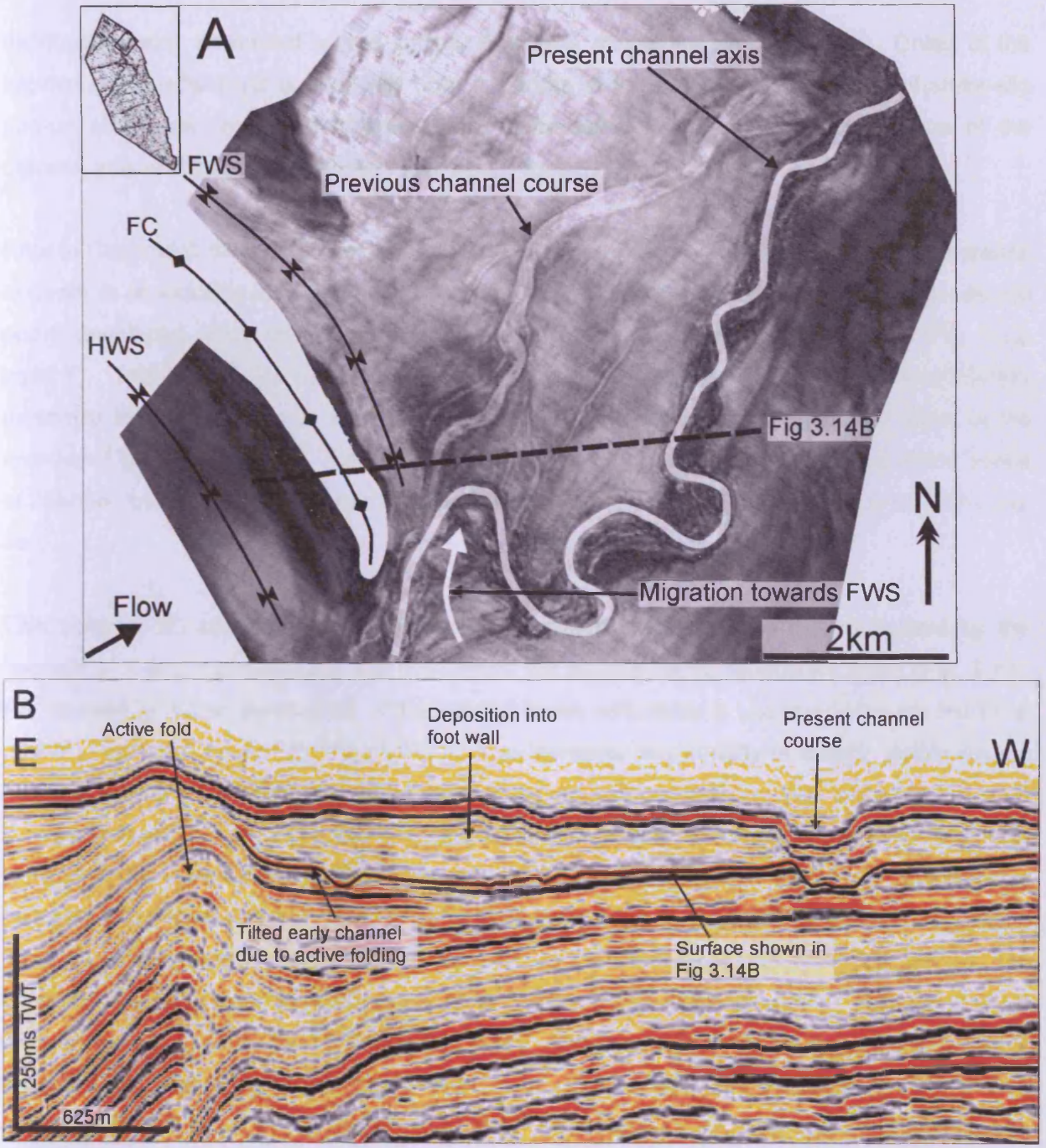

Figure 3.14: 3.14A: Amplitude map of the base Channel C surface. FWS = Footwall syncline, FC = Fold crest, HWS = Hanging-wall syncline. Increased lateral migration of the first meander occurs where Channel C exits the fold belt, with the direction of lateral migration being towards the footwall syncline to the north. An early, short lived small scale channel developed in this area at the apex of the first outwards facing meander bend after emergence of Channel C from the fold belt. 3.14B: Seismic profile showing increased tilting of the basal channel deposits contrasted with the undeformed top channel surface.

distribution being controlled by the surrounding folds and strike slip structures. Onlap of the internal levee reflections is observed onto the limbs of folds and onto the flanks of strike-slip pop-up structures, indicate that pre-channel deformation which controls the location of the channel axis and levee distribution in this area (Fig. 3.12C).

Prior to Channel C emerging from the fold belt the channel depth profile shows a sharp increase in depth in association with a straight (sinuosity = 1) channel segment in which the levees are poorly developed, showing limited thickness and lateral extent from the channel axis (Fig. 3.12, point F). This part of Channel C passes downstream into an area showing thick and laterally extensive levees covering an area of 22km^2 in association with a high sinuosity reach of the channel (Fig. 3.12, point G). The thickest levee deposits (up to 14m) occur on the inside bends of channel meanders and immediately downstream of the point where Channel C exits the fold belt.

This zone of increased sinuosity and levee deposition is confined to the south-west by the forelimb of a thrust propagation fold onto which the internal levee reflections onlap (Fig. 3.14). An increase in the angle of onlap of the internal levee reflections is observed towards the base of the Channel C sequence (Fig. 3.14). The increase in sinuosity is clearly visible on the seafloor and is also expressed morphometrically as a broad peak which correlates with an increased channel W:D ratio. This is in contrast to the isolated sinuosity peaks associated with sharp changes in channel course which correlate with low W:D ratios. Channel C also displays an earlier channel developed at the base of the sequence in this area. This channel appears to have been relatively short lived and was followed by an avulsion to form the present day channel. The avulsion node (sensu Kolla et al. 2007) occurs at the base of the north-west levee where Channel C exits the fold belt (Fig 3.14). The point of avulsion is associated with a decrease in channel erosional depth (Fig 3.13). This channel is relatively straight with a sinuosity of 1.1, near the avulsion node it is 150m wide and c.7m deep, with the width increasing to 260m towards the north where it eventually rejoins Channel C. No levees are observed to be associated with this channel but several linear small scale channels are present, typically having widths of 50m (Fig 3.14). These small scale channels emerge from the outer bank close to the position where the first meander (which developed subsequently) is now located. They join the course of the avulsed channel with the exception of one which joins the course of Channel C.

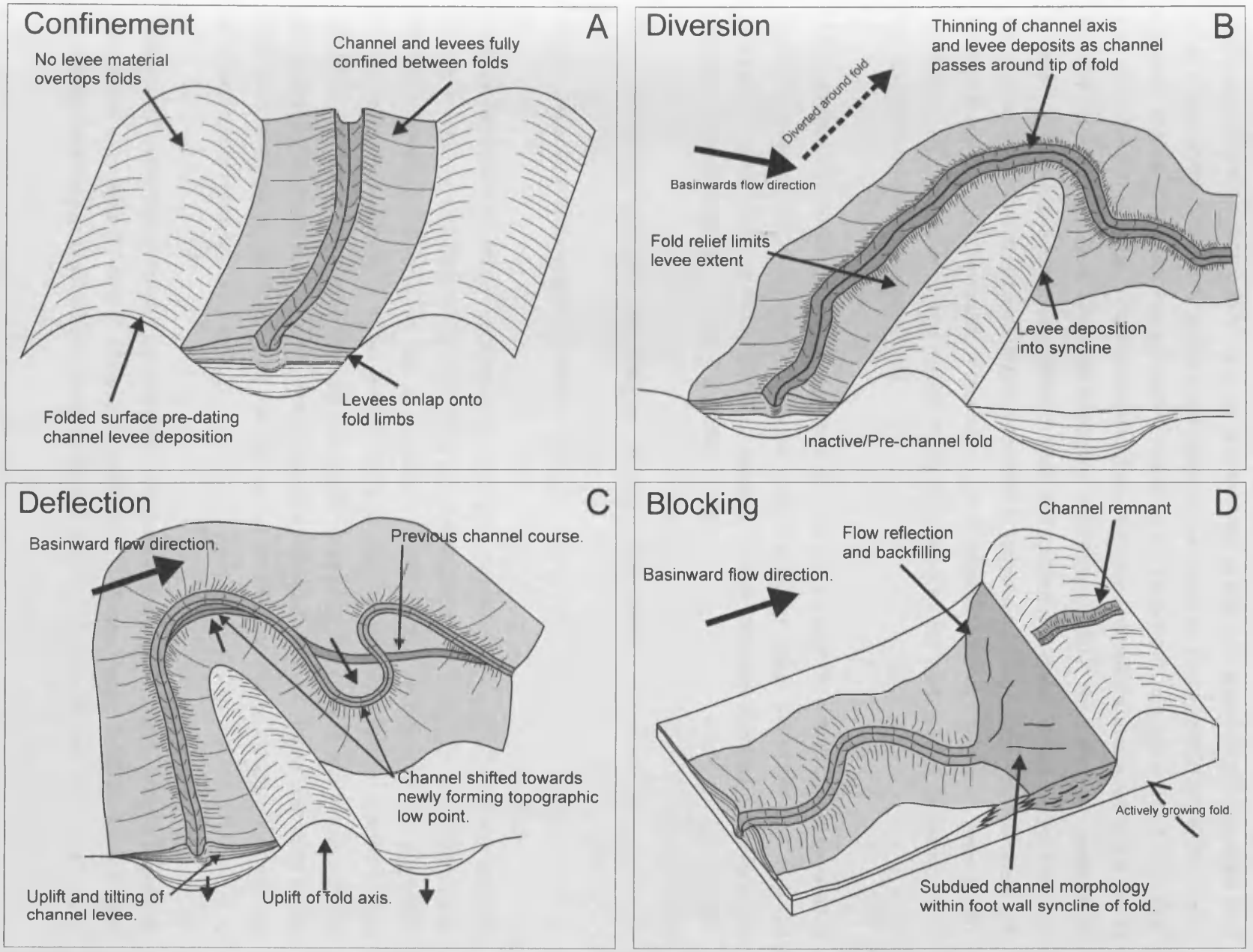

Figure 3.15: Block diagrams illustrating the four end member interactions between submarine channel development and underlying deformation. Compare with Figure 2 which shows an unconfined channel levee system. See text for details.

3.5 Discussion

The channel systems described in the previous section all show examples of channel development influenced by deformation resulting from compressional salt tectonics which affects this area. Based on the various examples of channel levee systems interacting with many separate structures within this area, and comparing this with unpublished examples from other areas where channel-structure interactions occur (such as Deepwater Nigeria), four end-member channel structure interactions: 'Confinement', 'Diversion', 'Deflection' and 'Blocking' can be defined (Fig. 3.15). Each channel-structure interaction results in a specific pattern of channel development and provides important information about the temporal relationship between submarine channel development and deformation. In order to aid recognition and description of similar channel-structure interactions elsewhere, these four end-members are defined in more detail below, with reference to type examples described from the Levant Basin. Unconfined channel development is also briefly discussed for the purposes of comparison with the four end-member interactions.

Although each channel-structure interaction is defined individually for a particular area of each channel, many of the channels in this area are affected by more than one type of these interactions along their length. The full range of these channel-structure interactions is discussed in more detail in Chapter 6 – section 6.2.1.

3.5.1 Definitions of key submarine channel – structure interactions.

3.5.1.1 Unconfined channel development (Fig. 3.2):

Channel development that is unaffected by underlying deformation is associated with channel levees that thin exponentially away from the channel axis (Skene et al. 2002). The channel axis itself is only confined between the constructional relief of the levees and not physically constrained by the underlying slope. Sediment waves may be prominent on the channel levees and can either be parallel to the channel axis (such as at meander bends) or orthogonal to the channel axis (Normark et al. 2002). Where the channel is unconfined, lateral migration of the channel is relatively unrestricted, and this can result in development of a highly meandering, sinuous channel levee system (Fig. 3.2).

Examples of unconfined channel development are observed along the south-western segments of channel segments B and C (Figs 3.10 and 3.12). These areas typically have higher sinuosities and thicker channel and levee deposits (Fig 3.12, points A and G). In areas of

unconfined channel development, the thickness and lateral extent of the channel levees is approximately symmetrical about the channel axis in the along-channel orientation (Fig. 3.10).

3.5.1.2 Confinement (Fig. 3.15a):

Confinement of a submarine channel is defined as the restriction of the course of a channel and its overbank deposits as a result of pre-existing structures (Fig 3.15a). Due to these structures constraining the channel course, confinement limits the ability of the channel to laterally migrate and develop a sinuous planform geometry. If the confining structures are no longer active, then aggradation of the submarine channel can lead to the degree of confinement decreasing over time as the channel infills accommodation space. This process is similar to the well recognised fill and spill model of enclosed mini-basin development described from the Gulf of Mexico (Prather et al. 1998; Beaubouef and Friedmann 2000) but here applies specifically to the development of submarine channel systems. As well as limiting lateral migration, confinement can also limit the thickness and distribution of the channel levee deposits, due to the available accommodation space being restricted by the enclosing structures.

The effects of confinement on channel development are very clearly illustrated by the example of Channel C. In this example, confinement is caused by strike slip faulting and folding, the axis of which is parallel to the channel course (Fig. 3.12, points D, E and F). In both cases the location of the channel axis, as well as levee deposits, are physically constrained by the folding induced topography (Fig 3.12, points D, E and F). Where strike slip faulting affects Channel C, levee development is asymmetric, with preferential deposition occurring within the areas of decreased relief formed by pull-apart structures (Fig. 3.12, point B). Confinement of Channel C results in limited lateral migration (Fig 3.12, point F) causing a decrease in sinuosity in those areas where confinement occurs.

3.5.1.3 Diversion (Fig. 3.15b):

Diversion is defined as a change in channel course resulting from a pre-existing structure (or series of structures) obstructing the flow pathway of the channel by modifying the slope gradient. Diversion is commonly caused by a pre-existing structure that is orientated at a high angle to the channel flow pathway which causes the channel to flow around the obstacle. Once the channel is diverted around the structure, it can resume its original down-slope course. Diversion of submarine channels in this study is associated with increased deposition of levee material into the synclines as the channel is diverted around the zones of positive seafloor topography above underlying thrust faulting (Fig. 3.10). Diversion can affect the courses of

submarine channels at either a local or regional scale. Local diversions can involve the channel pathway being shifted by hundreds of metres laterally as the submarine channel flows around a single obstacle. Regional diversions cause a lateral shift in the course of the submarine channel of several to tens of kilometres and result from arrays of linked or overlapping structures obstructing the down slope channel pathway.

An example of a local diversion around a single fold is observed along Channel B, where diversion occurs 1km to the south east around a single thrust fold (fold 2 in Fig. 3.10). Diversion of Channel B results in preferential levee deposition towards the north west, into the depression formed by the hanging-wall syncline associated with fold 2 (Fig. 3.10). The example of regional scale diversion of Channel C is caused by multiple folds and pop-up structures along strike slip faults, the combined effects of which result in a shift in the channel pathway of over 8km to the north-west until Channel C exits the fold belt (from point C to point G, Fig. 3.12). Large scale channel diversion by multiple structures affecting Channel C is associated with confinement into local depressions adjacent to the diverting structures (Fig. 3.12, point C).

3.5.1.4 Deflection (Fig. 3.15c):

Deflection is defined as a progressive shift in channel position away from the axis of uplift of an adjacent growing structure, causing a shift in channel position to occupy the newly forming topographic low point. Deflection causes successive changes in channel course over time. This is distinct from diversion, which involves a single lateral shift in channel position around a passive obstacle to flow. The two types of interaction are therefore similar, with the relative timing of channel development and deformation being the key factor which sets diversion and deflection apart. Lateral accretion surfaces on the side of the channel adjacent to the structure, and erosion on the opposite side are indications that the channel pathway is being shifted away from the adjacent structure (see also Mayall et al. 2006). Deflection by an uplifting structure such as a growing fold may result in an abandoned channel or accretion surface perched above the present channel thalweg. This is a result of the channel's course being shifted to occupy the local gravity base over time. Examples of submarine channel deflections by active structures (salt diapirs) have been documented from the Angolan slope (Gee and Gawthorpe 2006).

An excellent example of deflection can be seen as Channel C emerges from the fold belt at the point where two oppositely verging thrust folds terminate against a transfer fault (Fig. 3.14). This area is characterised by the deposition of a lobe-like deposit covering approximately 22km^2, with the thickest channel levee deposits concentrated against the forelimb of the fold to

the north west and, to a lesser extent, against the back limb of the fold to the south east (Fig. 3.14B). The temporal evolution of Channel C in this area involves successive shifts in channel position towards the lowest bathymetric point over time – in this case the low point is the footwall of the fold to the northwest of the channel (Fig. 3.14). During deflection of this channel, an avulsion occurred during the lateral migration of the channel position. The avulsed channel is located at the base of the channel sequence at the first downstream facing meander bend after emergence of Channel C from the fold belt. This avulsed channel is associated with small scale, linear channels developed in the overbank areas adjacent to the avulsed channel (Fig. 3.14). Following abandonment of the avulsed channel, the high sinuosity, present day channel segment progressively evolved over time from an originally less sinuous course.

3.5.1.5 Blocking (Fig. 3.15d):

Blocking of a submarine channel is defined as a structure orientated at a high angle to the channel flow direction preventing downstream sedimentation due to structural relief and the upstream facing slope causing reflection of individual flow events along the submarine channel. Blocking can result from a relative rate of fold growth or uplift which exceeds the erosional and aggradational rates of the channel across the fold crest and the adjacent synclines. Blocked submarine channels may show an unfilled channel remnant preserved downstream of the blocking structure, whereas the channel segment upstream will have a subdued morphology due to backfilling and flow reflections from the blocking structure (e.g. Bursik and Woods 2001).

Channel A is an excellent example of a system which has become blocked due to fold uplift perpendicular to the channel, in a similar manner to that of a defeated fluvial system (Burbank et al. 1996). Continued activity of Channel A has resulted in increased deposition upstream of the blocking fold (Fig. 3.8) which has partially healed over the constructional relief generated by this channel. Downstream of the blocking fold, a channel remnant is preserved which retains its original relief due to the relief of the fold preventing any downstream sedimentation.

3.5.2 Implications of submarine-channel interactions

The recognition and description of four end member types of submarine channel-structure interactions in a deepwater fold and thrust belt setting may have implications for reservoir development in any deep marine system where submarine channel development occurs on a structurally active slope. These interactions may be applicable, for example, to other slope settings, particularly those undergoing gravity driven collapse. Examples include the Niger Delta (Heinio and Davies 2007; Morgan 2004), the Angolan Margin (Gee and Gawthorpe 2005) and

offshore Brazil (Viana et al. 2003). It is hoped that the recognition of these four channel-structure interactions will be a useful starting point for a descriptive framework for submarine channels within structurally active slope settings.

Thickness and lateral extent of channel levees within a confined channel are controlled by the available local accommodation space, which is in turn related to the nature of the confining structures (Fig. 3.12, point F). This could limit the development of any potential reservoir to between the confining structures, particularly if structural relief prevents lateral migration. An example of this is seen where Channel C is confined by multiple folds and strike slip pop-up structures (Fig. 3.12).

Local diversion of submarine channels around the tips of folds or faults results in a shift in overall channel direction until the channel passes around the structure. In the case of channel diversion around the edge of a fold, levee deposition is concentrated within the hangingwall and footwall syncline while the channel axis passes around the fold (Fold 2, Fig. 3.10). Increased deposition of levee material within these synclines could result in preferential development of crevasse splays and sheet sands localised in these areas, with important consequences for reservoir development in fold belt settings where channel levee systems are developed (Fig. 3.14). Regional scale diversion of submarine channels also involves a degree of confinement, as is shown by Channel B (Fig. 3.12).

Deflection can result in the development of amalgamated, potentially sand-rich channel axis deposits adjacent to the uplifting structure as the channel's position is shifted away from the axis of uplift and towards the newly forming low point. Deflection can also be associated with development of avulsions (Fig. 3.14) and increased deposition of crevasse splays and sheet deposits into structural lows forming during ongoing deformation. This too may have implications for reservoir prediction, in that lateral amalgamation of individual channels could result in a more prolific reservoir than a comparable channel where there has been no history of deflection.

Blocking can result in dramatic changes in submarine channel thicknesses upstream and downstream of the blocking structure. In the example in this study, channel development within the footwall syncline upstream of the blocking fold has resulted in a highly sinuous channel with potentially sand-rich lateral migration deposits. Blocking may also result in loss of connectivity within the channel axis deposits across the blocking structure, particularly if the channel becomes more erosive across the fold crest (Heinio and Davies 2007).

3.5.3 Timing relationships between submarine channels and structural deformation.

Establishing the correct timing of the interactions between submarine channels and structures affecting their development is a key factor in predicting the depositional response to active deformation of the slope and will affect which of the four end-member interactions is most likely to occur. This study documents several different relative timings of deformation with respect to submarine channel development:

1. Deformation pre-dates channel development: This is seen where Channel C is confined and diverted by multiple fold and strike-slip structures. In this case the surface resulting from faulting and folding controls the slope gradients as well as the available accommodation space into which levee deposition can occur.
2. Deformation post-dates channel development: An example of this is where Channel A is blocked by a fold which developed perpendicular to the channel flow direction.
3. Deformation is coeval with channel development: This is seen where Channel C is diverted towards the footwall when it emerges from the fold belt (Fig 14). Another example occurs along Channel B which is affected by underlying folding which does not result in a channel diversion (Fig. 3.10).

In this study the most commonly observed interactions involve deformation which pre-dated submarine channel deposition. This is evident from the channel isopach maps, particularly as the channels pass through the fold belt (Fig. 3.12). These examples show that the thickness and lateral extent of the channel levees (as well as the location of the channel axis) are controlled by the pre-channel deformation surface (Fig. 3.12c).

Channel levees can be used as an indicator to assess the relative timing of deformation with respect to channel development. In situations where levee deposition from a submarine channel is unconstrained, the levee package thins exponentially away from the channel axis (Skene et al. 1998; Broucke et al. 2002; Deptuck et al. 2003). Internal reflections within the levees are often highly continuous but converge laterally away from the channel axis, this convergence often appearing as apparent downlap on seismic data.

Where a structure which pre-dates the submarine channel is present, channel diversion or confinement can result in the internal levee reflections showing downlap onto the flank of the structure (Fig. 3.12c). In addition, the gross shape of the levee package will differ from that seen where channel deposition is unconfined - compare levee geometry seen in Figure 3.12 with that in Figure 3.2.

If structural relief initially pre-dates channel development, but subsequent deformation is coeval with channel deposition, the gross geometry of the levee package will be similar to the previous case. The geometry of the internal levee reflections will differ however, as the basal levee reflections will become progressively rotated by the growing structure (in this case a fold) over time (Fig. 3.14). This will result in the basal levee reflections becoming tilted towards the channel axis, with the degree of rotation of the levee reflections decreasing upwards. An example of this relationship is observed for Channel C (Fig. 3.14B).

In the case of a structure which post-dates channel deposition, the levee will become incorporated into the growing structure and the internal levee reflections may become rotated and appear to onlap onto the flank of the structure. The levee should still retain its gross geometry however, and show tapering away from the channel axis. This relationship is not seen in the systems studied here as deposition of the channel systems post-dates deformation.

3.5.3.1 Using morphology to assess the timing of channel-structure interactions:

The submarine channels in this study area are all significantly affected by the fold belt as they cross it. In the case of channel B however, there is no diversion when this channel crosses Fold 1 (Fig. 3.10). This is in contrast to the second fold, which diverts this channel, and also contrasts markedly with the 8km diversion to the NW observed along Channel C (Fig. 3.12).

The erosional depth profile of Channel B shows a strong similarity to the cross sectional profile of the underlying fold, which is asymmetric with the fold crest flanked by a broad hangingwall syncline and a narrow footwall syncline (Fig. 3.11). Thus the increase in erosional depth observed over the hangingwall and footwall synclines and the decrease in erosional depth across the fold crest mirrors the geometry of the underlying fold profile. This similarity between the shape of the erosional depth profile underlying fold is interpreted to result from folding superimposed onto a normal erosional depth profile over the course of the channel's development. This is in contrast to areas where underlying deformation does not affect, or post-dates channel development (Fig. 3.11). In these areas, the difference between the erosional depth and the channel thalweg depth profile is fairly constant (Fig 3.11). Comparison of the erosional depth profile with the thalweg depth profile of Channel C across fold 1 (Fig. 3.11) reveals a contrast between the magnitude of folding that has affected the two profiles, with the erosional depth profile showing a more pronounced resemblance to the underlying fold than the thalweg depth profile The difference observed between these two profiles as Channel A crosses the edge of the fold is interpreted here to represent fold growth which was coeval with

the development of this channel. Therefore, the difference between these two morphological parameters is a useful record of the response of this channel to uplift. Comparison of these two profiles where Channel B crosses the fold crest (Fig. 3.11) shows that increased deposition occurs across the synclines with relatively less deposition occurring across the fold crest.

3.6 Conclusions

1. This study documents a series of submarine channel levee systems which developed within a deepwater fold belt setting. The channel levee systems described are typically 500m in width and are dominantly aggradational, with well developed levee deposits. Where no underlying structures are present, the channels in this area typically have a sinuous planform geometry.
2. Evidence of the response of submarine channel systems to the structurally formed slope is exhibited by levee asymmetry which results from the surrounding structures which determine the available accommodation space for levee development.
3. In deepwater fold belt settings, where submarine channel systems develop on a structurally deformed seafloor, four end member channel-structure interactions can be defined: Confinement, diversion, deflection and blocking.
4. These interactions can occur in combination with each other but each will result in a specific pattern of channel development, this can have implications for potential reservoir sand body distribution, thickness and connectivity, particularly around folds.
5. Recognition of these interactions provides a useful framework for describing submarine channel evolution in structurally active areas.
6. Channel-structure interactions also provide information about the relative timing of deformation vs channel development. For example, confinement and diversion result from pre-channel deformation, whereas deflection and blocking result from deformation which is coeval and post dates channel development respectively.
7. Variations in morphological parameters such as erosional depth vs thalweg depth can also be used to assess the timing and response of the channel to deformational features which are active over the time period of channel development.
8. The results of this study should be applicable to many other deepwater fold belt settings in which submarine channels are developed on a structurally active seafloor.

Chapter 4

This chapter has been submitted in revised form after being peer reviewed for inclusion into a special issue of the Journal of Sedimentary Research on the topic of seafloor geomorphology.

The work presented in this chapter is that of the lead author (IRC), editorial support was provided by the project supervisor, JAC in accordance with a normal thesis chapter.

CHAPTER 4

INTERACTIONS BETWEEN COEVAL SEDIMENTATION AND DEFORMATION FROM THE NIGER DELTA DEEPWATER FOLD BELT

4.1 Abstract

The deepwater fold and thrust belt of the Western Niger Delta provides an ideal natural setting in which to study interactions between coeval sedimentation and deformation. Deformation in this area takes the form of folding resulting from the up-dip gravitational collapse of the Niger Delta above the overpressured shale detachment of the Akata formation. The seafloor relief formed by folding is initially orientated perpendicular to the downslope sediment transport direction. This results in a significant barrier to the basinwards transport of material and in the creation of accommodation space within the hangingwall and footwall areas of the fold. Coeval sedimentation during uplift results in deposition of a growth sequence comprised of a compensationally stacked vertical succession of mass transport deposits (MTDs), channel levee systems (CLSs), and hemipelagic drape deposits (HD). Variations in the along-strike structural style and relief of a large scale fold c.40km in length control variations in growth sequence geometry. These variations in fold style along strike also determine sediment flow pathways around the positive relief formed at the seafloor during fold uplift. Switching of sedimentation between the two structurally induced flow pathways around the fold is related to the compensational stacking patterns within the hangingwall which cause a shift in flow pathways from one fold edge to another. The combined structural-stratigraphic approach to the interpretation of sedimentation in deepwater fold belts is a useful method for reconstructing the development of relief during folding.

4.2 Introduction

Deepwater fold belts found on passive margins are characterised by zones of thrusts, and overlying thrust-related folds which develop to accommodate up-dip extensional structures at the head of large gravity spreading deformational systems (Bornhauser, 1958; Winker, 1982; Jackson, 1995; Letouzey et al., 1995; Morley and Guerin, 1996). The gravitational collapse of large prograding sediment wedges above ductile substrates such as salt or overpressured shale is typical of many of the world's large deltaically driven depocentres on passive margins such as the Gulf of Mexico, the Niger Delta, the Kwanza-Congo Deltas, the Amazon Cone and the Nile Cone (McClay et al., 2003; Rowan et al., 2004; Cartwright and Jackson, 2008). Compression in these settings is often expressed at the seafloor as asymmetric folds which typically have a

positive relief of several hundred metres (Cohen and McClay 1996; Demyttenaere et al., 2000; Heinio & Davies, 2006) and act as significant barriers to the downslope transport of sediment. This results in complex slope topography with multiple depressions acting as focal points for sedimentation as well as positive bathymetric barriers to down-slope sediment transport, all of which contribute to highly complex, tortuous flow pathways in these settings (Smith, 2004).

In deepwater fold belt settings, the main drivers for sediment accumulation are the interactions between slope topography and sediment transport and deposition. The interplay between accommodation space evolution controlled by fold amplification and sediment transport are the first order controls on sediment architecture and facies (reservoir) distribution, and influence, for example, reservoir-seal juxtapositions (Cartwright, 1989; Prather, 1998; Prather et al., 2003). Due to water depths of up to 4000m, the influence of eustatic sea level in directly controlling available accommodation space is secondary in such deep water settings, but can still influence long term variations in sediment supply and in conditioning the shelf-slope boundary zone for net bypass or accumulation (e.g. Jervey, 1988).

Gravity driven sedimentation in deepwater fold belt settings can be separated into two well recognised end member processes, defining a depositional continuum (e.g Reading and Richards, 1994). Firstly, turbidity current driven sedimentation results in the formation of channel levee complexes (e.g. Babonneau et al., 2002; Kolla et al., 2007; Wynn et al., 2007) but can also include more unchannelised, early stage sheet-like deposits (e.g. Beaubouf & Friedmann, 2000). Secondly, mass wasting processes can mobilise and displace large volumes of sediment over varying distances downslope through a range of transport mechanisms such as debris flows, sliding and slumping (Martinsen & Bakken, 1990; Mulder and Cochonat, 1996; Frey-Martinez et al., 2005).

Coeval sedimentation during folding results in the formation of growth sequences adjacent to the fold limbs (Cartwright, 1989; Suppe et al., 1992). The preservation potential of these growth sequences is much higher in deepwater fold belts than in any other setting (e.g. inverted rift basins (Cartwright, 1989) or foreland basins). Growth sequences are characterised by stratal thinning or onlap onto the fold crest and expansion of sedimentary packages into the forelimb or backlimb of the fold, as well as a progressive increase in stratal rotation with depth (e.g. Salvini and Storti, 2002, for review). Growth sequences are commonly studied in the context of structural geology and provide important indicators of the mechanism of folding (Suppe et al., 1992; Poblet et al., 1997; Bernal & Hardy, 2002; Salvini & Storti, 2002). Understanding the mechanism of folding is important as the type of fold will determine the rate of uplift over time and also the shape of the fold which can affect sedimentation during fold growth (Salvini &

Storti, 2002). Growth sequences can also provide information on the relative rates of uplift vs sedimentation (Burbank & Verges, 1994; Burbank et al., 1996). Detailed analysis of sediment-structure interactions between features such as submarine channels and emerging topographic relief within a regime of active deformation can provide detailed information which can be used to refine conceptual models of fold growth based upon larger scale features such as growth stratal architecture. Deepwater confined channels are highly sensitive indicators of gradient change (Huyghe et al., 2004; Heinio & Davies, 2007; Ferry et al., 2005; Clark & Cartwright, 2009) and one of the aims of this chapter is to show how they can be used to identify subtle changes in fold amplitude and surface relief that otherwise would be undetectable from analysis of seismic profiles alone.

Deepwater fold belts in which sedimentation is coeval with deformation have been extensively described from a structural viewpoint, namely in the Gulf of Mexico (Wu et al., 1990; Trudgill et al., 1999), the Nile Delta (Letouzey et al., 1995; Gaullier et al., 2000; Cartwright and Jackson, 2008), and the Niger Delta (Damuth, 1994; Morley & Guerin, 1996; Wu & Bally, 2000). However, comparatively few studies address the interactions between the structural deformation and sedimentation in these or equivalent settings (Cartwright, 1989; Hagen et al., 1994; Huyghe et al., 2004; Heinio & Davies, 2007; Noda et al., 2008). 3D seismic data from deepwater fold belts provide ideal datasets to study sediment-structure interactions and to study growth sequences adjacent to folds, because the entire growth sequence architecture can be imaged in detail and placed in its structural context.

This study is based on a high resolution 3D seismic survey from the deepwater western Niger Delta and aims to present a detailed analysis of a growth sequence associated with a single, well defined fold. The main aims of the paper are to address the following questions:

1. How can detailed stratigraphic information from the growth sequence be used to reconstruct the seafloor relief during fold growth?
2. What is the architecture of the growth sequence in three dimensions and how does this relate to the filling of accommodation space created by folding over time?
3. What are the primary sediment pathways during fold growth and how do these change over time?

The underlying theme of this paper is to demonstrate how an integrated structural and stratigraphic analysis of growth sequences can not only be used to aid in reconstructing the structural evolution, but also help to refine depositional models in deepwater fold belts.

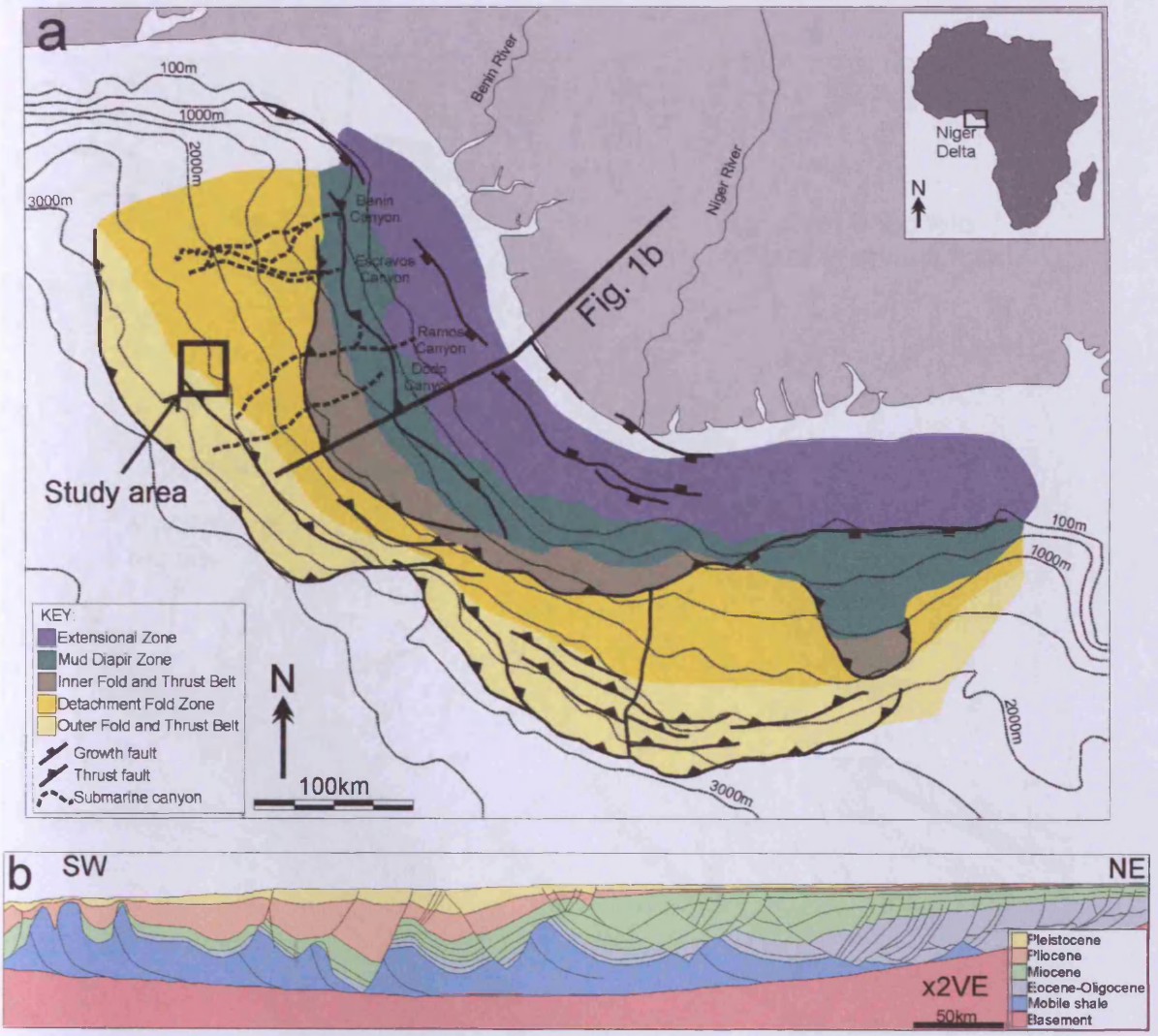

Figure 4.1: **4.1a** shows the location of the 3D seismic survey described in this paper. The survey is located at the boundary between the detachment fold belt and the outer fold and thrust belt. Structural zonation of the offshore Niger Delta is modified after Corredor et al (2005) and the positions of the submarine canyons are modified from Deptuck et al (2007). Fig. **4.1b** (modified from Haack et al 2000) shows a cross section through the western Niger Delta. The updip extensional domain passes into one of downdip compression where this study is located. The system of linked extension – compression occurs above a detachment layer of overpressured shales. **Fig. 4.1c** (next page) shows a seabed dip attribute map of the seafloor of the study area with several key features identified which are referred to later in the paper.

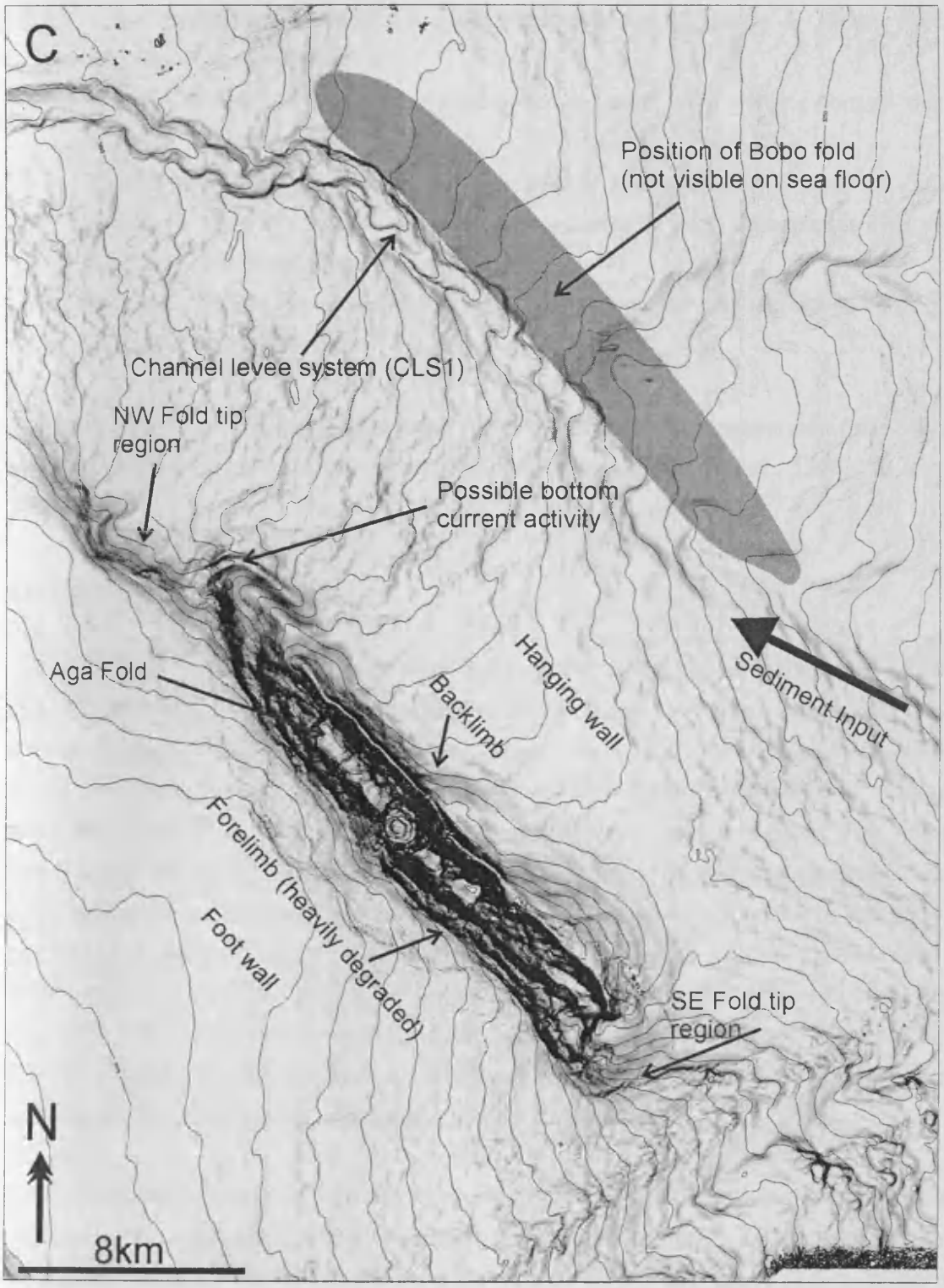
C
Position of Bobo fold
(not visible on sea floor)
Channel levee system (CLS1)
NW Fold tip
region
Possible bottom
current activity
Aga Fold
Backlimb
Hanging wall
Sediment Input
Forelimb (heavily degraded)
Foot wall
SE Fold tip
region
N
8km

2. A mud diapir zone beneath the upper continental slope (Morley & Guerin, 1996) with inter-diapir depocenters.
3. An inner fold and thrust belt, characterised by basinward verging thrusts and folds including detachment folds.
4. A transitional detachment fold zone beneath the lower continental slope characterised by areas of little or no deformation but with occasional large detachment folds above a structurally thickened Akata formation.
5. An outer fold and thrust belt characterised by basinward and hinterland verging thrust faults and associated folds.

The outer fold and thrust belt is separated into two distinct regions, separated from each other by the northern culmination of the Charcot fracture zone (Conners et al., 1998; Wu and Bally, 2000).

4.3.2 Study area and methods.

The study area is located inboard of the outer fold and thrust belt of the western Niger Delta (Fig. 4.1) in water depths ranging from 2000 to 2300m below sea level. Structurally, the study area is relatively simple and shows the development of two folds – the Aga and Bobo folds (Fig. 4.1c). Both these structures can be described as thrust propagation folds (Mitra, 1990) in that along the greater part of their strike they are underlain by large thrust faults. The Aga fold is clearly visible on the present day sea floor (Fig. 4.1c), the Bobo fold was reactivated at a late stage but is now buried below sediments which have accumulated within the hangingwall of the Aga fold. This paper focuses on the most recent, and most clearly imaged, upper section of the growth sequence deposited during the latest phase (Plio-Pleistocene) of growth of the Aga fold (Fig. 4.2). This sequence provides an ideal interval in which to study sediment-structure interactions and three dimensional stacking architectures within the growth sequence, as well as being the within the highest resolution interval of the dataset.

The 3D seismic data used in this study covers an area of c.2000 km^2 and is zero phase time migrated with a positive polarity reflection (black) representing an increase in acoustic impedance. The data are sampled at 4ms intervals with a line spacing of 12.5m. Where given, estimates of depth assume an interval velocity of 2000 m/s, calibrated by nearby wells. The dominant frequency of the upper 1.5s of data is approximately 45Hz, giving a tuning thickness estimated at 12.5m.

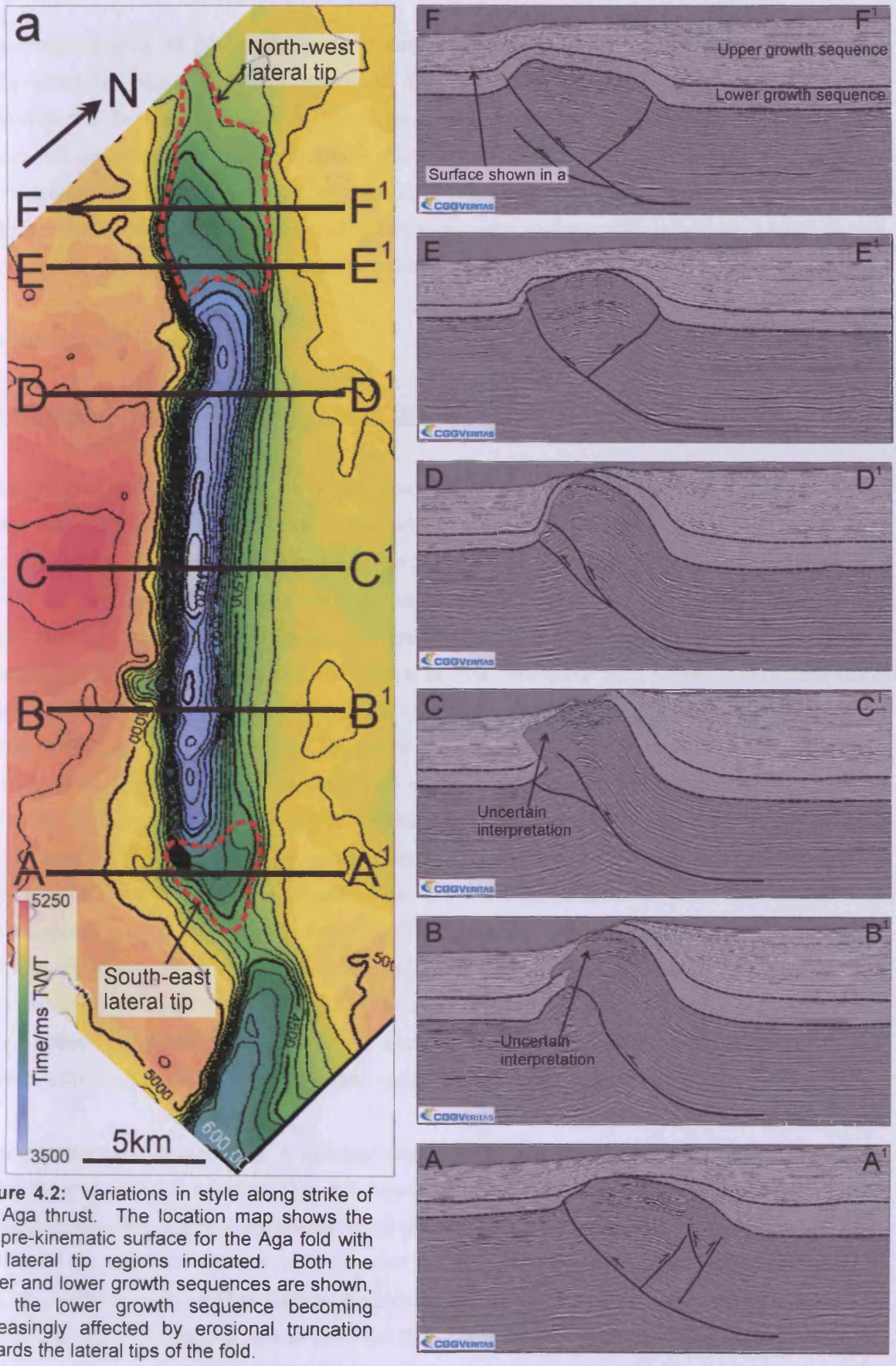

Figure 4.2: Variations in style along strike of the Aga thrust. The location map shows the top pre-kinematic surface for the Aga fold with the lateral tip regions indicated. Both the upper and lower growth sequences are shown, with the lower growth sequence becoming increasingly affected by erosional truncation towards the lateral tips of the fold.

The methods used in this study involved detailed mapping of individual seismic-stratigraphic units within the growth sequence deposited adjacent to the Aga fold. The aim of this was to establish the three-dimensional architecture of the growth sequence and to document the effects of coeval uplift and deposition. Subdivision of the growth sequence into discreet architectural elements was based on standard seismic stratigraphic characteristics such as reflection continuity, amplitude, internal seismic character of the package and also relationships such as onlap, downlap and erosional truncation.

4.4 Results and observations.

4.4.1 Structural framework of the Aga thrust and fold.

This section provides an overview of the structural characteristics of the Aga thrust and fold in order to demonstrate the link between the underlying structural characteristics and the resulting fold topography. The primary Aga thrust verges towards the southwest, is continuous over a length of 40km, and has a displacement that reaches c. 500m in the central portion of the structure decreasing laterally towards the thrust lateral tips (Fig. 4.2). The fault plane is well imaged on the seismic data but the limbs of the overlying fold show severe amplitude attenuation in some areas, particularly within the forelimb which dips at a steeper angle than the backlimb (Fig. 4.2, lines B and C). The thrust ramps upwards from a detachment level located at the top of the Akata Formation, and increases in dip upwards into the overlying Agbada formation. Typical values for the dip of the fault plane are 14° near the detachment, increasing to 35° towards the fault tip. The primary thrust splits into several frontal splay thrusts which propagate into the forelimb and footwall: these are most well developed within the central area of the primary Aga thrust (Fig. 4.2, lines C and D). Towards the lateral tips of the primary thrust, north eastwards verging backthrusts are developed which tip out at a lower stratigraphic level that the primary thrust (Fig. 4.2, lines A, E and F). The dip of these backthrusts is typically 26°. The seafloor expression of the Aga fold exhibits significant mass wasting (see Heinio and Davies, 2007), with maximum degradation concentrated on the forelimb (Fig. 4.3).

The geometry of the Aga fold is typically asymmetric, with the forelimb dipping at a steeper angle compared to the backlimb (Fig. 4.2, lines C and D). At the seafloor, the dip of the forelimb is difficult to measure due to extensive mass wasting which has modified the fold geometry (Fig. 4.3), the backlimb has typical seafloor dips of c.6° (Fig. 4.2, lines B and C). The asymmetry of the fold decreases with fold amplitude towards both the north-western and south-eastern lateral tips of the fold. The lateral tips of the Aga fold extend just beyond the resolvable limit of the underlying thrust lateral tips. In these regions, the fold has a broader, less asymmetric profile

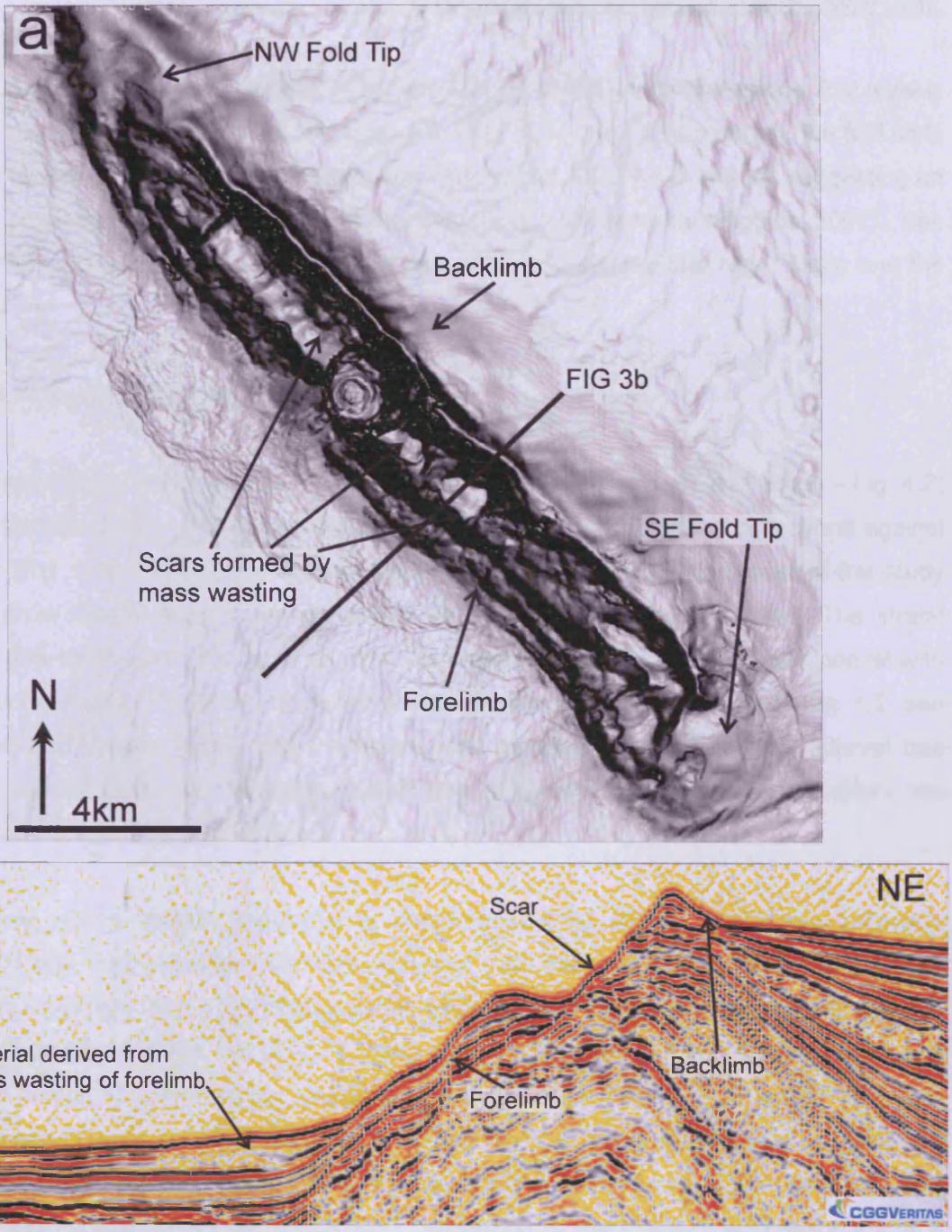

Figure 4.3: Seafloor dip map showing extensive mass wasting and degradation of the Aga fold forelimb, visible in **4.3a**. **4.3b** shows a representative seismic line though one of the prominent scars and shows material derived from mass wasting interbedded with the pelagic drape within the footwall.

with associated with decreased fold relief at the seafloor. In these lateral tip regions, fold style is similar to that of a faulted detachment fold (Fig. 4.2, lines A, E and F). In contrast, the fold style in the central portion is similar to fault propagation folding (Fig. 4.2, line C and D), suggesting an evolutionary sequence as fold amplitude and thrust displacement increase (Higgins, 2007). See also Chapter 6, section 6.2.2 for a comparison of fold styles between the Niger Delta and the Levant Basin.

4.4.2 Growth sequence geometry.

The hangingwall growth sequence can be subdivided into two units (lower and upper – Fig. 4.2) based on reflection continuity over the fold crest and onlap relationships of reflections against the backlimb (Fig. 4.2). The upper interval of the growth sequence forms the focus of this study as it is the most clearly imaged and contained entirely within the survey area. The stratal geometry of reflections within the upper growth sequence show that deposition was coeval with increased relative rates of uplift, compared to the lower growth sequence interval (Fig. 4.2, see also Burbank and Verges,1994). This increased rate of relative uplift over this interval has resulted in clear interactions between uplift and sedimentation, particularly within the hangingwall of the Aga thrust and fold.

The lower unit of the growth sequence is characterised by largely continuous reflection packages that thin and converge over the fold crest with little observable onlap against the backlimb of the Aga fold (Fig. 4.2). Mass wasting of the fold forelimb has removed much of this sequence from the front of the fold (Figs. 4.1 and 4.2c). The lower growth sequence is eroded by the upper growth sequence at the fold lateral tips where erosional truncation by the upper growth sequence can be seen (Fig. 4.2). The isochron map of the lower growth sequence unit shows an elongate zone of increased thickness deposited against the backlimb of the Aga fold which thins towards the north-west (Fig. 4.4a). Deposition of the lower growth sequence was also affected by the growth of a separate fold which extends out of the study area to the SE, and appears to link with the Aga fold described here (Fig. 4.4a).

The upper sequence shows a clear increase in thickness passing from the fold crest to the upslope limb with clear onlap of its internal reflections against the uppermost surface of the lower syn-kinematic sequence of the fold (Fig. 4.2). Thinning of this unit from the limb towards the crest is clearly seen on an isochron map of the upper syn-kinematic interval (Fig. 4.4b) which also shows a more general thickening of this sequence towards the SE corresponding to the entry point for sedimentation into the study area. The upper growth sequence is affected by late stage uplift of the smaller Bobo fold to the north east of Aga, resulting in thinning of the

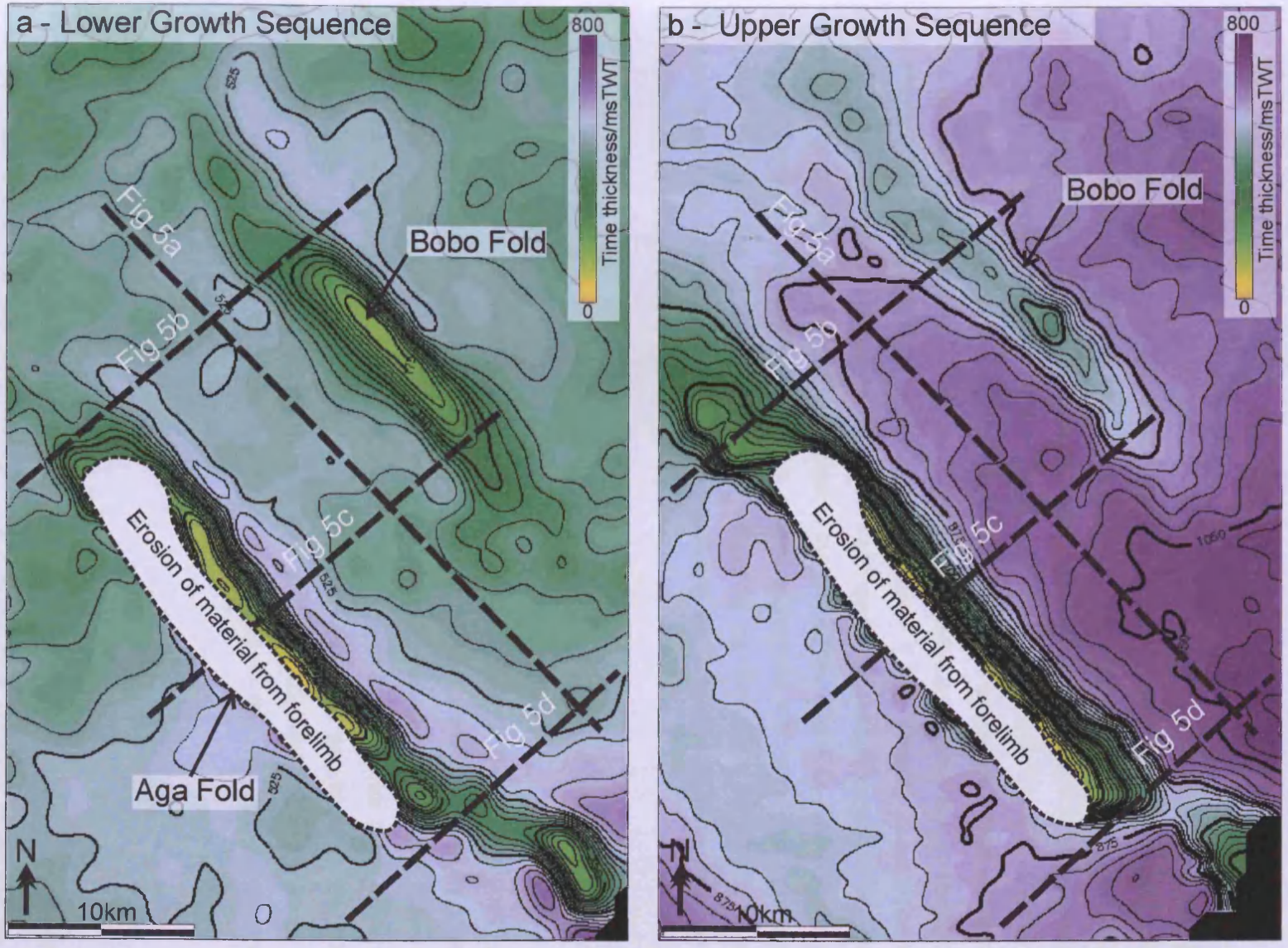

Figure 4.4: **4.4a** Isochron map of the lower growth sequence – both the Aga and Bobo folds were active over this interval resulting in an increase in thickness of the sedimentary package within the hangingwall and the footwall. **4.4b** Isochron map of the upper growth sequence showing a much greater increase in thickness associated with fold growth than that seen within the lower interval.

upper sequence across the fold crest, although the greatest amount of stratal thinning is observed during the lower growth sequence for the Bobo fold (Fig. 4.4b). These observations help to illustrate an important point with respect to analysing isochron maps of growth sequences: it is imperative to set the local fold within a broader context, to recognise larger scale thickness variations and to distinguish them from short-range effects related to folding and spatially varying sedimentation rates.

Variations in growth sequence geometry occur along the strike of the Aga fold. The growth sequence displays a progressive increase in the occurrence of onlap and thinning onto the backlimb towards the central zone of the fold (Fig. 4.2). The top of the lower growth sequence forms the onlap surface, and continued uplift of the Aga fold has resulted in progressive rotation of the points of onlap towards the base of the upper growth sequence (Fig. 4.5). At the south-east and north-west lateral hinges of the fold, the upper growth sequence stratal architecture is that of overlap where thinning but continuous reflection packages occur across the fold crest with little onlap onto the fold limbs observed (Figs. 4.5b & 4.5d). Overlap is accompanied by erosion of the lower growth sequence, as can be seen by the increased truncation of reflections against the base of the upper growth sequence at the fold edges (Fig. 4.2). The transition along strike from the lateral fold tips to the central area is associated with a change from erosional truncation and overlap of the lower growth sequence by the upper sequence to one of increasing conformity between the two, with increasing development of onlap onto the lower syn-kinematic sequence (Fig. 4.5c).

4.4.3 Seismic stratigraphic architecture of the upper growth sequence.

This section describes the principal seismic stratigraphic units which make up the upper growth sequence within the hangingwall of the Aga fold. The growth sequence in this study consists of a more diverse range of depositional elements compared to the previous chapter. Description of each seismic stratigraphic unit is followed by its interpretation. The three dimensional stacking patterns of these units throughout fold growth are then described in the following section. The distribution of these units is illustrated in figure 4.5, which shows a series of dip orientated lines as well as a profile parallel to the strike of the Aga fold to illustrate the distribution of the growth sequence elements.

4.4.3.1 Channel levee systems (CLSs):

Submarine channel levee systems and their architectural elements have been extensively described from many different basin settings (e.g. Abreau et al., 2003; Deptuck et al., 2003;

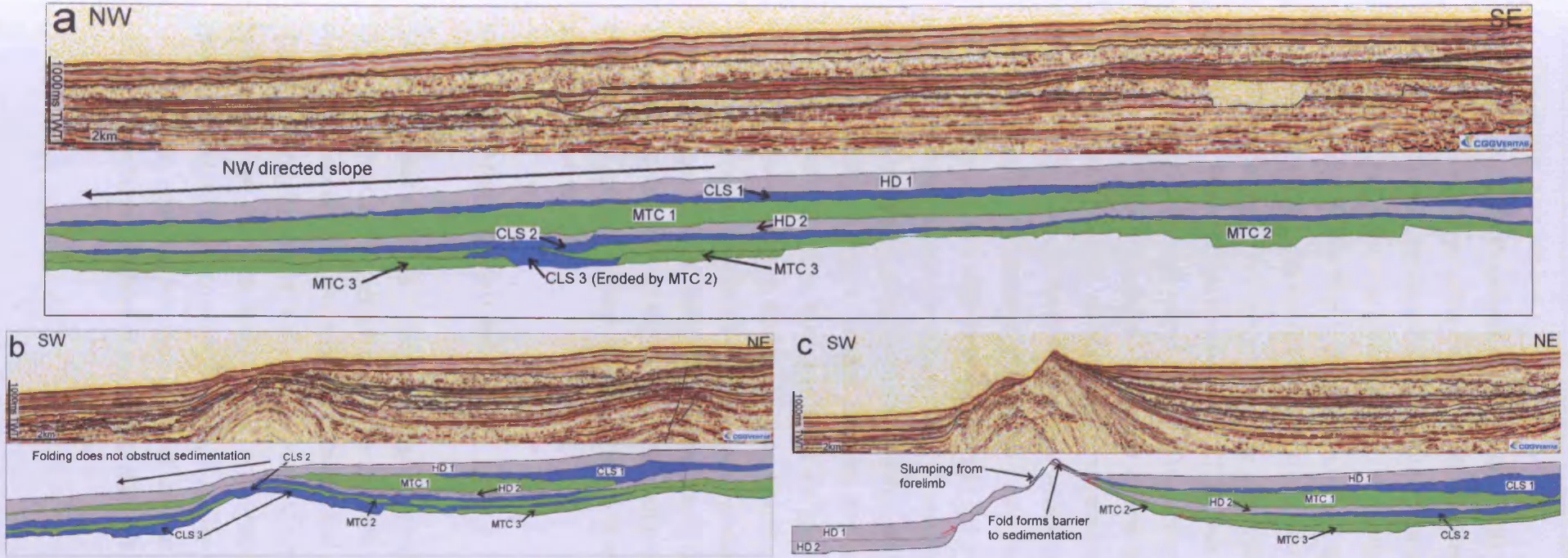

Figure 4.5: Series of seismic profiles across the upper growth sequence within the hanging wall of the Aga fold. For line locations, see figure 4.4. Each seismic profile is accompanied by an interpretation which shows the seismic stratigraphic units described in this paper and shows the links to the relevant figures which show isochron maps of each unit. **4.4a** shows a profile orientated parallel to the strike of the Aga fold showing an overall north-west dipping slope. Profiles **4.4b**, **4.4c** and **4.4d** show a series of profiles across the north-west fold tip, the central area of the fold and the south-east fold tip respectively. At the lateral fold tips (profiles **4.4b** and **4.4d**), the fold relief is not sufficient to block sedimentation resulting in overlap by the various seismic stratigraphic units. At the central area (profile **4.4c**) the increased fold relief results in onlap and confinement of sedimentation within the hanging wall.

Posamentier, 2003; Posamentier and Kolla, 2003). Many of the architectural elements identified from these previous studies can be identified here, and we describe only the key features of each system as a detailed description of all of the architectural elements is beyond the scope of this study. Channel levee systems (CLS) are a common component of the growth package in the hangingwall of the Aga fold. Three channel systems are described here, and are termed CLS 1-3, with CLS 1 being most recently deposited (Fig. 4.6). The channel levee systems show a significant variation in scale, morphology and architectural complexity, (see next section). The youngest of these channel systems, CLS 1, lies below a recent c.100ms thick package of parallel reflections which cover most of the survey area, interpreted to result from hemipelagic draping. CLS 1 displays large scale outer levees that flank a channel belt up to 2km wide (Fig. 4.6). The channel axis of all of these systems is typically U shaped and infilled with high amplitude, often discontinuous reflections which terminate against the margins of the channel axis. The depth of incision of the channel axis varies between different channel systems but generally shows some degree of incision into the pre-channel sequence (Fig. 4.6b). CLS 1 also displays terraces related to meaner loop abandonment and channel incision as well as semi-circular scarps due to collapse of the channel sidewalls (Fig. 4.6a). In contrast to large scale channels such as CLS 1, smaller systems are also observed (See CLS 2 described later). Smaller channel systems, such as CLS 2 are typically no more than 500m in width and do not show the same level of architectural complexity as the larger channel levee systems. A common characteristic of all channel levee systems in this area is that they display a high sinuosity, regardless of the scale of the system (See Figs. 4.6, 4.9c and 4.11). Levees are clearly recognisable from all CLS by the characteristic tapering of the levee away from the channel axis, with individual reflections within levee packages showing downlap onto a basal surface (Fig. 4.6b).

4.4.3.2 Mass transport deposits (MTDs):

Mass transport deposits (MTDs) are a common element of the syn-kinematic sequence (e.g. Fig. 4.4). They are easily recognisable as units of generally low amplitude, chaotic seismic character in contrast to the higher amplitude and more continuous channel sequences which often incise into them (Fig. 4.6). Three major MTDs can be identified and traced throughout the hanging wall of the Aga fold. These units exhibit a number of key characteristics widely recognised within these types of deposit (e.g. Frey-Martinez et al., 2005; Bull et al., 2008):

1. Basal grooves are common and consist of linear erosional scours incised into the detachment surface of each MTD (Fig. 4.7).

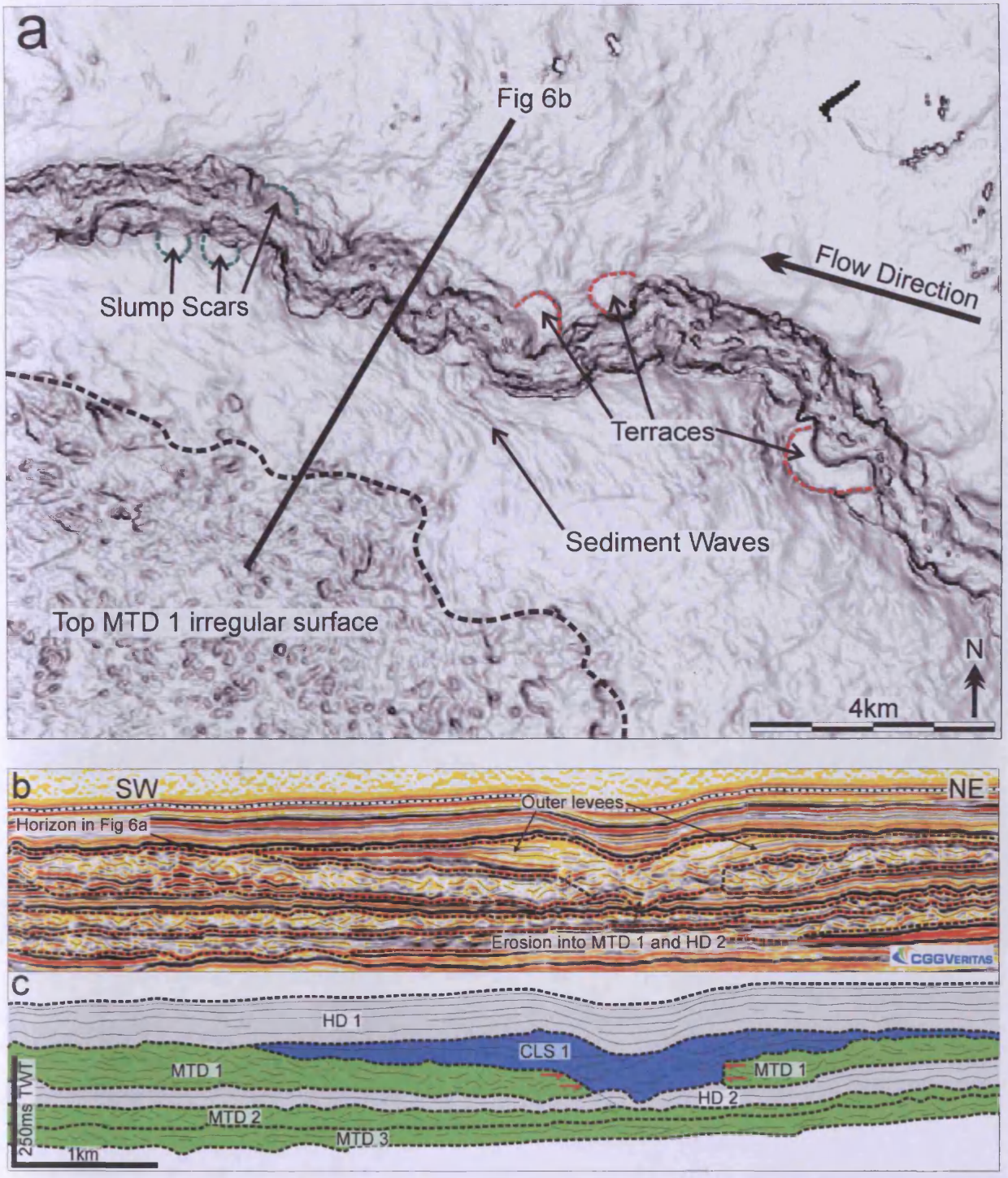

Figure 4.6: **4.6a** shows a dip attribute map of the upper surface of CLS 1. Key features include a sinuous channel axis, terraces formed by abandoned meander loops and slump scars formed by collapse of the channel sidewalls. Sediment waves orthogonal to the channel axis are also apparent on the channel levees. **4.6b** shows a seismic line through CLS 1 illustrating some key CLS features including channel levees, internal levees/terraces and the channel axis which incises into the underlying deposits. **4.6c** shows interpreted depositional units which make up the seismic section shown in **4.6b**.

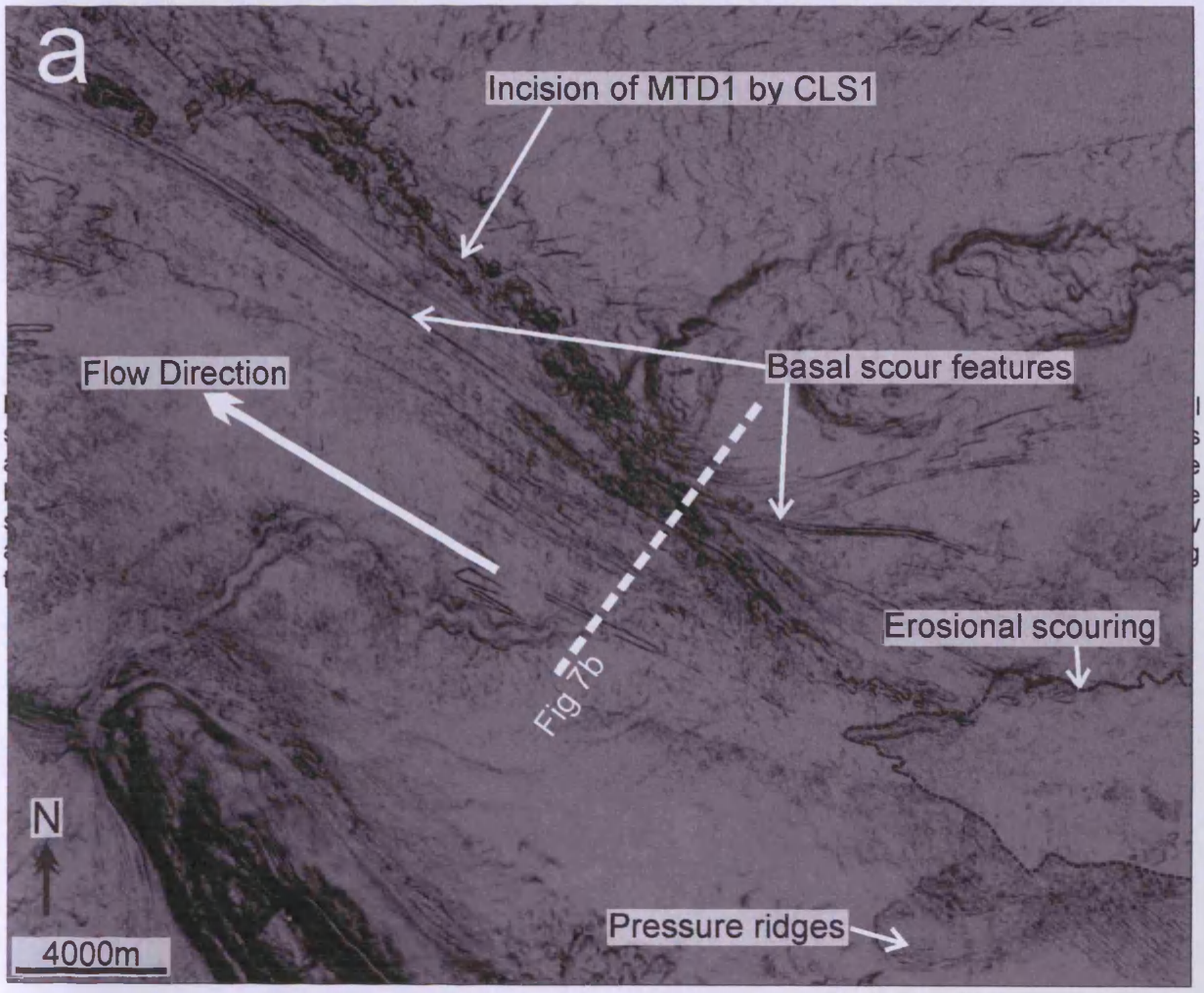
a
Incision of MTD1 by CLS1
Flow Direction
Basal scour features
Fig 7b
Erosional scouring
N
4000m
Pressure ridges

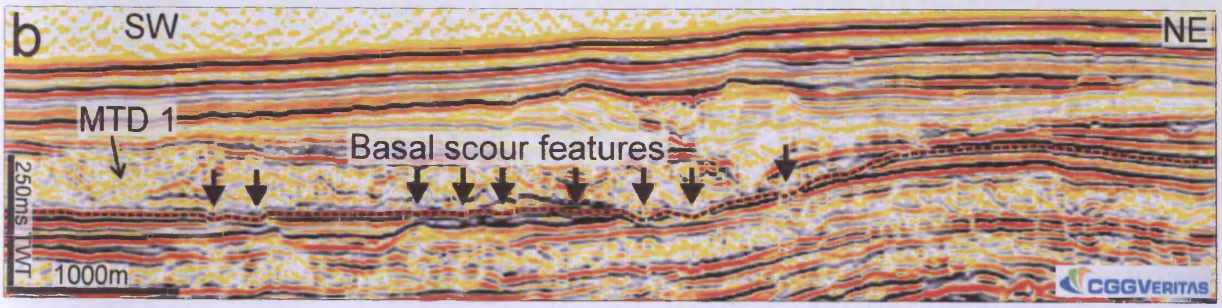
b
SW
NE
MTD 1
Basal scour features
250ms TWT
1000m
CGGVERITAS

2. Step-like erosional depressions also occur, and are often infilled by material of similar seismic character to the surrounding MTD. These depressions have very sharp lateral boundaries and are rectangular in cross section (See MTD 2 described later)
3. Compression ridges and thrusting are also observed at the base and at the top of several MTDs, these features provide useful kinematic indicators for the direction of transport (Bull et al., 2009, also Fig. 4.7).

All of the MTDs identified in this study extend outside of the area of data coverage, both in an upslope and downslope direction, and are assumed to be sourced from the east of the survey area according to the orientation of features such as the prominent basal grooves and also features such as pressure ridges (Fig. 4.7). Within the upper syn-kinematic sequence there is a clear and predictable stratigraphic relationship between MTDs and the CLS where in all cases, channel systems tend to incise into a previously deposited MTD. It is unclear from this dataset alone whether this represents cyclic deposition or whether the relationship is coincidental simply arising because the MTD and CLS represent the most common depositional products within this part of the slope sequence.

4.4.3.3 Hemipelagic drape deposits (HDs):

These deposits possess a seismic facies comprised of high amplitude, continuous reflections that can often be traced across the whole study area. Reflections making up this sequence typically exhibit configurations that passively drape onto the previous topography of the underlying unit (Brown and Fisher, 1977). Some thickness variations do occur within this unit however, and it is possible that this unit has been modified by bottom current activity in some areas, with reflection configurations and planform topography reminiscent of contourite drift deposits identified on 3D seismic elsewhere (c.f. Knutz and Cartwright, 2003). One such area can be seen on the present day seafloor (Fig. 4.1c – north-west fold tip area). Here, bottom current activity seems to have scoured a depression (moat) around the NW edge of the Aga fold.

4.4.4 Stacking patterns within the upper growth sequence and the effects of fold uplift on deposition

This section describes in chronological sequence the influence of fold development on the deposition of the most recent architectural elements of the upper growth sequence. We also highlight some of the characteristic relationships that reveal the interactions between fold-

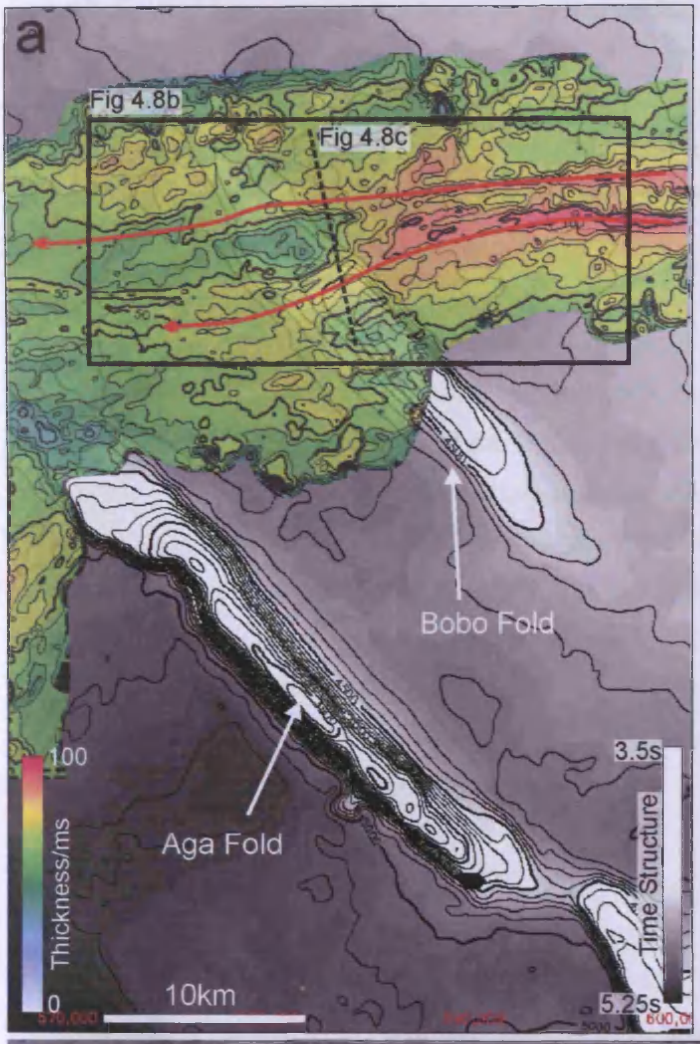

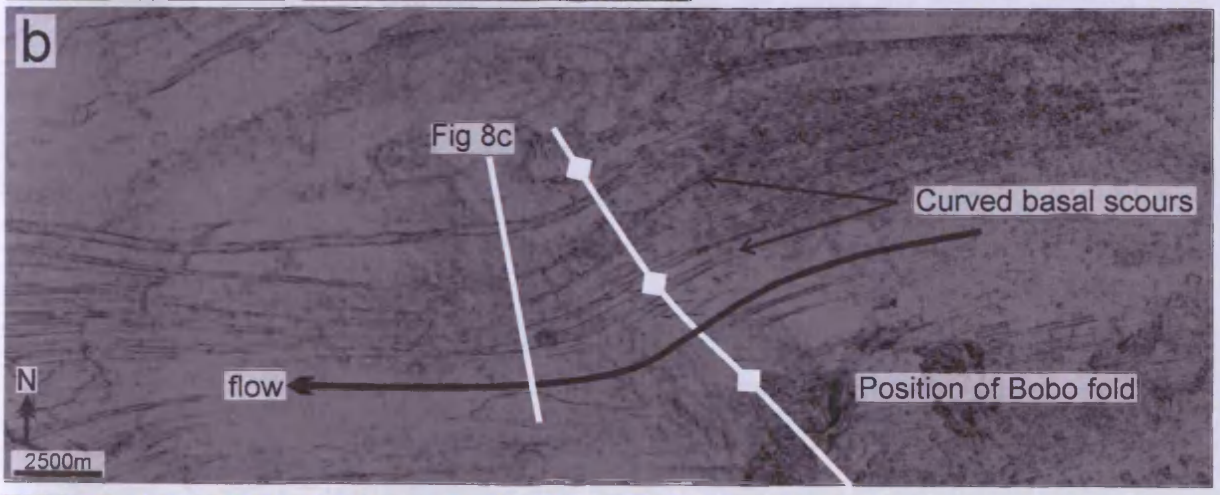

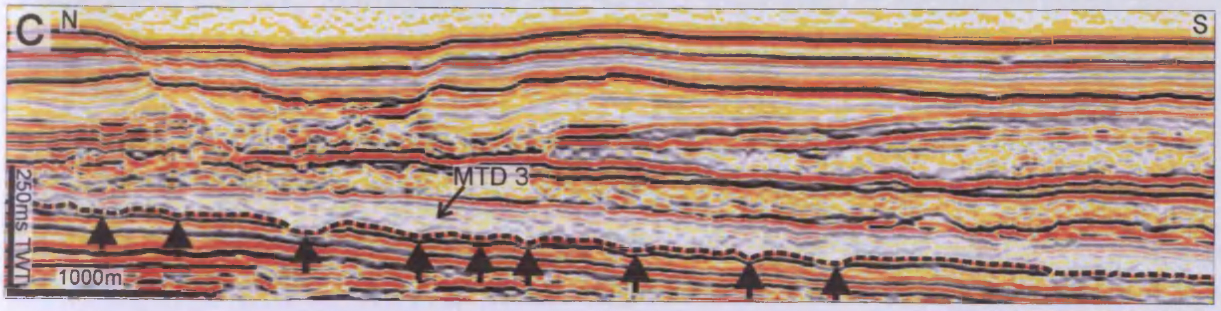

Figure 4.8: **4.8a** shows a simplified isochron map of MTD 3, and illustrates its strongly east to west component of flow. The zones of increased thickness seen in this deposit correlate strongly to the prominent basal scours seen on the coherence image in **4.8b**. These scours show a change in orientation as they cross the position of the Bobo fold and this is interpreted to be as a result of subtle fold topography influencing the depositional pathway of MTD 3.

controlled topography and deposition. These relationships include deflection of the basal scours of MTDs, and changes in submarine channel morphology in response to uplift of the Aga fold. The original isochron maps from which these interpretations are drawn are presented at the end of this thesis in Appendix A2.

At the base of the mapped interval within the upper growth sequence, MTD 3 exhibits an east-west oriented thickness trend, with the thickest portions of the deposit concentrated above a set of prominent basal scour features at the base of this deposit, these scours are up to 500m wide and 20m deep (Fig. 4.8). The orientation of these scours and the thickness distribution of the overlying deposit indicate that MTD 3 was sourced from the east, outside of the study area. Importantly, the prominent scours imaged on the basal surface of this MTD show a change in orientation on crossing the subtle relief due to the Bobo fold (Fig. 4.8). This highlights a potential use of recognising basal scour features associated with MTDs in revealing subtle variations in topography over which the flow passed. MTD 3 tapers towards its southern margin, where erosion by CLS 3 has partially removed material.

CLS 3 lies stratigraphically above MTD3, which is incised by this channel in some areas (Fig. 4.9). The pathway of this channel within the hangingwall of the Aga fold is controlled by the southwards thinning and pinch out of MTD3 (Fig. 4.9), and thus provides a good example of a compensational relationship between channel positioning and pinch out of an underlying MTD deposit. This channel also exhibits a clear example of a diversion related to fold-controlled topography as it passes around the north-west lateral tip of the Aga fold (see also Clark and Cartwright 2009). Diversion of this channel shows no significant change in sinuosity as CLS 3 passes from the hangingwall to the footwall (Fig. 4.9c) possibly suggesting little change in gradient upon passing from the hangingwall to the footwall (see also Ferry et al 2005). The only change in channel morphology associated with this transition is a thickening of the channel levee deposits and deposition of a high amplitude, sheet like deposit beginning at the forelimb to footwall transition (Fig. 4.9c). This channel system has also suffered significant erosion in the north-east where it enters the survey area by the overlying MTD 2, with erosion appearing to preferentially remove the channel levees (Fig. 4.9b). Preservation of the channel levees within the forelimb may be a result of the decreased thickness of the overlying MTD 2 in this area.

The distribution of MTD 2 is much more extensive compared to MTD 3 and shows a general thinning to the north of the survey area, with this deposit being sourced from the east of the study area with the direction of transport being westwards, as indicated by the thickness trends seen within this unit (Fig. 4.10). There are several key controls on the deposition of MTD 2. Firstly, relief resulting from aggradation of the channel levees deposited by CLS 3 results in run-

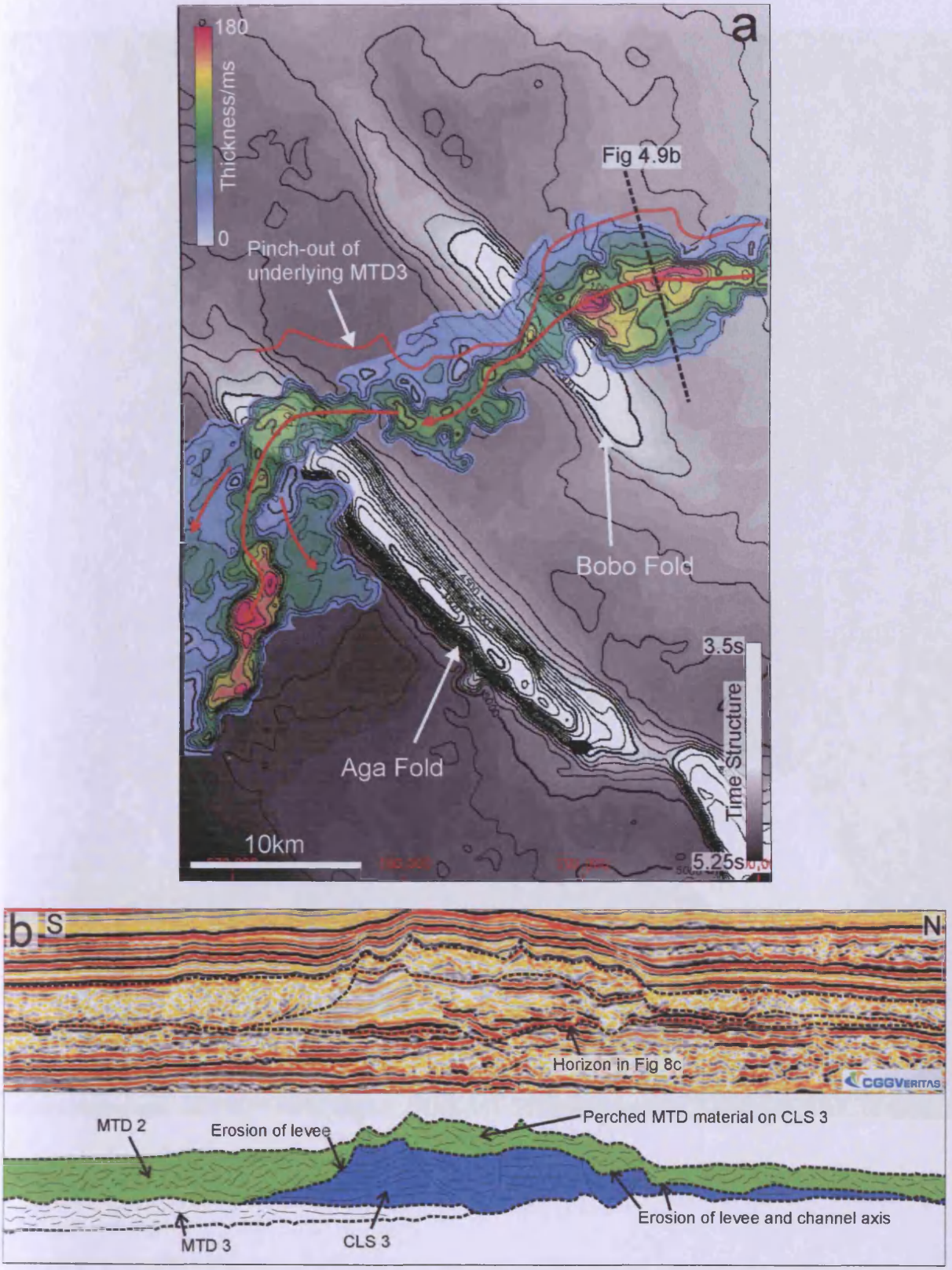

Figure 4.9: The isochron map of CLS 3 seen in **4.9a** has been extensively modified by erosion caused by the overlying MTD 2. Erosion by MTD 2 has resulted in removal of significant volumes of levee material and also formation of positive relief caused by 'perched' MTD material on top of CLS 3, this can clearly be seen in **4.9b**. Figure **4.9c** (next page) shows an amplitude map of the base CLS 3 surface. This highly sinuous nature of the channel can be seen as well as the change in depositional style of the earliest channel deposits upon crossing into the foot wall.

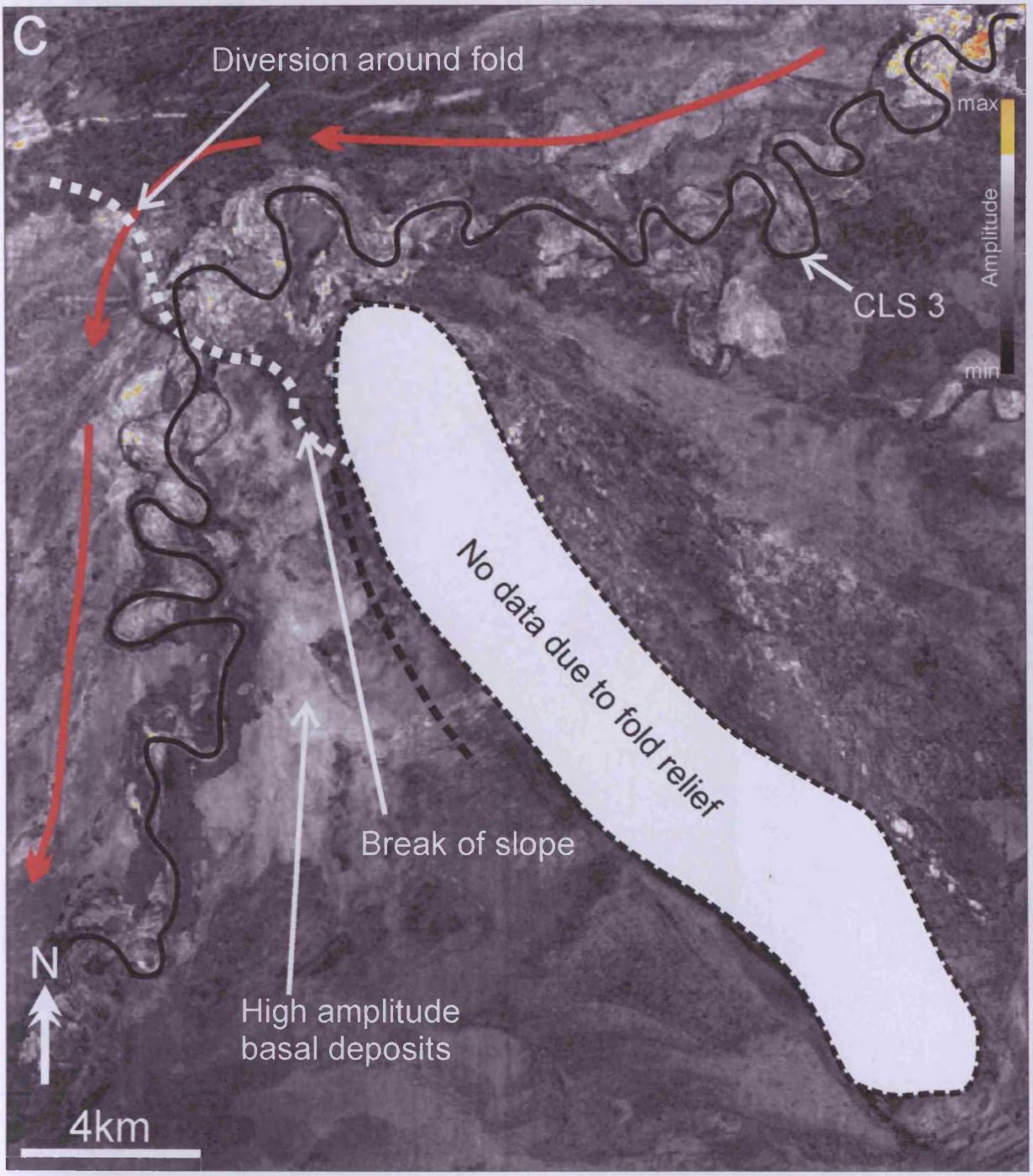
C
Diversion around fold
max
Amplitude
min
CLS 3
No data due to fold relief
Break of slope
N
High amplitude
basal deposits
4km

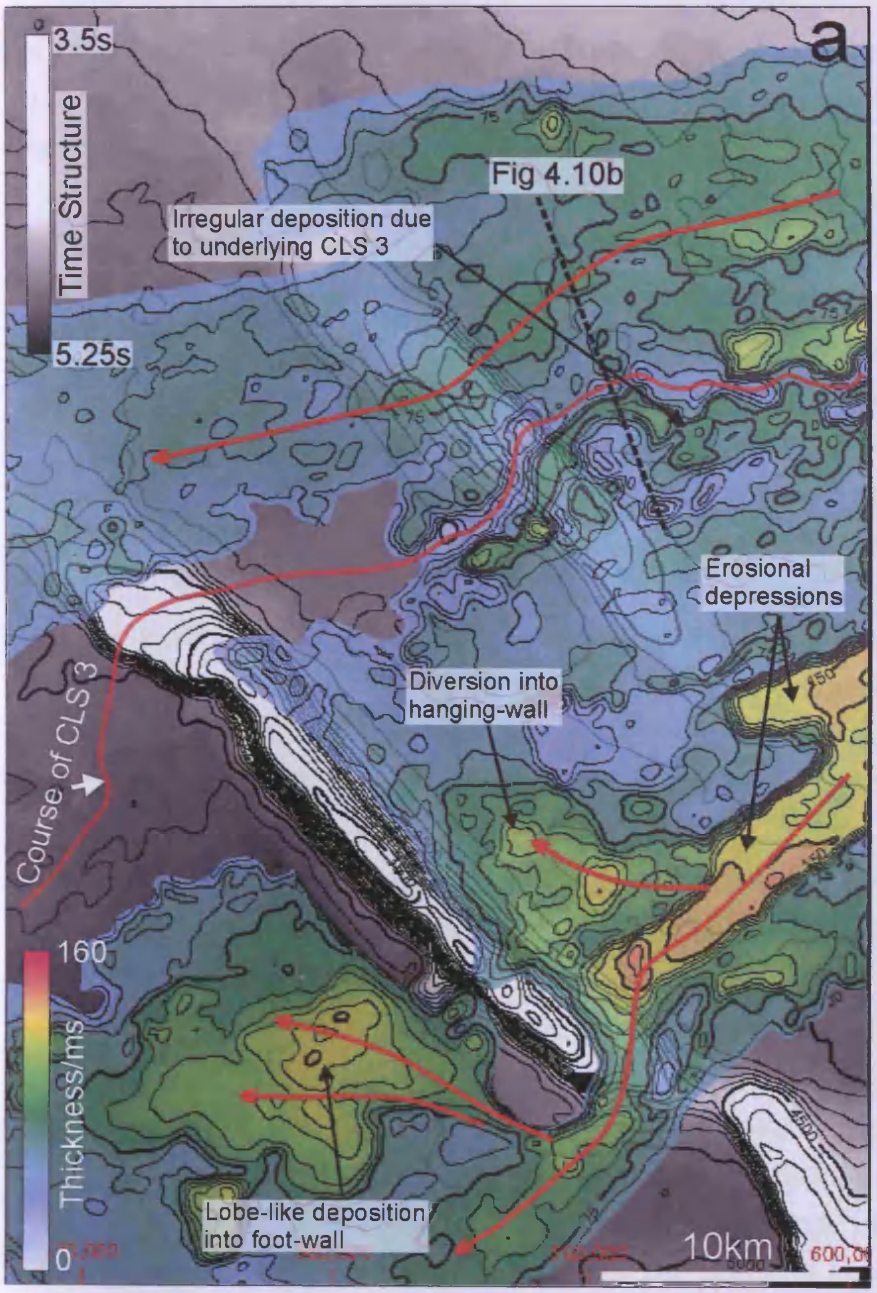

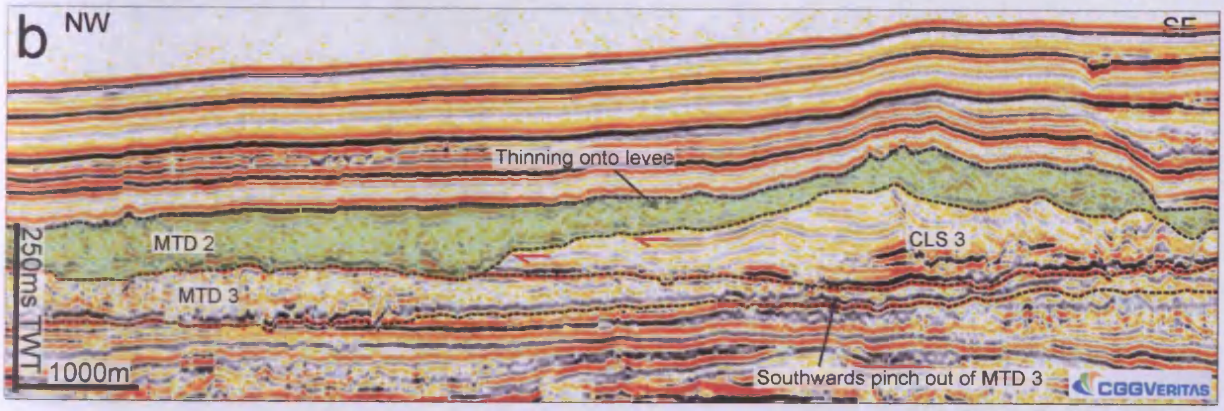

Figure 4.10: **4.10a** shows an isochron map of MTD 2. This deposit is concentrated around the south-east fold tip region where diversion is observed into the hanging wall and into the footwall. Diversion of material into the footwall results in a lobe-like depositional geometry of the MTD in this area as it responds to the available accommodation space within this area. 10b demonstrates the compensational relationship between levee relief and overlying MTD deposition where MTD material thins against the underlying channel levee. Perched MTD material can still be seen on this section, see also Fig. **4.10b** for comparison.

up relationships where the material from MTD 2 thins against the wedge shaped levees which obstruct deposition (Fig. 4.10b). In the north-east of the survey area, MTD 2 has resulted in significant erosion of the channel levees of CLS 3, leaving only the channel axis preserved (Fig. 4.10b). Erosion of the underlying channel system is concentrated in the north-east where MTD2 enters the survey area. The isochron map of CLS 3 shows that the channel levees have been removed during emplacement of MTD 2, particularly on the southern margin of the channel where MTD 2 increases in thickness (Fig. 4.10a). The second control on the distribution of MTD 2 is the relief of the Aga fold and its primary role in shaping the accommodation space upslope and in obstructing the down-slope flow pathway of this deposit (Smith et al., 2004; Prather et al., 2003; Beaubouef and Friedmann, 2000). This results in thinning of the MTD against the backlimb and diversion of material around the south-east lateral tip of the fold (Fig. 4.10). In this area deposition of MTD 2 within the footwall resulted in the formation of a lobe like deposit which infilled negative relief within the footwall of the Aga fold (Fig. 4.10a). Basal grooves are also observed to be diverted around the lateral hinge and diverge within the footwall. This echoes the relationship already noted for MTD3, whereby basal grooves carry important directional information that reveals subtle gradient changes (Bull et al., 2008).

Following the emplacement of MTD 2, a small scale channel-levee system – CLS 2 was deposited (Fig. 4.11) that is up to 500m in width with the channel axis being no more than 50m deep. This channel system is sourced from the east and exhibits a clear diversion around the north-west lateral tip of the Aga fold. The levee distribution for CLS 2 is uniform within the backlimb of the Aga fold, with levee thickness and lateral extent approximately equal on each flank of the channel (Fig. 4.11a). Thickening of the channel and levee deposits is observed upon crossing from the forelimb to the footwall and is associated with a localised increase in channel migration in this area. See for example, the abandoned meander loop in Fig. 4.11b. The change in channel morphology is located at the transition from forelimb to footwall, in a similar manner to that previously observed for CLS 3.

The deposition of CLS 2 was followed by a hemipelagic interval (unit HD 2, Fig. 4.5). This unit shows no systematic thickness variations due to structural growth but some material has been eroded by MTD 1 which overlies this interval.

Deposition of MTD 1 was influenced by both the Aga and Bobo folds, as can be seen from the thinning of this deposit against the backlimb of the Aga fold and against the forelimb of the reactivated Bobo fold (Fig. 4.12). Basal grooves are also present at the base of this deposit (Fig. 4.6a) and, combined with the isochron map show that MTD1 was sourced from the east with deposition being confined entirely to the hangingwall of the Aga fold. The basal grooves of

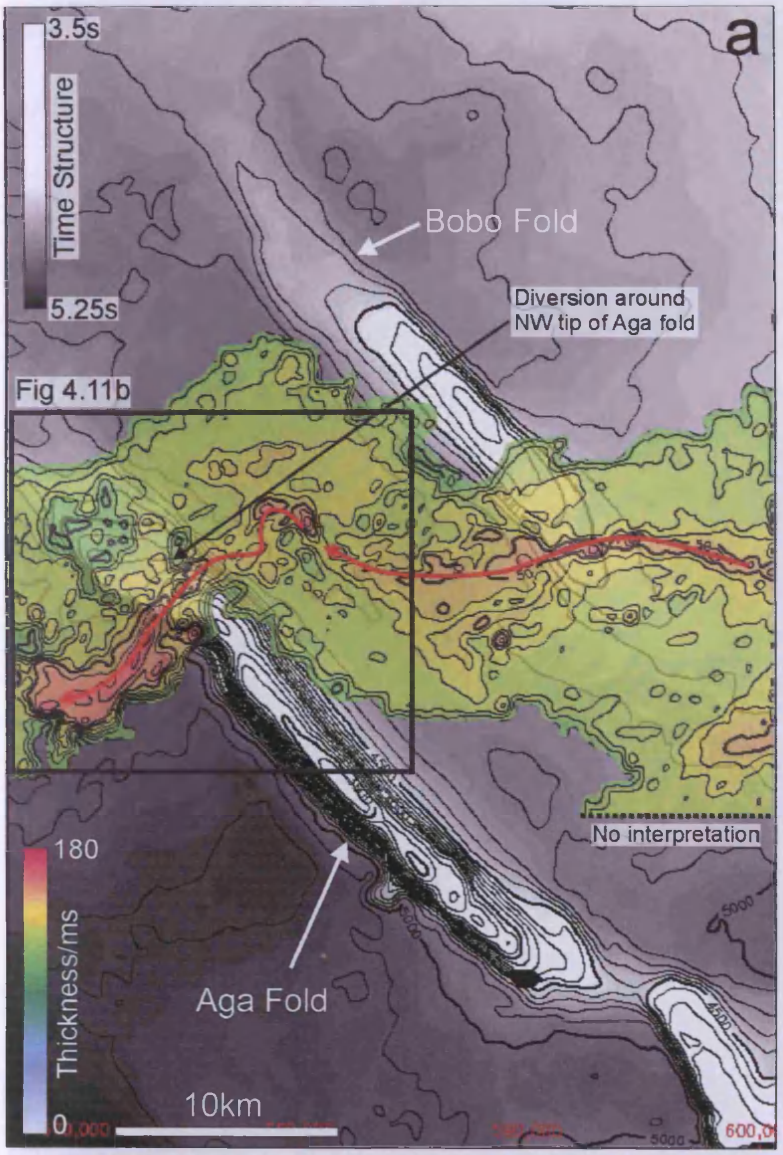

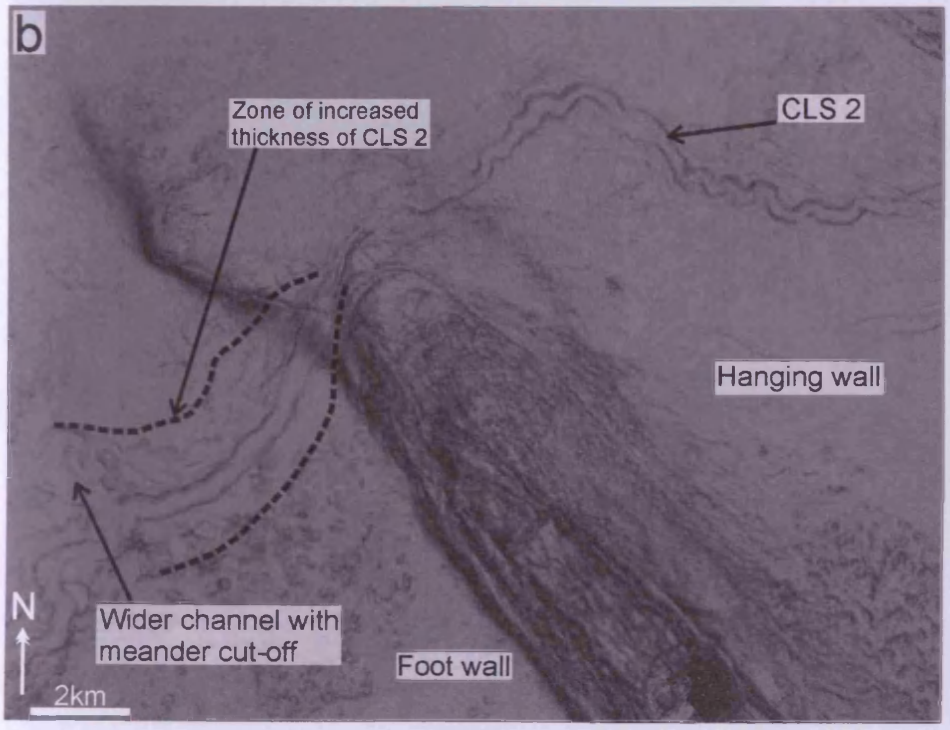

Figure 4.11: **4.11a** shows the isochron for this channel interval. The channel levees are symmetrical about the channel axis in plan view within the hanging wall. As the channel is diverted around the NW fold edge, levee distribution becomes asymmetric due to the confining effect of fold relief. Also apparent is the increase in thickness of the channel deposits within the footwall, immediately down-dip from the forelimb to footwall break of slope. The change in channel morphology is emphasised in 10b, which shows a coherence slice flattened to the top of CLS 2. In this image, the channel shows increased lateral migration limited to the footwall area, with the formation of an abandoned meander loop labelled in Fig. **4.11b**.

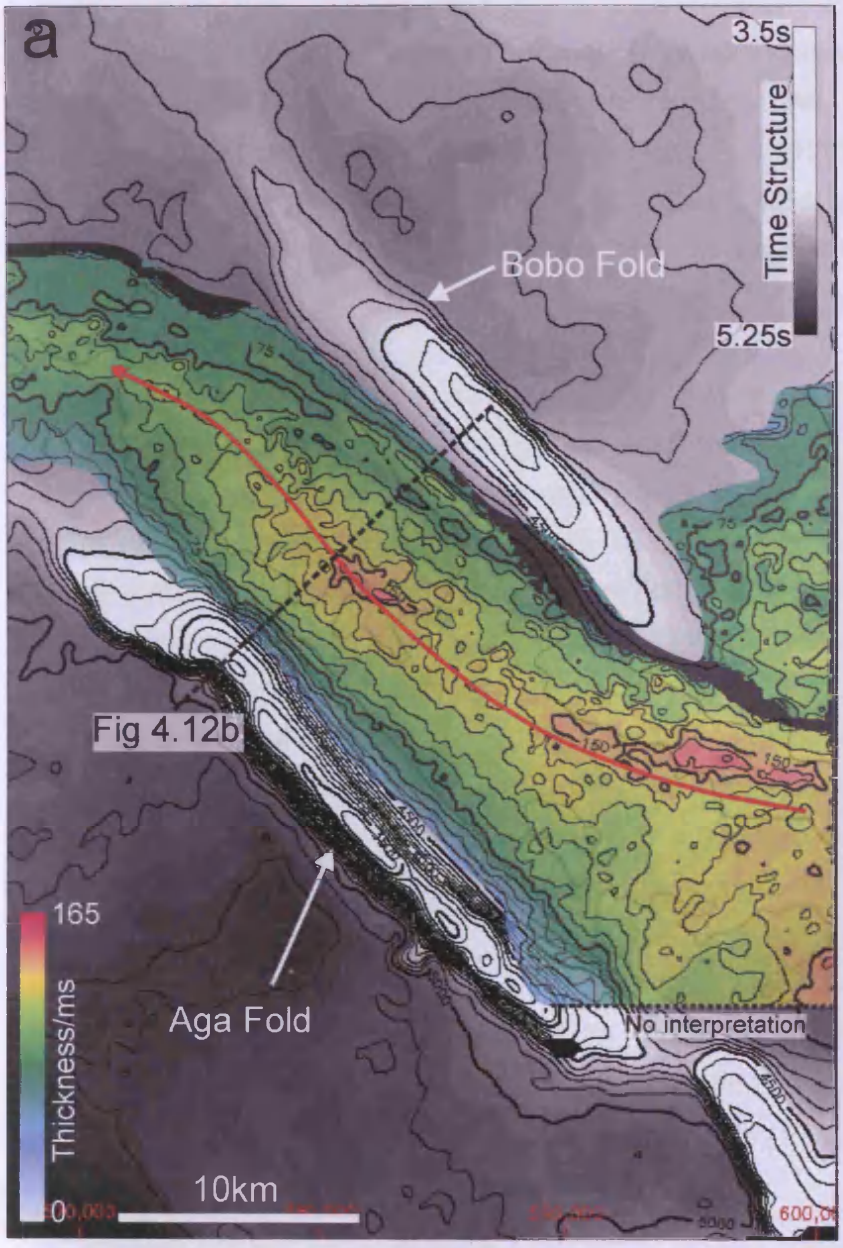

Figure 4.12: The isochron map of MTD 1 in **4.12a** shows a strong south-east to north-west orientation in deposition due to confinement of this deposit against the backlimb of the Aga fold and the forelimb of the reactivated Bobo fold. **4.12b** shows a seismic line which further illustrates the confined nature of this MTD deposit. Note the location of the overlying channel levee system (CLS 1), the axis of which is located between the pinch out of MTD 1 and the axis of uplift of the Bobo fold.

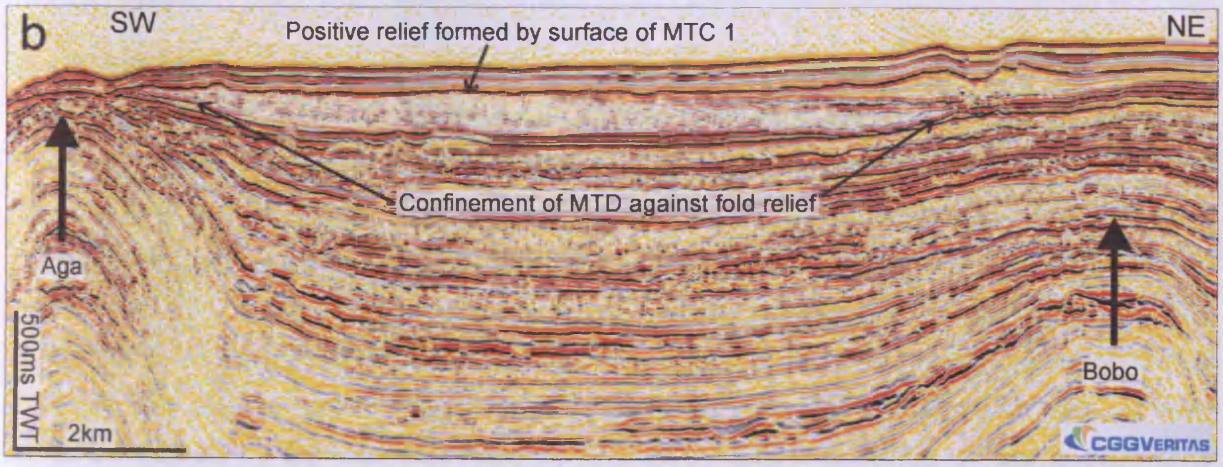

MTD 1 show convergent and divergent relationships in response to the relief present at the time of deposition by the forelimb of the Bobo fold, which has resulted in confinement of this deposit into the accommodation space between the two folds (Fig. 4.12b). MTD 1 is entirely confined within the hangingwall of the Aga fold and cannot be traced into the footwall (Fig. 4.12a), indicating that the seafloor relief prior to deposition was sufficient to confine MTD 1 within the hangingwall.

The isochron map of CLS1, the most recent channel system, shows that the levees are evenly distributed on either side of the channel axis but that the overall thickness of this system and the lateral extent of the levees decreases towards the west (Fig. 4.13). The positioning of this channel within the study area is related to the northwards thinning and pinch-out of the underlying MTD 1 unit to the south-west and the Bobo fold towards the north east. Late stage of uplift of the Bobo fold is shown by tilted levee relationships seen along this channel (Fig. 4.13b). Despite tilting of the channel levees caused by uplift of the Bobo fold, the lowermost levee reflections onlap the fold, demonstrating that fold-controlled relief controlled the course of CLS 1 early on in its development. Relatively rapid subsequent sedimentation due to levee deposition then resulted in overlap of the fold crest. This was followed by a phase of renewed uplift resulting in the folded levee geometry observed in Figure 4.13b.

The final and youngest stratigraphic unit (HD1) is composed mainly of parallel –reflections that drape the relief of the underlying channel levee system (Fig. 4.4a). Within the forelimb of the Aga fold, the extensive degradation resulted in local mass wasting deposits which are intercalated with the draping facies (Fig. 4.3).

4.5 Discussion

The detailed description of the architectural elements comprising the upper growth sequence illustrates a number of key processes regarding the interaction between structurally controlled topography and depositional processes and products. These include the three dimensional stacking of individual architectural elements comprising growth sequence and also the more detailed interactions between deposition of these units and structurally induced relief present at the time of deposition. These generic themes are observable on similar folds in many deepwater fold belts, or indeed within inverted rift systems (Cartwright, 1989) or foreland basins (Burbank and Verges, 1994). These themes are discussed further below, in an effort to draw some wider conclusions that may help in predictive studies in areas of active deepwater exploration.

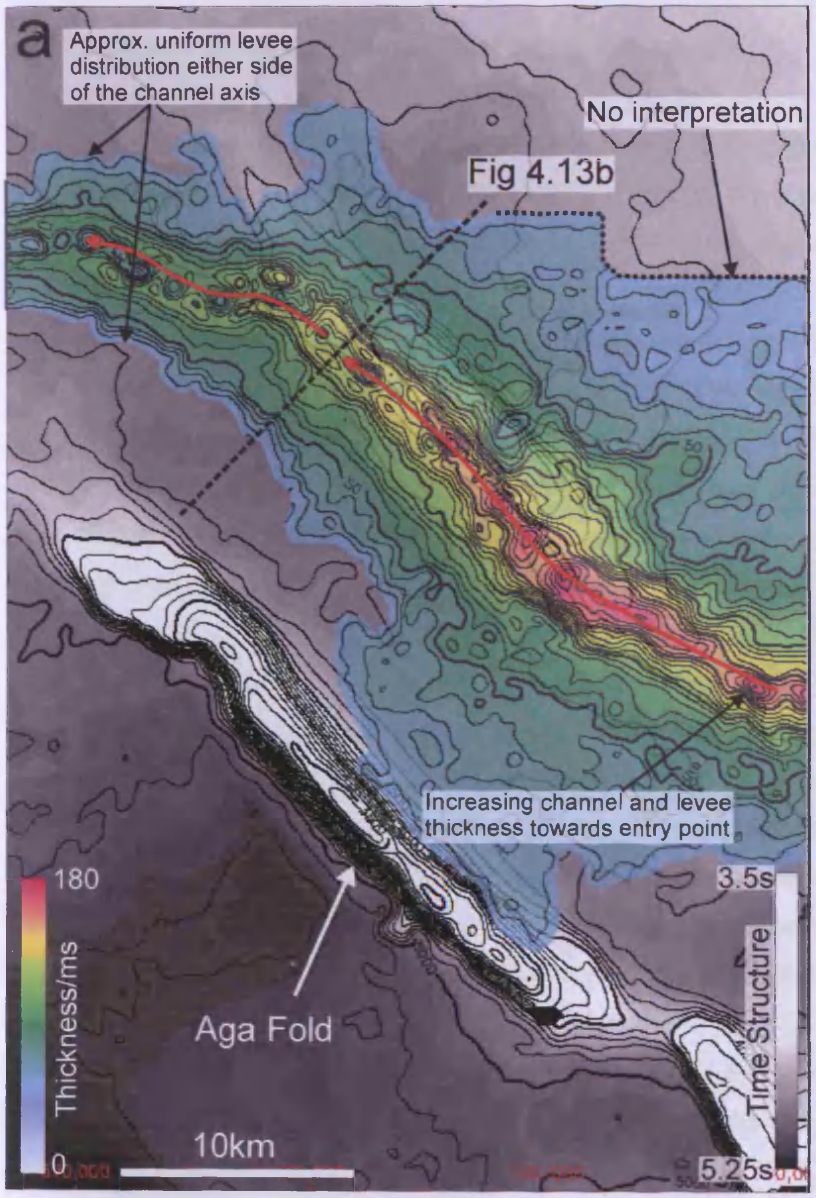

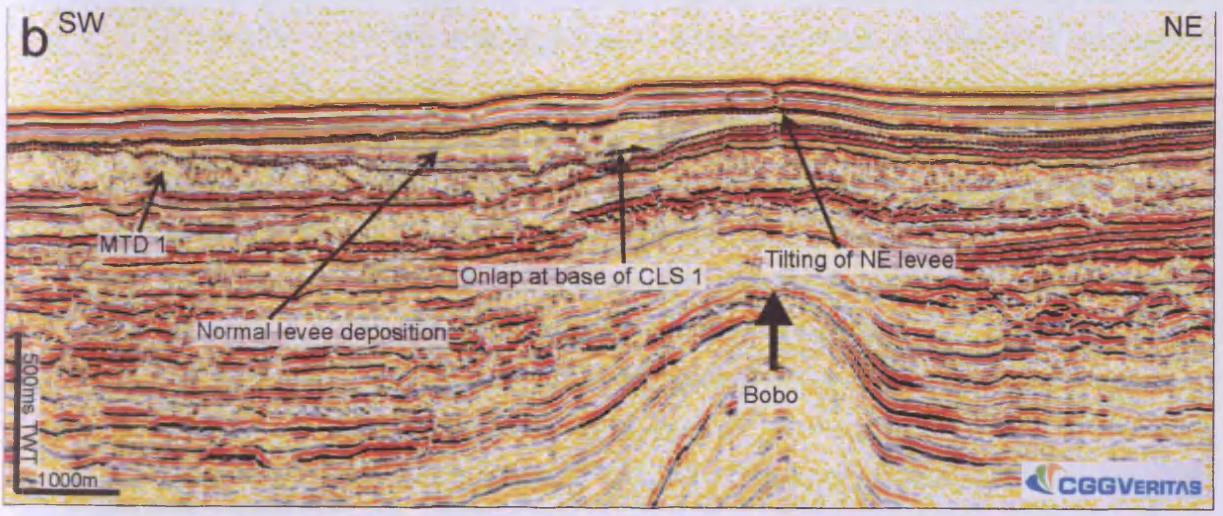

Figure 4.13: **4.13a** shows the isochron of CLS 1 showing a uniform levee distribution about the channel axis. The levees and channel fill thicken towards the source direction, indicating that this channel was backfilled during the latest stage of its deposition. **4.13b** shows that reactivation of the Bobo fold has uplifted the north-east channel levee, resulting in a unique levee geometry compared to the south-west channel levee which is undeformed.

4.5.1 Development of bathymetric relief during fold growth

Considerable insights into relief development during folding can be obtained when analysing growth folds, by comparing the central most highly deformed region with the lateral tips of the structure. At the lateral tip regions of the Aga fold, for example, the observed pattern of thinning of the upper growth sequence across the fold crest and lack of onlap against the backlimb suggest that no opposing slope was developed in these areas to block sediment transport into the footwall (c.f. Burbank and Verges, 1994; Burbank et al., 1996). This is in contrast to the central area of the fold, where the upper growth sequence onlaps the backlimb of the Aga fold, indicating that the fold formed positive seafloor relief resulting in a barrier to flow across this area of the fold (Fig. 4.2). Although no opposing slope developed at the lateral tip regions during deposition of the upper growth sequence, an overall basinwards dipping slope was maintained during uplift – as can also be seen on the present day seafloor (Fig. 4.1c).

Evidence that a basinward dipping slope was maintained during fold growth at the forelimb to footwall transition can be seen in the subsurface where CLS 2 and CLS 3 are diverted around the north-west lateral hinge (Figs. 4.9 and 4.11). Thickening of CLS 2 occurs as it is diverted around the Aga fold, resulting in increased deposition localised in the immediate footwall (Fig. 4.11). Another example of how the depositional style of channel levee systems changes at the forelimb-footwall transition is shown by the amplitude map at the base of CLS 3 (Fig. 4.9c). This shows development of a fan-like feature characterised by high seismic amplitudes, located at the base of slope of the forelimb-footwall transition. CLS 3 also shows an increase in overall channel deposit thickness within the footwall and slight ponding of the left hand levee against the forelimb (Fig. 4.9). These observations suggest that:

1. At the scale of individual flow events, there is a change in flow character at the backlimb to forelimb transition caused by the decrease in slope. The decrease in slope at this transition point results in flows becoming increasingly depositional within the footwall. This could be a result of processes such as hydraulic jumps (Garcia, 1993) occurring as a response to the change in gradient from the steep forelimb to the reduced slope of the footwall.
2. At the larger scale of slope architectural elements, the increased deposition within the footwall may be caused by the local perturbation in the base level of the channel profile due to folding. The channel response to this local lowering of gradient is to aggrade within the forelimb of the fold in order to reach its hypothetical equilibrium profile (Pirmez et al., 2000; Ferry et al., 2004).

At the lateral tips of the Aga fold, the relief resulting from fold growth did not create an opposing slope to block sedimentation around the fold. The curvature seen within the upslope limb close to the lateral tip regions reflects progressive rotation during uplift towards the base of the sequence during sedimentation, and not actual fold relief expressed on the seafloor (Fig. 4.5). An estimate can be obtained of the magnitude of uplift which has occurred during deposition of the upper growth sequence by taking the change in thickness of the upper growth sequence across the fold crest at the lateral tip regions of the Aga fold (see Masaferro et al., 2002 for more detail). Using an average interval velocity of $2000ms^{-1}$, the upper growth sequence records approximately 430m of uplift at the lateral tips of the Aga fold. This compares to at least 1000m of cumulative positive relief being developed towards the central area of the fold over the same interval. Note that due to the increasing occurrence of onlap towards the central portion of the Aga fold, this estimate only provides a minimum value for fold relief in this area.

Evidence of low slope gradients during submarine channel deposition can be assessed based on observations of channel morphology. Large scale sinuosity variations of submarine channel systems down-slope have been documented by Clark et al. (1992), Pirmez and Imran (2003) and Babbonneau et al. (2002). Submarine channel systems also exhibit localised morphological variations in response to varying slope gradients (Ferry et al., 2004; Huyghe et al., 2004; Gee and Gawthorpe, 2006), these responses can be summarised as:

- Increases in slope gradient result in localised increased channel incision, often associated with a decrease in sinuosity.
- Decreases in slope gradient result in localised channel aggradation, corresponding to a local increase in sinuosity.

There is also some evidence that highly sinuous submarine channels only occur where the underlying slope gradient is below a certain threshold value. Clark et al. (1992) also have shown that sediment calibre of the flows forming submarine channel systems also play a key role in determining the maximum sinuosity for a variety of given slope values. Babbonneau et al. (2002) suggested that a slope value of 0.3° acts as the threshold value for the Zaire and Amazon systems. Whilst it is not known whether this figure is generally applicable to all submarine channel systems, the implication is that wherever highly sinuous submarine channels occur, it will be in association with a certain underlying slope gradient for a given series of flows with particular characteristics in terms of sediment calibre. CLS 2 displays high sinuosity along its length throughout the study area, despite being diverted around the NW lateral hinge of the fold (Fig. 4.10). The high sinuosity of this system is evidence that low gradients (possibly below 0.5°) were present at the seafloor despite active uplift of the Aga fold during deposition of the upper growth sequence. These low seafloor gradients implied by

submarine channel morphology reflect a rapid relative rate of sedimentation compared to uplift at the fold lateral tip. This is not surprising: the lateral tip regions are often the preferential flow pathways around the fold, and a laterally increasing sedimentation rate is thus to be expected. This is in turn controlled by lateral variations in the structural style of the fold along strike, and in particular by the way in which fold relief varies along strike, which can be affected by factors such as synthetic and antithetic thrust fault linkages (Higgins et al., 2007). Other examples of the strong control exerted by changes in gradient around a fold which diverts submarine channels is presented in Chapter 5 – see section 5.5.4.

Analysis of isochron data for individual architectural elements which make up the upper growth sequence shows that development of sufficient fold relief to block deposition into the footwall only occurred after, or during, the deposition of unit HD2 (Compare Figs. 4.10 and 4.12). Deposition of MTD 1 is not associated with any overspill of sediment into the footwall due to the backlimb of the Aga fold forming an obstacle to flow against which MTD 1 terminates along its south west margin (Fig. 4.12). Deposition of MTD 1 was also affected by a late stage reactivation of the Bobo fold, which caused partial confinement of this deposit and diversion of the basal grooves around the edges of the topography created by reactivation of this fold. This reactivation is a relatively late stage event in the development of the upper growth sequence and is associated with a shift in the direction of sedimentation from being fold-perpendicular (MTDs 3 and 2 and CLSs 3 and 2) to fold parallel (MTD 4.1 and CLS 4.1). Based on this information a two phase model of growth sequence development can be described (Fig. 4.14):

1. The first phase of growth sequence development (Fig. 4.14a-d) involves a significant element of deposition that is perpendicular to the strike of the fold. This can be seen where CLSs 3 and 2 are diverted around the NW fold edge, and MTD 2 is diverted around the SE lateral hinge to deposit within the forelimb. During this phase of deposition, only the central area of the fold presented an obstruction to flow.
2. The second phase of deposition (Fig. 4.14e and f) was preceded by uplift of the Aga fold and also by reactivation of the Bobo fold. Following this renewed period of uplift, the deposition of MTD 1 and CLS 1 do not show diversion around the fold tips and are confined to the upslope limb of the Aga fold.

This change in the sediment distribution pathways from fold-perpendicular to fold-parallel results from increased relative uplift rates compared to sedimentation, which may be the result of an increase in the rate of shortening and uplift causing rapid development of positive relief, or alternatively a decrease in sediment volume input into hangingwall of the Aga fold. With lack of chronostratigraphic information and the limited coverage of this 3D dataset, it cannot be

determined which of these two mechanisms is responsible for the change in sedimentation patterns over time.

4.5.2 Three dimensional growth sequence architecture and implications for reservoir development.

From the observations presented above, we suggest that the three-dimensional stacking relationships seen within the upper growth sequence are controlled primarily by two factors:

1. Compensational relationships within the hangingwall area upslope of the zone affected by fold relief. Here, deposition of each successive unit is affected partly by the topography resulting from the previous deposit.
2. The relief generated by the Aga fold which results in ponding and onlap of deposits onto the backlimb and diversion of sedimentation around the fold lateral tips resulting in overlap.

Compensational relief is largely generated by the deposition of MTD units and also results to some extent from the positive relief constructed during deposition of channel levees. The location of CLS 3 within the hanging wall occurs at the southward pinch out of the underlying MTD 3 (Fig. 4.9). Thus the relief generated by the previous MTD deposit has also influenced this channels course in addition to the effect of the Aga fold whose structurally induced relief results in channel diversion around the north-west lateral hinge. The effect of compensational relief formed by a channel levee system within the hanging wall can also be seen where MTD 2 thins against the levees of CLS 3 (Fig. 4.10b). Overall, a shift in the locus of deposition towards the south of the study area is seen over the depositional interval represented by MTD 3 to MTD 2 (Figs. 4.14a-d). This is accompanied by southward shift in the input points into the study area.

This southwards shift in sedimentation within the hanging wall is also associated with a shift in sediment pathways around the fold edges. During deposition of MTD 3 and CLS 3 and 2, the north-west lateral hinge was the preferred flow pathway for sediment to deposit within the footwall. However deposition of MTD 2 was shifted to the south, due to compensational effects from the levee relief of CLS 3 and due to the southwards shift in the input point into the study area. MTD 2 utilises the south-east lateral tip, where diversion of material is seen around the hinge and is associated with lobe-like deposition of sediment within the forelimb (Fig. 4.10). Switching of the primary flow pathways between the north-west and the south-east fold lateral tips is related to the compensational stacking and southwards shift in deposition away from the north-west lateral tip of the Aga fold.

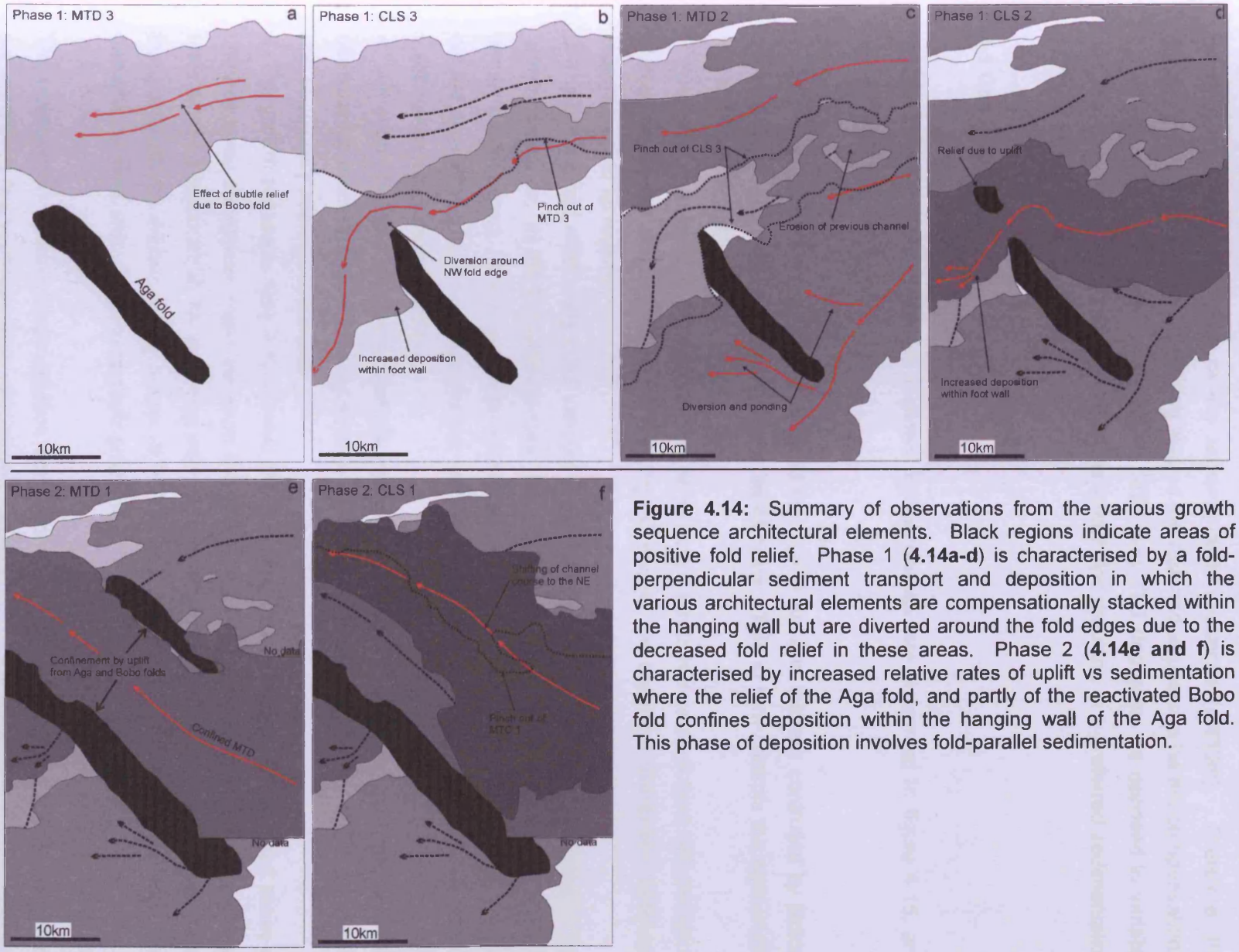

Figure 4.14: Summary of observations from the various growth sequence architectural elements. Black regions indicate areas of positive fold relief. Phase 1 (**4.14a-d**) is characterised by a fold-perpendicular sediment transport and deposition in which the various architectural elements are compensationally stacked within the hanging wall but are diverted around the fold edges due to the decreased fold relief in these areas. Phase 2 (**4.14e and f**) is characterised by increased relative rates of uplift vs sedimentation where the relief of the Aga fold, and partly of the reactivated Bobo fold confines deposition within the hanging wall of the Aga fold. This phase of deposition involves fold-parallel sedimentation.

The structural relief which developed during the upper growth sequence can be assessed by comparing the thickness change from the upslope limb to the fold crest. As discussed above, both of the fold lateral hinge regions show relatively equal amounts of structural relief development during deposition of the upper growth sequence (c.430m). Therefore, the dominant control on flow path switching around the Aga fold appears to be the compensational backfilling of the hangingwall by alternating MTD and CLS deposition as opposed to variable shortening and differences in fold relief at the lateral tips resulting in a preferred sedimentation pathway around the fold.

4.6 Conclusions

In conclusion, the central themes explored in this chapter are presented in figure 4.15, and summarised as follows:-.

1. Variations in structural style along strike of the Aga thrust and fold are controlled by factors such as shortening and the development of backthrusts. This in turn controls the style of the fold and its relief at the seafloor.
2. Fold relief developed at the seafloor and its evolution through time combined with the effect of compensational stacking within the hangingwall control the sediment distribution pathways around the fold tip regions.
3. The varying fold relief along strike controls the response seen in the stratal geometries of the growth sequence. At the fold lateral hinges, the growth sequence displays overlap and thinning across the fold crest, as well as erosional truncation of the underlying sequences. Across the central area of the fold, onlap against the fold limb results from an increased relative rate of uplift compared to sedimentation.
4. Although the fold geometry controls the accommodation space in the hanging wall, stratigraphic architectures are controlled by a combination of compensational stacking patterns and structurally confined deposition.
5. The growth sequence itself is comprised of a complex, three dimensionally stacked series of channel levee complexes, mass transport deposits and hemipelagic intervals. Many of these units exhibit a response to the emerging relief during fold growth which can be assessed using features such as scours at the bases of MTDs and changes in channel morphology and depositional style which respond to slope gradient.

The relationships between sedimentation and deformation documented in this case study are not specific to this particular area, and similar expressions of the interplay between tectonics

and sedimentation have been observed by us in many other deepwater fold belts. As such, we suggest that these examples may be used as a reference set to base more general exploration play models wherever a slope system is being actively deformed, as well as forming a basis for further work involving comparative studies of the interactions between sedimentation and deformation from separate deepwater fold belt settings.

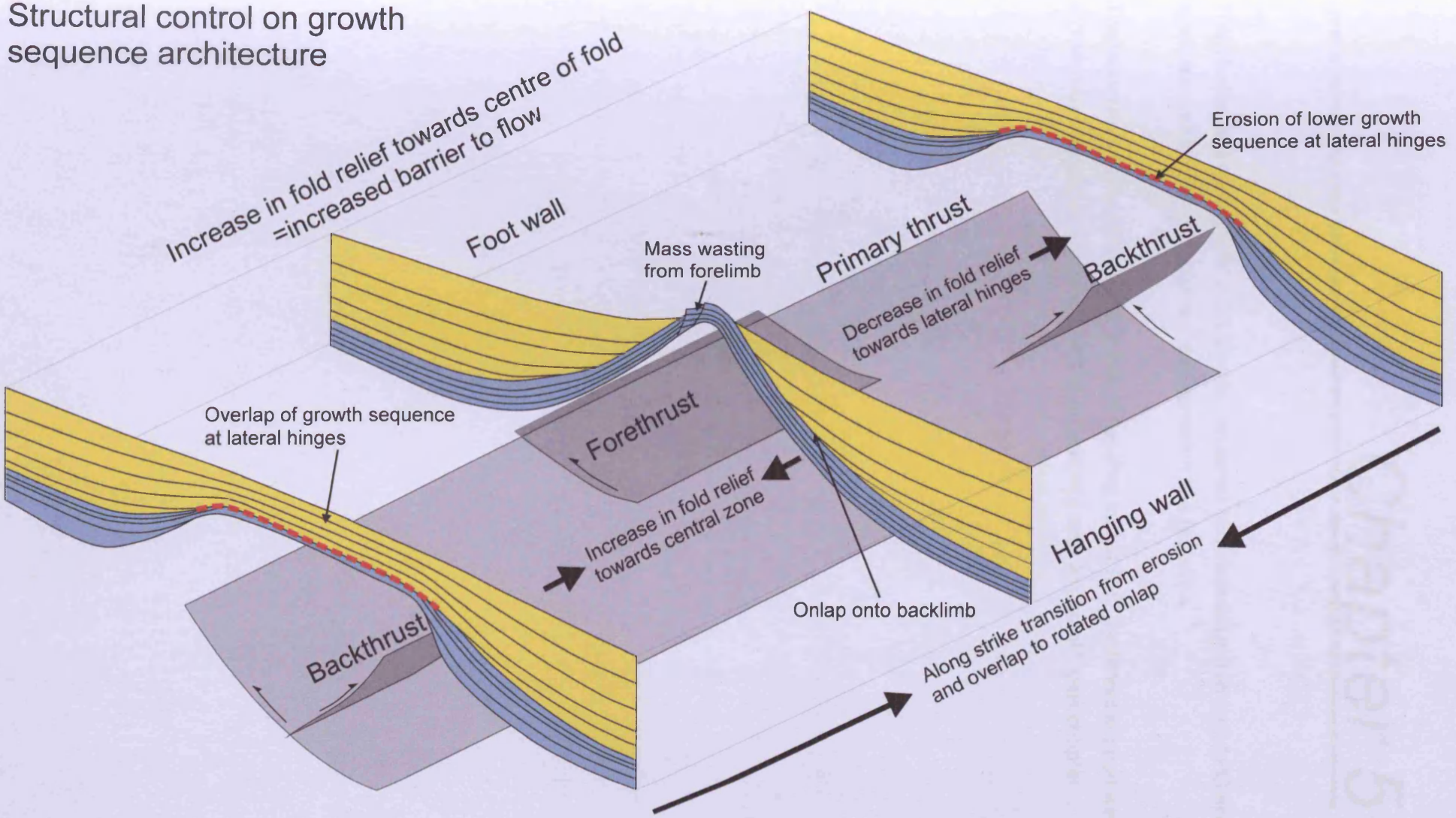

Figure 4.15: Conceptual model of the key factors affecting the evolution of the growth sequence in this study area.

Chapter 5

This chapter has been submitted to be peer reviewed and included within an AAPG special publication on interactions between sedimentation and tectonics.

The work presented in this chapter is that of the lead author (IRC), editorial support was provided by the project supervisor, JAC in accordance with a normal thesis chapter.

CHAPTER 5

A CASE STUDY OF THREE DIMENSIONAL FOLD AND GROWTH SEQUENCE DEVELOPMENT AND THE LINK TO SUBMARINE CHANNEL-STRUCTURE INTERACTIONS IN DEEPWATER FOLD BELTS.

5.1 Abstract

Compressional deformation within deepwater fold and thrust belts is commonly associated with the formation of growth folds where sedimentation is coeval with deformation. This typically results in the formation of growth packages adjacent to the fold limbs. Growth sequence geometry can be a useful indicator of how the relative rates of uplift and sedimentation vary over time. In this study, we consider how the relative rates of sedimentation and uplift vary in three dimensions along strike of a series of folds from the Levant Basin, eastern Mediterranean. In many deepwater fold and thrust belts, submarine channel levee systems form important depositional systems and are often key targets for hydrocarbon exploration. This study documents examples of growth sequences that are comprised almost exclusively of submarine channel-levee complexes and examines their three-dimensional development over time in conjunction with the evolving three dimensional fold relief. The development of these channel systems is characterised by spatial variations in sinuosity in response to underlying deformation. We demonstrate that growth sequence architecture and its variation along strike are key factors which affect the response of submarine channel systems to fold growth. The aim of these results is to improve our understanding of the links between sedimentation and deformation in these settings and to demonstrate that the resulting conceptual models benefit greatly from linking structural and stratigraphic observations at the scale of the overall growth sequence and at the more detailed scale of individual channel levee systems.

5.2 Introduction

Syn-kinematic sediments are deposited coevally with growing folds and faults and form geometrically distinctive growth sequences on the forelimbs and backlimbs of folds (Suppe et al. 2002). Growth sequences associated with thrust related folds have received much interest in the context of structural geology, as they provide a useful means of reconstructing the kinematics of fold growth (e.g. Suppe et al. 1992; Poblet et al. 1997; Bernal & Hardy, 2002; Salvini & Storti 2002). However, there have been surprisingly few detailed studies of growth sequences in marine fold belts where preservation potential is high, and where availability of 3D

seismic data allows a fully three-dimensional approach to be taken (Higgins et al. 2009 ; Morley and Leong, 2008).

Variations in the internal and external geometry of growth sequences such as the positioning and configuration of onlapping and overlapping sedimentary units can be used to constrain the evolution of topographic or bathymetric relief during folding. This analytical approach, which focuses on the stratigraphy is critical for understanding how sedimentary systems respond to growing folds (Puidefabregas et al. 1992 ; Burbank et al. 1996 ; Burbank and Verges 1994). Growth sequences are also progressively incorporated into the fold limbs during deformation. If the syn-kinematic sediments include reservoir prone lithologies, inclusion of these into the growing fold can result in potential hydrocarbon reservoirs contained within fold closure or on the fold limbs. From a hydrocarbon exploration perspective, it is important to understand how the interactions between sediment deposition and coeval fold growth control the distribution of reservoir and seal units, as well as considering how these are affected by any emergent fold relief.

Growth sequences are commonly observed from thin-skinned deep water fold and thrust belts associated with gravitational collapse of passive margins. Examples include the Angolan Margin (Brun and Fort 2003), North-West Borneo (Morley 2009; Morley and Leong 2008), the Mississippi Fan Fold Belt (Rowan 1997), the Niger Delta (Damuth 1994) and the Eastern Nile Delta (Gradmann et al 2005). In deepwater fold belt settings, growth sequences are commonly composed of deposits derived from gravity currents and mass transport processes, interspersed with background hemipelagic sedimentation (e.g. Stow and Mayall 2000). All of these sedimentary processes may interact with the emerging fold relief which will in turn determine the architecture of the growth sequence (Morley 2009; Morley and Leong 2008). The previous chapter, for example, documents the role of mass transport complexes in infilling fold-created accommodation space. Another key factor influencing the sedimentary response to uplift is the along-strike, three dimensional evolution of folds over time (Higgins et al 2009). Lateral propagation of folds can exert a strong control on sedimentary pathways and the location of depocenters through time (Demyttenaere et al 2000; Burbank et al 1996; Morley and Leong 2008).

The aim of this study is to link structural and stratigraphic observations of fold growth in three dimensions. These observations are then linked to the detailed response of submarine channel systems to fold growth over time. An emphasis is placed here on describing along-strike variations in fold geometry through time so that the three-dimensional evolution of the system is documented. We attempt to show how these variations can be critical in determining sediment

transport routes, and ultimately in the geometry of the growth sequence. Knowledge of the way in which submarine channel systems respond to uplift during syn-kinematic sedimentation will be of wider use in deep water exploration in these settings in predicting the location or absence of potential reservoir units.

5.3 Geological setting and database

5.3.1 Pre-Messinian development of the Levant Basin.

The Levant Basin is located in the Eastern Mediterranean Sea and is bounded to the east by the passive continental margin of Israel, Lebanon and Syria, to the south by the north-eastern lobe of the Nile Deep Sea Fan, to the west by Eratosthenes seamount and to the north by the subduction zone and transform fault of the Cyprus Arc (Fig. 5.1, Ben-Avraham et al. 1988; Ben-Avraham et al. 1995; Vidal et al. 2000). Formation of the Levant Basin and the adjacent margin is related to a sequence of rifting events occurring from Early Permian to Middle Jurassic times associated with the initial break-up of Pangaea (Garfunkel, 1998). Final continental break-up and the initiation of ocean spreading occurred at the end of Middle Jurassic (Garfunkel and Derin 1984). Compression in the Late Cretaceous and the development of the Syrian Arc Foldbelt and resulted in a series of NE-SW orientated folds along the Levant Margin (Eyal 1996; Buchbinder and Zilberman 1977; Garfunkel 1998). During the Oligocene, a system of submarine canyons developed along the Levant Margin. Headward extension of these canyons occurred throughout the Miocene due to intermittent uplift and emergence of the Levant Margin (Druckman et al. 1995; Buchbinder and Zilberman 1997).

5.3.2 Messinian Salinity Crisis and post-Messinian basin development.

Near the end of the Miocene (5.9Ma), narrowing of the connection between the Mediterranean Sea and the Atlantic Ocean led to the Messinian Salinity Crisis (Hsu et al. 1978). This resulted in a rapid sea level fall estimated at between 800-1200m in the Eastern Mediterranean Sea (Druckman et al. 1995; Bertoni and Cartwright, 2007) and the subsequent deposition of a thick evaporitic sequence up to 2km thick in some parts of the basin. The fall in sea level was accompanied by erosion along the marginal areas of the Levant Basin, resulting in the incision of a series of prominent canyons around the basin margin (Cita and Ryan 1978; Garfunkel and Almagor 1987).

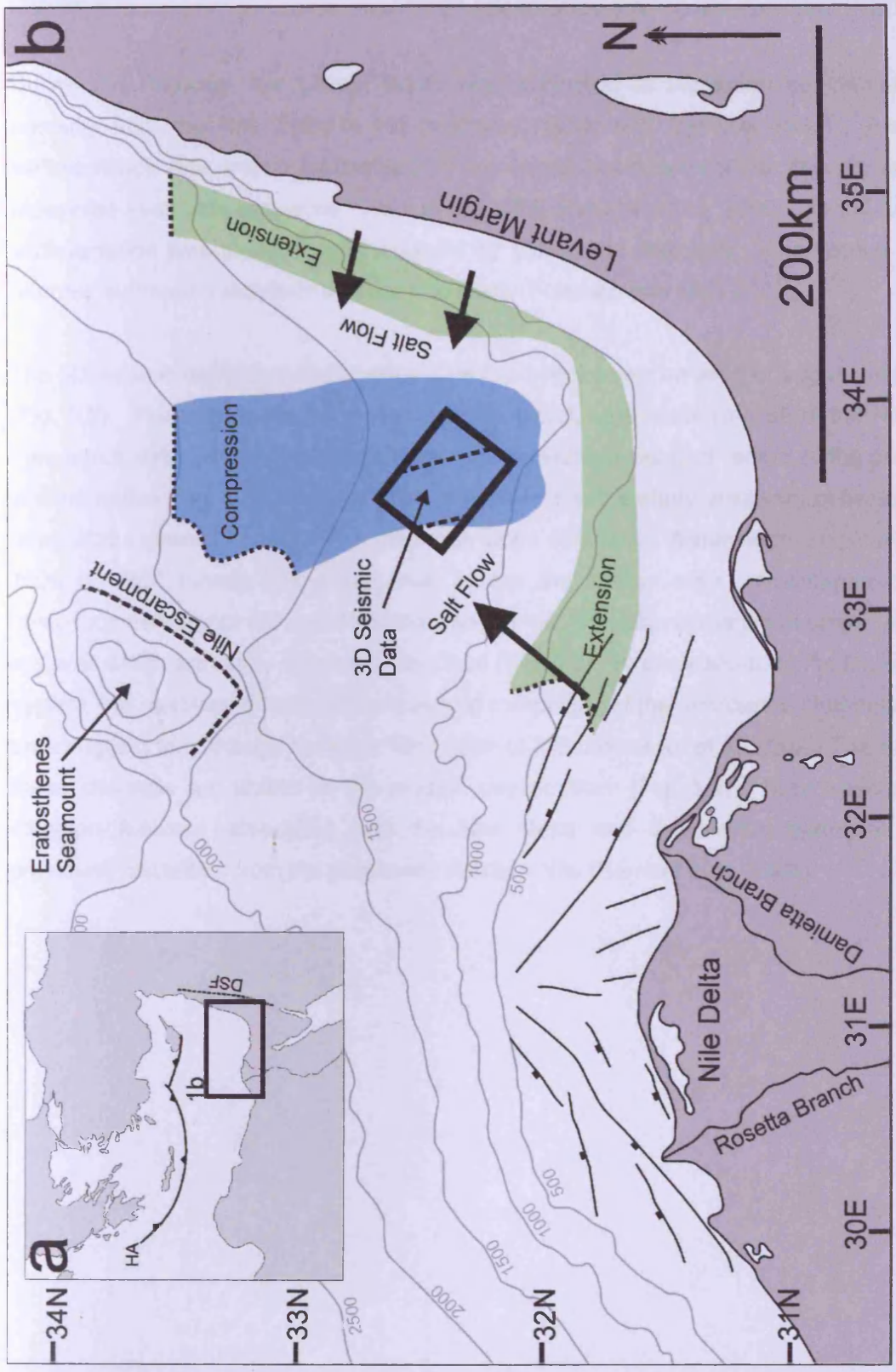

Figure 5.1: Location of the survey area within the context of the Nile Delta. 1a (inset) shows the area of interest in the Eastern Mediterranean sea, HA = Hellenic arc, DSF = Dead sea fault system. 1b shows the setting of the Nile Delta and the location of the seismic survey used in this study, which covers a portion of the eastern deep sea fan which is currently being affected by thin-skinned compression. The zone of compression within the Levant basin is driven by the gravitational collapse of both the Nile Delta and the Levant Margin. Figure adapted from Garziglia et al 2008; Netzeband et al 2006 and Gradmann et al 2005.

During the Pliocene, the Levant Basin was subjected to increased sedimentation derived primarily from the Nile Delta to the southwest (Mart and Ben-Gai 1982). An increase in sedimentation rate was accompanied by increased basin subsidence due to loading of the Messinian evaporitic sequence (Tibor et al. 1992; Ben-Gai et al. 2005). In the Levant Basin, sedimentation was predominantly sourced by submarine channels. The source of these NE oriented submarine channels was the Nile Delta (Folkman and Mart 2008).

The 3D seismic data used in this study (Gal C survey) cover an area of approximately 1400km^2 (Fig. 5.2). This survey covers a portion of the distal, north-eastern area of the Nile Deep Sea Fan, which extends into the Levant Basin and provides a detailed record of the post-Messinian sedimentation (Fig. 5.2). Average seafloor gradients in the study area vary between 0.38° in the down-slope direction and 0.02° in the cross slope direction. Water depths typically range from 1000 to 1350 meters below sea level across the survey area. Submarine channels are ubiquitous throughout the post-Messinian sequence, typically consisting of single, channel levee systems which are rarely erosionally confined (Fig. 5.2). In comparison to the larger scale slope system, the relatively small scale and lack of complexity of the submarine channels in this study area suggest they occupy the lower fan region (c.f. Babboneau. et al. 2002). The most recent of these channels are visible on the present day seafloor (Fig. 5.2). Submarine channels are common features associated with the Nile Delta and subsurface examples have been previously described from the deepwater Western Nile (Samuel et al. 2003).

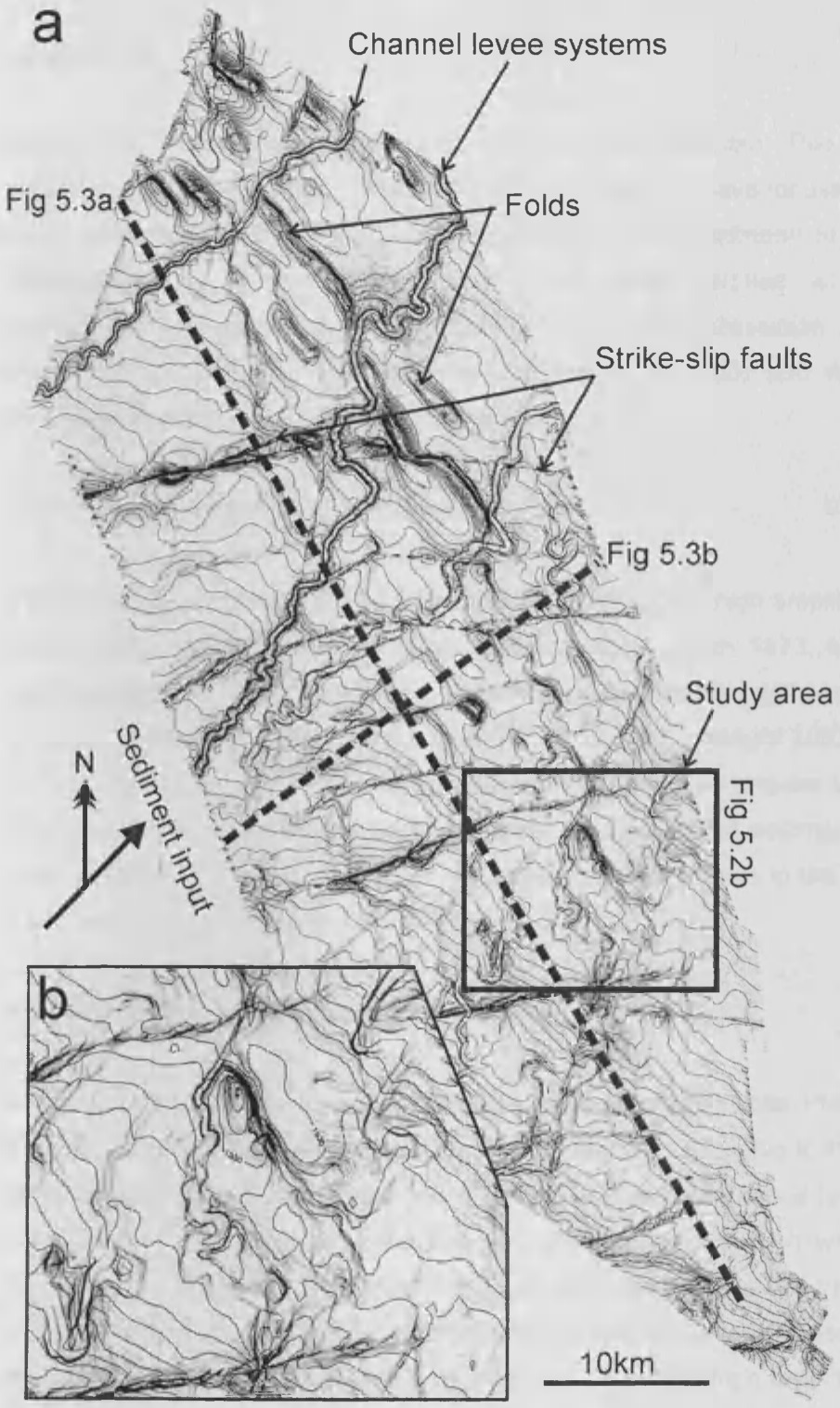

Figure 5.2: 2a shows a seafloor dip (darker shades indicate increases in gradient) attribute map of the seismic survey area. This map is overlain by two way travel time contours spaced at 10ms intervals. Submarine channel systems sourced from the Nile to the south-west cross the seafloor and their development is affected by strike-slip fault structures and a series of folds whose strike is perpendicular to the submarine channel flow direction. These folds become progressively buried towards the south-east due to the increasing thickness of the syn-kinematic interval Unit PM3 – see figure 5.3. 2b shows the detailed study area, note the irregular seafloor expression of two folds, and the prominent, partially buried submarine channel levee system.

5.3.3 Seismic stratigraphy

This study focuses on the uppermost sequence of the post-Messinian, Plio-Quarternary sedimentary section in the Levant Basin. Recent studies from this area have focussed on either the Messinian sequence (e.g. Bertoni & Cartwright 2005,2006,2007; Gradmann et al 2005), or along the marginal areas of the Levant Basin (e.g. Frey-Martinez et al 2005). Chronostratigraphic and lithological data, where given, for the Post Messinian sedimentary cover is based on unpublished well reports (Frey-Martinez et al 2005) and there are no published wells within the more basinal Gal C survey area.

5.3.3.1 Messinian Evaporite Sequence (6.7-5.2Ma)

The top of the Messinian sequence is marked by Horizon M – a regional high amplitude positive reflection recognisable throughout the entire Mediterranean Basin (Ryan 1973, see also Fig. 5.3). Internally, the Messinian sequence shows evidence of deformation with multiple thrust detachment levels observed (Cartwright & Jackson 2008; Bertoni & Cartwright 2007). Over the more marginal areas of the Levant Basin, Horizon M may represent an angular unconformity between the lower, deformed Messinian evaporites and the post Messinian sedimentary section (Bertoni & Cartwright 2007). However, this does not appear to be the case in the Gal C area, where the two sequences are seismically concordant (Fig. 5.3).

5.3.3.1 Post Messinian Sequence (5.2Ma-Present)

The post-Messinian overburden can be subdivided into three intervals (Units PM1, PM2 and PM3) based on seismic stratigraphic characteristics as well as the relationship to the extensive thin-skinned deformation throughout the study area (Fig. 5.3). The PM3 interval is the focus of this study as it is this sequence which comprises the syn-kinematic section which records coeval post-Messinian compression and sedimentation in this area, and is described in more detail below. Units PM1 and PM2 comprise the pre-kinematic section and were deposited prior to the deformational phase. Unit PM1 consists of locally continuous, high amplitude parallel reflections displaying low relief channel forms up to 500m in width. These channels provide useful kinematic indicators for the many strike-slip faults throughout the study area. Unit PM2 consists of low to medium amplitude, locally continuous reflections interlayered with minor packages of low amplitude, chaotic reflections which pass laterally into continuous packages. Unit PM2 shows internal thickness variations related to the development of channel-levee complexes, which are clearly visible within this interval (Fig 3.5, chapter 3). The uppermost part

of unit PM2 consists of a package of low-amplitude, parallel reflections in which channel levee development is absent (Fig. 5.3).

Unit PM3 is considered to form the syn-kinematic sequence throughout the study area and is the focus of this study. The base of this unit records the first appearance of onlap associated with folding throughout the study area, with the exception of several folds where the first occurrence of onlap is observed c.50ms below the base of this unit. Over the scale of the survey area, the thickness of this unit increases towards the south-east (see Fig. 3.6, chapter 3). At the kilometre scale, sedimentation within unit PM3 is strongly controlled by numerous NW-SE trending folds (Figs 5.2 and 5.3). Unit PM3 shows systematic thinning of sedimentary packages across fold crests accompanied with thickening into hangingwalls and footwalls of the folds. This can be clearly observed on seismic profiles and also on the isochron map of this interval (Fig. 5.3). This geometry is typical of growth sequences associated with sedimentation coeval with uplift (e.g. Burbank and Verges 1994; Suppe et al 1995; Masaferro et al 2002; Cartwright, 1989; Morley, 2009) The stratigraphic architecture of unit PM3 consists of a vertical sequence of channel levee systems, many of which are strongly affected by post-Messinian deformation (Fig. 5.2). These channel levee systems typically have widths of 500m and depths of up to 60m. Many are highly sinuous (average value of 1.51), although variations can occur when channels are confined and diverted around the NW-SE trending folds (Clark and Cartwright, 2009). Diversion and deflection of channels are common when the strike of the folds and their associated bathymetric relief is perpendicular to the channel flow direction.

5.3.4 Post Messinian thin skinned deformation

The Gal C survey area is located in the contractional domain of a gravity driven, linked extensional-compressional system in the Eastern Mediterranean (Cartwright and Jackson, 2008; Gradmann et al 2005). Thin-skinned contractional structures result from a combination of the gravity-induced collapse of the Nile Cone above the ductile Messinian evaporite sequence (Loncke et al 2006; Gradmann et al 2005). This is combined with westward tilting and thin-skinned collapse of the Levant margin (Cartwright and Jackson, 2008). Together, the effects of these variably oriented marginal collapses interact with a buttressing effect due to the Eratosthenes seamount, resulting in changes in orientation of the thrust, fold and strike-slip structures that characterise this complex area (Loncke et al 2006).

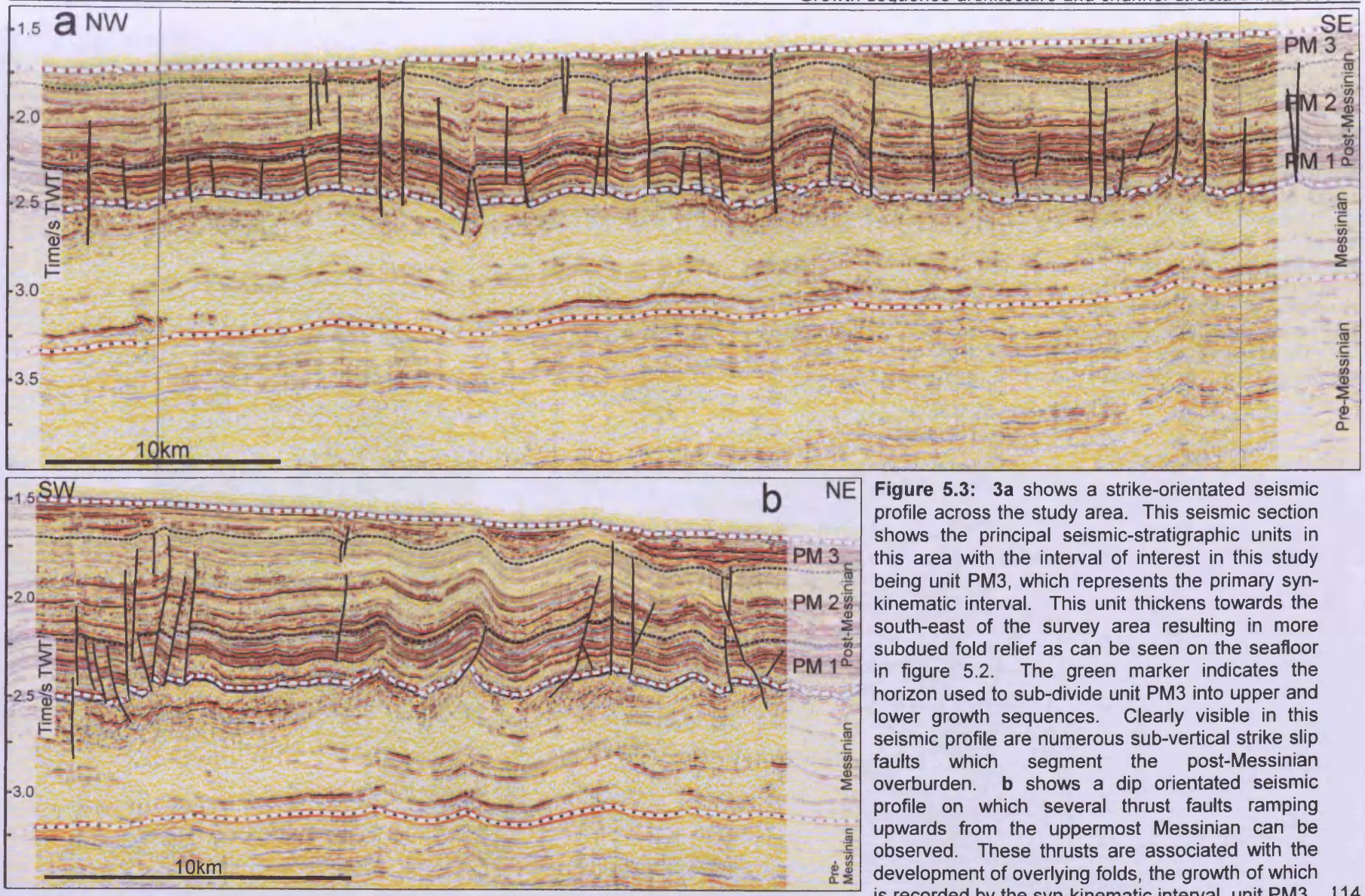

Figure 5.3: **3a** shows a strike-orientated seismic profile across the study area. This seismic section shows the principal seismic-stratigraphic units in this area with the interval of interest in this study being unit PM3, which represents the primary syn-kinematic interval. This unit thickens towards the south-east of the survey area resulting in more subdued fold relief as can be seen on the seafloor in figure 5.2. The green marker indicates the horizon used to sub-divide unit PM3 into upper and lower growth sequences. Clearly visible in this seismic profile are numerous sub-vertical strike slip faults which segment the post-Messinian overburden. **b** shows a dip orientated seismic profile on which several thrust faults ramping upwards from the uppermost Messinian can be observed. These thrusts are associated with the development of overlying folds, the growth of which is recorded by the syn-kinematic interval, unit PM3.

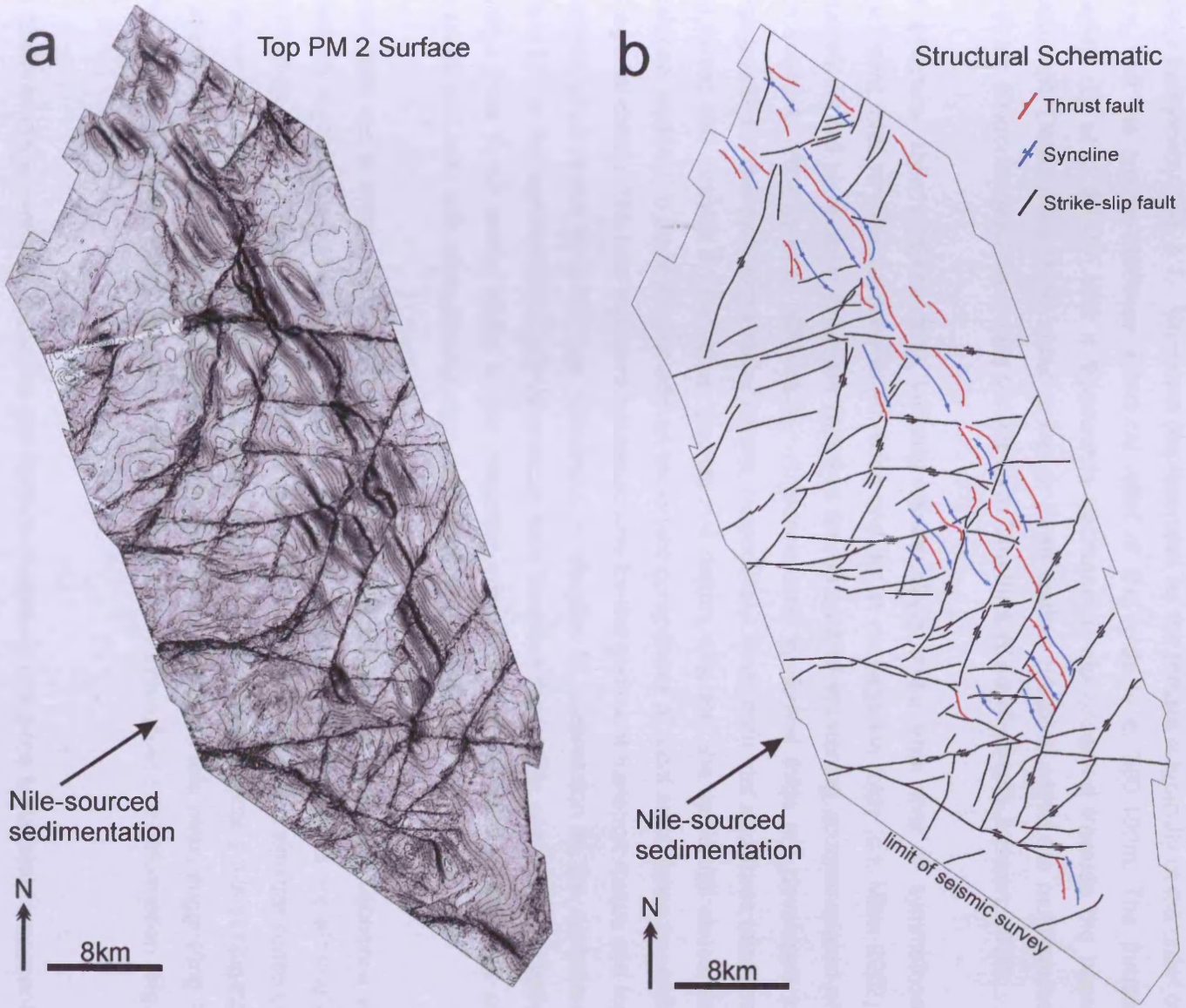

Figure 5.4: **a** Dip attribute map of the top PM2 horizon (see figure 5.3 for location). This map represents the top of the pre-kinematic sequence throughout the survey area and more clearly shows the SE-NW orientated fold belt a conjugate set of strike slip faults which segment many of the thrusts and folds. **b** Schematic map showing the distribution of thrusts underlying the folds, as well as synclines which form within the hanging-walls and foot-walls of many folds in this area.

Deformation within the Gal C survey area is characterised by NW-SE striking thrust faults which show a predominant vergance towards the NE (Fig 5.4). These thrusts detach within the uppermost Messinian and ramp upwards into the overlying section, typically to terminate below the seafloor within the base of the unit PM3 (Fig. 5.3). A small number (c.5) of these thrusts verge towards the SW towards the NW of the survey area (Fig. 5.4). All of these thrust faults are associated with the formation of overlying folds, and these exert a key control on the seafloor bathymetry (Fig. 5.2). Maximum displacement on the thrusts is typically of the order of 500m, and the typical maximum structural relief of the folds is c. 300-400m. The thrusts generally dip at c. 30-40°, with a downwards decrease in dip observed towards the basal detachment. Detachment levels occur at two or three distinct horizons within the multilayered Messinian evaporite sequence, which can be up to 2km thick (Cartwright and Jackson, 2008).

The structural style of these folds typically varies along strike from that of symmetrical detachment folds to thrusted detachment folds and thrust propagation folds (c.f. Mitra 2002). Variations in fold style along strike are linked to the amount of shortening accommodated on each structure (Higgins et al 2007;2009). Antiformal and synformal folds are developed in hangingwalls and footwalls to the major thrusts, respectively. The antiformal structures raise the local folded and thrusted layers above the regional datum, whereas the synformal structures developed adjacent to the fold crest add an important component of local subsidence beneath the regional datum. This has important consequences for the sediment transport routes and for accommodation space evolution (see discussion in chapter 6). Depression of the synformal regions below the regional datum is only possible here because the mobile salt is preferentially depleted from these areas, and a similar response would not be expected in the case of deepwater fold belts with shale detachments (c.f Briggs et al. 2006).

A conjugate set of strike slip faults that detach within the uppermost Messinian sequence is present throughout the survey area (Figs. 5.3 and 5.4). These strike slip faults are strikingly linear in map view, and show two dominant trends: An E-W trending set with a sinistral sense of displacement and a dextral NE-SW trending set (Fig. 5.4). The angle bisecting this conjugate set of strike-slip faults is orthogonal to the orientation of the thrust and fold axes, suggesting a consistent NE direction for the maximum compressive stress throughout the deformation (Fig. 5.4).

The displacement direction of the strike slip faults is measured using the horizontal component of the relative offset of channels developed at the top Messinian level and within unit PM1. Typical strike slip displacements are of the order of 200-500m (see Fig.3.4, chapter 3). Zones of

local transtension and transpression occur where strike slip fault segments link, these form push-up structures with a relief of up to 90m above the present day seafloor and also pull-apart structures that are up to 60m deep (Fig 5.2). These push-up and pull apart structures can be used to constrain the timing of the strike-slip faults, because sediments post-dating the strike slip activity show onlap and infilling of the push-up and pull-apart structures respectively. These stratal relationships show that the timing of strike-slip fault activity can be constrained to the top of Unit PM2, synchronous with the onset of folding in many of the thrust/fold structures (Fig. 5.3).

5.4 Methods

Growth sequences can be described qualitatively using relationships such as onlap, overlap and offlap (Burbank and Verges 1994; see also Fig. 1.3, chapter 1). Such relationships, combined with observations of the reflection geometry within the growth sequence can be used to assess relative rates of sedimentation versus uplift (Burbank and Verges 1994; Cartwright, 1989; Puidefabregas et al. 1992; Suppe et al 1992;). In this study, the growth sequence represented by unit PM3 can be sub-divided into two intervals termed the upper and lower growth sequences (Fig. 5.3). This sub-division is based on the gross geometrical style of the sequence (e.g. onlap or overlap) and also on the response of submarine channel systems within the growth sequence to uplift (see section 5.5.4). It should be noted that growth sequence geometry varies significantly along strike in response to variations in the relative rates of uplift versus sedimentation. Thus, an understanding of the along-strike variations in uplift combined with the nature of sedimentation is critical to understanding the three dimensional stratigraphic response to uplift in these settings. Isochron maps can be a useful tool in interpreting three dimensional growth sequence architectures as they show gross patterns of thinning over fold crests and thickening adjacent to the fold limbs (e.g. Salvini and Storti 2002). Overlapping growth sequences are revealed on isochron maps by thinning across the fold crests, whilst onlap results in stratal terminations against the emergent relief.

To quantify the three dimensional variations in fold uplift and growth sequence geometry, we undertook along strike measurements of the structural relief and growth sequence expansion factor. The measurements of structural relief were taken using a similar method to that previously described by Masaferro et al. (1999) and Poblet et al. (2004) for measuring crestal structural relief of folds (Fig. 5.5). This method is based on the assumptions that measured horizons were deposited horizontally, and that no limb-parallel shearing occurred during fold growth (Masaferro et al 1999). Where an overlapping growth sequence is observed, the thickness difference of the package between the footwall and the fold crest is interpreted to

represent the cumulative fold uplift which occurred over the time interval in which the growth sequence was deposited (Fig. 5.5, see also Poblet et al. 2004, Masaferro et al. 1999). An overlapping growth sequence geometry also implies that any positive fold relief that developed was healed over due to high relative rates of sedimentation compared to uplift (Burbank and Verges 1994). In the case of onlapping growth sequences, the minimum value of crestal structural relief is equal to the thickness recorded in the growth sequence adjacent to the fold limbs (Fig. 5.5). The onlap terminations onto the fold limbs imply that the sedimentation rate was not sufficient to heal over the growing fold, resulting in positive relief at the depositional surface.

Measurements of crestal structural relief were taken at 100m intervals along strike-perpendicular seismic profiles for the folds studied here. Where the onlap geometry closely resembled a parallel onlap fill, it was assumed that the gross thickness of the onlapping units as measured in the flank areas was equivalent to the structural relief extant during the onlap interval. In the case of strongly convergent onlap, the relief measured using this method should be regarded as a cumulative relief developed during this interval.

These measurements were taken for both the lower and upper growth sequences in order to gain a finer resolution of along strike fold development than is represented by the whole of the syn-kinematic package, which has a total thickness of over 200m. Reference points for measuring stratigraphic thickness were taken between the fold crest and the lowest point of the adjacent footwall syncline. A regional datum was not imposed due to the close (less than 2km) spacing of the measured folds and the development of synclines within the footwalls of each fold. Taking a reference datum using the relatively undeformed top pre-kinematic surface (top PM2 marker) towards the west of the survey area it is apparent that the formation of negative relief occurs adjacent to the positive relief of the antiform itself. The negative relief formed by the synclines is important in terms of generating localised depocenters adjacent to the positive relief formed by the uplifting fold crest (see Fig. 5.1).

The expansion factor of each growth sequence was measured using the methodology defined for growth sequences associated with normal faults (Thorsen 1963; Roux 1979). For growth sequences associated with folds, the expansion factor E is defined as $E = Z'/Z$, where Z' is the thickness of the growth sequence within the footwall or hangingwall and Z is the thickness over the fold crest. These measurements were taken for both lower and upper growth sequences at along strike intervals of 100m, and the data is given in Appendix A3.

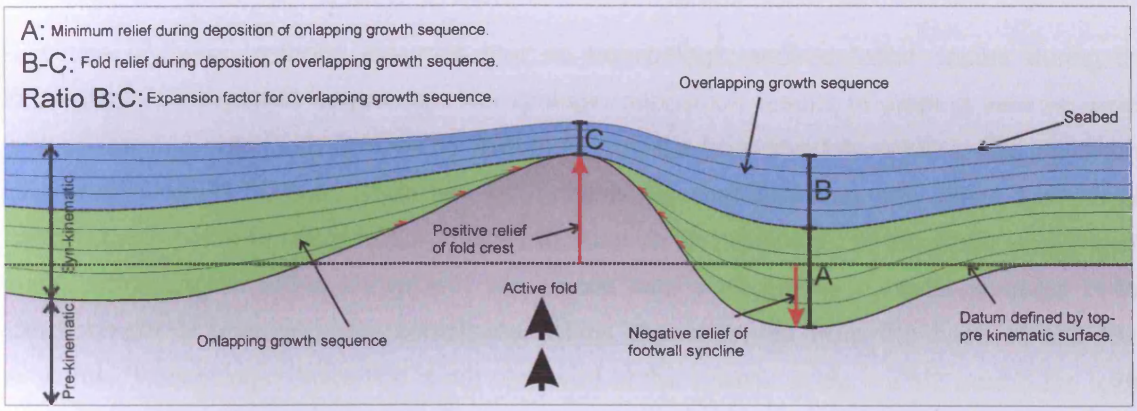

Figure 5.5: Methods used to characterise growth sequence development along strike in this study. The style of folding in this area involves depression of the footwall and hangingwall below the datum marked by relatively undeformed pre-kinematic level. The minimum structural relief of the onlapping (green) growth sequence is equal to the thickness A. Structural relief developed during the overlapping (blue) interval is given by B-C. These measurements were taken along strike at 100m intervals.

The use of these methods assumes that no hemipelagic sedimentation occurs during the deposition of the growth sequence. Hemipelagic deposition results in draping seismic facies across the fold crest with little or no thickness change from the fold crest to the fold limbs (Cartwright, 1989). Thus, deposition of hemipelagic sedimentation can make the correct interpretation of the onset of folding difficult to observe and quantify. In this study, the primary mode of deposition within the growth sequences was from gravity currents involved in the development of channel levee complexes, which are observed from the base of unit PM3 onwards. Hemipelagic deposition is not observed at the seismic scale in PM3 across the folds, and we assume here that the growth sequences are predominantly composed of deposition from density currents.

5.5 Results and observations

The results section is structured in an attempt to describe the interactions between sedimentation and deformation from large to small scale. An summary of key observations linked to the appropriate figures, is presented at the end of this section in table 5.1. The section begins with an overview of the main structural features of the detailed study area within the Gal-C survey, and introduces the nomenclature used in the following sections, as well as establishing the relative timing of deformation. This is followed by a description of the quantitative results relating to along-strike relief development and growth sequence expansion factor. The growth sequence isochron maps are then described in relation to the preceding measurements, before finally describing the interactions and development of individual channel levee systems which comprise the growth sequences in this area.

5.5.1 Along strike structural development and growth sequence evolution

Growth sequence development within the detailed study area is primarily affected by two fold structures (Folds 1 and 2). These folds both exhibit significant structural variation along strike (Fig. 5.6). The folds and their underlying thrust faults terminate laterally against SW-NE trending strike slip faults that act to compartmentalise the compressional belt and limit the lateral extent of individual thrusts and folds (Figs. 5.6 and 5.7). The zones of intersection between the thrust/fold pairs and the strike slip faults are recognisable as steep, sub vertical 'scarps' expressed on the pre-kinematic surface with a structural relief of up to 120m. (Fig. 5.7). Fold 1 is 3.8km in length, with structural relief along strike showing a non uniform distribution such that relief is concentrated at two peaks at each end of the fold where terminations occur against the bounding strike slip faults, and with a minimum value of relief in the central zone of the fold (Fig. 5.7). A more typical distribution of relief expected in deepwater fold belts would predict the

maximum fold relief axio-symmetrically along the fold, but this applies where underlying thrusts tip out in either axial direction without any hard linkage to adjacent structures (Salvini and Storti 2002; Higgins et al. 2009). Fold 2 is 5.6km in length and again shows asymmetric distribution of structural relief along strike – in this case the maximum structural relief has developed at the north-western termination against its bounding strike slip fault (Fig. 5.7). Fold 2 is segmented where the zone of maximum uplift occurs by the same strike slip fault against which fold 1 terminates at its north-western end (Figs. 5.6 and 5.7).

Periclinal synclines are developed on the back limb of the hangingwall and in the footwall to Folds 1 and 2 (Fig. 5.6). These synclinal structures were expressed as closed depressions on the palaeosurface which marks the onset of fold growth (Fig. 5.7). The location of maximum depth within each basin was adjacent to the central zone of each fold, excepting the footwall depression of Fold 2, where the topographically lowest point was asymmetrically disposed towards the southeastern termination even though the maximum structural relief is located at the northwestern termination (Fig. 5.7).

5.5.2 Timing of Growth

The onset of folding is marked by the first occurrence of onlap onto the fold forelimbs and backlimbs, on the basis that density current deposition responds to the presence of seabed topography created by folding with the final deposit resulting in an onlap configuration (e.g. Kneller 1995; Alexander and Morris 1994). Onlap systematically directed towards the fold crests is first recorded at the base of unit PM3 for both folds (Fig. 5.6). However, onlap at the base of unit PM3 is not consistently observed along strike, particularly in the case of Fold 1. The central zone of Fold 1 shows no observable onlap onto the fold limbs, indicating that the areas of maximum structural relief observed against the lateral terminations also record the earliest onset of folding. These observations illustrate that without good three-dimensional control, it would be easy to misinterpret the onset of growth of this structure.

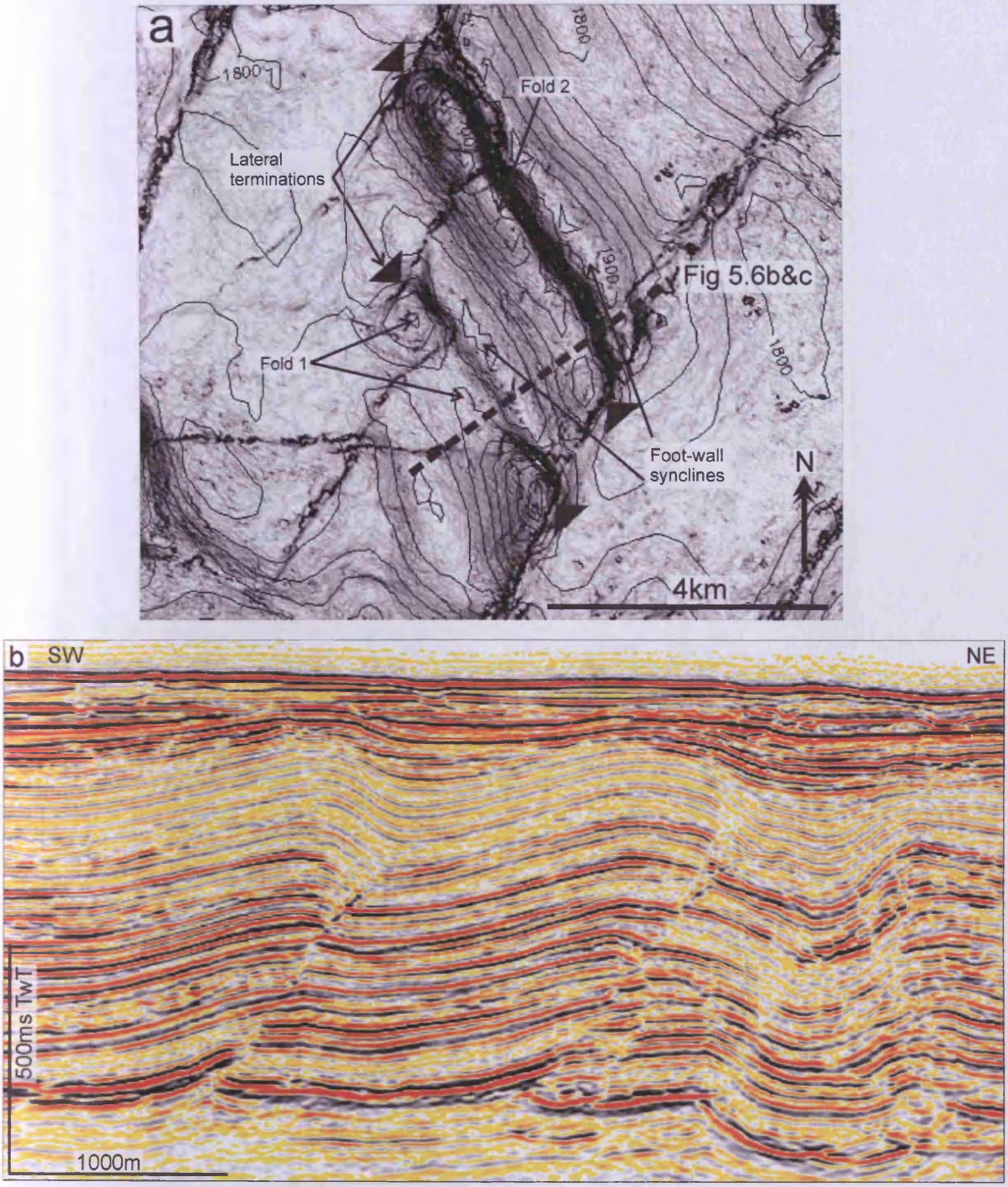

Figure 5.6: Nomenclature used within the results section of this study. **a** shows a dip attribute map of the top PM2 surface of the detailed study area. Folds 1 and 2 are indicated, as are the foot-wall synclines adjacent them. Red triangles mark the positions of lateral terminations of the folds against strike-slip faults. **b** shows an uninterpreted seismic profile showing folds 1 and 2 and the growth sequence. **c (next page)** is a line drawing interpretation of the same seismic profile showing the subdivision of the PM3 interval into lower and upper growth sequences. Channel levee systems described from the lower and upper growth sequences are termed the lower and upper channel levee systems, respectively.

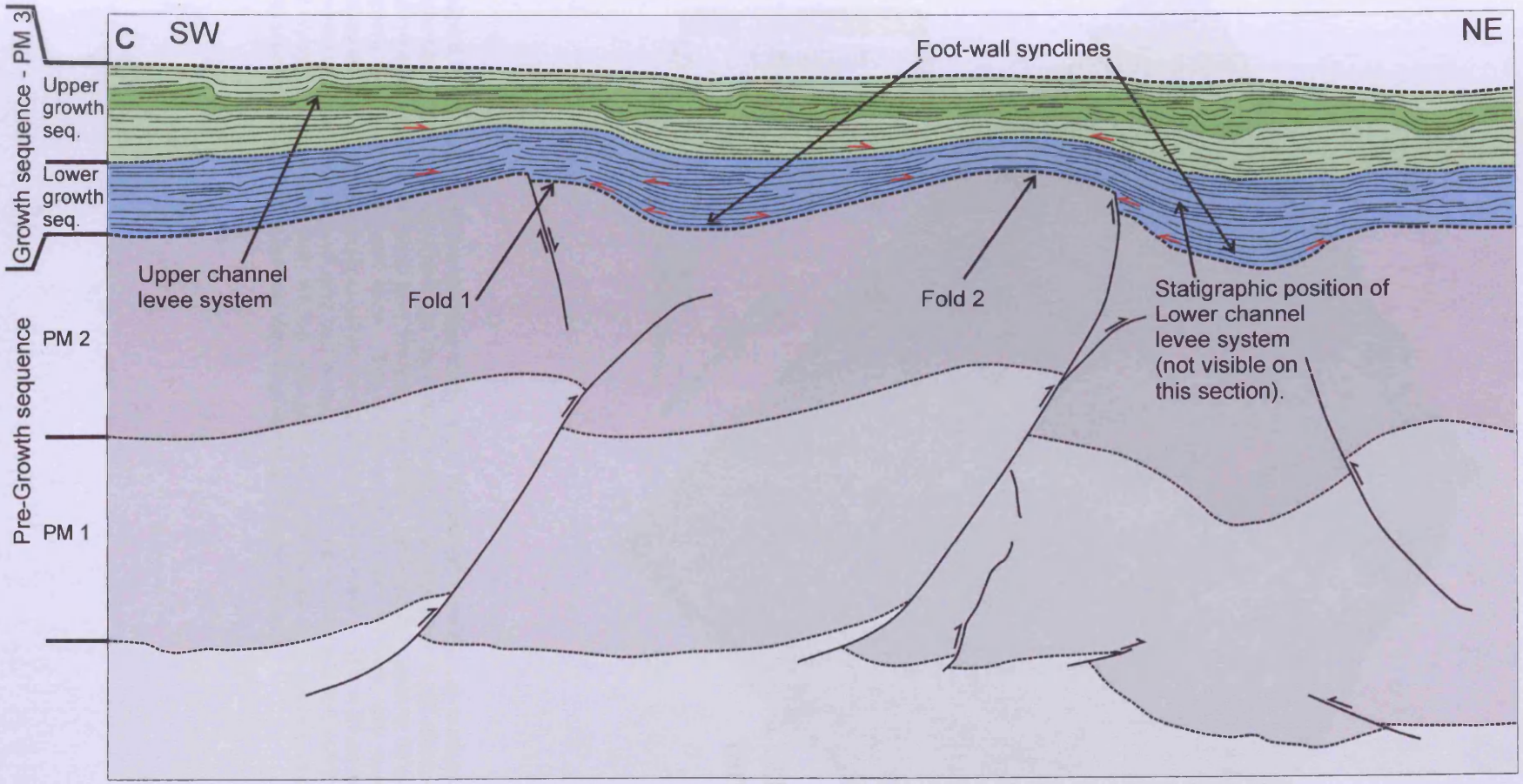
C SW
NE
Foot-wall synclines
Growth sequence - PM 3
Upper growth seq.
Lower growth seq.
Upper channel levee system
Fold 1
Fold 2
Statigraphic position of Lower channel levee system (not visible on this section).
Pre-Growth sequence
PM 2
PM 1

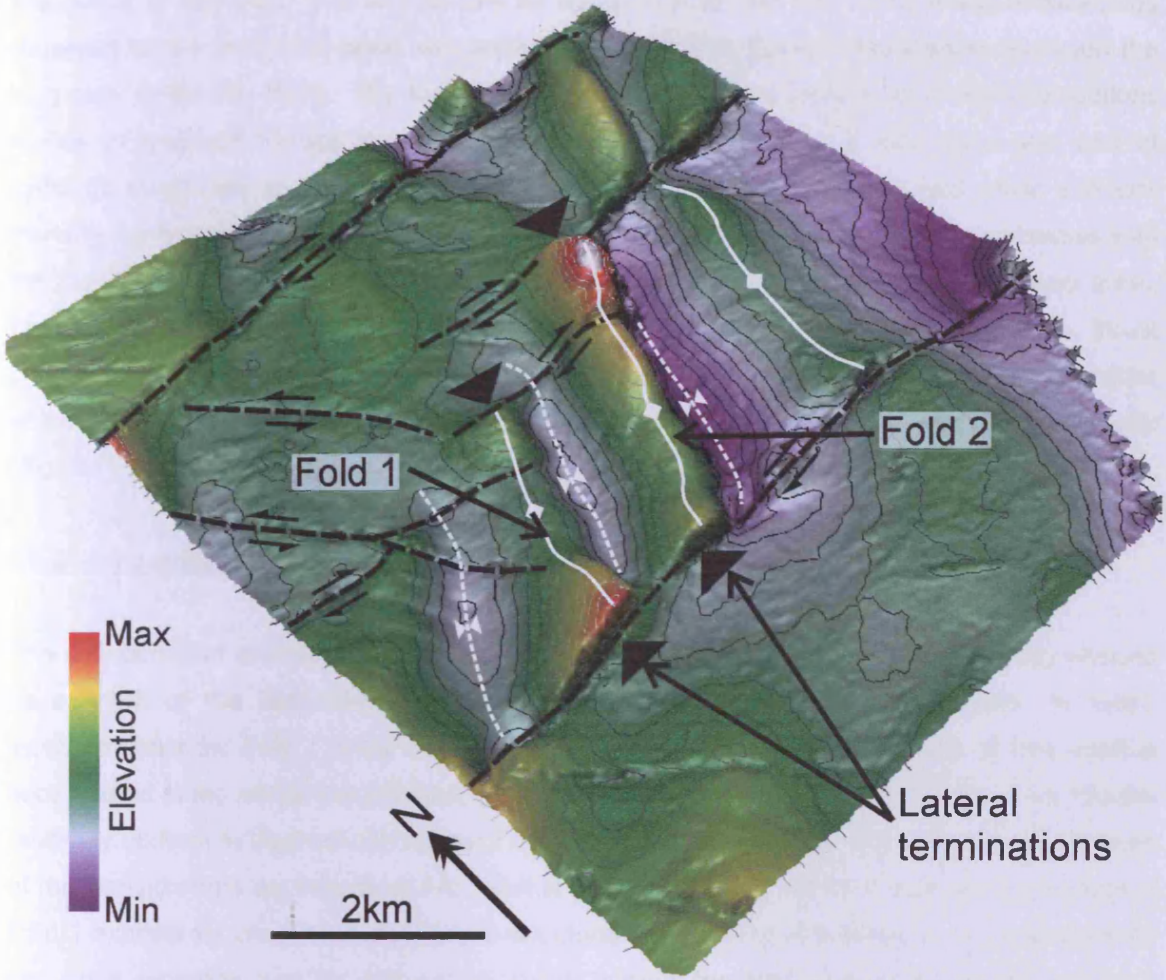

Figure 5.7: 3D surface of the detailed study area, generated from the top surface of the pre-growth sequence. This surface illustrates the non-uniform lateral distribution of uplift along strike of each fold. Maximum fold uplift is concentrated towards the lateral terminations against strike-slip faults which segment individual thrusts and folds. The sense of offset for the strike slip fault systems can be determined from channel systems within the pre-growth sequence. Where these terminations occur, sub-vertical scarps are formed, and can be seen at south eastern lateral fold terminations. The foot-wall synclines associated with folding can also be seen, these form closed depressions in three dimensions, as indicated by the two way time contours (25ms Interval).

The timing of strike-slip fault activity can be dated in a similar way using onlap relationships observed for the many pull-apart and pop-up structures that form at intersections between the conjugate strike slip faults. The local positive or negative topography at these intersections relates to localised transtension and transpression along the main fault trace and was of sufficient magnitude to result in well resolved onlap relationships. The basal onlap surfaces marking the creation of positive and negative relief related to strike slip faulting correlates with the top PM2 surface which also records the onset of the folding throughout the survey area.. These onlap relationships indicate that strike-slip faulting occurred coevally with thrust propagation and fold amplification. Many of the strike slip faults and folds continue to be active at the present day, as can be seen from their expression in the modern seafloor topography (Fig. 5.1).

5.5.2 Along strike measurements of structural relief and expansion factor.

The distribution of structural relief for the lower and upper growth sequences is highly skewed as a result of the hard-linked intersections with the confining strike slip faults. In detail, measurements for Fold 1 show clearly the extent to which the development of fold relief is accentuated at the lateral terminations, whereas relief values over the central part of the fold are relatively uniform throughout deposition of the growth sequence (Figs. 5.8 and 5.9). An example of this considerable asymmetry in fold relief is apparent where the southeastern termination of Fold 1 exhibits an increase in cumulative structural relief during deposition of the upper growth sequence, whereas over the same stratigraphic interval the northwestern termination shows a decrease when compared to the lower growth sequence (Figs. 5.8 and 5.9).

The distribution of along strike relief for Fold 2 shows a distinctive zone of structural relief spanning 2km at the northwestern lateral termination during deposition of the lower growth sequence (Fig. 5.8). The remainder of the fold exhibits uniform structural relief, albeit approximately twice that seen on average when compared to Fold 1 (Fig. 5.8). The upper growth sequence records a shift in the locus of uplift away from the north-west lateral termination towards the central area. Here, the magnitude of structural relief shows a general decrease along strike towards the south-east (Fig. 5.8). This is also evident from the isochron map covering the upper growth sequence interval (See next section – Fig. 5.11).

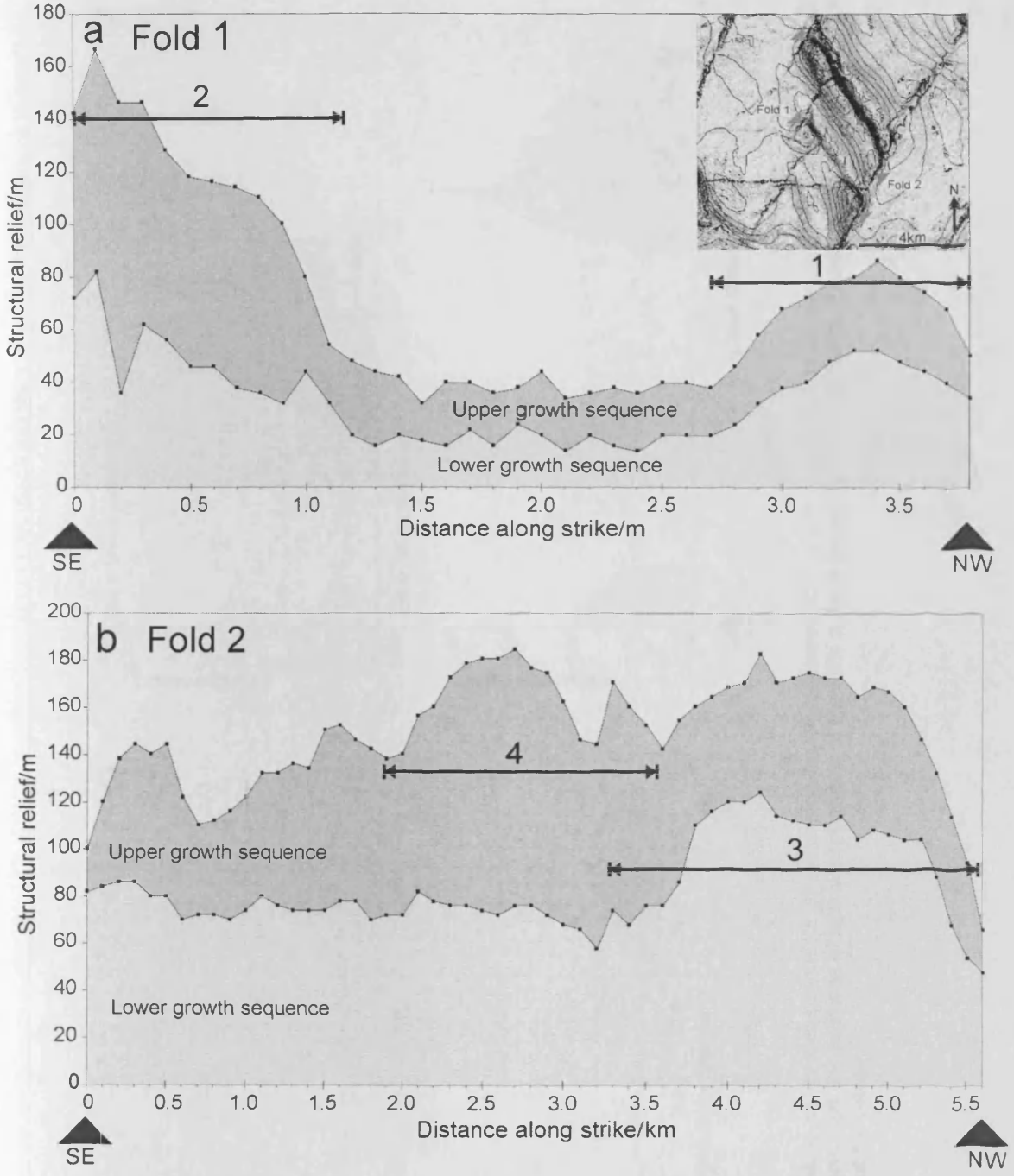

Figure 5.8: Along strike distribution of uplift for folds 1 (**a**) and 2 (**b**). **a** shows that both lower and upper growth sequences display areas of increased uplift located at the lateral fold terminations. Inset map shows both folds with lateral terminations marked by triangles. 1 and 2 mark the zones of increased uplift observed at the lateral terminations for fold 1, see also Fig. 5.7. **b** shows a constant distribution of uplift along strike over the lower growth sequence for fold 2, with the exception of the north-east termination which shows a greatly increased uplift over the same interval (marked 3). The upper growth sequence shows a shift in the area of maximum uplift towards the central part of the fold (marked 4).

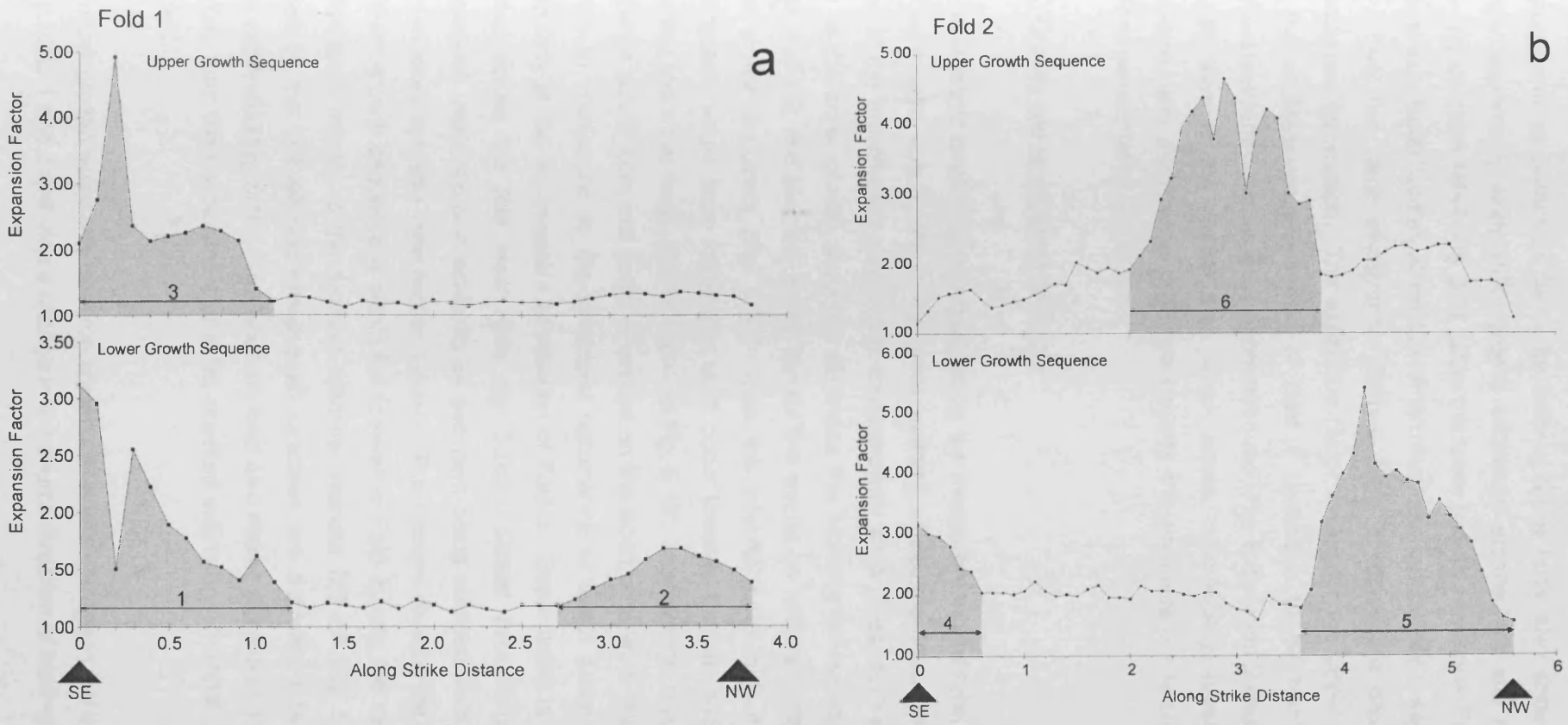

Figure 5.9: Graphs showing along strike measurements of expansion factor measured for folds 1 and 2 (see text) over the lower and upper growth sequence intervals. Black triangles mark the positions of lateral terminations of the folds against bounding strike-slip faults. Shaded regions indicated zones of increased fold activity. See text for details.

Measurements of expansion factor for both of these folds also show the development of a strongly asymmetric along-strike growth sequence architecture and mirror the observations above for structural relief (Fig. 5.9). Over the lower growth sequence, Fold 1 shows a maximum in expansion factor located at the lateral terminations, particularly towards the south-east (Fig. 5.9). Over the same stratigraphic interval, Fold 2 shows the greatest expansion at the northwestern termination. The expansion factor values for the upper growth sequence show that the southeastern termination of Fold 1 continues to be highly active, whereas the northwestern termination is much more subdued (Fig. 5.9). Fold 2 displays a shift in the locus of uplift towards the central area which shows dramatically increased growth sequence expansion, with a decrease observed towards the northwestern lateral termination observed over the same interval (Fig. 5.9b).

5.5.3 Growth sequence isochron maps.

The style of fold development suggested by the measurements of relief and expansion factor is also expressed very clearly in the gross patterns of sedimentation recorded by the isochron maps of the growth sequence in the detailed study area (Figs. 5.10 and 5.11). The isochron map of the lower growth sequence illustrates the asymmetric evolution of structural relief of Folds 1 and 2, and also the strong control this exerts on sediment distribution throughout the lower growth sequence (Fig. 5.10). Over this interval, both folds display a pattern of fold amplification where local maxima in uplift occur towards the lateral terminations against the bounding strike slip faults (Points 1 to 4 on Fig. 5.10). Stratigraphic thinning of the lower growth sequence across both fold crests is evident on the isochron map in figure 5.10, and is seen on profiles to correspond to the enhanced occurrence of basal onlap against the fold limbs, particularly at the northwestern termination of Fold 2. Basal onlap is generally succeeded by overlap across the fold crest (See Fig. 5.6c). Stratal thickening into the footwall and hangingwall depressions is achieved by sediment being sourced from a series of NE directed channel levee systems (see section below). The primary depocentre during the deposition of the lower growth sequence is within the footwall of Fold 2, with the maximum thickness at the northwestern margin of the footwall syncline (marked MT on Fig. 5.10). The depocentres formed by the footwall and hangingwall synclines are delimited laterally by the intersecting strike-slip faults (Fig. 5.10). The isochron map also shows the extent of the thickness variations resulting from the development of a NE oriented submarine channel system (marked CLS on Fig. 5.8).

The upper growth sequence isochron shows a dramatic change in the areas of active uplift along Folds 1 and 2 and also a change in the source direction of sediment input into the

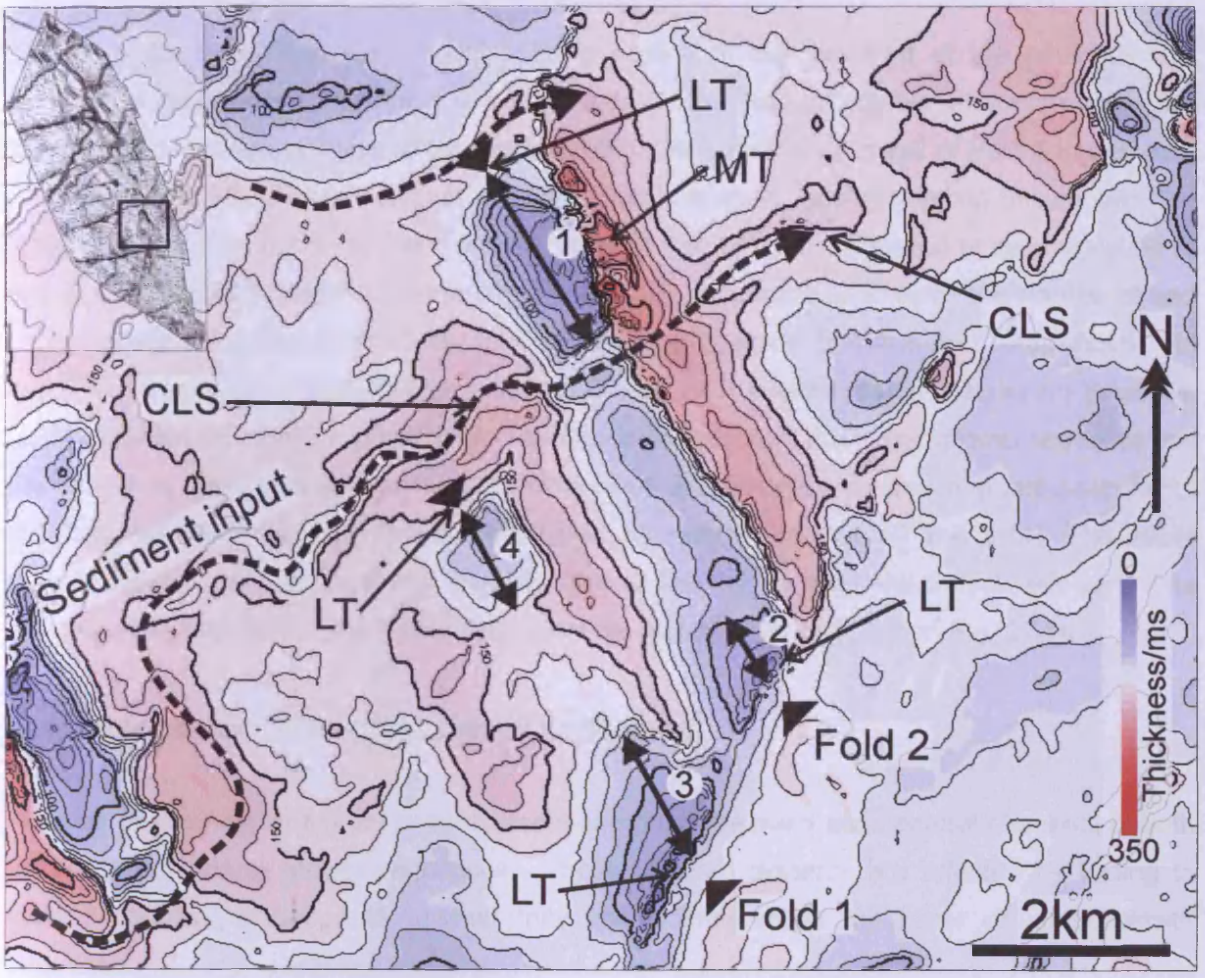

Figure 5.10: Isochron map of the lower growth sequence, contours spaced at 25ms intervals. Dashed black arrows indicate the directions of sedimentary input for the deposits making up this sequence. LT = Lateral terminations, MT = Maximum thickness, CLS = Channel levee system. Note that uplift along folds 1 and 2 is distributed unevenly along strike, with areas of increased uplift being concentrated towards the lateral terminations of the folds against strike slip faults (marked LT). Points marked 1-4 correspond to the zones where an increase in expansion factor is observed, refer to figure 5.9.

detailed study area (Fig. 5.11). Uplift along Fold 1 is concentrated at the south-eastern termination (see points marked LT in Fig. 5.11). This has a notable effect on sediment distribution: a marked increase in thickness occurs within the hangingwall of Fold 1 in this area (marked MT on Fig. 5.11). Towards the northwest only minor stratal thinning occurs over the crest of Fold 1 (Fig. 5.11) indicating a lower relative rate of uplift compared to sedimentation in this area of the fold. Relief development for fold 2 is concentrated towards the northwest and central areas of the fold, linked to an increase in onlap towards the northwest. Amplification of fold 2 decreases along strike towards the southeast, to a position where almost no growth is visible near the intersection (Fig. 5.11). The depocentres within the upper growth sequence are not limited by the lateral terminations of Folds 1 and 2 against the intersecting strike-slip faults and become more open towards the southeast (compare figures 5.10 and 5.11). The upper growth sequence shows a general thinning towards the north-west, where thickness variations are caused by the development of a channel levee system (marked CLS on Fig. 5.11).

5.5.4 Growth sequence submarine channel development

A series of submarine channel levee systems comprise the main architectural elements of both the lower and upper growth sequences. These channel systems are affected by folding to various degrees according to whether they are located within the lower or upper growth sequence.

5.5.4.1 Lower channel levee system

The lower growth sequence contains three channel levee systems, all of which have a flow direction perpendicular to fold strike (Fig. 5.12). Two of these channel levee systems do not cross Folds 1 and 2 and are not discussed further. A third channel (the lower channel levee system) crosses the crest of Fold 2, this channel is the youngest of the three channels comprising the lower growth sequence and is described here. The lower channel levee system is typically 500m in width and up to 20m in depth. Seismic amplitude attributes of this channel (Fig. 5.12) show that a decrease in sinuosity and lateral migration is observed as this channel crosses the fold crest and footwall syncline of Fold 2. The lack of diversion (c.f. Clark and Cartwright 2009) observed in this channel levee system is consistent with observations from seismic profiles and from the isochron map of the lower growth sequence: These show an overlapping stratal geometry above the crests of Folds 1 and 2 with variable thinning occurring along strike linked to changes in structural relief (see previous section). Reflection packages which are continuous across the fold crest but thin as they pass over it can be interpreted to

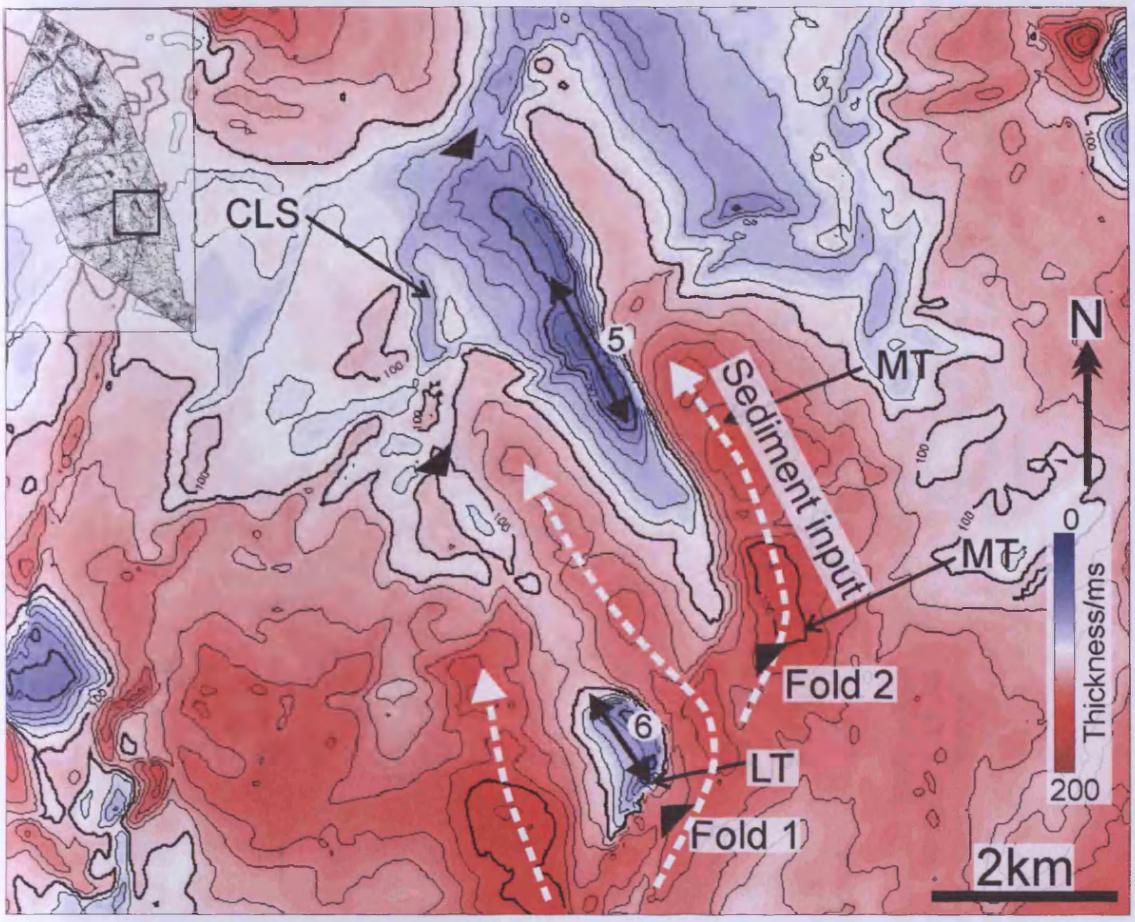

Figure 5.11: Isochron map of the upper growth sequence, contours spaced at 25ms intervals. Dashed white arrows indicate the sedimentary input directions. Points 5 and 6 correspond to the measured zones of increased expansion factor in figure 5.9 LT = lateral terminations, MT = Maximum thickness, CLS = Channel levee system. See text for details.

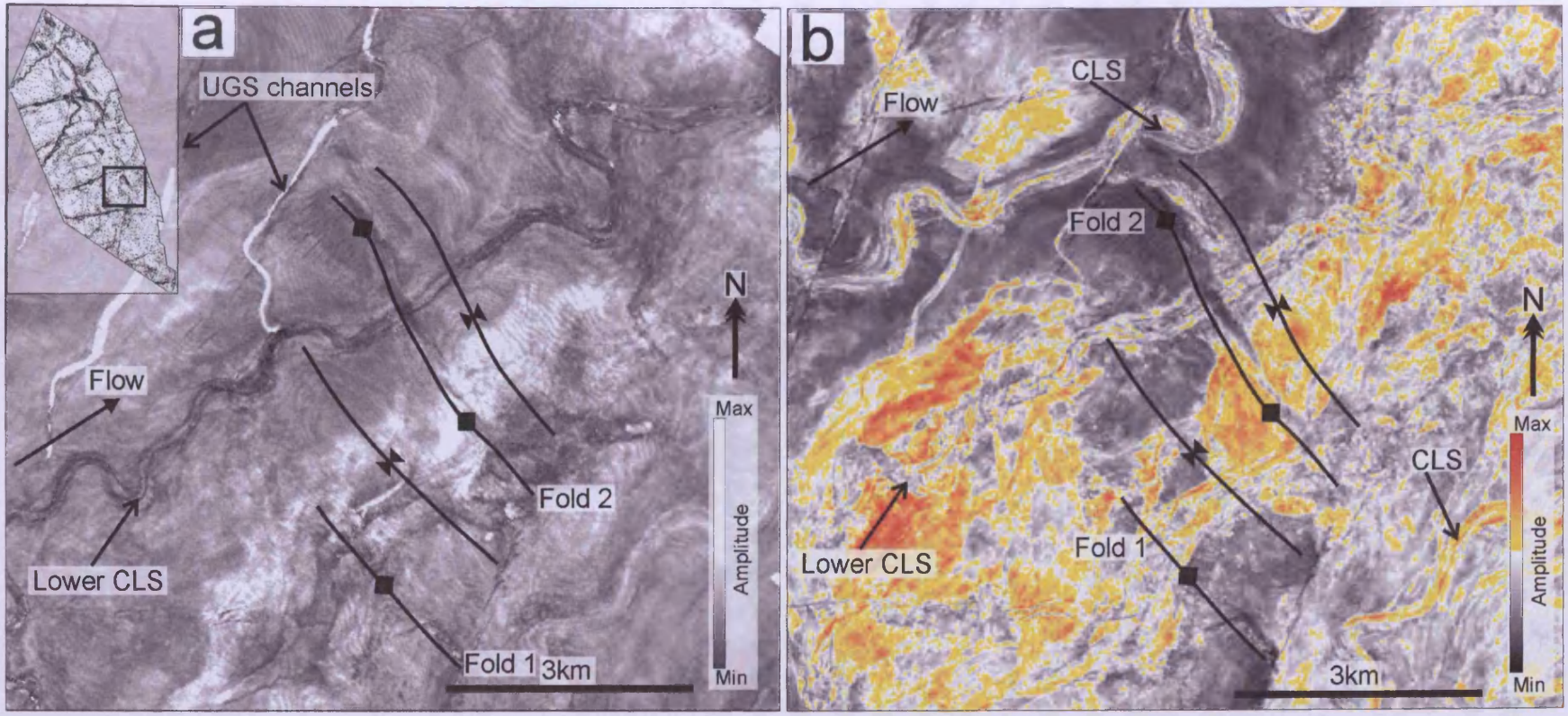

Figure 5.12: **a** shows a amplitude map of the top lower growth sequence surface. UGS (Upper growth sequence) Channels mark upper growth sequence channel levee systems that have partially incised down to this stratigraphic level but are not part of the lower growth sequence. The lower channel levee system crosses the crest of fold 1 where a decrease in channel sinuosity is observed. Otherwise the course of this channel is unaffected by development of folds 1 and 2. **b** shows RMS amplitude extracted over a 60ms window below the top surface of the lower growth sequence. The map shows two channel levee systems (marked CLS) which also flow perpendicular to the strike of folds 1 and 2 but do not cross the fold crests.

represent a lack of positive relief at the depositional surface during fold growth due to the increased relative rate of sedimentation compared uplift. This interpretation is consistent with the results observed here where folding did not obstruct the flow path of this particular channel levee system (see also: Burbank et al 1996).

5.5.4.1 Upper channel levee system

The upper channel levee system shows significant differences in channel morphology and development compared to the lower channel levee system (Fig. 5.13). This channel enters the study area from the south-west, with an avulsion site located immediately downstream of the south-eastern lateral termination of Fold 1 (Fig 5.13). Upstream of the avulsion site, two highly sinuous channel segments are developed (Fig. 5.13), with the segment to the west being the most recent. This can be observed from the vertical stacking relationships between the two channel segments. The eastern channel segment displays a uniformly high sinuosity associated with a high degree of lateral migration of individual meander loops, as is apparent from the base channel amplitude map (Fig. 5.13). The western channel segment displays a variable sinuosity, with higher values observed within the hanging-wall of Fold 1, followed by a decrease where the channel segment is diverted around the north-western lateral termination (Fig. 5.13). The western channel segment also shows increased occurrence of meander cut-off loops within the hanging wall of Fold 2 associated with the higher values of sinuosity in this area (Fig. 5.13).

Table 5.1: Summary of the observations presented in the preceeding section.

Results	***Growth sequence***	***Key Observations***
Structural relief measurements.	**Upper**	• Both folds show asymmetric relief development. • Fold 1 shows maximum relief recorded towards the south-east, with little additional relief developed at the north-west termination. • Fold 2 shows a shift in the location of maximum relief development towards the central zone of the fold.
	Lower	• Fold 1 and fold 2 show maximum relief developed at the fold-strike slip fault terminations, and a decreased relief relative to these areas across the central part of each fold.
Growth sequence expansion factor.	**Upper**	• Expansion factor along strike mirrors the observations above – expansion is concentrated towards the fold:strike-slip fault terminations. • Fold 1 shows little expansion at its previously active north-west termination. • Fold 2 shows increased expansion shift away from the north-west termination towards the central zone.
	Lower	• Maximum growth concentrated at terminations of folds 1 and 2 against strike-slip faults.
Isochron maps.	**Upper**	• Change in direction of sediment input to fold-perpendicular directed sedimentation. • Only the south-east termination of fold 1 obstructs deposition. • Fold 2 shows increased uplift within its central area and towards the north-west termination.
	Lower	• Sedimentation perpendicular to fold orientation. • Deposition within hangingwall and footwall synclines. • Thinning observed where lateral terminations of folds occur against strike-slip faults, which also limit deposition within the synclines.
Submarine channel system development.	**Upper**	• Upper channel levee system is strongly affected by the relief of both folds resulting in avulsion and spatial variations in sinuosity and lateral migration.
	Lower	• Lower channel levee system flows perpendicular to fold 2 and crosses the fold crest without diversion. • Planform morphology of this channel shows a clear decrease in sinuosity as the fold crest is crossed.

5.6 Discussion

The observations presented above from the detailed case study of the deepwater fold belt of the Levant margin show a system of thrusts and overlying folds that are highly compartmentalised by a series of coeval conjugate strike slip faults. Both of these structural elements influenced seafloor topography to a varying degree according to the magnitude of uplift which is non-uniform along strike. The evolution of fold structural relief was conditioned in part by the intersections between thrust and strike slip faults. Fold propagation, and notably along strike development was thus more asymmetrical than would be traditionally expected (e.g. Salvini and Storti 2002). The following discussion considers in more detail the manner in which sedimentary pathways were controlled by the evolution of structural relief and its effect on seafloor topography. This discussion attempts to explore in more detail some of the factors affecting the architecture of growth sequences and their along strike variations, as a means of emphasising the possible problems confronting interpretations solely based on limited outcrop or 2D seismic profiles. We also attempt to examine in more detail the link between growth sequence geometries and development of submarine channel systems.

5.6.1 Submarine channel development during folding: The link with growth sequence geometry

Studies from subaerial channel systems (e.g. Burbank et al 1996; Snow and Slingerland 1990) show that several factors influence the response of channel systems to underlying fold growth. These include the rates of growth and 3D geometry of multiple fold structures, the flow characteristics of the channel system, and the presence of any pre-existing topography which will influence flow pathways prior to any affects of subsequent deformation. Transverse channel systems, whose orientation is often perpendicular to fold strike, must maintain a sufficiently high ratio of aggradation upstream of the fold as well as erosion across the fold crest in order to avoid becoming 'defeated' and subsequently blocked by the growing structure (see also: Burbank et al 1996 for a summary of these concepts as applied to subaerial systems).

When attempting to apply these concepts to submarine channel-structure interactions it is important to note some key differences in terms of channel evolution between subaerial and submarine systems (e.g. Kolla et al 2007). Firstly, submarine channel systems often show significantly increased component of vertical aggradation compared to subaerial channels. Secondly, a significant proportion of the flow in submarine systems can overspill the channel levees, particularly at the downstream facing outer banks of channel meanders (Peakall et al 2000; Kolla et al 2007; Straub et al 2008; Corney et al 2006). Thus, the role of increased aggradation in submarine channel systems should be taken into account when assessing

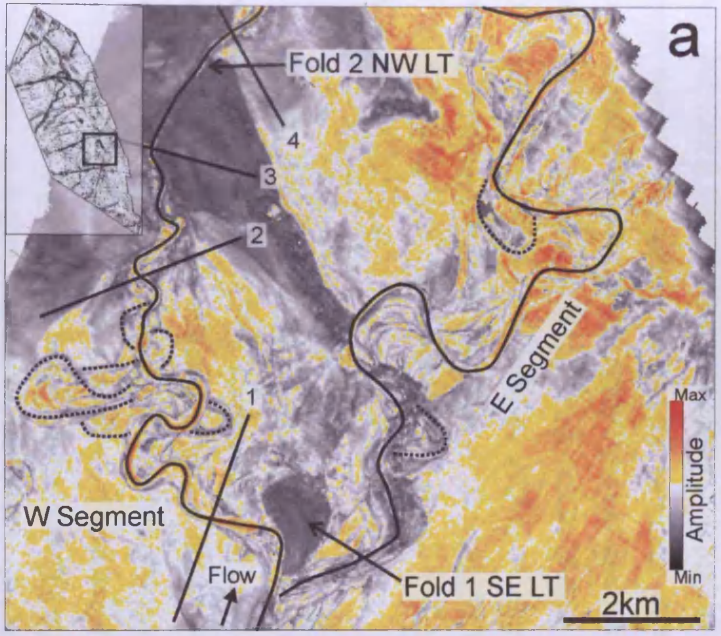

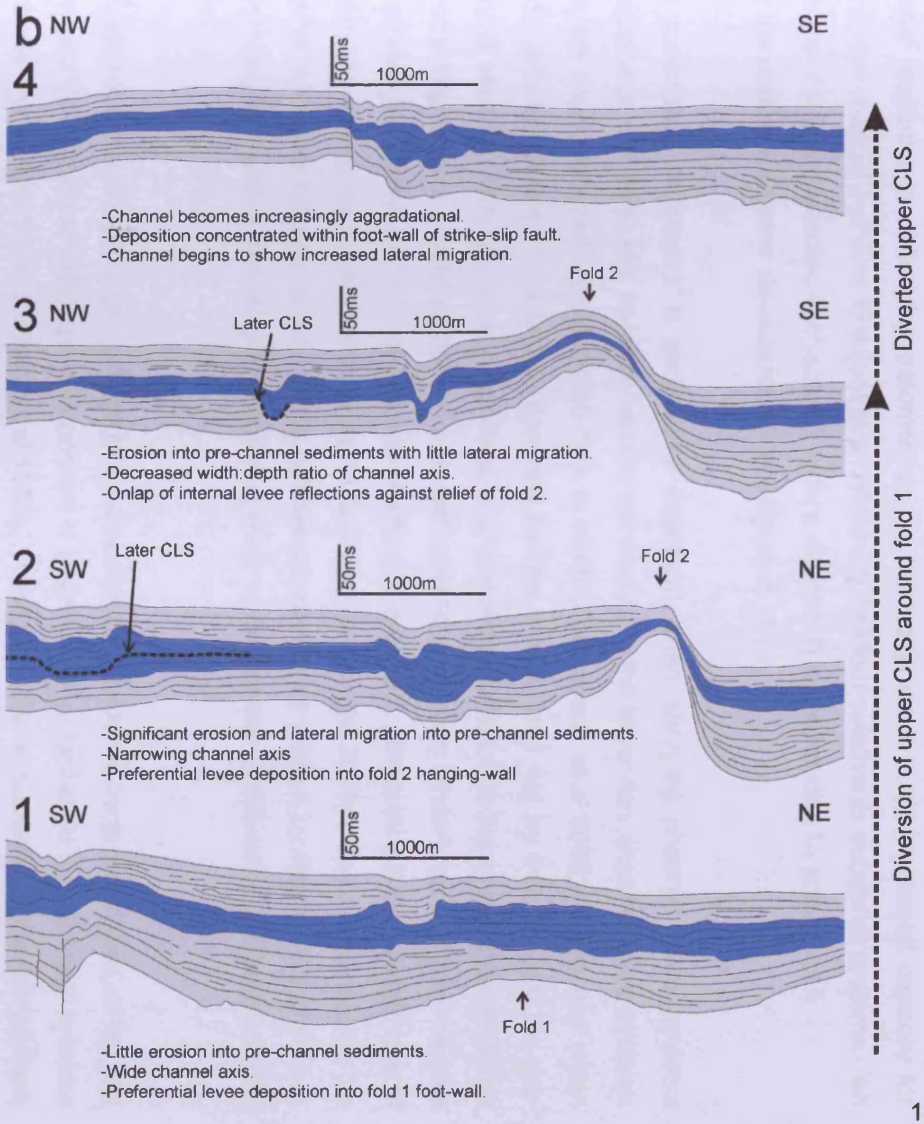

Figure 5.13: **a** shows the amplitude map at the base of the upper channel levee system. This channel splits at the south-east lateral termination of fold 1 into western and eastern segments, of which the western segment is the younger. The western segment shows spatial variability in channel lateral migration and in the formation of cut-off loops (dashed lines). **b** shows a series of interpreted seismic profiles of the upper growth sequence, with the upper channel interval marked in blue. These profiles illustrate the change in channel morphology as it is diverted around the relief formed by fold 2 over the upper growth sequence interval.

channel response to underlying deformation, as this may result in an increased capacity for submarine channel systems to adjust to a deforming seafloor relative to subaerial systems. An example of this is presented in chapter 3, where channel B is responding to active uplift over the period of channel development - see figure 3.11.

This conceptual framework is particularly important when studying channel levee systems developed on the lower fan, as is the case in our study. In the lower fan, channel levee systems often are relatively small – typically 0.5-1km in width (Babonneau et al 2002; Pirmez and Imran 2003), with the channel axis largely confined by the levees, and not by incision into the pre-channel section. The increased magnitude of channel aggradation in lower fan channel levee systems implies that a channel flowing perpendicular to a growing underlying fold may be able to maintain its course and will not become blocked or diverted, particularly if the relative rate of uplift is low compared to sedimentation (c.f. Clark and Cartwright 2009). This appears to be the case for the lower channel levee system, whose course is not altered by the growth of Fold 2, even though a more subtle morphological response – a decrease in sinuosity, is observed (Fig. 5.12a).

The general link between large scale growth sequence architectures such as overlap, onlap and offlap and the pattern of drainage development is already well established for subaerial systems (Burbank and Verges 1994; Burbank et al 1996). Previous work on subaerial systems (Burbank et al 1996) and the recent studies from deepwater fold and thrust belts (Huyghe et al 2004; Morley and Leong 2008) show that where overlapping growth sequence architectures occur, drainage tends to be perpendicular to the fold axis. Onlapping growth sequence architectures are characteristic of a drainage system that is parallel to fold axes, where diversion occurs around the lateral regions of folds (Burbank et al 1996). This case study also demonstrates that this set of structure-channel relationships applies in deepwater systems, but that channel levee development within growth sequences can vary greatly in their spatial and temporal evolution. The ultimate cause of this is likely to be the three-dimensional variability in underlying deformation.

An example of this relationship is seen in the lower channel levee system which flows perpendicular to the strike of Fold 2, which is developed within an overlapping growth sequence (Fig. 5.12). The overlapping stratal geometry implies that, at the scale of the seismic data used here, no positive topography developed during the growth of Fold 2 over the time interval represented by the lower growth sequence. Sinuosity of submarine channel systems has been demonstrated to be linked, in general, to the underlying slope gradient by several studies (See chapter 1; Ferry et al 2005; Pirmez et al 2000; Huyghe et al 2004; Babonneau et al 2002). The

planform geometry of the lower channel levee system seen here is consistent with a channel response to an increased underlying gradient in the downstream direction, resulting in a decrease in channel sinuosity across the crest of fold 2 (Fig. 5.12). The decrease in sinuosity in this area is associated with a localised channel course which shows little lateral migration (Fig. 5.12). The important implication of this is that although the growth sequence architecture implies no positive seafloor relief due to folding took place, the imprint of the underlying deformation still results in a decrease in channel sinuosity as it crosses the fold crest and footwall.

The evolution of the upper submarine channel system is characterised by the diversion of the western branch around the emerging topography of Fold 2. Diversion of this channel levee system, combined with the increasing occurrence of onlap onto the limbs of fold 2 within the upper growth sequence (Fig. 5.13) indicate that a higher relative rate of uplift compared to sedimentation characterised this sequence. The western branch of the upper channel shows an increase in sinuosity within the hangingwall of Fold 2, with the zone of increased sinuosity being associated with frequent meander cut-off loops (6) (Fig. 5.13). This is in contrast to the eastern branch, which shows prominent lateral migration with meander cut-off being much less common, with only two clear cut-offs observed. The eastern branch also shows less spatial variation in sinuosity compared to the western branch (Fig. 5.13). The strong preferential development of sinuosity observed for the eastern branch of the upper channel is developed within the hangingwall syncline of Fold 2. The spatial association between this zone of high sinuosity and the underlying formation of negative relief suggests an important accommodation space control on the development of this particular reach of the upper channel (see also discussion, Fig. 6.7). This relationship is likely to be found in other deepwater channels interacting with structurally controlled topography.

5.6.2 Factors affecting growth sequence architecture along strike

The along-strike variation in fold amplitude is a key parameter in determining the final three dimensional growth sequence geometry (Salvini and Storti 2002). The examples documented here are excellent case studies in how the along-strike transition between onlap and overlap depends on variable relative rates of uplift versus sedimentation, that have wider implications for the way we interpret growth sequences in deepwater fold and thrust belt settings. The folds in this study show increased uplift relative to sedimentation at lateral terminations with strike-slip faults which compartmentalise the thrusts and folds. This is in contrast to systems where the maximum fold amplitude is located in the centre of the fold and decreases towards the lateral tip regions (Salvini and Storti 2002; Morley 2009; Higgins et al. 2009). The development of

structural relief along strike is also a key factor which determines the sedimentary transport pathways around the fold (see examples in previous section). Folds 1 and 2 documented here both illustrate a mode of fold growth that is highly skewed and non-uniform both spatially and temporally (e.g. Figs. 5.10 and 5.11). The effects of this non-uniform spatial and temporal uplift pattern can be seen in the evolution of sediment flow paths and in net sediment accumulation, and attests to the coupled nature of the interactions between sediment transport and structural evolution in this type of deepwater fold belt.

The folds throughout this study area are characterised by the development of synclines within the footwall and hangingwall (Fig. 5.7). These are key features affecting sediment pathways in that the negative relief of these depressions causes local gradient changes that combine with the effects of positive relief over the fold crestal regions. An excellent example of this is where the eastern branch of the upper channel levee system displays an increased sinuosity associated with a number of meander cut-off loops within the hangingwall of Fold 2. Channel morphology in this area contrasts significantly with the reach downstream which is diverted around the north-west lateral termination of Fold 2, which is much straighter with limited lateral migration (Fig. 5.13). This example is a simple illustration of the strong controls exerted on channel morphology by structurally induced gradient changes.

Growth sequences can record important variations in the relative rates of sedimentation and uplift, particularly when sub-divided into narrower intervals. One of the most difficult aspects of the interpretation of growth sequences is to relate lateral variations in sedimentation rate to variations in fold amplification (Fig 5.14). In the discussion above it has been tacitly assumed that growth sequence deposition was spatially uniform. However, the channel levee systems comprising the growth sequences are effectively linear sources in terms of sediment flux, with sedimentation rates decreasing rapidly away from the channel axis (Fig 5.14). This increase in the local rate of deposition towards the channel axis leads to increased deposit thicknesses in this region and can result in a growth sequence architecture that can easily be interpreted in terms of a misleadingly high rate of sedimentation relative to uplift. This could be a common pitfall in many deepwater fold belt settings, where channels are frequently diverted around the lateral tips of folds (Demytteneaere et al 2000; Morley 2009; Huyghe et al 2004; Clark and Cartwright, 2009). The key implication of this is that the interpretation of relative sedimentation and uplift rates around fold tip/termination regions requires a three dimensional perspective which takes into account the mechanism of sedimentation within the growth sequence to accurately interpret fold growth.

5.6.3 Summary: Conceptual model of deformation and sedimentation

Fold uplift during the lower growth sequence was non-uniform and concentrated towards the lateral terminations of Folds 1 and 2 (Fig 5.15a). The magnitude of uplift, from measurements of fold relief, was greater along Fold 2 compared to Fold 1. The growth sequence architecture is primarily one of overlap, indicating that no fold relief developed on the seafloor during this stage of folding (Fig 5.15b).

Submarine channel development during the lower growth sequence supports the observations above that no fold relief developed at the seafloor during deposition of the lower growth sequence (Fig. 5.15b). This resulted in development of channel levee systems which flowed perpendicular to the fold crest. Although channel development is perpendicular to the fold crest, underlying deformation was still sufficient to affect channel sinuosity over the fold crestal region and the footwall. This was most likely a result of subtle gradient changes causing the channel to re-adjust its planform geometry in order to achieve equilibrium at this location (e.g. Pirmez et al 2000).

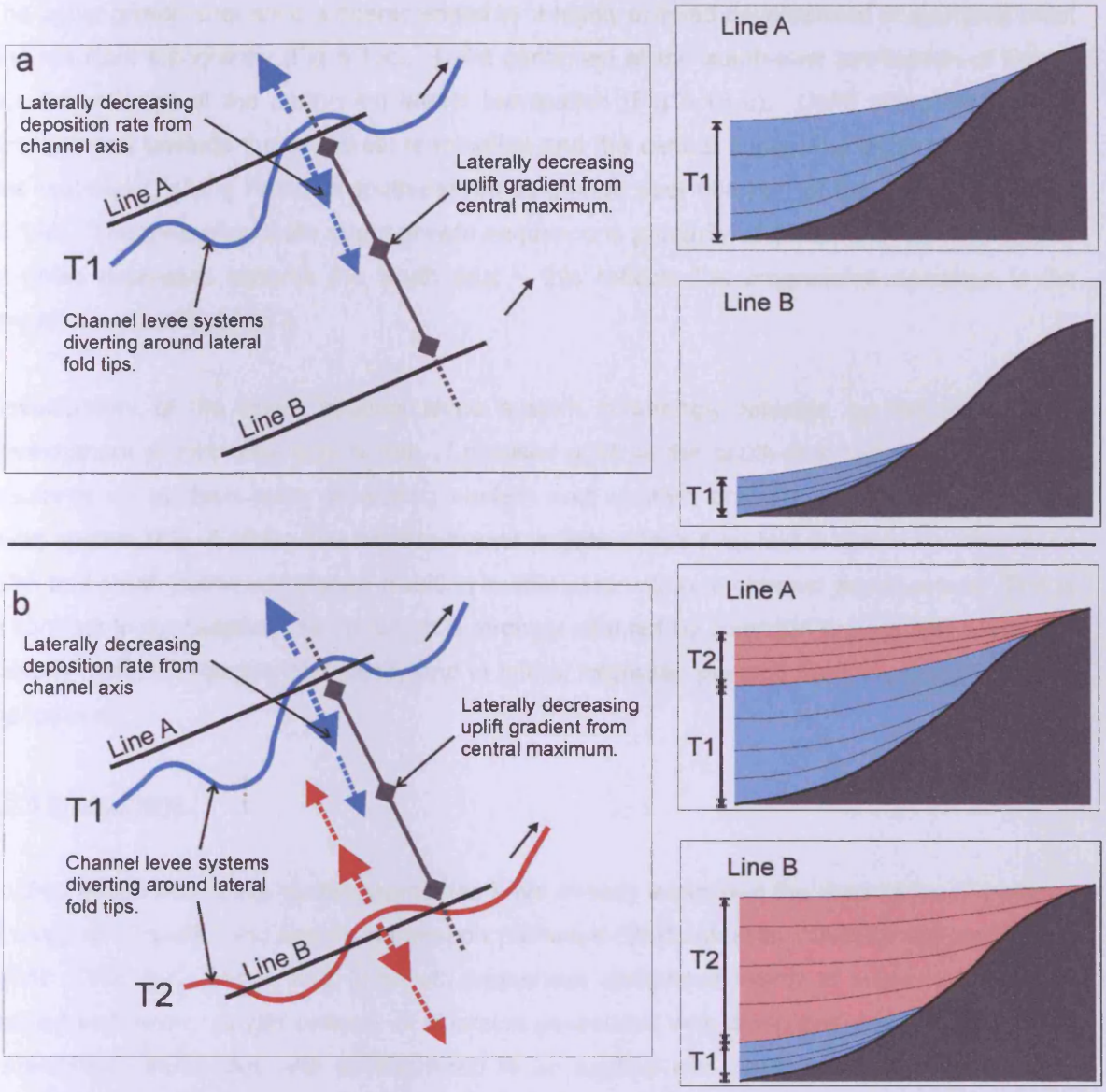

Figure 5.14: Schematic figure showing the effect of laterally decreasing deposition rates from submarine channel systems on growth sequence architecture. At T1 shown in **a**, the blue channel system deposits progressively thin away from the channel axis, resulting in an apparent decrease in the relative rate of sedimentation compared to uplift at line B. At T2 shown in **b**, a later channel levee system repeats the process to build the overall growth sequence architecture where apparent changes in the relative rates of sedimentation vs uplift are affected by lateral variations in deposition rate away from the channel axis as well as from fold uplift itself.

The upper growth sequence is characterised by a highly skewed development of structural relief and resultant topography (Fig 5.15c). Uplift continued at the south-east termination of Fold 1 but discontinued at the north-west lateral termination (Fig 5.15 c). Uplift along Fold 2 was concentrated towards the northwest termination and the central zones, but decreased towards the south-east, giving Fold 2 a south-eastwards plunge over this part of the growth sequence (5.15c). The geometry of the upper growth sequence is primarily of onlap, although the degree of onlap decreases towards the south east – this reflects the progressive decrease in the magnitude of uplift of fold 2.

Development of the upper channel levee system is strongly affected by the non-uniform development of fold relief (Fig. 5.15d). Localised uplift at the south-east termination of fold 1 results in an avulsion node separating eastern and western branches of the upper channel levee system (Fig. 5.15d). The eastern branch is little affected by fold 2 due to the decreased relief and south-eastwards plunge resulting in little obstruction to channel development. This is in contrast to the western branch, which is strongly affected by diversion around fold 1 and also exhibits marked changes in sinuosity and in lateral migration passing from the hanging wall to the footwall.

5.6.4 Implications

Studies based on growth stratal geometries have already examined the links between patterns of onlap and overlap and sediment transport pathways (Burbank et al. 1996; Morley and Leong 2008). This study shows that, in growth sequences comprised mainly of submarine channel-derived sediments, simple patterns of diversion associated with onlap and unconfined channel development associated with overlap need to be applied with caution. Instead, patterns of submarine channel development reveal a more subtle influence of underlying deformation than can be ascertained from the study of growth sequence geometries alone. These include preferential sinuosity development and associated variations in the degree of lateral migration which can vary dramatically over relatively short distances – 100s of metres in the case of the examples discussed here (see Fig. 5.13). These areas of increased lateral migration and sinuosity can be associated with potentially sand-rich lateral migration deposits (Abreau et al. 2003; see also Fig. 5.13). Thus a more detailed knowledge of where these areas occur in structurally deformed areas may be of use in predicting potential reservoir characteristics at greater depths in seismic surveys where resolution is poorer. In contrast, the lower channel levee system shows a
decreased sinuosity

5.15a Lower growth sequence - structure

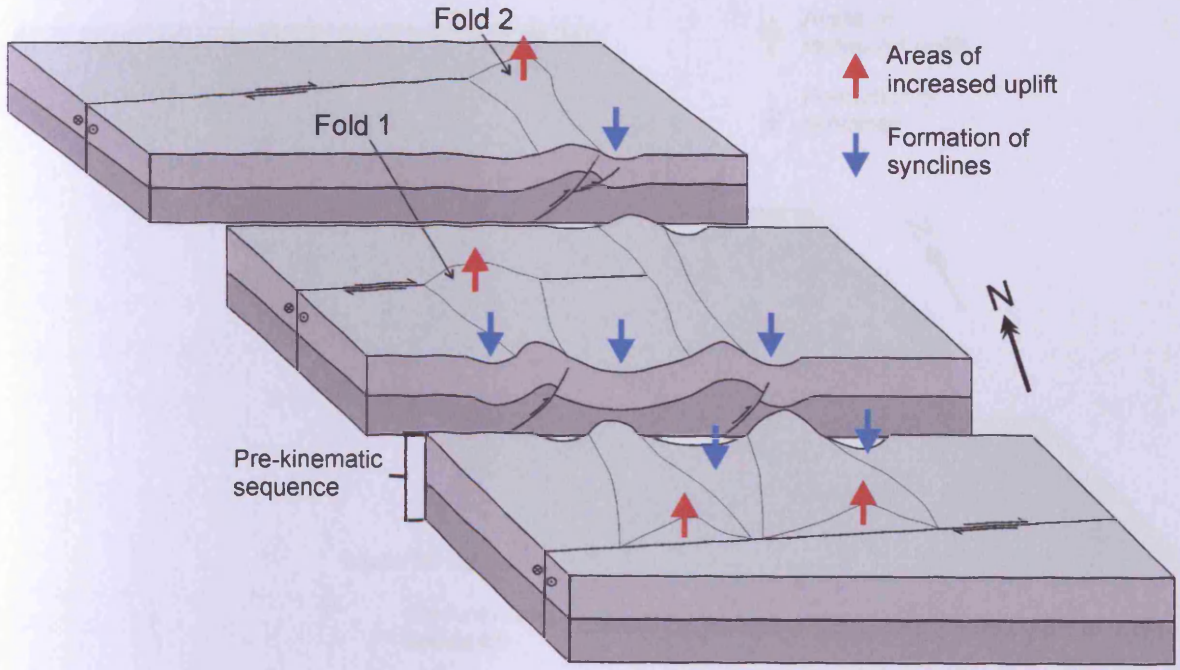

5.15b Lower growth sequence - sedimentation

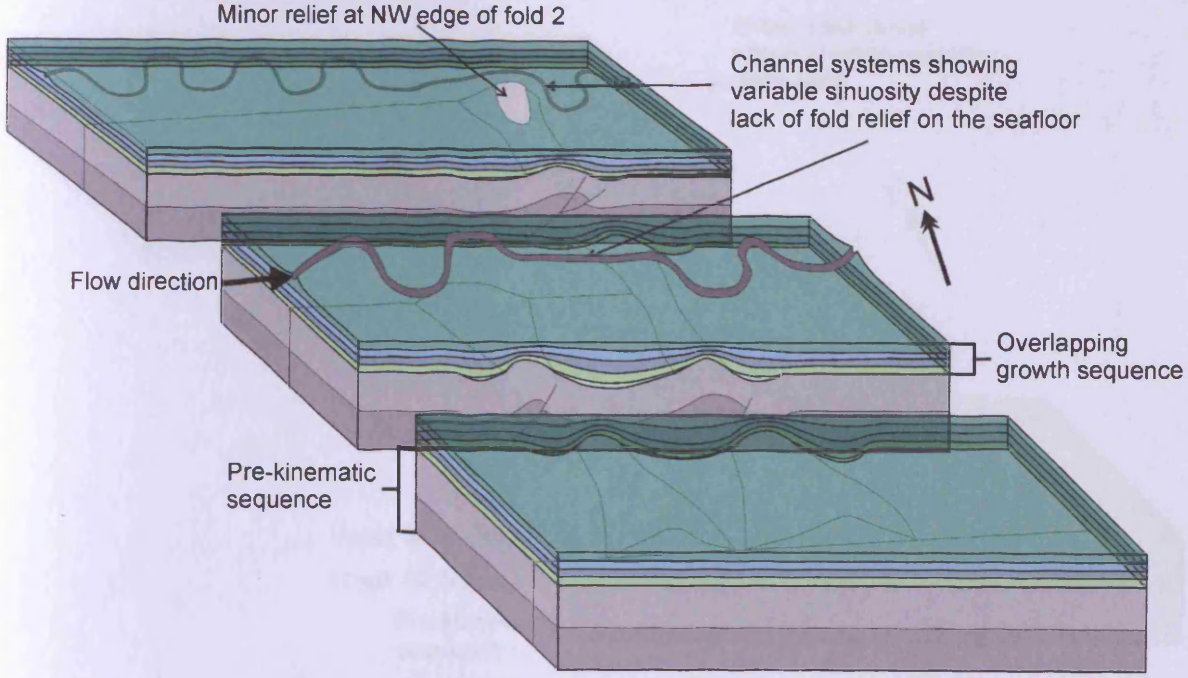

5.15c Upper growth sequence - structure

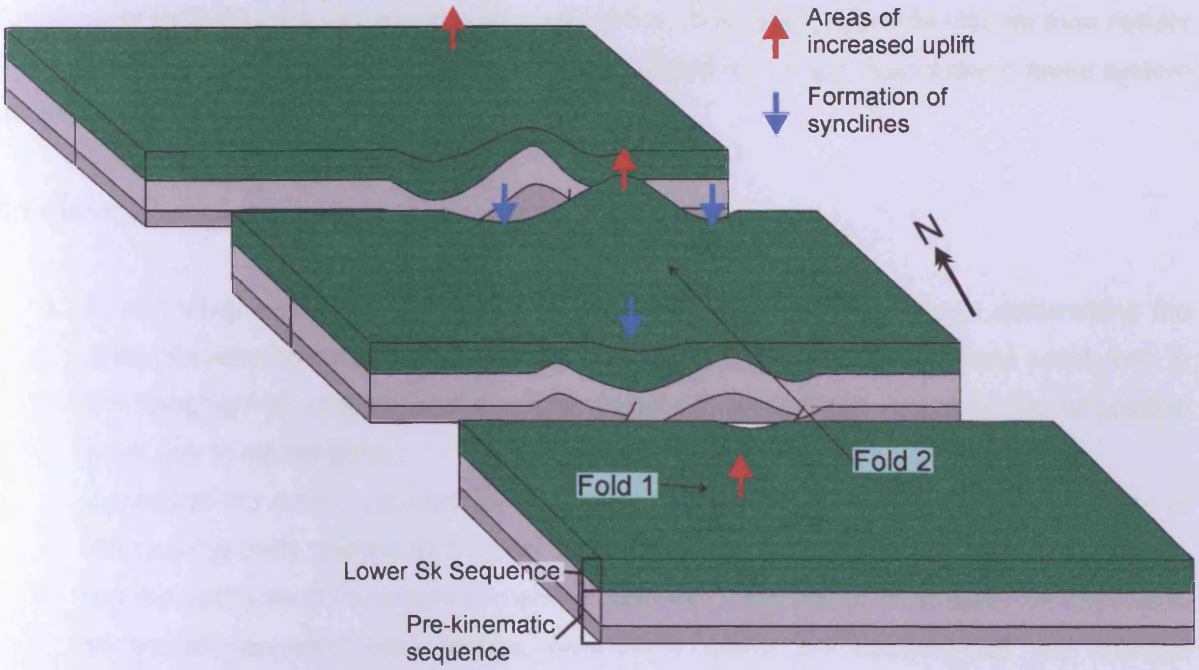

5.15d Upper growth sequence - sedimentation

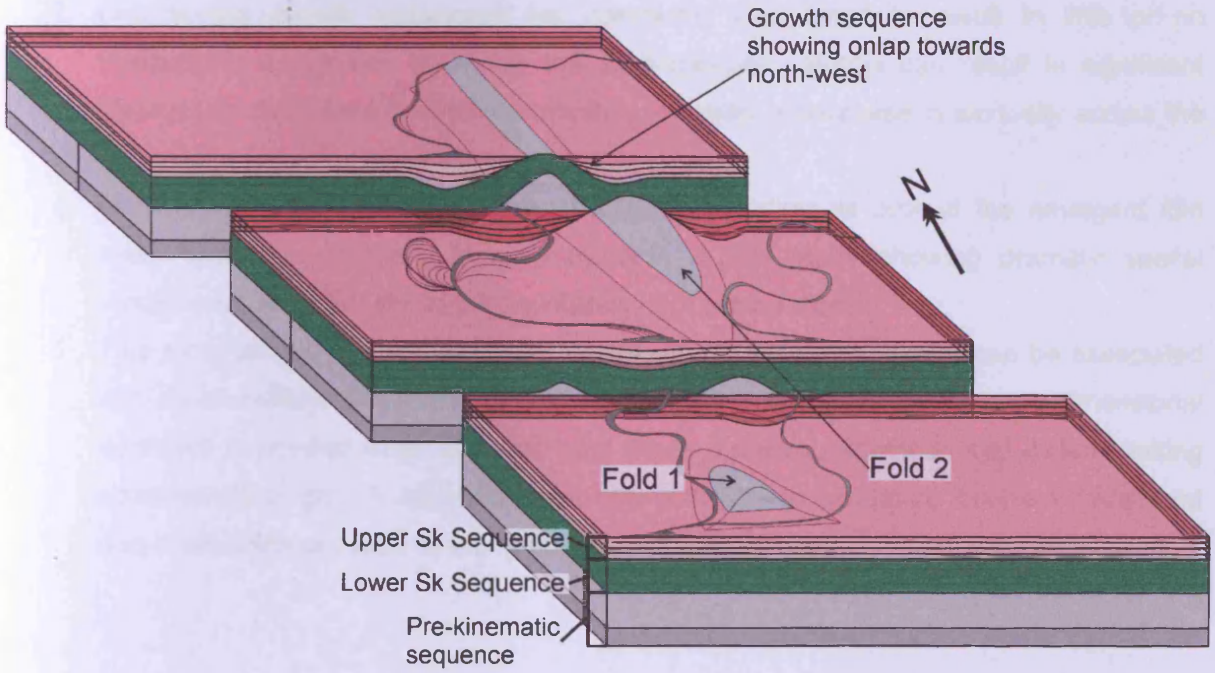

Figure 5.15: Conceptual model of fold development and growth sequence development. See text for details.

across the fold crest and this implies that channel levee systems may still be affected by underlying deformation, even when they develop within an overlapping growth sequence. Subsequent folding which incorporates this part of the channel into the fold closure then results in a greatly decreased potential reservoir volume compared to a sinuous channel levee system which is incorporated into the fold crest.

5.7 Conclusions

1. In this study area, the structural style of folding plays a critical role in determining the available accommodation space for sediment deposition. The depressions which form in the hanging-wall and foot-wall syncline areas are coeval with the evolution of positive relief due to crestal uplift.
2. Control of the evolving structural relief on channel sinuosity: Depending on the rate of structural growth relative to channel deposition, the sinuosity of the channel can vary greatly over a short (hundreds of metres) distance. This results in preferential deposition of laterally accreted sand bodies, particularly within the hanging-wall and footwall synclines of folds. Preferential sinuosity development in this way is usually associated with diversion and/or deflection of the channels around the fold so that a portion of the channel occupies the axis of the hanging-wall or foot-wall.
3. Overlapping growth sequences are commonly interpreted to result in little or no topographic expression of folding but in deepwater settings can result in significant changes in submarine channel morphology, causing a decrease in sinuosity across the fold crest.
4. Onlapping growth sequences imply diversion of sediments around the emergent fold relief, with the submarine channel systems in this study showing dramatic spatial variations in sinuosity and in the development of cut-off loops.
5. This study shows that folding during growth sequence development can be associated with a non-uniform distribution of uplift along strike. Therefore a fully three dimensional approach is needed when characterising these systems. Methods can include linking observations of growth sequence geometry with growth sequence isochron maps, and also measurements such as along-strike relief development.

Chapter 6

CHAPTER 6

SUMMARY AND DISCUSSION

6.1 Summary

The work presented in this thesis can be summarised within the conceptual framework presented in figure 6.1. Chapter Three describes the detailed interactions between submarine channel systems and folding, using examples from the eastern Nile deepwater fold belt. From this description a novel and coherent framework for classifying submarine channel-structure interactions was introduced. Chapter Four is a more focussed study on the detailed three dimensional stacking patterns within a single growth sequence from the western Niger Delta. This chapter forms a case study of how three-dimensional stacking patterns within a growth sequence vary over time, and provides a useful basis for comparing deepwater fold belts from different locations. Chapter Five broadens the description and analysis of submarine channel-structure interactions previously documented and attempts to link these detailed interactions to larger scale growth sequence geometries. In Chapter Five, the interactions between three-dimensional fold development and sedimentation are described, and from this it is shown that this can be an important control on more subtle responses of submarine channels to deformation, such as spatial sinuosity variations. These three chapters form a coherent set of studies which aim to address the nature of sediment-structure interactions in deepwater fold belts, firstly by concentrating on detailed studies and then attempting to link this with growth sequences, which represent the larger scale result of coeval sedimentation and deformation. This work also highlights the advantages of taking a fully three dimensional approach to understanding both growth sequence architecture (Chapter 4) and fold evolution over time (Chapter 5)

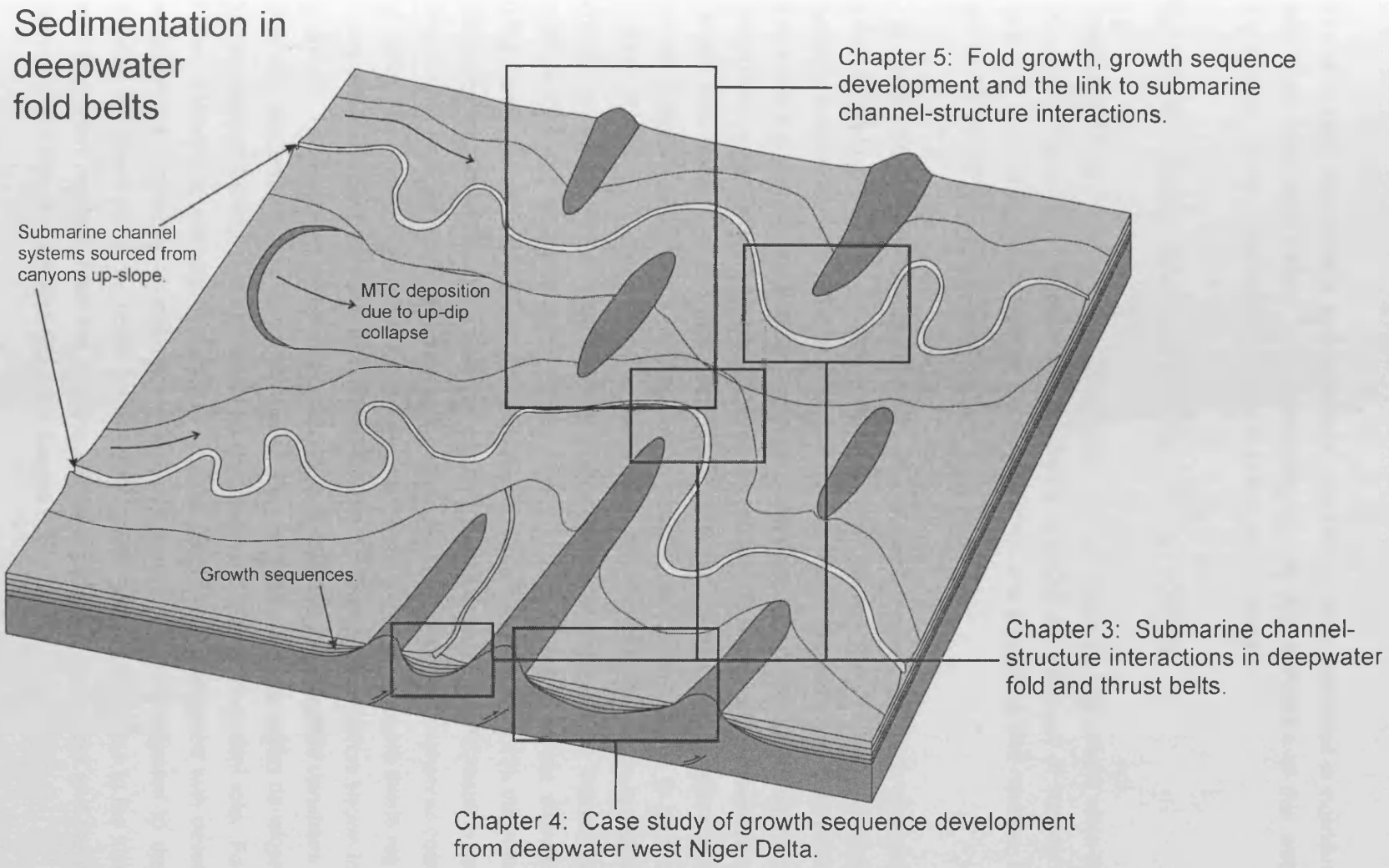

Figure 6.1: Conceptual model of a deep water fold-belt setting where sedimentation interacts with deformation to control the evolution of seafloor bathymetry. The themes covered in the three chapters in this thesis are placed within the context of this environment.

6.2 Discussion

The aim of this discussion is to draw together the main themes discussed in individual chapters and to develop them further. The general applicability and limitations of this work are also highlighted. Finally, some ideas for future research are presented.

6.2.1 Submarine channel-structure interactions as end-members

Chapter 3, which details a set of end-member channel structure interactions aims to provide a descriptive framework for describing submarine channel development in actively deforming settings. This section further refines this classification, and places the end-member interactions within the context of the timing of deformation.

The timing of deformation relative to sedimentation (pre-, post- or syn- channel development) is a key factor in controlling the type and style of interaction. Diversion and confinement form opposite end-members in terms of interactions which are governed by pre-channel deformation, and this is summarised graphically in figure 6.2. Both of these interactions require pre-existing bathymetry to be present to control the channel course. The transition between pure diversion (simple local diversions) and pure confinement (channel course and deposition of the channel levees is entirely physically constrained by surrounding structures) seems to be related to the number of structures which affect a channel's course. Simple diversions typically involve a change in channel course related to a single structure which obstructs the channel pathway, an example of which is presented in figure 6.2 (a and b) involving a simple channel diversion around a single fold from the Levant Basin. As seen in Chapter 3 (Fig 3.12), the influence of an increasing number of folds on a particular channel course is more likely to result in confinement, which in turn may be associated with larger scale diversions shifting the channel course by tens of kilometres laterally (Fig. 6.2, e and f). Between these two end-members exists regional scale diversions associated with only partial confinement, an example of which is shown in figure 6.2 (c and d). This example shows clear diversion and also significant spatial variations in channel sinuosity (see also Chapter 5, section 5.5.4), with the high sinuosity region developed with the hanging-wall of the fold. Fold style and spacing may also play an important role. For example, in the eastern Nile fold belt, the structural style of the folds is associated with development of prominent hangingwall and footwall synclines. These depressions adjacent to the fold may increase the ability of this particular fold style to confine sedimentation due to the increased net structural relief resulting from the combined positive elevation of the fold and the depression formed by the adjacent syncline (See also section 6.2.2).

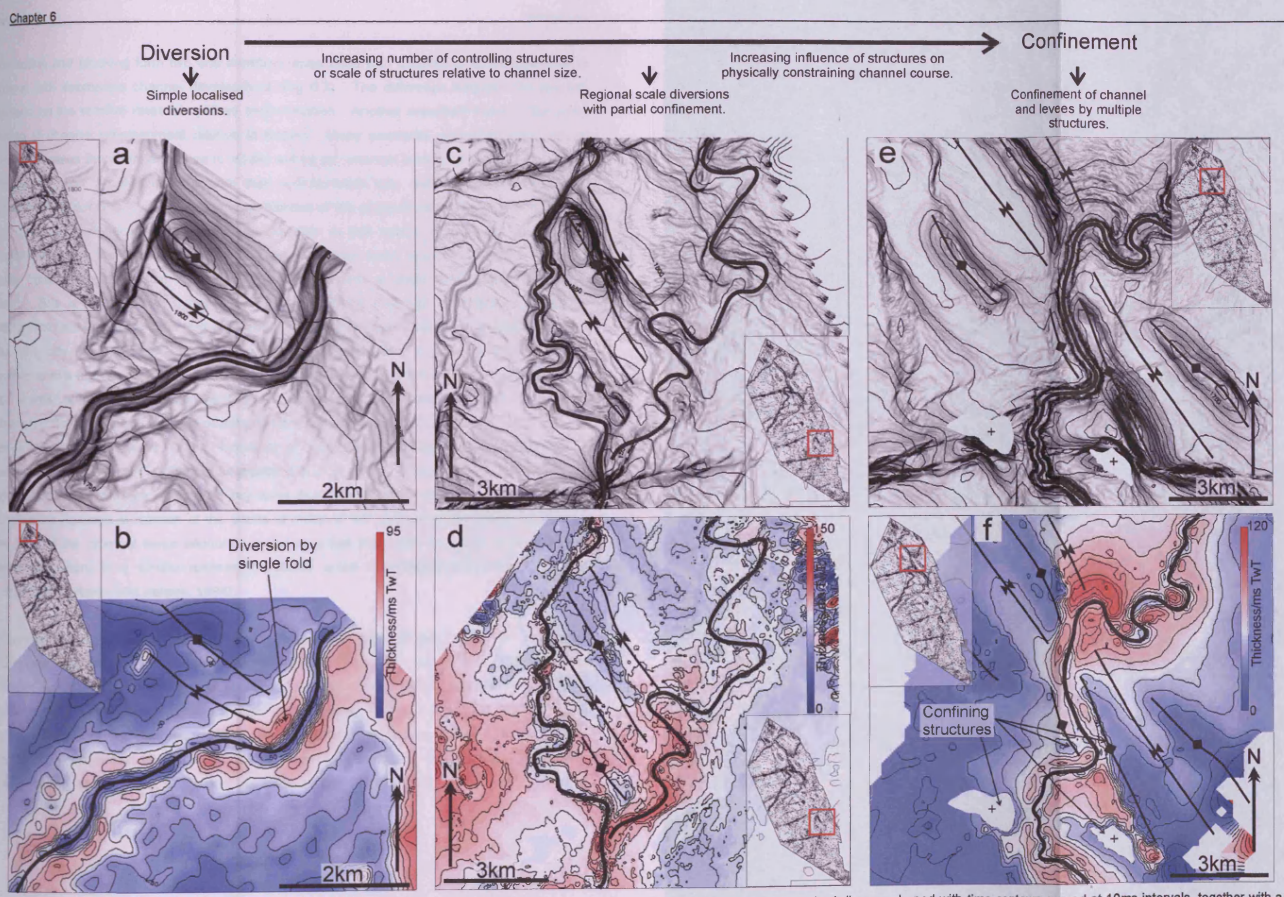

Figure 6.2. Examples of channel-structure interactions which show the transition from diversion to confinement. Each figure shows a seabed dip map draped with time contours spaced at 10ms intervals, together with a isochron map of the submarine channel with the folds marked as anticlines and synclines. Figures **a** and **b** illustrate a simple diversion around the tip of a fold which causes a shift in channel course of c.400m to the south east. Figures **c** and **d** show a diversion and avulsion caused by multiple folds (see chapter 5 for more details). The eastern channel segment is diverted for over 4 km by two folds which show non-uniform uplift along strike. Despite the influence of multiple folds on the channel course, this system is still relatively free to migrate and still exhibits a sinuous planform geometry. Figures **e** and **f** show a channel diverted by multiple structures but which is confined – this limits levee deposition and lateral migration of the channel.

Deflection and blocking form two end members associated with underlying deformation that is coeval with submarine channel development (Fig 6.3). The difference between the two will depend on the relative rates of uplift vs sedimentation. Another important factor is the initial timing of channel emplacement relative to folding. Many examples presented show that in nearly all cases the channel course is initially set by pre-channel folding. For situations where the rate of uplift is only slightly greater than sedimentation rate, deflection of the submarine channel will occur (Fig. 6.3). Accurate quantification of the absolute rate differences involved in this process of deflection have not been possible in this thesis, due to the lack of age constraints within the shallow stratigraphy. Deflection can result in a shift in channel position away from the focal point of uplift, or alternatively towards a newly forming bathymetric low point. This is illustrated in figure 6.3, where a channel meander is deflected towards a bathymetric low point over time (Fig 6.3a and b). Where the rate of uplift is significantly greater than the rate of deposition then blocking can occur, particularly if the growing structure is orientated at a high angle to the channel flow direction (Fig 6.3e and f). Blocking will also result in a sharply defined onlap relationship between the channel levee complex and the flank of the structure. Between these two end-members, intermediate modes of channel development may result in channel avulsions, or the formation of short-lived lobe-like deposits developed in particular at the base of the channel sequence (Fig 6.2c and d). The seismic profile shown in figure 6.2d also illustrates one of the key ways in which deflection can be recognised: The progressive increase in rotation of the points of onlap of the internal levee reflections towards the base of the channel levee sequence indicates active fold uplift during the time period of levee deposition, in a similar manner to rotated onlap relationships observed in growth sequences (Burbank and Verges, 1994).

Therefore, diversion and confinement may represent 'passive' responses of developing submarine channels to pre-existing structural relief. This is in contrast to deflection and blocking which represent the 'active' response of a developing submarine channel to coeval deformation. Recognition of these interactions provides a useful constraint on the timing relationships between deformation and folding where they can be recognised. Similar passive versus active responses are known from interactions between fluvial systems and neotectonic structures (e.g. Ouchi, 1985; Burbank et al., 1996; Burbank et al., 1999).

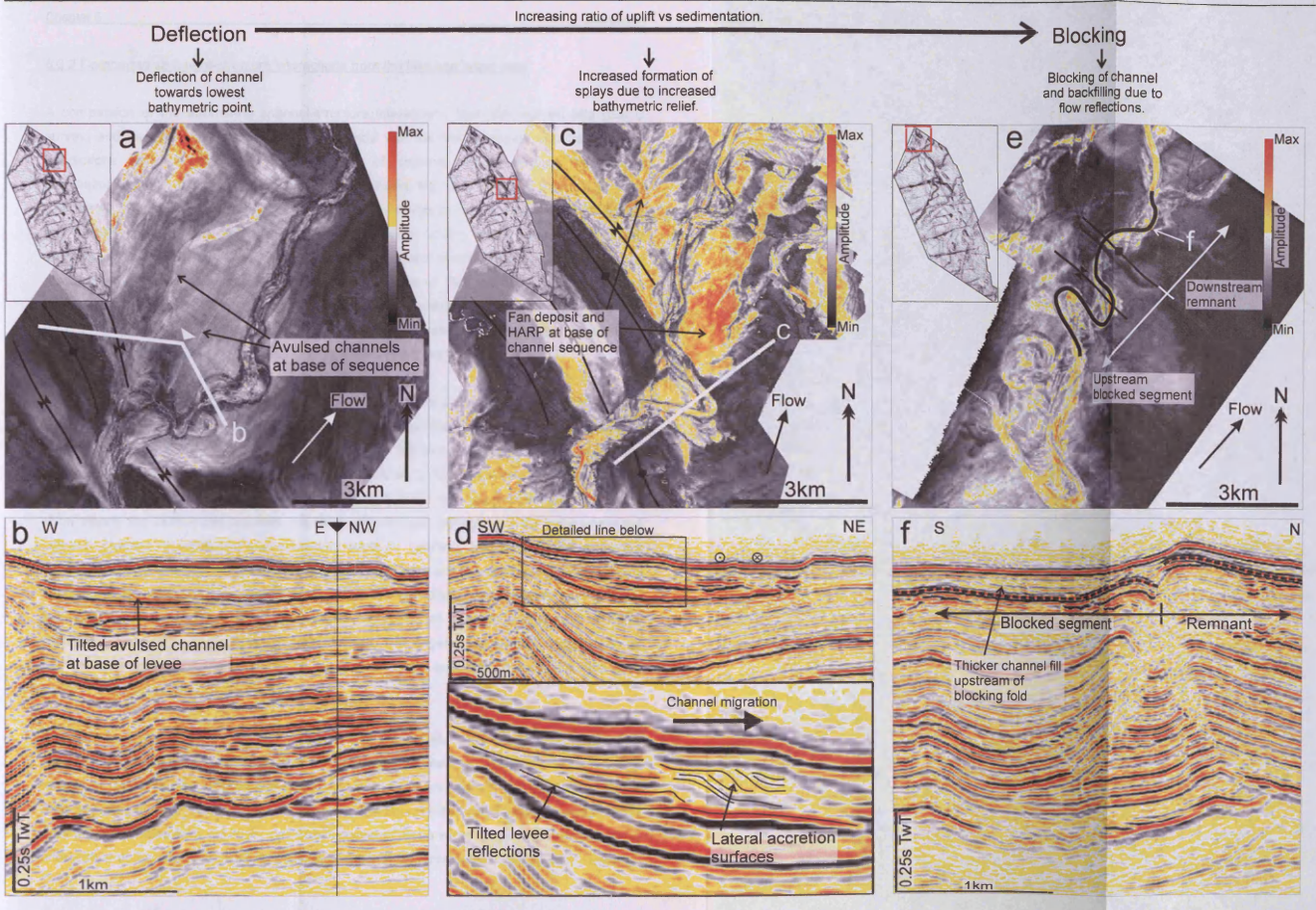

Figure 6.3. Examples of channel-structure interactions which show the transition from deflection to blocking. Each pair of figures shows a base channel sequence amplitude map together with a seismic profile illustrating some key characteristics. Figure a shows deflection of a single meander loop into a foot-wall syncline. This deflection is associated with a avulsion at the base of the channel sequence, which has become tilted due to subsequent folding, shown in profile b. Figures c and d show a deflection away from a growing fold, associated with the formation of a HARP unit (seen in c), the formation of lateral accretion surfaces facing away from the axis of uplift and internal levee reflections showing increased rotation towards the base of the levee package (d). Blocking is illustrated by e and f. The seismic profile shown in f is taken along the channel centreline and illustrates the increased thickness of channel deposits downstream of the fold which has caused blocking of this channel. A much thinner sequence of channel deposits is preserved upstream of the fold. See also chapter 3 for more details.

6.2.2 Comparing sediment-structure interactions from the Nile and Niger fans

A comparison of the submarine channel-structure interactions from the eastern Nile (Gal C survey) and the Niger delta (OPL322 Survey) show that the most common channel-structure interactions can be classified as diversions of channel course around the lateral terminations/tips of folds. Compare, for example, figure 6.2 with figures 4.9 and 4.11 from Chapter 4). Diversion of submarine channel systems around the lateral tips of the Aga Fold in the OPL322 survey occur immediately following onset of folding at the base of the growth sequence (Fig. 6.4). The diversionary paths of all subsequent channel levee systems within the growth sequence are then maintained around the edges of this fold during its subsequent development (Fig. 6.4). This is in contrast to some folds within the Gal C survey area which have a highly non-uniform history of along-strike uplift where rates of fold uplift and the locations of maximum uplift vary over time (See Chapter 5, figures 5.8 and 5.9).

Diversions of submarine channel systems in the Nigeria study do, however, differ from the Nile Delta examples in terms of channel morphology. The sharp changes in course observed as the Nile submarine channels are diverted around folds and strike-slip structures is often associated with a localised decrease in channel sinuosity, as is shown in figure 6.5(a-d). This figure shows several examples of diversions with the channel path overlaid onto the pre-kinematic surface to show clearly the relationship between structure and channel pathway. At the point where the channel crosses the fold, a low sinuosity reach is typically bounded upstream and/or downstream by zones of increased sinuosity which develop within hanging-wall and foot-wall synclines in examples from the Levant Basin (Fig. 6.5). In contrast, channel levee systems from the Niger Delta study which divert around the lateral tips of the Aga fold show much less variation in sinuosity over the diverted channel reach. The Niger delta channel systems also do not show the strong structural control on levee deposition shown by many of the Nile delta channel systems as they are diverted (Fig. 6.5).

It should be stated that the number of documented channel-structure interactions from the Nigeria study presented here is far fewer than those documented from the Nile data. One reason for this is that the Nile dataset records many more channel levee systems which show a more diverse range of interactions with fold growth compared to the examples from the Niger delta. Other studies from the Niger Delta have revealed that a wider range of channel-structure interactions do occur. These include incision of channel systems across folds and the formation

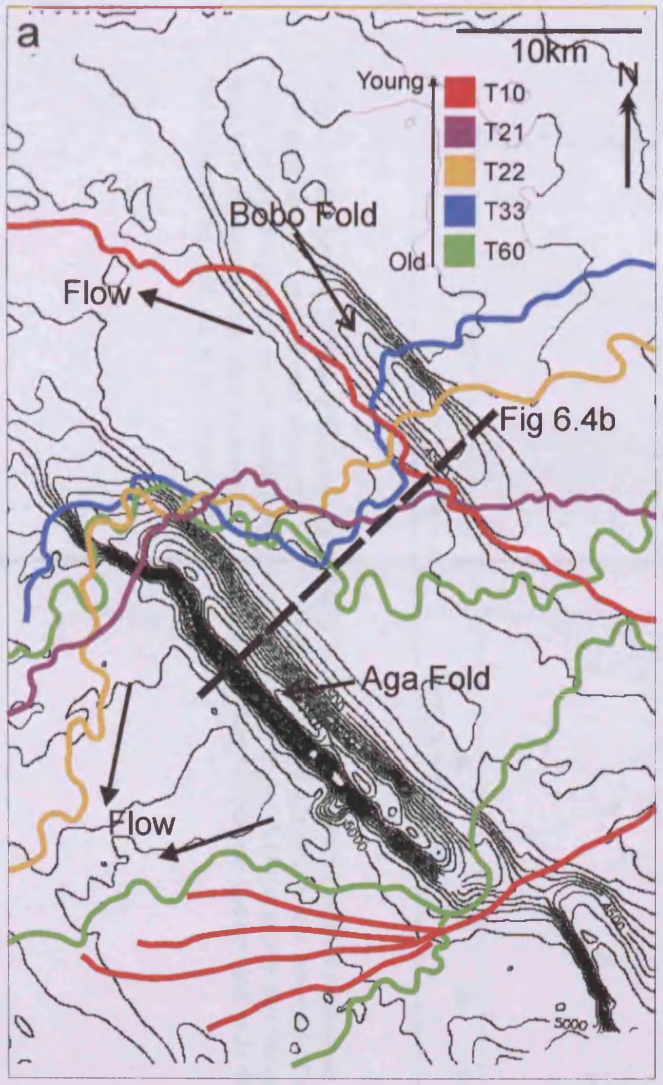

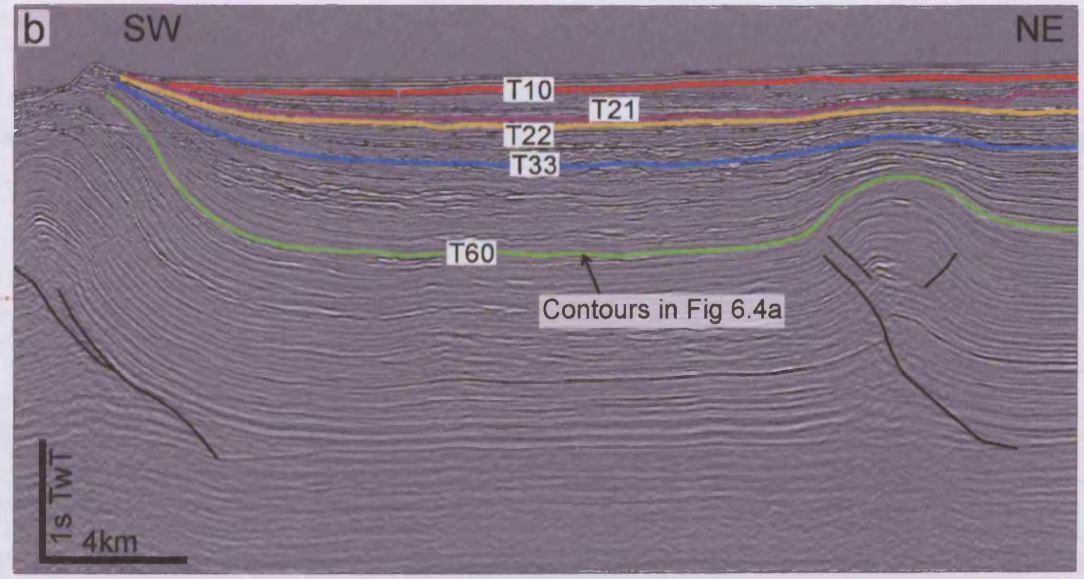

Figure 6.4: The contour map shown in **a** shows the time structure at the base of the growth sequence (T60 horizon in **b**) for the Niger Delta study area. Coloured lines represent the paths of several submarine channel systems located at various stratigraphic levels within the growth sequence, as shown in the seismic profile in **b**. This figure shows that, from the onset of growth of the Aga fold, submarine channel systems were diverted around the lateral tip regions of the fold with the location of the diversions remaining fairly constant – ie lateral propagation of the fold along strike was not a significant factor in controlling the pathways of submarine channel systems during growth of the Aga fold. Compare with the example of fold growth documented in chapter 5.

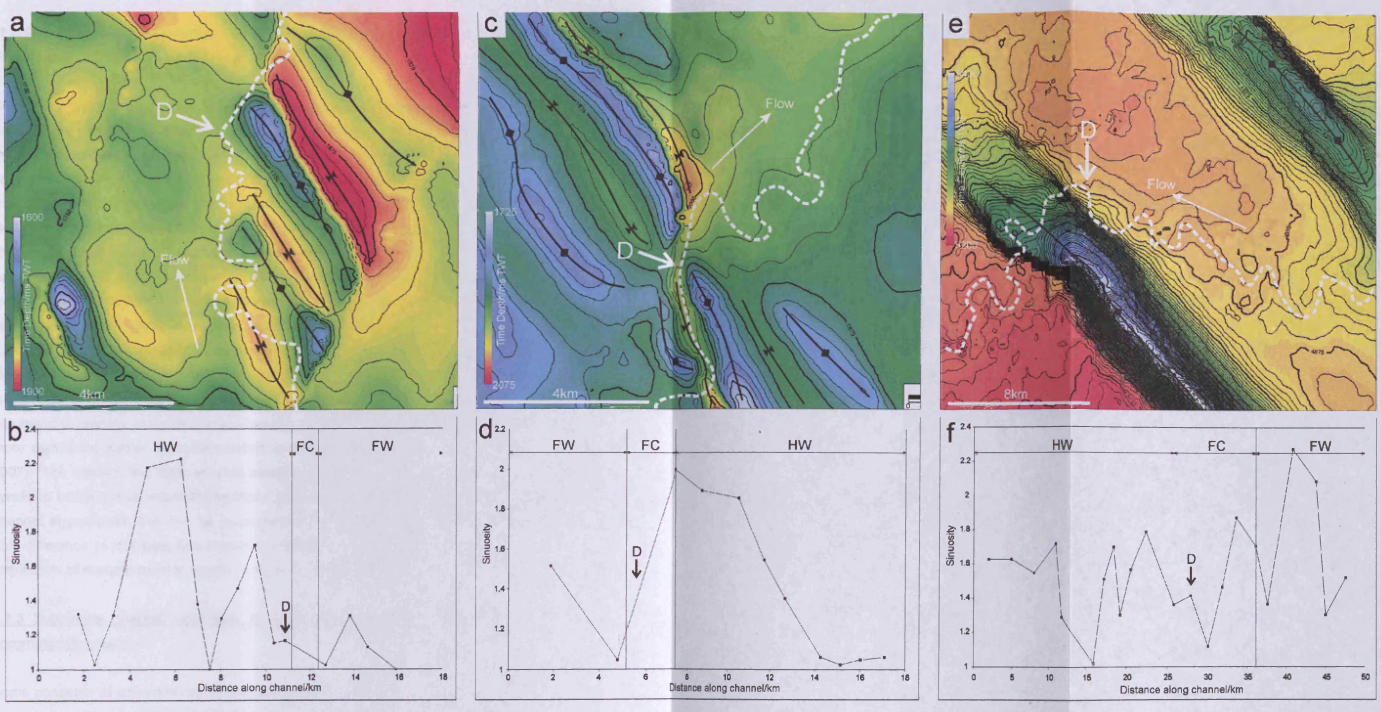

Figure 6.5. Series of time structure maps of the top pre-kinematic surface (a, c, e) with the axes of anticlines and synclines marked. Points marked D correspond to diversion points where a change in overall channel course is observed. The graphs b, d, and f show sinuosity measurements taken between inflection points in order to compare the eastern Nile and Niger Delta examples (see chapter 2). White dashed lines on figure a, c and e indicate the courses of submarine channel levee systems which structurally controlled. All of the channel courses are diverted but spatial variations in sinuosity occur as the channel is diverted around the fold. The channel systems in a and c show a pre-diversion and post-diversion sinuosity increase respectively, as can be seen on the corresponding graphs b and d. The Niger Delta channel (located at the base of the growth-sequence) shows a lesser range of sinuosity values associated with diversion of the channel compared to the eastern Nile examples in a to d.

of knickpoints (Heinio and Davies, 2007) and also spatial variations in channel morphology (Pirmez et al., 2000, their Fig. 11; Adeogba et al., 2005).

Comparing these two datasets reveals some important differences, both in terms of structure and also the morphological style of the submarine channel systems in each area. Structurally, the study area from the Niger Delta (Chapter 4, Fig. 4.1) is much simpler than that seen in the eastern Nile study, showing only two folds (with possible linkages extending beyond the survey limits – see Higgins et al., 2007) compared to the c.27 folds and numerous bounding strike slip faults observed in the eastern Nile area (Fig. 6.6). The folds in the Niger Delta study area are also larger, both in total crestal uplift and in lateral extent – the Aga and Bobo Folds have respective lengths of 26km and 21km, with the fold crests spaced 16km apart. Values of total crestal relief for the Aga and Bobo folds are 1800m and 720m respectively. In contrast, folds from the eastern Nile have an average lateral extent of 3.8km and an average crestal spacing of 2.8km (Fig 6.6). Crestal uplift values reach a maximum of up to 250m above the footwall. In the eastern Nile, fold lateral extent tends to be limited by the bounding strike-slip faults, whereas in the Niger Delta folds can link up and join along strike via underlying thrust fault linkages. This can result in laterally extensive structures 10s of km in along strike length, resulting in a much more significant barrier to sedimentation compared to the Levant examples (Higgins et al., 2007). The eastern Nile folds are also associated with below-regional footwall and hangingwall synclines which act as important localised depocentres and are related to zones of increased channel aggradation, this can be accompanied by a localised increase in channel sinuosity. This difference in fold style has important implications for sedimentation pathways and on the distribution of accommodation space. This is explored in more detail in the following section.

6.2.3 Submarine channel responses to folding and the relationship to local variations in accommodation space

Some concepts of accommodation space and equilibrium profile for deepwater slope systems have already been established (Prather et al., 1998; Pirmez et al., 2000; 2003; Booth et al., 2003; Smith, 2004). In a similar manner to that described for subaerial fluvial systems (Mackin, 1948), the large scale morphological evolution of submarine channel systems over time can be interpreted in terms of channel adjustment to reach a notional equilibrium profile, or graded slope. In this equilibrium state, the flows passing a particular point are neither net depositional or erosional (Pirmez et al., 2000; Kneller, 2003). This hypothetical profile is a concept most

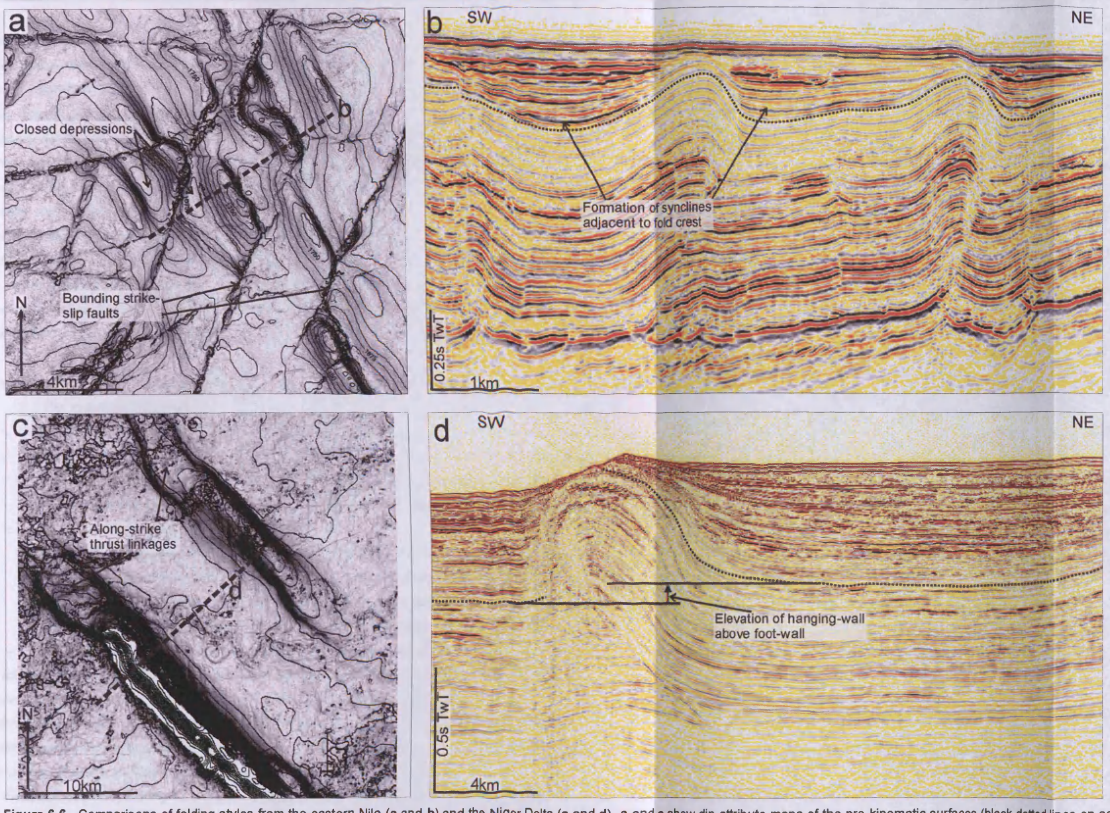

Figure 6.6. Comparisons of folding styles from the eastern Nile (**a** and **b**) and the Niger Delta (**c** and **d**). **a** and **c** show dip attribute maps of the pre-kinematic surfaces (black dotted lines on seismic profiles) with overlayed time structure contours. Folds from the eastern Nile have typical lateral extents of 3-4km due to segmentation by the numerous strike slip faults (**a**). Folding is also associated with the formation of foot-wall and hanging-wall synclines which form closed depressions in three dimensions. The Niger delta folds shown in **c** considerably more laterally extensive (10s of km) compared to the eastern Nile folds. These folds extend along strike via thrust fault linkages (see Higgins et al 2007). Closed depressions within the hanging-wall and foot-wall are not associated with the Niger Delta folds, instead elevation of the hanging-wall above the footwall occurs, along with extensive degradation of the fold at the seafloor (**d**).

157

easily applied to channel systems over geological time scales, as at the scale of individual flows, each event may vary in volume, grain size and concentration, and the equilibrium profile for one particular type of flow will differ from others due to variations in these characteristics (e.g. Kneller, 2003). Thus the equilibrium profile concept involves effectively averaging the flow characteristics over geological time scales, in addition to other factors such as deformation which also introduce perturbations along the slope profile. For submarine channel systems, the shape of the equilibrium profile is roughly concave with pinning points at the head of the feeder canyon (effectively the sediment source) and channel-lobe transition where flows become unchannelised (Pirmez et al., 2000; Kneller, 2003). It should be noted that in settings where sediment distribution is structurally controlled, the lowermost point of the equilibrium profile may be better described as the gravity base – the lowest point in the basin within which a flow can deposit (Kneller, 2003). The accommodation space is represented by the difference between the seabed and the equilibrium profile.

The slope of the equilibrium profile may vary over time due to several factors:

1. The character of the flows passing down the submarine canyon can vary over time (Kneller, 2003; Samuel et al., 2003). Decreases in flow density or thickness, or an increase in dominant grain size increases the gradient of the equilibrium profile resulting in the formation of accommodation space causing aggradation. The opposite to this case (erosion and loss of accommodation) can be caused by an increase in flow density or thickness, or a decrease in grain size.
2. Deformation resulting from, for example, thin-skinned gravitational collapse and salt tectonics or subduction and the formation of an accretionary prism can alter the slope of the equilibrium profile. Deformation will alter the position of the pinning points at either end of the concave profile to which the submarine channel is attempting to adjust, as well as modifying the slope profile (Pirmez et al., 2000).

In addition to these large scale variations in equilibrium profile, local structures on a deforming slope result in many local perturbations to the overall slope equilibrium profile (Ferry et al., 2002; Prather et al., 2003; Smith, 2004; Adeogba et al., 2005). When attempting to apply the equilibrium profile concept to explaining channel evolution over time, it is necessary to consider the effects of these multiple local structures. Each of which will introduce localised modifications to the slope profile resulting in a more complex overall response of the channel levee system over time.

Recognition of the differences in fold structural styles between the Nile and Niger delta study areas is relevant as the fold style act as an important local control on the distribution of accommodation space. The footwall and hangingwall synclines associated with the eastern

Nile foldbelt generate zones of locally increased accommodation space, similar to the ponded accommodation described for salt withdrawal mini-basins on the Gulf of Mexico slope (Prather et al., 1998; Satterfield and Behrens, 1990; Beauboeuf and Friedmann, 2000). The development of this ponded accommodation adjacent to the fold crest appears to affect channel development in the eastern Nile in two important ways:

1. The localised increase in accommodation space results in increased channel aggradation in order for the system to reach its local equilibrium profile. This response of the submarine channel to the local increase in accommodation is similar to the model described by Beaubouef and Friedmann (2000) for the sequential filling of multiple enclosed basins on the Gulf of Mexico slope.
2. Increased deposition of high amplitude, sheet-like bodies at the base of the submarine channel systems are often observed in the foot-wall and hangingwall synclines within the eastern Nile survey (Fig. 6.3).

The distribution of accommodation space associated with the Aga Fold from the Niger Delta study area is much simpler due to lack of foot-wall or hanging-wall synclines. Figure 6.7 shows examples of folds from the eastern Nile and the Niger Delta with profiles taken along the diversionary sedimentation pathways around the edges of the folds. Upon each of these profiles a hypothetical equilibrium profile has been imposed purely to illustrate the nature of accommodation space along each flow pathway (Fig. 6.7). Accommodation space associated with the style of folding observed for the Aga fold is healed slope accommodation (Chapter 1, see also Prather et al., 2003, for definition) within the footwall (Fig 6.7). Generation of this accommodation space is related to the fold crestal relief and also to the vertical separation between the hanging wall and footwall associated with this style of folding (see also Fig. 6.6). The response of submarine channel systems to this localised creation of accommodation space within the forelimb is a local increase in thickness at the forelimb to foot-wall transition (Chapter 4, Figs. 4.9, 4.10 and 4.11). However this increase in thickness does not seem to result in a marked increase in local sinuosity compared to the eastern Nile submarine channels. In contrast, the fold style in the eastern Nile involves formation of synclines adjacent to the fold crests, and these tend to increase the amount of accommodation space by adding a significant

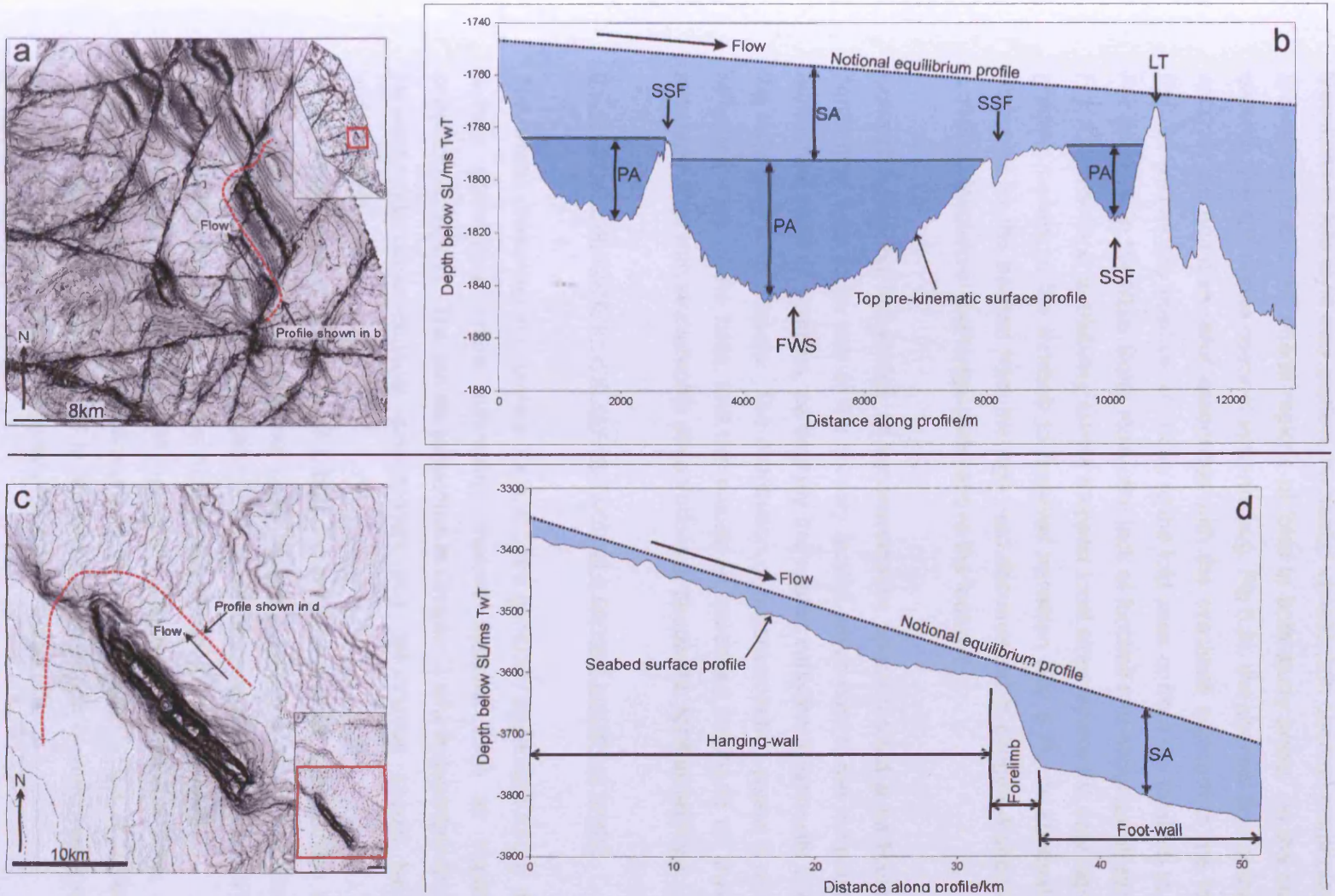

Figure 6.7: Surface profiles extracted from seismic horizons following the pathways of submarine channel systems during diversion around folds. The surface shown in **a** is the top-pre kinematic surface from the eastern Nile dataset. The graph in **b** shows the surface profile above which a notional equilibrium profile has been positioned to illustrate conceptually the distribution of accommodation space. Key structures controlling accommodation around these folds include foot-wall synclines (**FWS**), strike-slip faults (**SSF**) and lateral terminations (**LT**). Accommodation can be subdivided into ponded (**PA**) and slope (**SA**). The structural style of folding from the Niger Delta study area is not associated with the development of synclines adjacent to the fold crest (**c**) with the result that variations in accommodation space (**d**) along a submarine channel system diverting around the fold occur only at the forelimb to foot-wall transition where an increase in slope accommodation (marked **SA** on **d**) occurs.

component of ponded accommodation to the already established slope accommodation (Fig. 6.7).

Variations in fold style may explain the spatial variations in channel morphology associated with diversions around the lateral regions of folds in both study areas. In the case of the diverted eastern Nile submarine channel systems (e.g. Fig 6.2), the channel flow pathway must take into account the negative relief associated with the synclines adjacent to the fold crest (e.g. Fig. 6.5), as well as any positive relief due to the fold crest or from the forelimb to footwall transition. For the folds in the Niger Delta study, the lack of footwall and hangingwall synclines (Chapter 4, Fig, 4.2) results in a relatively simple stepped local slope where the only significant variation in gradient occurs at the forelimb to foot-wall transition (Fig 6.7). In contrast to the fold styles observed for the eastern Nile, the Aga Fold documented in chapter 4 shows significant (up to c.300m) elevation of the hangingwall above the footwall.

Understanding the distribution of accommodation space around a particular fold is therefore considered here to be one of the primary factors which control the morphological response of submarine channel systems, particularly the spatial variation in sinuosity observed in many of the examples in this thesis. The distribution of accommodation space is closely related to the structural style of the folds, and this places an increased emphasis on linking descriptions of structural style with stratigraphic observations in deepwater foldbelt settings.

6.2.4 General applicability and key elements of a general predictive model

The results presented in Chapters 3,4 and 5 are generally applicable to any deepwater fold belt setting, particularly where submarine channel systems form an important part of the depositional regime. The results presented in Chapter 3 which describes the basic interactions between submarine channel development and deformation should be applied with an understanding of:

1. Knowledge of the style of submarine channel and its approximate location within the larger scale canyon-channel levee system. Larger scale submarine channel systems may show different interactions due to larger scale or more frequent flow events which will alter the relative rates of erosion and deposition versus uplift.
2. The structural style of folding which affects the particular area, for example, the formation of synclines adjacent to the fold crests. This is important in terms of controlling local variations in accommodation space to which submarine channels will show a morphological response (see also Chapter 5).

The basic set of submarine channel-structure interactions can also be applied to different structural settings, and are not specific to deepwater fold belts. Some examples include the numerous channel diversions caused by salt diapirism documented by Gee and Gawthorpe (2006) from offshore Angola. Salt diapirism in the Gulf of Mexico also results in channel diversions and confinement (Sawyer et al., 2007). Other zones where channel-structure interactions could commonly be expected are from areas of extension and growth faulting (e.g. Anderson et al., 2002; Hooper et al., 2002; Ferry et al., 2005).

Chapters 4 and 5 present results which link the detailed stratigraphic and structural observations from Chapter 3 to the larger scale result of structural-stratigraphic interactions – growth sequences. Growth sequences are a commonly observed feature of deepwater fold belts, and the work presented here provides some new insights into interpreting growth sequences in terms of their linked stratigraphic and structural evolution. The key parameter in linking observations of growth sequence geometry with detailed interactions between sedimentation and the growing fold is the evolution of positive fold relief over time. This can be assessed qualitatively by observations such as onlap and overlap, and quantitatively by measurements such as growth sequence expansion factor using a similar method originally defined for extensional growth faults (Thorsen, 1963; Roux, 1979).

The work presented here, as well as previously published literature examples of sedimentation in structurally active deepwater settings (Hubbard et al., 2008; Gee and Gawthorpe, 2007; Ferry et al., 2004; Smith, 2004) suggest that there are several key controls which need to be considered when assessing the potential effect of seafloor deformation on submarine channel development:

- The relative rates of sedimentation and uplift over time.
- Orientation of deformational structures relative to flow pathways.
- Structural style of deformation and its control on local accommodation space.
- The location of deformation on the overall channel profile.

The importance of each of these factors is briefly discussed below in the context of practically applying these concepts to predict submarine channel development.

6.2.4.1. Relative rates of uplift and sedimentation: The relative rates of uplift and sedimentation can be assessed by observing the geometry of the growth sequence within which the reservoir is deposited (see also Chapter 1, section 1.2.2). Overlap indicates that the relative rate of sedimentation was greater than uplift and that deformation most likely did not result in positive

topography during reservoir deposition. Onlap indicates that positive relief was present and was significant enough to affect sediment deposition. At a basic level, these observations reveal whether sedimentation was able to bypass seafloor topographic features (overlap) or whether these features caused diversion of sedimentation pathways (onlap). Within an overlapping growth sequence however, spatial variations in the sinuosity of submarine channel systems can still result in poor reservoir development across the crest of the developing fold, an important factor which could degrade any potential reservoir developed directly over the fold crest. Onlapping growth sequences signify diversion of sedimentation around topography, but reservoir development can be strongly affected by the nature of the diversionary path (e.g. factors such as the level of confinement - Fig. 6.2). The formation of growth sequences can also occur during the formation of normal faults and salt diapirs and the use of growth sequence geometries can provide easily observable and useful insights in many deepwater settings to more detailed structural-stratigraphic interactions (see also Fig. 6.8).

6.2.4.2. Orientation of structure relative to sedimentation pathways: The orientation of submarine channel systems to deformational features acts as an important control on the final channel geometry and development. The examples presented in this study generally consider relatively small scales of deformation, typically individual folds, although these can be up to 40km in lateral extent, as shown by the case study presented in Chapter 4. A higher angle between sedimentation pathways and deformational structures results in an increased likelihood of diversion, and may result in a connected tortuous corridor style of sedimentation at the slope scale when multiple structures affect the channel course (Smith, 2004). Alternatively, if deformation post-dates an already established structure-perpendicular channel system, the channel course may become increasingly incised, in a similar manner to an antecedent fluvial system (Burbank et al., 1996). Where sedimentation pathways are parallel to deformational structures, confinement will play an increased role in determining the pattern of sedimentation, and limit lateral migration. ? Hubbard et al 2008 example?

6.2.4.3. Structural style: The structural style of folds can vary according to geological settings, for example the Eastern Nile fold-belt differs greatly in the structural style of folding compared to the Western Niger Delta (see section 6.2.2). The structural style plays a critical role in determining the local accommodation space, which is believed to be a key control on sedimentary architecture in these systems (see also section 6.2.3). The development of local accommodation around individual structures is a concept which can also be easily applied to other systems such as salt diapirs and extensional faults.

6.2.4.4. Location of the sedimentary system on the slope profile: This factor is strongly linked the relative rates of uplift and sedimentation discussed in section 6.2.6.1. Submarine channel systems located on the upper to middle slope tend to be much larger scale systems and often possess a strong component of erosional confinement of the channel axis, suggesting an increased capacity for incision and bypass of any underlying structural obstacles compared to the smaller scale channel levee systems on the lower slope (such as the ones shown in chapters 3 and 5). Essentially, the more proximal the submarine channel, the greater its potential for erosion and bypass of underlying deformational features.

6.2.5 Implications for reservoir development

The research presented in this thesis could have important implications for where likely reservoir deposition will occur in structurally active, deep-water depositional systems. Understanding the nature of the submarine channel-structure interactions that may have occurred is a key factor in determining the development of any potential reservoir unit as many interactions involve localised changes in levee deposition and channel sinuosity over distances of 100s of meters. Deposits from the channel axis (including those related to lateral migration over time), as well as the channel levees, can form potential hydrocarbon reservoirs (Cross et al., 2009; Mayall et al., 2006; Abreau et al., 2003; Clemenceau et al., 2000). Diverted and confined channels can potentially degrade the reservoir potential of the channel levee system due to localised structures resulting in a static channel planform in which the coarse grained material in the channel axis is vulnerable to erosion from by-passing flows (Fig. 6.2e and f). Deflection may be result in more laterally extensive sand bodies formed by gradual lateral migration over time away from the focal point of uplift. Coeval deformation and channel deposition may also promote the formation of HARPs at the base of channel levees, and also features such as crevasse splays which could form potentially good quality, laterally extensive sheet-like reservoirs (Fig. 6.3c).

Understanding the way in which submarine channel systems develop within growth sequences can also have important implications for the location of channel reservoirs which become incorporated into a growing fold (Fig. 6.8). An overlapping growth sequence in which the channel shows spatial variations in sinuosity as it crosses the location of the underlying fold crest may result in the best potential reservoir bodies located off the fold crest and within the fold limbs (Fig 6.8a). An example of this is presented in Chapter 5 (Fig. 5.12). Here, a channel levee system developed within an overlapping growth sequence shows spatial variations in sinuosity across the crest of a growing fold, with a local decrease in sinuosity across the fold

crest, accompanied by a lack of lateral migration. Thus, we could expect any potential reservoir sands across the fold crest itself to be highly limited in terms of lateral extent, or even potentially eroded by bypassing flows. The more sinuous portions of the channel levee system would form better potential reservoirs located within the fold limbs (Fig 6.8a). The connectivity of these two reservoirs on either fold limb would depend on the evolution of the low sinuosity segment which crosses the fold crest. Localised bypass and erosion in this area could isolate the two sand bodies located in the fold limbs, for example.

Within onlapping growth sequences, channel diversion may again result in spatial variations in sinuosity with incorporation of the lateral migration deposits into the fold limb which originally caused the change in channel course (Fig. 6.8b). The final configuration of potential reservoir units will result in reservoir sands derived from the channel axis concentrated on one fold limb, whilst the other limb may consist of levee-derived deposits depending on the degree of channel diversion (Fig. 6.8b). No connectivity should be expected across the crest of the fold in this case as the positive relief at the time of channel deposition would have formed a depositional barrier. This can be inferred from the onlapping growth sequence geometry.

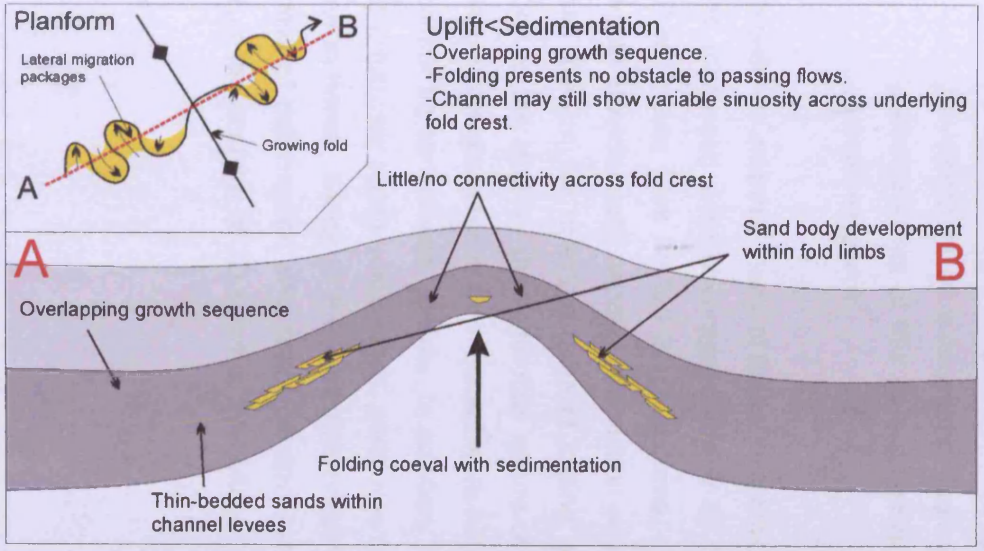

Figure 6.8a: Schematic figure illustrating the potential effects on reservoir development of a submarine channel developed within an overlapping growth sequence. Although the overlapping growth sequence geometry implies little/no positive seafloor relief, the channel system still displays a decrease in sinuosity across the fold crest, resulting in potentially poor reservoir development in this area. Further folding results in laterally extensive reservoirs located off of the fold crest within the limbs.

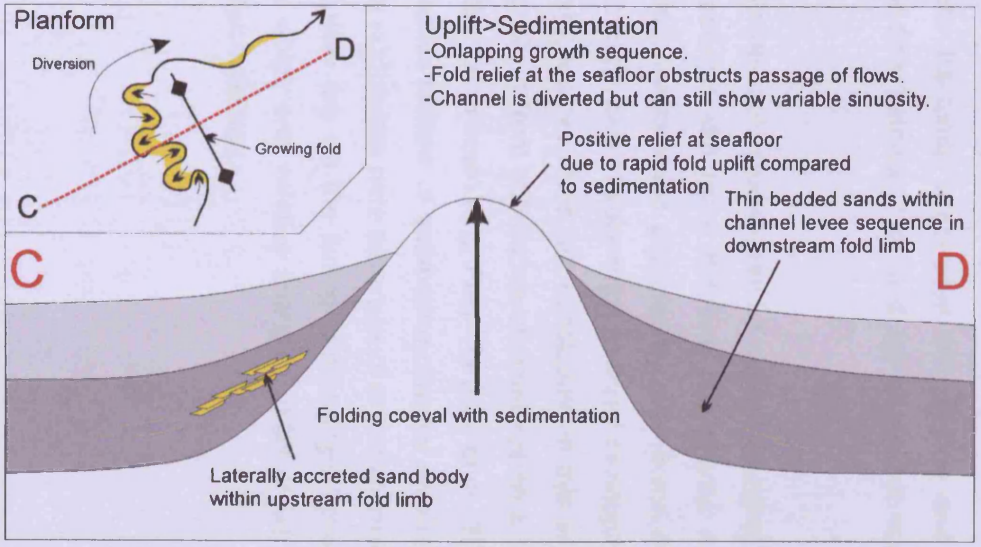

Figure 6.8b: Schematic figure showing submarine channel development within an onlapping growth sequence due to a relatively high rate of uplift compared to sedimentation. The result is channel diversion around the fold resulting in potential reservoir deposition within one fold limb only. Connectivity across the fold crest is not possible as fold relief would have prevented deposition.

6.2.7Further work

One of the most fundamental questions which the work in this thesis raises regards the response of deepwater sedimentary systems to perturbations of the equilibrium profile. In order to properly address this question however, more work needs to be undertaken in usefully applying the equilibrium profile concept to deepwater systems. A key problem in applying this concept is that despite the ever increasing coverage of 3D seismic data, individual surveys often only image a segment 10s of km in length of the much larger scale canyon-channel-lobe system which can be 100s of km in length. Application of the equilibrium profile concept to individual seismic surveys is difficult in practice as it is difficult to establish where the particular survey lies with reference to the overall equilibrium slope which governs the amount of accommodation space. In order to address this problem, further consideration needs to be given to the location of the pinning points which limit the upper and lower extents of the equilibrium profile. In a submarine fan undergoing thin-skinned gravitational collapse, the location of these pinning points could change over time, as well as increased deformation resulting in tortuous sedimentation pathways (c.f. Smith, 2004) which act to lengthen the slope profile. Thus, fitting the equilibrium profile to the slope, especially in structurally deformed systems, would appear to be a key prerequisite to establishing where changes in accommodation space along the slope occur. From this it may then be possible to anticipate changes in submarine channel morphology which may have a impact on the deposition of potential hydrocarbon reservoirs (see also Fig. 6.7).

Another key control on the evolution of submarine channel systems over time is the characteristics of the flows, such as the frequency, volume and grain size (Pirmez and Imran, 2003; Kneller, 2003; Kane et al., 2008). How these characteristics control channel evolution in areas of complex seafloor bathymetry is, so far, an unexplored avenue of research. This is despite a generally good understanding of the way in which unchannelised gravity flows respond to bathymetric obstacles (e.g. Alexander and Morris, 1994; Bursik and Woods, 2000; Woods et al., 1998; Sinclair and Cowie, 2002; Lamb et al., 2005; Kneller et al., 1991). Further work utilising numerical and physical models of submarine channel development would greatly complement process-based interpretations from 3D seismic data.

Chapter 7

CHAPTER 7

CONCLUSIONS

This study represents the first results from the utilisation of 3D seismic data to systematically study and understand the interactions between sedimentation and deformation from deep-water fold and thrust belts. The studies presented here illustrate how this type of data can yield insights into these interactions at several scales. These range from the detailed interactions between submarine channel systems and folds presented in chapter three, to the larger scale formation of growth sequences associated with folding presented in chapters four and five. Presented below are some general concluding remarks, followed by chapter-specific conclusions.

7.1 General conclusions

- 3D seismic data can provide important insights into the spatial and temporal interactions between sedimentation and tectonics in deepwater fold-belt settings.
- The studies presented here highlight the importance of taking a combined structural-stratigraphic approach to the analysis of these systems.
- The morphological response of submarine channel systems in deepwater fold-belts is ultimately governed by adjustment of the channel course to reach its equilibrium profile. In detail, channel response to deformation is related to the style of accommodation space developed around a particular fold.
- In order to apply the results presented in this thesis, an understanding of the structural style of folding is necessary as fold style critically controls the distribution of local accommodation space in these depositional systems.

7.2 Conclusions from Chapter 3 – Channel-structure interactions from the Levant Basin

- The Levant basin forms an ideal area to study the effects of recent (post-Messinian) thin skinned deformation on sedimentation derived from the Nile Delta.

- Several submarine channel levee systems where characterised qualitatively using channel isochron maps and quantitatively using measurements of channel morphometric parameters.
- From this study, four basic interactions between submarine channel development and deformation can be described:
    - Confinement: Restriction of a submarine channel axis and the channel levees by surrounding structures which physically constrain deposition.
    - Diversion: A change in channel course caused by a pre-existing structure or series of structures which obstruct the flow pathway via modifying the slope gradient.
    - Deflection: A progressive shift in channel course away from the axis of uplift, or towards a newly forming bathymetric low point. A key difference from diversion is that deflection causes successive changes in channel course over time.
    - Blocking: Blocking results from relative rates of uplift that are far greater than the rates of deposition and erosion from the submarine channel. Structural relief prevents sedimentation downstream of the blocking structure.
- These interactions are described as end-members, and are intended to form a framework for describing the behaviour of submarine channel systems in structurally active settings.
- Each interaction is associated with a specific style of submarine channel development, thus recognition of these interactions may have practical implications in terms of predicting reservoir geometries. This cannot be fully assessed using just 3D seismic data however.
- Recognition of these channel-structure interactions provides information regarding the relative timing of deformation and channel development. In particular, levee internal reflection geometries and measurements of channel morphometric parameters can provide important information on detailed timing relationships over the period of channel development.
- Diversion and confinement represent end-members with the transition between each interaction being controlled by the number of structures influencing the channel course and also the magnitude of uplift. These interactions represent the response of channel development to the pre-depositional structurally controlled slope.

- The transition between deflection and blocking is controlled by the ratio of uplift to sedimentation. These two interactions represent the channel response to active deformation during sedimentation.

7.3 Conclusions from Chapter 4 – Coeval sedimentation and deformation from the western Niger Delta.

- A growth sequence associated with 32km in length fold structure (the Aga fold) was mapped in detail in order to provide a case study of three dimensional growth sequence development from the western Niger Delta.
- The growth sequence in this is comprised of a three-dimensionally stacked interval of channel-levee complexes, mass transport deposits and hemipelagic intervals. Mass transport deposits and submarine channel systems respond to the emerging relief during fold growth and this can be assessed using features such as basal scours and also changes in channel morphology in response to folding-induced gradient changes.
- Variations in the structural style of the large scale (32km in length) Aga fold is controlled by factors such as shortening and the development of back-thrusts. The low relief areas at the fold lateral tip regions are characterised by the formation of back-thrusts, whereas the high relief central area of the Aga fold is characterised by the development of fore-thrusts.
- The accommodation space within the hanging-wall is controlled by the fold style, but growth sequence architecture is also strongly affected by compensational stacking within a vertical sequence of mass transport deposits and submarine channel systems.
- This compensational stacking controls the switching of sedimentation pathways from one fold edge to another during the fold growth.

7.4 Conclusions from Chapter 5 – The link between growth sequence architecture and channel-structure interactions.

- In this study area, the structural style of folding plays a critical role in determining the available accommodation space for sediment deposition. The depressions which form in the hanging-wall and foot-wall syncline areas are coeval with the evolution of positive relief due to crestal uplift.

- Control of the evolving structural relief on channel sinuosity: Depending on the rate of structural growth relative to channel deposition, the sinuosity of the channel can vary greatly over a short (hundreds of metres) distance. This results in preferential deposition of laterally accreted sand bodies, particularly within the hanging-wall and footwall synclines of folds. Preferential sinuosity development in this way is usually associated with diversion and/or deflection of the channels around the fold so that a portion of the channel occupies the axis of the hanging-wall or foot-wall.
- Overlapping growth sequences are commonly interpreted to result in little or no topographic expression of folding but in deepwater settings can result in significant changes in submarine channel morphology, causing a decrease in sinuosity across the fold crest.
- Onlapping growth sequences imply diversion of sediments around the emergent fold relief, with the submarine channel systems in this study showing dramatic spatial variations in sinuosity and in the development of cut-off loops.
- This study shows that folding during growth sequence development can be associated with a non-uniform distribution of uplift along strike. Therefore a fully three dimensional approach is needed when characterising these systems. Methods can include linking observations of growth sequence geometry with growth sequence isochron maps, and also measurements such as along-strike relief development.

References

Abreu, V., Sullivan, M., Pirmez, C., Mohrig, D. 2003. Lateral accretion packages (LAPs): an important reservoir element in deep water sinuous channels. Marine and Petroleum Geology, 20, 631-648.

Adeogba, A.A., McHargue, T.R., Graham, S.A. 2005. Transient fan architecture and depositional controls from near surface 3-D seismic data, Niger Delta continental slope. AAPG Bulletin, 85, 627-643.

Alexander, J., and Morris, S., 1994, Observations on experimental, nonchannelized, high concentration turbidity currents and variations in deposits around obstacles: Journal of Sedimentary Research, v. A64, p. 899–909.

Alonso, B., Ercilla, G., Small turbidite systems in a complex tectonic setting (SW Mediterranean Sea): morphology and growth patterns. Marine and Petroleum Geology, v.19, p.1225-1240.

Antobreh, A.A., Krastel, S., 2006. Morphology, seismic characteristics and development of Cap Timiris Canyon, offshore Mauritania: a newly discovered canyon preserved off a major arid climatic region. Marine and Petroleum Geology 23, 37–59.

Avbovbo, A. A., 1978, Tertiary lithostratigraphy of the Niger Delta: AAPG Bulletin, v. 62, p. 295–300.

Babonneau, N., Savoye, B., Cremer, M., Klein, B., 2002. Morphology and architecture of the present canyon and channel system of the Zaire deep-sea fan. Marine and Petroleum Geology 19, 445–467.

Badalini, G., Kneller, B., and Winker, C., 2000, Architecture and processes in the Late Pleistocene Brazos–Trinity turbidite system, Gulf of Mexico continental slope, in Weimer, P., Slatt, R.M., Coleman, J., Rosen, N.C., Nelson, H., Bouma, A.H., Styzen, M.J., and Lawrence, D.T., eds., Deep water reservoirs of the world, SEPM, Gulf Coast Section, 20th Annual Bob F. Perkins Research Conference, p. 16–33.

Beauboeuf, R.T., Friedmann, S.J., 2000, High-resolution seismic/sequence stratigraphic framework for the evolution of Pleistocene intra slope basins, Western Gulf of Mexico: depositional models and reservoir analogs, in Weimer, P., Slatt, R.M., Coleman, J., Rosen, N.C., Nelson, H., Bouma, A.H., Styzen, M.J., and Lawrence, D.T., eds., Deep-Water Reservoirs

of the World: Gulf Coast Society of the Society of Economic Paleontologists and Mineralogists Foundation, 20th Annual Research Conference, p. 40–60.

Ben-Avraham, Z., Tibor, G., Limonov, A.F., Leybov, M.B., Ivanov, M.K., Tokarev, M.Y., Woodside, J.M. 1995. Structure and tectonics of the Eastern Cyprean Arc. Marine and Petroleum Geology, 12, 263-271.

Ben-Avraham, Z., Kempler, D., Ginzburg, A. 1988. Plate convergence in the Cyprus Arc. Tectonophysics, 146, 231-240.

Ben-Gai, Y., Ben-Avraham, Z., Buchbinder, B., Kendall, C. G.StC. 2005. Post-Messinian evolution of the Southeastern Levant Basin based on two-dimensional stratigraphic simulation. Marine Geology, 221, 359-379.

Bernal, A., Hardy, S., 2002, Syn-tectonic sedimentation associated with three dimensional fault-bend fold structures: a numerical approach. Journal of Structural Geology, v. 24, p. 609-635.

Bertoni, C., Cartwright, J.A. 2005. 3D seismic analysis of circular evaporite dissolution structures, Eastern Mediterranean. Journal of the Geological Society, London, 162, 909-926.

Bertoni, C., Cartwright, J.A. 2006. Controls on the basinwide architecture of late Miocene (Messinian) evaporites on the Levant margin (Eastern Mediterranean). Sedimentary Geology, 188-189, 93-114.

Bertoni, C., Cartwright, J.A. 2007. Major erosion at the end of the Messinian Salinity Crisis: evidence from the Levant Basin, Eastern Mediterranean. Basin Research, 19, 1-18.

Bilotti, F.D. & Shaw, J.H., 2005, Deepwater Niger Delta fold and thrust belt modelled as a critical-taper wedge: the influence of elevated of elevated basal fluid pressure on structural styles. AAPG Bulletin, v. 89, p. 1475-1491.

Bornhauser, M., 1958, Gulf Coast tectonics: AAPG Bulletin, v. 42, p. 339-370.

Bouma, A.H., Stelting, C.E., Coleman, J.M., 1985b. Mississippi Fan: Gulf of Mexico. In: Bouma, A.H., Barnes, N.E., Normark, W.R. (Eds.), Submarine Fans and Related Turbidite Sequences. Springer, Berlin, pp. 143–150.

Briggs, S.E., Davies, R.J., Cartwright, J.A., Morgan, R., 2006, Multiple detachment levels and their control on fold styles in the compressional domain of the deepwater west Niger Delta. Basin Research, v. 18, p. 435-450.

Brown, L.F.Jr., Fisher, W.L., 1977, Seismic stratigraphic interpretation of depositional systems: Examples from Brazillian rift and pull-apart basins. In: Payton, C.E.(ed): Seismic stratigraphy – Applications to hydrocarbon exploration, American Association of Petroleum Geologists Memoir v. 26, p.213-248.

Brown, A. R., 1999. Interpretation of Three-Dimensional Seismic Data. AAPG Memoir 42, 5th edition.

Broucke, O., Temple, F., Rouby, D., Robin, C., Calassou, S., Nalpas, T., Guillocheau, F. 2004. The role of deformation processes on the geometry of mud-dominated turbiditic systems, Oligocene and Lower-Middle Miocene of the Lower Congo basin (West African Margin). Marine and Petroleum Geology, 21, 327-348.

Brun, J.-P., and X. Fort, 2004, Compressional salt tectonics (Angolan margin): Tectonophysics, v. 382, p. 129–150.

Buchbinder, B., Zilberman, E. 1997. Sequence stratigraphy of Miocene-Pliocene carbonate siliclastic shelf deposits in the eastern Mediterranean margin (Israel): Effects of eustasy and tectonics. Sedimentary Geology, 112, 7-32.

Bull, S., Cartwright, J., Huuse, M., 2009, A review of kinematic indicators from mass transport complexes using 3D seismic data. Marine and Petroleum Geology, v. 26, p. 1132-1151.

Burbank, D.W., Verges, J., 1994, Reconstruction of topography and related depositional systems during active thrusting. Journal of Geophysical Research, v. 99, p. 281-297.

Burbank, D., Meigs, A., Brozovic, N., 1996. Interactions of growing folds and coeval depositional systems. Basin Research, v8, 199-223.

Burke, K. C. B., Dessauvagie, T. F. J. and Whiteman, A. J., 1971, The opening of the Gulf of Guinea and the geological history of the Benue Depression and the Niger Delta. Nature Phys. Sci. v. 233, p. 51-55

Bursik, M.I., Woods, A.W. 2000. The effects of topography on sedimentation from particle laden turbulent density currents. Journal of Sedimentary Research, 70, 53-63.

Cartwright, 1989, The kinematics of inversion in the Danish Central Graben. Geological Society of London Special Publications, v. 44, p. 153-175.

Cartwright, J.A., Jackson, M.P.A. 2008. Initiation of gravitational collapse of an evaporitic basin margin: The Messinian saline giant, Levant Basin, eastern Mediterranean. GSA Bulletin, 120, 399-413.

Chaumillon, E., Mascle, J. 1997. From foreland to forearc domains: New multichannel seismic reflection survey of the Mediterranean Ridge Accretionary complex (Eastern Mediterranean). Marine Geology, v.138. p.237-259.

Cita, M.B., Ryan, W.B.F. (eds), 1978. Messinian Erosional Surfaces in the Mediterranean. Marine Geology, 27, 366pp.

Clark, I. R., Cartwright, J. A., 2009. Interactions between submarine channel systems and deformation in deepwater fold belts: Examples from the Levant Basin, Eastern Mediterranean sea. Marine and Petroleum Geology, v. 26, p.1465-1482.

Clemenceau, G.R., Colbert, J., Edens, D., 2000. Production Results from Levee-Overbank Turbidite Sands at Ram/Powell Field, Deepwater Gulf of Mexico. In: Weimer, P., Slatt, R.M., Coleman, J., Rosen, N.C., Nelson, H., Bouma, A.H., Styzen, M.J., Lawrence, D.T. (Eds.), Deep-Water Reservoirs of the World, GCSSEPM Foundation 20th Annual Research Conference, pp. 241–251.

Cobbold, P.R., Szatmari, P. 1991. Radial gravitational gliding on passive margins. Tectonophysics, 188, 249-289.

Cohen, H. A., and K. McClay, 1996, Sedimentation and shale tectonics of the northwestern Niger Delta front: Marine and Petroleum Geology, v. 13, p. 313-328.

Connors, C. D., Denson, D. B., Kristiansen, G., Angstadt, D. M., 1998, Compressive anticlines of the mid-outer slope, central Niger Delta: AAPG Bulletin, v. 82, no. 10, p. 1903.

Corney, R.K.T., Peakall, J., Parsons, D.R., Elliott, L., Amos, K.J., Best, J.L., Keevil, G.M., Ingham, D.B., 2006. The orientation of helical flow in curved channels. Sedimentology 53, 249–257.

Corredor, F., J. H. Shaw, and F. Bilotti, 2005, Structural styles in the deepwater fold-and thrust belts of the Niger Delta: AAPG Bulletin, v. 89, no. 6, p. 753– 780.

Cross, N. E., Cunningham, A., Cook, R. J., Taha, A., Esmaie, E., El Swidan, N. 2009. Three-dimensional seismic geomorphology of a deep-water channel slope system: The Sequoia field, offshore west Nile Delta, Egypt. AAPG Bulletin, v.93, p.1063-1086.

Curray, J.R., Emmel, F.J., Moore, D.G., 2003. The Bengal Fan: morphology, geometry, stratigraphy, history and processes. Marine and Petroleum Geology 19, 1191–1223.

Damuth, J.E., Flood, R.D., 1984. Morphology, sedimentation processes, and growth pattern of the Amazon deep-sea fan. Geo Marine Letters 3, 109–117.

Damuth, J.E., Flood, R.D., 1985. Amazon Fan, Atlantic Ocean. In: Bouma, A.H., Normark, W.R., Barnes, N.E. (Eds.), Submarine Fans and Related Turbidite Systems. Springer, New York, pp. 97–106.

Damuth, J.E., Flood, R.D., Kowsmann, R.O., Belderson, R.H., Gorini, M.A., 1988. Anatomy and growth pattern of Amazon deep-sea fan as revealed by long-range side-scan sonar (GLORIA) and high resolution seismic studies. Bulletin of the American Association of Petroleum Geologists 72, 885–911

Damuth, J. E., R. D. Flood, C. Pirmez, and P. L. Manley, 1995, Architectural elements and depositional processes of Amazon deep sea fan imaged by long-range side-scan sonar (GLORIA), bathymetric swath-mapping (SeaBEAM), high-resolution seismic, and piston-core data, in K. T. Pickering, R. N. Hiscott, N. H. Kenyon, F. Ricci Lucchi, and R. D. A. Smith, eds., Atlas of deep water environments: architectural style in turbidite systems: London, Chapman and Hall, p. 105–121.

Damuth, J. E., 1994, Neogene gravity tectonics and depositional processes on the deep Niger Delta continental margin: Marine and Petroleum Geology, v. 11, no. 3, p. 320– 346.

Demyttenaere, R., J. P. Tromp, A. Ibrahim, P. Allman-Ward, and T. Meckel, 2000, Brunei deep water exploration: From sea floor images and shallow seismic analogues to depositional models in a slope turbidite setting: Gulf Coast Section SEPM Foundation 20th Annual Research Conference Deep-Water Reservoirs of the World, December 3–6, 2000, 304–317.

Deptuck, M.E., Steffens, G.S., Barton, M., Pirmez, C. 2003. Architecture and evolution of upper fan channel belts on the Niger Delta slope and in the Arabian Sea. Marine and Petroleum Geology, 20, 649-676.

Deptuck, M.E., Sylvester, Z., Pirmez, C, O'Byrne, C. 2007 Migration-aggradation history and 3-D seismic geomorphology of submarine channels in the Benin-major Canyon, western Niger Delta slope, Marine and Petroleum Geology, v. 24, 406-433.

Doust, H. and Omatsola, E. (1990) Niger Delta. In: Divergent/Passive Margin Basins (Eds. J. D. Edwards and P. A. Santogrossi), AAPG Memoir, No 48, p. 201-238

Droz, L., Rigaut, F., Cochonat, P., Tofani, R., 1996. Morphology and recent evolution of the Zaire turbidite system (Gulf of Guinea). Geological Society of America Bulletin 108, 253–269.

Droz, L., Marsset, T., Ondre´ as, H., Lopez, M., Savoye, B., Spy-Anderson, F.-L., 2003. Architecture of an active mud-rich turbidite system: the Zaire Fan (Congo-Angola margin southeast Atlantic): results from Zai¨Ango 1 and 2 cruises. Bulletin of the American Association of Petroleum Geologists 87, 1145–1168.

Druckman, Y., Buchbinder, B., Martinotti, G.M., Siman Tov, R., Aharon, P. 1995. The buried Afiq Canyon (eastern Mediterranean, Israel): a case study of a Tertiary submarine canyon exposed in Late Messinian times. Marine Geology, 123, 167-185.

Evamy, B. D., J. Haremboure, P. Kamerling, W. A. Knaap, F. A. Molloy, and P. H. Rowlands, 1978, Hydrocarbon habitat of Tertiary Niger Delta: AAPG Bulletin, v. 62, p. 277– 298.

Eyal, Y. 1996. Stress field fluctuations along the Dead Sea Rift since the Middle Miocene. Tectonics, 15, 157-170.

Fairhead, J.D., Binks, R.M., 1991. Differential opening of the Central and South Atlantic oceans and the opening of the West African rift system. Tectonophysics v. 187, p. 191-203.

Ferry, J.N., Mulder, T., Parize, O., Raillard, S. 2005. Concept of equilibrium profile in deep water turbidite systems: effects of local physiographic changes on the nature of sedimentary processes and the geometries of deposits. In: Hodgson, D.M., Flint, S.S. (eds), Submarine Slope Systems: Processes and Products, Geological Society Special Publication 244, London, pp181-193.

Fildani, A., Normark, W.R., 2004. Late Quaternary evolution of channel and lobe complexes of Monterey Fan. Mar. Geol. 206 (1–4), 199–223.

Flood, R. D., and J. E. Damuth, 1987, Quantitative characteristics of sinuous distributary channels in the Amazon deep-sea fan: Geological Society of America Bulletin, v. 98, p. 728–738.

Flood, R., Hiscott, R. N., Aksu, A. E., 2009. Morphology and evolution of an anastomosed channel network where saline underflow enters the Black Sea. Sedimentology, v.56, p.807-839.

Frey-Martinez, J., Cartwright, J.A., Hall, B. 2005. 3D seismic interpretation of slump complexes: examples from the continental margin of Israel. Basin Research, 17, 83-108.

Fonnesu, F., 2003, 3-D seismic images of a low-sinuosity slope channel and related depositional lobe (west Africa deepoffshore): Marine and Petroleum Geology, v. 20, p. 615–629.

Ford, M., Williams, E.A., Artoni, A., Verge´s, J., Hardy, S., 1997. Progressive evolution of a fault-related fold pair from growth strata geometries, Sant Llorenc¸ de Morunys, SE Pyrenees. J. Struct. Geol. 19 (3– 4), 413–441.

Folkman, Y., Mart, Y. 2008. Newly recognised eastern extension of the Nile deep-sea fan. GSA Bulletin, v.36, p.939-942.

Garfunkel, Z. 1998. Constraints on the origin and history of the Eastern Mediterranean basin. Tectonophysics, 391, 5-35.

Garfunkel, Z., Almagor, G. 1987. Active salt dome development in the Levant Basin, southeast Mediterranean. In: Lerche, I., O'Brien, J. (eds), Dynamical Geology of Salt and Related Structures. Academic Press, London, pp.263-300.

Garfunkel, Z., Derin, B. 1984. Permian-Early Mesozoic tectonism and continental margin formation in Israel and its implications for the history of the Eastern Mediterranean. In: Dixon, J.E., Robertson, A.H.F. (eds), The Geological Evolution of the Eastern Mediterranean, Geological Society Special Publication 17, 187-201.

Gaullier, V., Vendeville, B.C. 2005. Salt tectonics driven by sediment progradation: Part II – Radial spreading of sedimentary lobes prograding above salt. AAPG Bulletin, 89, 1081-1089.

Gaullier, V., Y.Mart, G. Bellaiche, B. Vendeville, J. Mascle, T. Zitter, and the second leg "PRISMED II" scientific party, 2000a, Salt tectonics in and around the Nile deep-sea fan: insights from the "PRISMED II" cruise, in B. C. Vendeville, Y. Mart, and J. L. Vigneresse, eds., Salt, shale, and igneous diapirs in and around Europe: Geological Society (London) Special Publication v. 174, p. 111–129.

Gee, M.R., Gawthorpe, R.L. 2006. Submarine channels controlled by salt tectonics: Examples from 3D seismic data offshore Angola. Marine and Petroleum Geology, 23, 443-458.

Gee, M.R., Uy, H.S., Warren, J., Morley, C.K., Ferguson, A., Lauti, S., and Lambiase, J.J., 2007, The Brunei Slide: A giant submarine landslide on the North West Borneo Margin revealed by 3D seismic data: Marine Geology, v. 246, p. 9–23.

Gradmann, S., Hubscher, C., Ben-Avraham, Z., Gajewski, D., Netzeband, G. 2005. Salt tectonics off northern Israel. Marine and Petroleum Geology, 22, 597-611.

Hagen, R.A., Bergersen, D.D., Moberly, R., and Coulbourn, W.T., 1994, Morphology of a large meandering sub marine canyon system on the Peru-Chile forearc: Marine Geology, 119, 7–38.

Hart, B. S., 1999. Definition of subsurface stratigraphy, structure and rock properties from 3-D seismic data. Earth-Science Reviews, v.47, p.497-518.

Heezen, B.C., Menzies, R.J., Schneider, E.D., Ewing, W.M., Granelli, N.C.L., 1964. Congo submarine Canyon. AAPG Bulletin 48, 1126–1149.

Heinio, P., Davies, R.J., 2006, Degradation of compressional fold belts: Deep Water Niger Delta. AAPG Bulletin, v. 90, p. 753-790

Heinio, P., Davies, R.J. 2007. Knickpoint migration in submarine channels in response to fold growth, western Niger Delta. Marine and Petroleum Geology, 24, 434-449.

Hesse, S., Back, S., Franke, D. 2009. The deep water fold-and-thrust belt offshore NW Borneo: Gravity-driven versus basement-driven shortenting. GSA Bulletin, v.121. p.939-953.

Higgins, S. Davies, R.J., Clarke, B. 2007. Antithetic fault linkages in a deep water fold and thrust belt. Journal of Structural Geology, 29,1900-1914.

Hooper, R.J., Fitzsimmons, R.J., Grant, N., Vendeville, B.C., 2002. The role of deformation in controlling depositional patterns in the southcentral Niger Delta, West Africa. Journal of Structural Geology 24 (4), 847–859.

Hovland, M., Gallagher, J.W., Clennell, M.B., Lekvam, K., 1997. Gas hydrate and free gas volumes in marine sediments: examples form the Niger Delta front. Marine and Petroleum Geology 14, 245–255.

Hsu, K.J., Montadert, L., Bernoulli, D., Cita, M.B., Erickson, A., Garrison, R.E., Kidd, R.B., Melieres, F., Muller, C., Wright, R.H. 1978. Initial reports of the Deep Sea Drilling Project, c42 (1): Washington D.C., U.S. Government Printing Office, 1249p.

Huyghe, P., Foata, M., Deville, E., Mascle, G. 2004. Channel profiles through the active thrust front of the southern Barbados prism. Geology, 32, 429-432.

Imran, J., Parker, G., Katopodes, N., 1998, A numerical model of channel inception on submarine fans: Journal of Geophysical Research, v. 103, p. 1219–1238.

Imran, J., Islam, M.A., Huang, H., Kassem, A., Dickerson, J., Pirmez, C., Parker, G., 2007. Helical flow couplets in submarine gravity underflows. Geology 35, 659–662.

Jackson, M.P.A, 1995, Retrospective salt tectonics, in Jackson, M.P.A., Roberts D.G., and Snelson, S., eds, Salt Tectonics, A Global Perspective, American Association of Petroleum Geologists Memoir, v. 65, p.1-28.

Jegou, I., Savoye, B., Pirmez, C., Droz, L. 2008. Channel-mouth lobe complex of the recent Amazon Fan: The missing piece. Marine Geology, v.252, p62-77.

Kane, I. A., McCaffrey, W. D., Peakall, J. 2008. Controls on sinuosity evolution within submarine channels. Geology, v.36, p.287-290.

Keary, P., Brooks, M., Hill, I. 2002. An introduction to geophysical exploration. Blackwell Science.

Keevil, G.M., Peakall, J., Best, J.L., Amos, K.J., 2006. Flow structure in sinuous submarine channels: velocity and turbulence structure of an experimental submarine channel. Marine Geology, 241, 241-257.

Keevil, G.M., Peakall, J. and Best, J.L. (2007) The influence of scale, slope and channel geometry on the flow dynamics of submarine channels. Mar. Petrol. Geol., 24, 487–503.

Khripounoff, A., Annick, V., Babonneau, N., Crassous, P., Dennielou, B., Savoye, B., 2003. Direct observation of intense turbidity current activity in the Zaire submarine valley at 4000m water depth. Marine Geology 194, 151–158.

Khripounoff, A., Vangriesheim, A., Crassous., P., Etoubleau, J. 2009. High frequency of gravity flow events in the Var submarine canyon (Mediterranean Sea). Marine Geology, v.263, p.1-6.

Kneller, B. C., 1995, Beyond the turbidite paradigm: physical models for deposition of turbidites and their implications for reservoir prediction: Geological Society (London) Special Publication, v. 94, p. 31–49.

Kneller, B. C. 2003. The influence of flow parameters on turbidite channel slope architecture. Marine and Petroleum Geology, v.20, p.901-910.

Kneller, B. C., & Buckee, C. (2000). The structure and fluid mechanics of turbidity currents: a review of some recent studies and their geological implications. Sedimentology, 47, 62–94.

Knighton, A.D., 1998. Fluvial Forms and Processes: A New Perspective. Arnold, London, 383pp.

Knox, G.J., Omatsola, E.M., 1989, Development of the Cenozoic NigerDelta in terms of the 'Escalator Regression' Model and Impact on Hydrocarbon Distribution. Proceedings KNGMG Symposium 'Coastal Lowlands, Geology and Geotechnology' (pp. 181-202). Kluwer Academic Publishers, Dordrecht.

Knutz, P.C., Cartwright, J., 2003, Seismic stratigraphy of the West Shetland Drift: Implications for later Neogene paleocirculation in the Faeroe-Shetland gateway. Palaeoceanography, v. 18, p1-11.

Kolla, V. 2007. A review of sinuous channel avulsion patterns in some major deep-sea fans and factors controlling them. Marine and Petroleum Geology, 24, 450-469.

Kolla, V., Coumes, F., 1987. Morphology, internal structure, seismic stratigraphy and sedimentation of Indus Fan. Bulletin of the American Association of Petroleum Geologists 71, 650–677.

Kolla, V., Posamentier, H.W., Wood, L.J., 2007, Deep water and fluvial sinuous channels-characteristics, similarities and dissimilarities, and modes of formation. Marine and Petroleum Geology, v. 24, p. 388-405.

Kukowski, N., Schillhorn, T., Huhn, K., von Rad, U., Husen, S., Flueh, E., R. 2001. Morphotectonics and mechanics of the central Makran accretionary wedge off Pakistan. Marine Geology, v.173. p.1-19.

Lamb, M.P., Toniolo, H., Parker, G. 2005. Trapping of sustained turbidity currents by intraslope minibasins. Sedimentology, 1-14.

Laursen, J., Normark, W.R., 2002. Late Quaternary evolution of the San Antonio submarine canyon in the central Chile forearc (w338S). Marine Geology 188, 365–390.

Letouzey, J., Colletta, B, Vialli, R., and Charmette, J-C., 1995, Evolution of salt-related structures in compressional settings, in Jackson, M.P.A., Roberts D.G., and Snelson, S., eds, Salt Tectonics, A Global Perspective, American Association of Petroleum Geologists Memoir, v. 65, p. 41-60.

Loncke, L., Gaullier, V., Mascle, J., Vendeville, B., Camera, L. 2006. The Nile deep-sea fan: An example of interacting sedimentation, salt tectonics, and inherited subsalt paleotopographic features. Marine and Petroleum Geology, 23, 297-315.

Lopez, M. 2001. Architecture and depositional pattern of the Quaternary deep sea fan of the Amazon. Marine and Petroleum Geology, 18, 479-486.

Mackin, J.H. 1948. The concept of the graded river. GSA Bulletin, v.59. p.463-512.

Mart, Y., Ben Gai, Y. 1982. Some depositional patterns at continental margin of southestern Mediterranean Sea. AAPG Bulletin, 66, 460-470.

Martinsen, O.J., Bakken, B., 1990, Extensional and compressional zones in slumps and slides in the Namurian of County Clare, Ireland. J. Geol. Soc. London, v.147, p. 153-164.

Masaferro, J., Poblet, J., Bulnes, M., Eberli, G.P., Dixon, T., McClay, K.R., 1999. PalaeogeneeNeogene/present day growth folding in the Bahamian foreland of the Cuban fold and thrust belt. Journal of the Geological Society v.156, p.617-631.

Mayall, M., and I. Stewart, 2000, The architecture of turbidite slope channels, in P. Weimer, R. M. Slatt, J. Coleman, N. C. Rosen, H. Nelson, A. H. Bouma, M. J. Styzen, and D. T. Lawrence, eds., Global deep-water reservoirs: Gulf Coast Section SEPM Foundation 20th Annual Bob F. Perkins Research Conference, p. 578–586.

Mayall, M., Jones, E., Casey, M. 2006. Turbidite channel reservoirs – key elements in facies prediction and effective development. Marine and Petroleum Geology, 23, 821-841.

McClay, K.R., Dooley, T. & Zamora, G., 2003, Analogue models of delta systems above mobile shales. In: Subsurface SedimentMobilization (Ed. by P.Van Rensbergen, C.Morley, R. Hillis& J.Cartwright),Geol. Soc. Lond. Spec.Publ., v. 216, p. 411-428.

McHargue, T.R., Webb, J.E., 1986. Internal geometry, seismic facies and petroleum potential of canyons and inner fan channels of the Indus Submarine Fan. AAPG Bulletin, 70, 161–180.

Metivier, F., Lajeunesse, E., Cacas, M.C., 2005. Submarine canyons in the bathtub. Journal of Sedimentary Research 75, 6–11.

Mitra, S. 1990. Fault-Propogation Folds: Geometry, Kinematic Evolution, and Hydrocarbon Traps. AAPG Bulletin, 74, 921-945.

Mitra, S. 2002. Fold-accomodation faults. AAPG Bulletin, 86, 671-693.

Mohrig, D., Buttles, J., 2007. Deep turbidity currents in shallow channels. Geology 35, 155–158.

Morgan, R. 2004. Structural controls on the positioning of submarine channels on the lower slopes of the Niger Delta. In: Davies, R.J., Cartwright, J.A., Stewart, S.A., Lappin, M., Underhill, J.R. (eds), 3D Seismic Technology: Application to the Exploration of Sedimentary Basins. Geological Society Memoirs, 29, 45-51.

Morley, C.K., 2009. Growth of folds in a deep-water setting. Geosphere, v.5. p.59-89.

Morley, C.K., and Guerin, G., 1996, Comparison of gravity-driven deformation styles and behaviour associated with mobile shales and salt, Tectonics, v. 15, p.1154-1170.

Morley, C.K., and Leong, L.C., 2008, Evolution of deepwater synkinematic sedimentation in a piggy-back basin, determined from 3D seismic reflection Geosphere, April 2009 89 data: Geosphere, v. 4, p. 939–962.

Moore, G. F., Shipley, T. H., Stoffa, P. L., Karig, D. E., Taira, A., Kuramoto, S., Tokuyama, H., Suyehiro, K. 1990. Structure of the Nankai Trough Accretionary zone from multichannel seismic reflection data. In: Special section on the role of fluids in sediment accretion, deformation, diagenesis, and metamorphism in subduction zones, Langseth, M.G., Moore, J. C., (eds). Journal of Geophysical Research, v.95, p.8753-8765.

Mulder, T. & Cochonat, H.P, 1996, Classification of offshore mass movements. J. Sediment. Res., v. 66, p. 43-57.

Noda, A., TuZino, T., Furukawa, R., Joshima, M., Uchida, J., 2008. Physiographical and sedimentological characteristics of submarine canyons developed upon an active forearc slope: The Kushiro Submarine Canyon, northern Japan. GSA Bulletin, 120, 750-767.

Normark, W. R., & Piper, D. J. W. (1983). Navy Fan, California Borderland: growth pattern and depositional processes. Geo-Marine Letters, 3(2–4), 101–108.

Normark, W.R., Piper, D.J.W., Posamentier, H.W., Pirmez, C., Migeon, S. 2002. Variability in form and growth of sediment waves on turbidite channel levees. Marine Geology, 192, 23-58.

Ouchi, S. 1985. Response of alluvial rivers to slow active tectonic movement: GSA Bulletin, v.96, p.504-515.

Paull, C.K., Ussler, W., Greene, H.G., Keaten, R., Mitts, P., and Barry, J., 2003, Caught in the act: The 20 December 2001 gravity fl ow event in Monterey Canyon: Geo-Marine Letters, v. 22, p. 227–232.

Peakall, J.,W.D.McCaffrey, and B. C. Kneller, 2000, A process model for the evolution, morphology and architecture of meandering submarine fan channels: Journal of Sedimentary Research, v. 70, p. 434–448.

Peakall, J., Ashworth, P.J., Best, J.L., 2007. Meander-bend evolution, alluvial architecture, and the role of cohesion in sinuous river channels: a flume study. Journal of Sedimentary Research 77, 197–212.

Peel, F. J., C. J. Travis, and J. R. Hossack, 1995, Genetic structural provinces and salt tectonics of the Cenozoic offshore US Gulf of Mexico: a preliminary analysis, in M. P. A. Jackson, D. G. Roberts, and S. Snelson, eds., Salt tectonics: a global perspective: AAPG Memoir 65, p. 153–175.

Pickering, K.T., Coleman, J., Cremer, M., Droz, L., Kohl, B., Normark,
W., O'Connell, S., Stow, D., Meyer-Wright, A., 1986. A high sinuosity, laterally migrating submarine fan channel–levee-overbank: results from DSDP Leg 96 on the Mississippi Fan, Gulf of Mexico. Marine and Petroleum Geology 3, 3–18.

Pirmez, C., and Flood, R.D., 1995, Morphology and structure of Amazon channel, in Flood, R.D., Piper, D.J.W., Klaus, A., and Peterson, L.C., eds., Proceedings of the Ocean Drilling Program, Initial Results: College Station, Texas, Ocean Drilling Program, p. 23–45.

Pirmez, C., Beaubouef, R.T., Friedmann, S.J., Mohrig, D.C. 2000. Equilibrium profile and baselevel in submarine channels: Examples from Late Pleistocene systems and implications for the architecture of deepwater reservoirs. GCSSEPM Foundation 20th Annual Research Conference: Deep-Water reservoirs of the World.

Pirmez, C., Imran, J., 2003. Reconstruction of turbidity currents in Amazon Channel. Marine and Petroleum Geology 20, 823–849.

Poblet, J., Hardy, S., 1995. Reverse modeling of detachment folds; application to the Pico del Aguila anticline in the South Central Pyrenees (Spain). Journal of Structural Geology 17, 1707-1724.

Poblet, J., McClay, K., Storti, F., Munoz, J.A., 1997, Growth strata geometries associated to single layer detachment fold. Journal of Structural Geology, v. 19, p. 369-381.

Poblet, J., Mun˜oz, J.A., Trave´, A., Serra-Kiel, J., 1998. Quantifying the kinematics of detachment folds using the three-dimensional geometry: application to the Mediano anticline (Pyrenees Spain). GSA Bull. 110, 111 – 125.

Popescu, I., Lericolais, G., Panin, N., Normand, A., Dinu, C., Le Drezen, E., 2004. The Danube submarine canyon (Black Sea): morphology and sedimentary processes. Marine Geology 206 (1–4), 249–265.

Posamentier, H.W. 2003. Depositional elements associated with a basin floor channel-levee system: a case study from the Gulf of Mexico. Marine and Petroleum Geology, 20, 667-690.

Prather, B. E. 2003. Controls on reservoir distribution, architecture and stratigraphic trapping in slope settings. Marine and Petroleum Geology, 20, 529-545.

Puigdefàbregas, C., Muñoz, J. A., and Vergés, J., 1992, Thrusting and foreland basin evolution in the southern Pyrenees, in McClay, K. R., ed., Thrust tectonics: London, Chapman and Hall, p. 247–254.

Reading, H.G., Richards, M., 1994, Turbidite system in deep-water basin margins classified by grain size and feeder system: American Association of Petroleum Geologists, Bulletin, v. 78, p. 792–822.

Riba, O., 1976. Syntectonic unconformities of the Alto Cardener, Spanish Pyrenees: a genetic interpretation. Sediment. Geol. 15, 213– 233.

Ross, W. C., Halliwell, B. A., May, J. A., Watts, D. E., & Syvitski, J. P. M. (1994). Slope readjustment: a new model for the development of submarine fans and aprons. Geology, 22, 511–5114.

Rowan, M.G., 1997. Three-dimensional geometry and evolution of a segmented detachment fold, Mississippi fan foldbelt, Gulf of Mexico. Journal of Structural Geology v.19, p.463-480.

Rowan, M. G., F. J. Peel, and B. C. Vendeville, 2004, Gravity-driven fold belts on passive margins, in K. R. McClay, ed., Thrust tectonics and hydrocarbon systems: AAPG Memoir 82, 157– 182.

Ryan, W.B.F., Hsu, K.J. et al (eds). 1973. In: Rep. Deep Sea Drill. Proj., vol. 13. 1447pp.

Salvini, F., Storti, F., 2002, Three-dimensional architecture of growth strata associated to fault-bend, fault-propogation and decollement anticlines in non-erosional environments. Sedimentary Geology, v. 146, p. 57-73.

Samuel, A., Kneller, B., Raslan, S., Sharp, A., Parsons, C. 2003. Prolific deep-marine slope channels of the Nile Delta, Egypt. AAPG Bulletin, 87, 541-560.

Satterfield, W. M., & Behrens, E. W. (1990). A Late Quaternary canyon/ channel system, northwest Gulf of Mexico continental slope. Marine Geology, 92, 51–67.

Sawyer, D. E., P. B. Flemings, and R. C. Shipp,2007, Seismic geomorphology, lithology, and evolution of the late Pleistocene Mars-Ursa turbidite region, Mississippi Canyon area, northern Gulf of Mexico: AAPG Bulletin, v. 91, p. 215–234

Schwenk, T., Spieß, V., Breitzke, M., Hu¨ bscher, C., 2005. The architecture and evolution of the Middle Bengal Fan in vicinity of the active channel–levee system imaged by high-resolution seismic data. Marine and Petroleum Geology 22, 637–656.

Segev, A., Rybakov, M., Lyakhovsky, V., Hofstetter, A., Tibor, T., Goldshmidt, V., Ben-Avraham, Z. 2006. The structure, isostasy and gravity field of the Levant continental margin and the southeast Mediterranean area. Tectonophysics, 425, 137-157.

Shaw, J.H., Suppe, J., 1994. Active faulting and growth folding in the eastern Santa Barbara Channel California. GSA Bull. v.106, p.607– 626.

Sheriff, R. E., Geldart, L. P. 1995. Exploration Seismology. Cambridge University Press.

Short, K. C., and A. J. Stauble, 1965, Outline of geology of Niger Delta: AAPG Bulletin, v. 51, p. 761–779.

Skene, K.I., Piper, D.J.W., Hill, P.S. 2002. Quantitative analysis of variations in depositional sequence thickness from submarine channel levees. Sedimentology, 49, 1411-1430.

Smith, R. 2004. Silled sub-basins connected to tortuous corridors: Sediment distribution systems on topographically complex slopes. In: Lomas, S. A. & Joseph, P. (eds) 2004, Confined Turbidite Systems. Geological Society, London, Special Publications, v. 222, p. 23-43.

Smith, D.P., Kvitek, R., Iampietro, P. J., Wong, K. 2007. Twenty nine months of geomorphic change in the Upper Montery Canyon (2002-2005). Marine Geology, v.236, p.79-94.

Snow, R.S., Slingerland, R.L., 1990. Stream profile adjustment to crustal warping; nonlinear results from a simple model. Journal of Geology 98 (5), 699–708.

Soh, W., Tokuyama, H., Fujioka, K., Kato, S., and Taira, A., 1990, Morphology and development of a deep-sea meandering Canyon (Boso Canyon) on an active plate margin, Sagami Trough, Japan: Marine Geology, 91, 227–241

Storti, F., Poblet, J., 1997. Growth stratal architectures associated to decollement folds and fault propagation folds. Inferences on fold kinematics. Tectonophysics 282, 353– 373.

Stow, D. A. V., & Mayall, M. (2000). Deep-water sedimentary systems: new models for the 21st century. Marine and Petroleum Geology, 17, 125–135.

Straub, K.M., Mohrig, D., McElroy, B., Buttles, J., Pirmez, C. 2008. Interactions between turbidity currents and topography in aggrading sinuous submarine channels: A laboratory study. GSA Bulletin, v.120, p.368-385.

Suppe, J., G. T. Chou, and S. C. Hook, 1992, Rates of folding and faulting determined from growth strata, in K. McClay, ed., Thrust tectonics: London, Chapman & Hall, p. 105–121.

Thorsen, C.E. 1963. Age of growth faulting in Southeast Louisiana. Transactions, Gulf Coast Association of Geological Societies, v.13, p.103-110.

Tibor, G., Ben-Avraham, Z. 1992. Late Tertiary seismic facies and structures of the Levant passive margin off central Israel, eastern Mediterranean. Marine Geology, 105, 253-273.

Trudgill, B. D., M. G. Rowan, J. C. Fiduk, P. Weimer, P. E. Gale, B. E. Korn, R. L. Phair, W. T. Gafford, G. R. Roberts, and S. W. Dobbs, 1999, The Perdido fold belt, northwestern deep Gulf of Mexico, Part 1: Structural geometry, evolution and regional implications: AAPG Bulletin, v. 83, p. 88–113.

Viana, A., Figueiredo, A., Faugeres, J.C., Lima, A., Gonthier, E., Brehme, I., Zaragosi, S. 2003. The Sao Tome deep sea turbidite system (southern Brazil Basin): Cenozoic seismic stratigraphy and sedimentary processes. AAPG Bulletin, 87, 873-894.

Vidal, N., Alvarez-Marron, J., Klaeschen, D. 2000. Internal configuration of the Levantine basin from seismic reflection data (Eastern Mediterranean). Earth and Planetary Science Letters, 180, 77-89.

Von Rad, U., Tahir, M., 1997. Late Quaternary sedimentation on the outer Indus shelf and slope (Pakistan): evidence from high-resolution seismic data and coring. Marine Geology 138, 193–236.

Westbrook, G. K., Ladd, J. W., Buhl, P., Tiley, G.J. 1998. Cross section of an accretionary wedge: Barbados Ridge Complex. Geology, v.16. p.631-635

Whiteman, A., 1982, Nigeria: its Petroleum Geology, Resources, and Potential, v. 1 and 2, Graham and Trotman, London, 394 pp

Winker, C.D., 1982, Cenozoic shelf margins: Northwestern Gulf of Mexico, Gulf Coast Association of Geological Societies Transactions, v. 32, p. 427-448.

Winker, C.D., and Booth, J.R., 2000, Sedimentary dynamics of the salt-dominated continental slope, Gulf of Mexico: integration of observations from the sea floor, near-surface and deep subsurface, in Weimer, P., Slatt, R.M., Coleman, J., Rosen, N.C., Nelson, H., Bouma, A.H., Styzen, M.J., and Lawrence, D.T., eds., Deep-Water Reservoirs of the World: Gulf Coast Society of the Society of Economic Paleontologists and Mineralogists Foundation, 20th Annual Research Conference, p. 1059–1086

Wu, S., A. W. Bally, and C. Cramez, 1990, Allochthonous salt, structure and stratigraphy of the northeastern Gulf of Mexico, part II: structure: Marine and Petroleum Geology, v. 7, p. 334–370.

Wu, S., and A. W. Bally, 2000, Slope tectonics— Comparisons and contrasts of structural styles of salt and shale tectonics of the northern Gulf of Mexico with shale tectonics of offshore Nigeria in Gulf of Guinea, in W. Mohriak and M. Talwani, eds., Atlantic rifts and continental margins: Washington, D.C., American Geophysical Union, p. 151– 172.

Wynn, R.B., Cronin, B.T., Peakall, J., 2007, Sinuous deep-water channels: Genesis, geometry and architecture. Marine and Petroleum Geology, v. 24, p. 341-387.

Yu, B., Cantelli, A., Marr, J., Pirmez, C., O'Byrne, C. and Parker, G. (2006) Experiments on self-channelized subaqueous fans emplaced by turbidity currents and dilute mudflows. J. Sed. Res., 76, 889–902.

Zapata, T.R., Allmendinger, R.W., 1996. Growth stratal records of instantaneous and progressive limb rotation in the Precordillera thrust belt and Bermejo basin, Argentina. Tectonics 15 (5), 1065– 1083.

Appendices

APPENDIX A1

A1.1 Additional seismic profiles showing changes in channel morphology

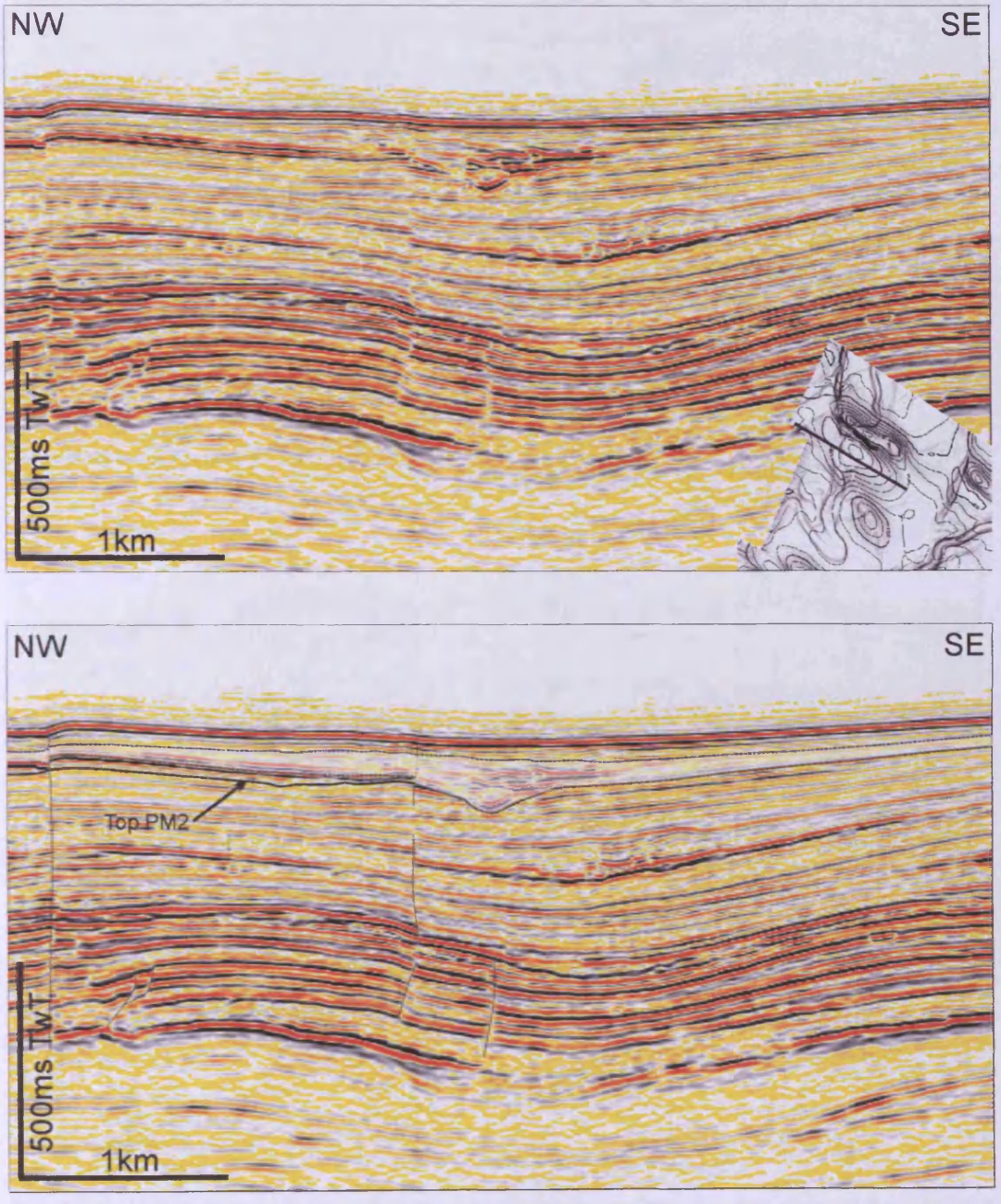

Fig. A1.1: Uninterpreted and partly interpreted seismic profiles showing channel A upstream of a fold which blocks this channel levee system.

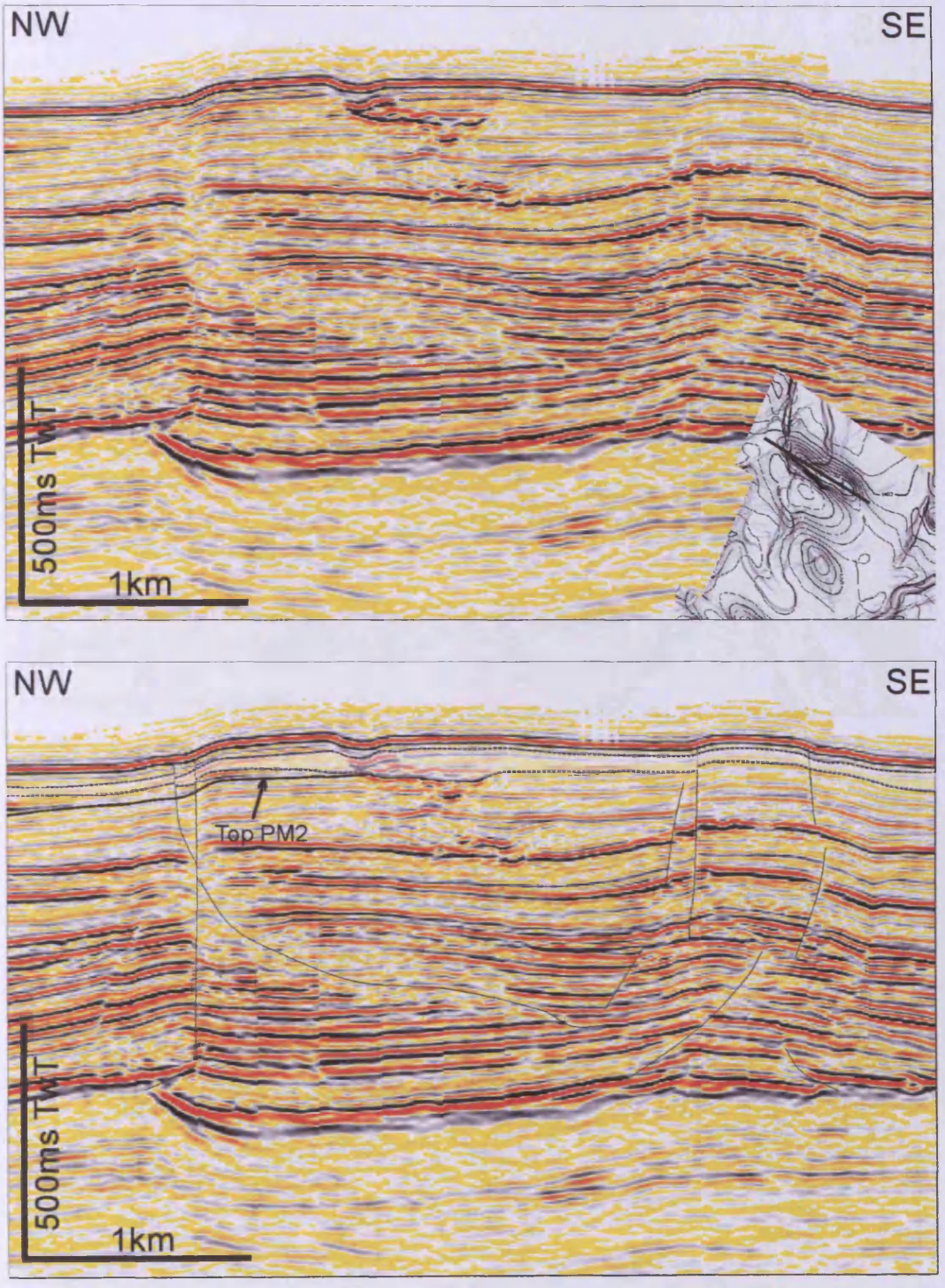

Fig. A1.2: Uninterpreted and partly interpreted seismic profiles showing channel A crossing the crest of the fold which blocked channel sedimentation.

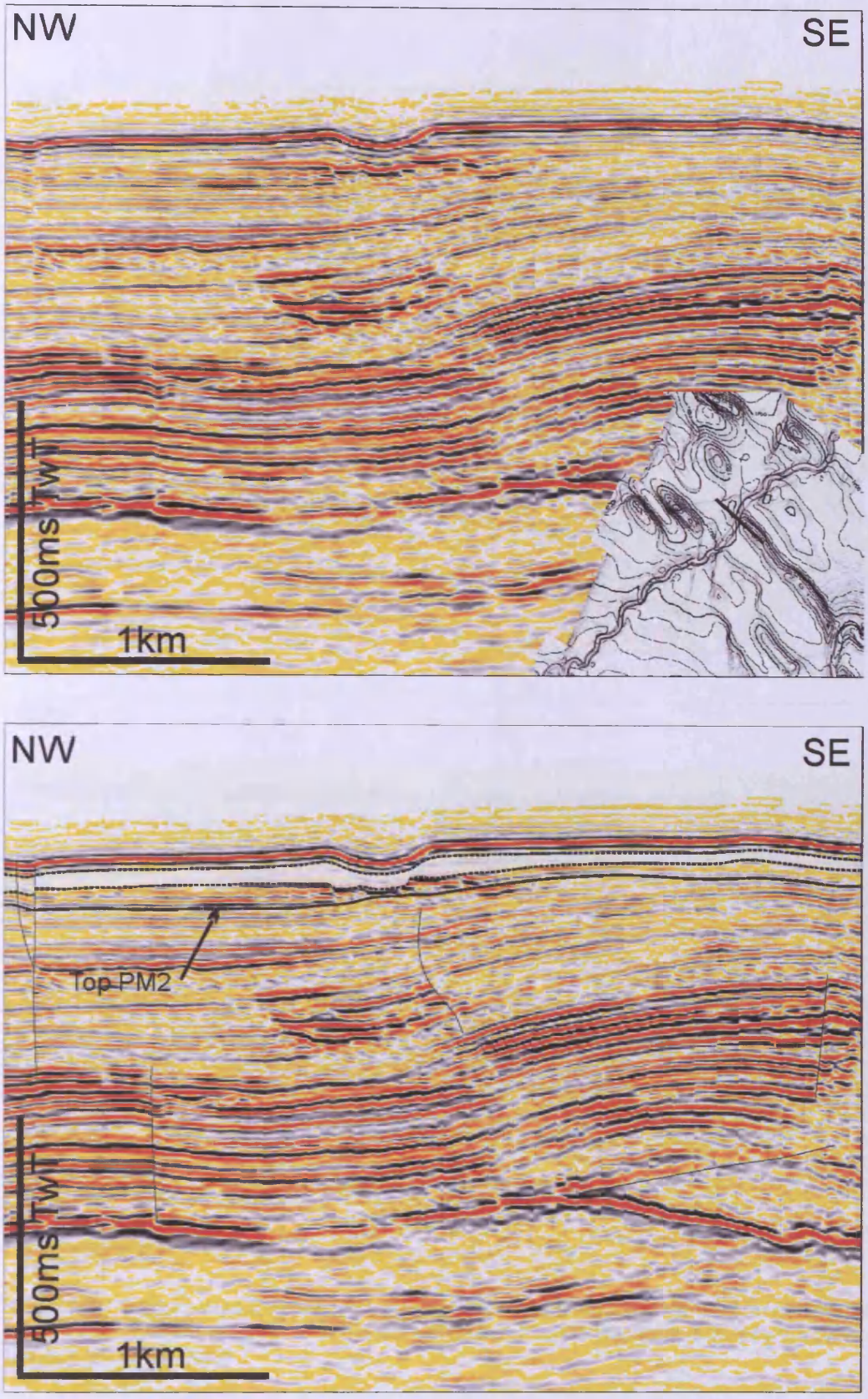

Fig. A1.3: Uninterpreted and partly interpreted seismic profiles showing channel B crossing the crestal region of a laterally propagating fold perpendicular to the channel flow direction.

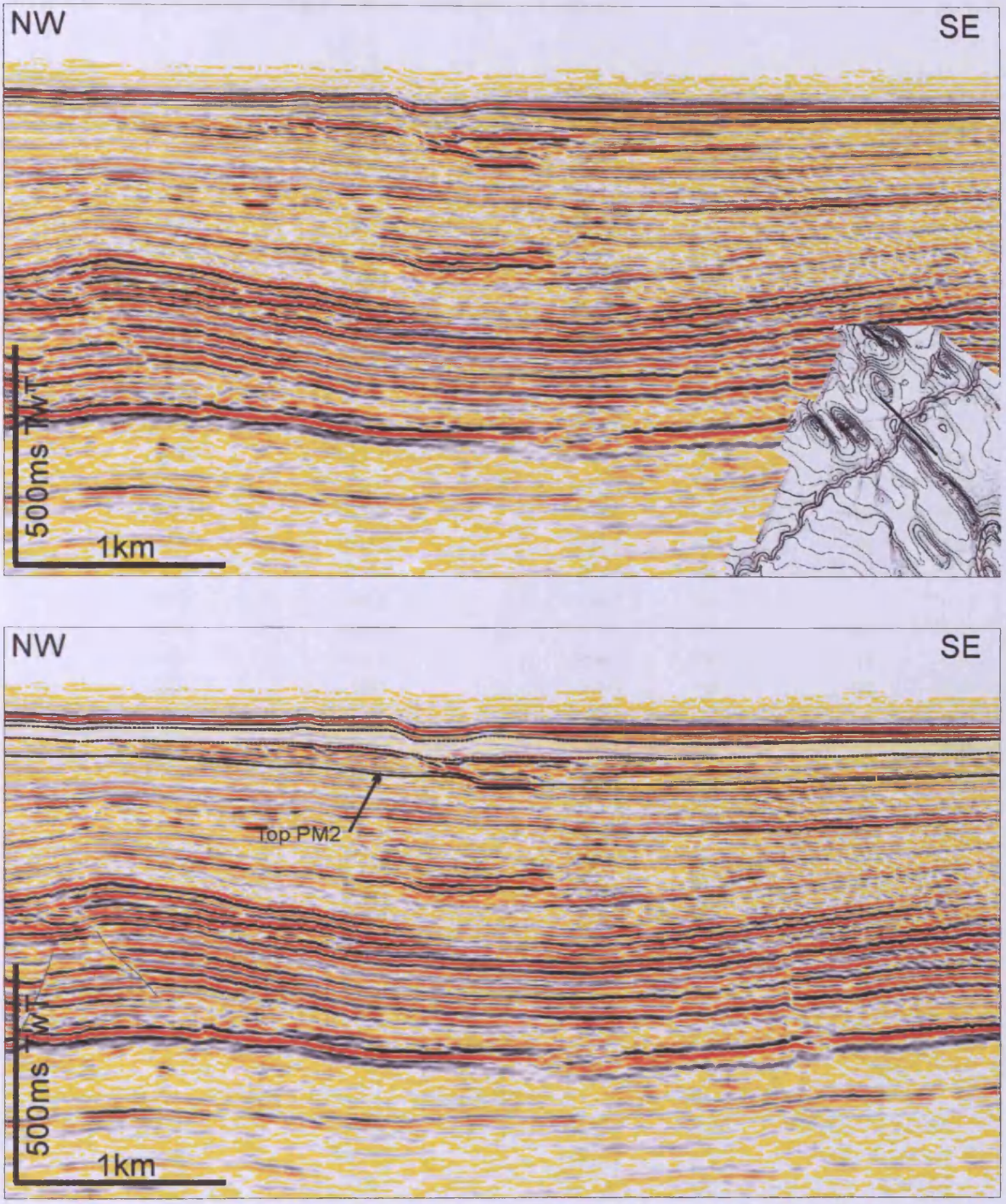

Fig. A1.4: Uninterpreted and partly interpreted seismic profiles showing channel B crossing the foot-wall syncline and showing increased levee deposition into the accommodation space created by folding towards the south-east.

A1.2 Channel A morphology measurements

Dist along channel/m	Channel Depth/mbsl	Erosional depth/mbsl	Channel Width/m	Relief/m	W:D Ratio
0	1345.5	1435.5	182	8	22.75
500	1354.5	1442.5	216	8	27.00
1000	1360.5	1416.5	221	18	12.28
1500	1366.5	1418.5	231	21	11.00
2000	1368	1424	192	18	10.67
2500	1375.5	1431.5	225	19	11.84
3000	1375.5	1427.5	226	19	11.89
3500	1371	1425	206	25	8.24
4000	1371	1421	174	18	9.67
4500	1371	1413	165	28	5.89
5000	1366.5	1422.5	171	67	2.55
5500	1372.5	1428.5	177	41	4.32
6000	1366.5	1440.5	155	28	5.54
6500	1380	1438	177	35	5.06
7000	1396.5	1480.5	165	29	5.69
7500	1398	1492	138		
8000	1402.5	1498.5	161		
8500	1408.5	1470.5	143	27	5.30
9000	1414.5	1484.5	136	16	8.50
9500	1422	1494	119	20	5.95
10000	1410	1470	127	26	4.88
10500	1341	1421	168	18	9.33
11000	1359	1405	158	21	7.52
11500	1378.5	1450.5	145	19	7.63
12000	1396.5	1466.5	121	22	5.50
12500	1405.5	1449.5	168	16	10.50
13000	1408.5	1446.5	177	22	8.05
13500	1407	1441	236	21	11.24

A.1.3 Channel B morphology measurements

Dist along channel/m	Channel depth/mbsl	Erosional depth/mbsl	Width/m	Relief/m	W:D Ratio
0	1233.00	1291.82	309	18.00	17.166667
500	1233.00	1308.29	338	19.88	17.006289
1000	1236.00	1301.88	280	12.00	23.333333
1500	1239.00	1302.53	340	16.88	20.148148
2000	1245.00	1303.82	318	16.88	18.844444
2500	1251.00	1312.18	268	18.75	14.293333
3000	1254.00	1325.76	253	19.50	12.974359
3500	1251.00	1314.53	274	15.00	18.266667
4000	1251.75	1325.87	273	11.63	23.483871
4500	1254.00	1315.18	396	20.25	19.555556

5000	1257.75	1334.22	277	19.88	13.937107
5500	1257.00	1324.06	312	17.25	18.086957
6000	1258.50	1325.56	337	18.75	17.973333
6500	1260.00	1316.47	327	19.88	16.45283
7000	1262.25	1319.90	354	29.63	11.949367
7500	1263.00	1319.47	334	21.00	15.904762
8000	1265.25	1314.66	337	20.63	16.339394
8500	1266.00	1318.94	336	16.88	19.911111
9000	1271.25	1319.49	341	20.25	16.839506
9500	1276.50	1327.09	313	20.25	15.45679
10000	1281.75	1339.40	336	21.75	15.448276
10500	1284.00	1341.65	340	22.13	15.367232
11000	1284.75	1340.04	304	20.63	14.739394
11500	1290.00	1345.29	343	21.75	15.770115
12000	1291.50	1355.03	332	21.75	15.264368
12500	1293.00	1353.00	308	20.63	14.933333
13000	1293.00	1351.82	386	19.50	19.794872
13500	1296.00	1357.18	316	19.88	15.899371
14000	1301.25	1363.60	323	19.50	16.564103
14500	1308.00	1368.00	332	21.38	15.532164
15000	1308.00	1375.06	320	19.88	16.100629
15500	1312.50	1377.21	322	19.50	16.512821
16000	1317.00	1384.06	278	19.88	13.987421
16500	1320.00	1397.65	360	15.00	24
17000	1321.50	1429.74	354	7.88	44.952381
17500	1322.25	1410.49	359	11.25	31.911111
18000	1320.00	1401.18	352	19.50	18.051282
18500	1325.25	1374.66	332	21.00	15.809524
19000	1332.75	1402.16	395	13.88	28.468468
19500	1333.50	1429.97	350	14.25	24.561404
20000	1332.00	1383.76	357	21.00	17
20500	1335.00	1402.06	358	21.00	17.047619
21000	1336.50	1395.32	356	16.50	21.575758
21500	1338.75	1389.34	343	21.00	16.333333
22000	1341.75	1398.22	350	21.00	16.666667
22500	1345.50	1409.03	385	16.13	23.875969
23000	1347.75	1408.93	367	12.75	28.784314
23500	1349.25	1415.13	309	17.25	17.913043
24000	1347.75	1428.93	347	15.75	22.031746
24500	1353.00	1407.12	377	20.25	18.617284
25000	1359.00	1409.59	372	18.38	20.244898
25500	1369.50	1433.03	440	18.75	23.466667
26000	1374.00	1424.59	353	18.00	19.611111

A1.4 Channel C morphology measurements

Distance along channel/m	Channel depth/mbsl	Erosional depth/mbsl	Width/m	Relief/m	W:D Ratio

0	1158.00	1195.40	614	36.00	17.06
200	1158.00	1197.10	694	34.13	20.34
400	1157.25	1198.90	687	33.38	20.58
600	1158.75	1195.30	415	36.75	11.29
800	1158.75	1196.15	390	34.50	11.30
1000	1158.75	1195.30	445	33.38	13.33
1200	1158.75	1196.15	434	32.25	13.46
1400	1161.75	1199.15	469	33.38	14.05
1600	1164.00	1202.25	544	33.75	16.12
1800	1164.75	1205.55	544	34.88	15.60
2000	1169.25	1204.95	465	38.63	12.04
2200	1170.00	1208.25	574	37.13	15.46
2400	1170.75	1208.15	545	36.38	14.98
2600	1173.75	1211.15	530	36.75	14.42
2800	1174.50	1214.45	681	36.75	18.53
3000	1176.75	1215.00	574	37.88	15.16
3200	1176.75	1213.30	658	33.38	19.72
3400	1178.25	1215.65	667	37.88	17.61
3600	1179.75	1216.30	553	35.25	15.69
3800	1181.25	1216.10	687	33.75	20.36
4000	1180.50	1215.35	505	33.75	14.96
4200	1181.25	1215.25	442	33.00	13.39
4400	1179.75	1217.15	501	29.63	16.91
4600	1179.75	1220.55	641	30.38	21.10
4800	1181.25	1222.90	587	30.75	19.09
5000	1182.00	1220.25	723	31.50	22.95
5200	1182.75	1219.30	861	33.75	25.51
5400	1185.00	1222.40	987	34.50	28.61
5600	1187.25	1222.95	893	39.00	22.90
5800	1187.25	1222.95	1037	36.75	28.22
6000	1188.00	1224.55	777	32.63	23.82
6200	1185.75	1222.30	520	28.50	18.25
6400	1189.50	1222.65	505	22.13	22.82
6600	1191.75	1222.35	460	34.50	13.33
6800	1191.75	1224.90	454	35.63	12.74
7000	1191.75	1225.75	421	28.13	14.97
7200	1191.75	1225.75	518	37.50	13.81
7400	1194.75	1230.45	618	27.00	22.89
7600	1195.50	1232.05	592	38.25	15.48
7800	1196.25	1242.15	457	36.75	12.44
8000	1197.75	1244.50	451	35.25	12.79
8200	1200.00	1245.90	619	33.00	18.76
8400	1199.25	1245.15	638	32.25	19.78
8600	1203.00	1242.10	553	32.25	17.15
8800	1200.75	1247.50	649	25.13	25.83
9000	1200.75	1247.50	479	27.00	17.74
9200	1201.50	1251.65	505	28.88	17.49
9400	1201.50	1248.25	525	30.75	17.07
9600	1200.75	1234.75	480	26.63	18.03
9800	1204.50	1254.65	531	29.63	17.92

10000	1206.00	1254.45	474	30.00	15.80
10200	1203.75	1257.30	414	29.25	14.15
10400	1206.75	1261.15	399	31.50	12.67
10600	1209.75	1266.70	449	30.38	14.78
10800	1212.75	1276.50	458	34.13	13.42
11000	1217.25	1272.50	479	35.25	13.59
11200	1218.75	1267.20	440	36.38	12.10
11400	1224.00	1269.05	426	36.00	11.83
11600	1227.75	1278.75	481	35.25	13.65
11800	1230.75	1285.15	489	34.50	14.17
12000	1226.25	1275.55	467	35.63	13.11
12200	1230.75	1286.85	467	34.13	13.68
12400	1233.75	1278.80	561	39.00	14.38
12600	1227.00	1281.40	613	33.38	18.37
12800	1227.00	1272.90	419	32.25	12.99
13000	1223.25	1277.65	467	28.88	16.17
13200	1224.00	1277.55	390	34.13	11.43
13400	1223.25	1273.40	370	32.25	11.47
13600	1224.75	1274.90	352	33.75	10.43
13800	1218.75	1268.90	381	26.25	14.51
14000	1218.75	1266.35	374	28.50	13.12
14200	1218.75	1266.35	322	27.38	11.76
14400	1220.25	1272.95	305	23.63	12.91
14600	1221.75	1268.50	390	26.63	14.65
14800	1227.75	1277.90	488	33.75	14.46
15000	1221.00	1269.45	593	25.50	23.25
15200	1224.00	1272.45	453	31.13	14.55
15400	1223.25	1269.15	454	30.38	14.95
15600	1223.25	1278.50	404	29.25	13.81
15800	1224.75	1275.75	417	27.38	15.23
16000	1224.75	1279.15	450	25.50	17.65
16200	1226.25	1277.25	418	25.50	16.39
16400	1228.50	1277.80	400	24.00	16.67
16600	1229.25	1281.95	420	25.13	16.72
16800	1227.75	1278.75	436	22.50	19.38
17000	1230.75	1283.45	443	24.75	17.90
17200	1235.25	1287.10	454	27.38	16.58
17400	1234.50	1285.50	476	21.75	21.89
17600	1238.25	1290.95	438	24.75	17.70
17800	1239.75	1297.55	459	24.38	18.83
18000	1241.25	1296.50	488	24.75	19.72
18200	1244.25	1296.10	424	24.38	17.39
18400	1242.75	1287.80	443	22.88	19.37
18600	1245.75	1299.30	408	22.13	18.44
18800	1247.25	1299.10	421	22.50	18.71
19000	1248.00	1299.85	418	22.50	18.58
19200	1248.75	1304.85	466	22.88	20.37
19400	1248.75	1306.55	466	21.75	21.43
19600	1252.50	1305.20	462	23.25	19.87
19800	1255.50	1304.80	407	26.25	15.50

20000	1257.75	1296.85	440	26.25	16.76
20200	1257.00	1302.90	419	23.63	17.74
20400	1260.00	1298.25	548	24.38	22.48
20600	1260.75	1301.55	583	24.75	23.56
20800	1262.25	1303.90	527	26.25	20.08
21000	1263.75	1302.85	498	25.88	19.25
21200	1265.25	1310.30	535	27.38	19.54
21400	1266.75	1321.15	502	28.88	17.39
21600	1266.00	1314.45	488	27.00	18.07
21800	1269.75	1326.70	488	29.63	16.47
22000	1272.00	1328.10	491	30.75	15.97
22200	1270.50	1330.00	533	30.00	17.77
22400	1272.75	1329.70	536	32.25	16.62
22600	1273.50	1326.20	522	33.75	15.47
22800	1272.75	1329.70	452	29.63	15.26
23000	1275.75	1330.15	483	36.00	13.42
23200	1278.00	1334.10	456	36.38	12.54
23400	1280.25	1332.95	669	39.00	17.15
23600	1280.25	1332.10	779	46.50	16.75
23800	1278.75	1327.20	844	37.50	22.51
24000	1278.75	1334.85	595	34.50	17.25
24200	1278.75	1329.75	553	33.38	16.57
24400	1278.00	1329.85	509	29.63	17.18
24600	1274.25	1326.95	513	27.75	18.49
24800	1272.00	1330.65	557	23.25	23.96
25000	1275.00	1330.25	567	25.50	22.24
25200	1275.75	1331.85	577	25.88	22.30
25400	1278.75	1337.40	677	25.50	26.55
25600	1283.25	1334.25	563	27.38	20.57
25800	1284.75	1345.10	618	24.00	25.75
26000	1284.75	1338.30	529	23.25	22.75
26200	1284.75	1341.70	597	22.13	26.98
26400	1285.50	1338.20	544	22.88	23.78
26600	1286.25	1341.50	537	25.50	21.06
26800	1284.75	1336.60	487	22.13	22.01
27000	1290.00	1341.85	419	27.38	15.31
27200	1287.75	1352.35	386	24.38	15.84
27400	1292.25	1350.90	401	25.50	15.73
27600	1287.75	1351.50	477	22.88	20.85
27800	1290.75	1351.95	545	25.88	21.06
28000	1294.50	1351.45	476	25.50	18.67
28200	1295.25	1358.15	531	30.38	17.48
28400	1290.75	1341.75	428	25.50	16.78
28600	1289.25	1347.90	480	23.25	20.65
28800	1290.75	1348.55	402	25.50	15.76
29000	1290.00	1349.50	462	21.75	21.24
29200	1290.75	1348.55	494	21.00	23.52
29400	1292.25	1351.75	561	24.00	23.38
29600	1292.25	1353.45	531	21.00	25.29
29800	1293.75	1355.80	539	24.00	22.46

30000	1293.75	1337.95	524	23.63	22.18
30200	1294.50	1342.10	488	22.50	21.69
30400	1295.25	1344.55	421	20.63	20.41
30600	1296.75	1352.85	441	16.13	27.35
30800	1298.25	1360.30	443	17.63	25.13
31000	1298.25	1360.30	422	14.63	28.85
31200	1301.25	1357.35	450	17.25	26.09
31400	1302.75	1360.55	438	16.88	25.96
31600	1304.25	1363.75	488	16.88	28.92
31800	1305.75	1364.40	475	17.63	26.95
32000	1308.75	1371.65	428	17.63	24.28
32200	1311.75	1375.50	412	16.50	24.97
32400	1314.75	1371.70	428	17.25	24.81
32600	1317.75	1380.65	404	18.38	21.99
32800	1320.75	1383.65	428	18.00	23.78
33000	1320.75	1384.50	428	12.00	35.67
33200	1323.00	1386.75	394	15.38	25.63
33400	1328.25	1369.90	329	19.88	16.55
33600	1329.00	1370.65	311	16.13	19.29
33800	1329.75	1375.65	295	18.38	16.05
34000	1332.75	1376.10	304	24.75	12.28
34200	1332.75	1375.25	352	27.00	13.04
34400	1330.50	1377.25	432	26.63	16.23
34600	1331.25	1377.15	512	23.63	21.67
34800	1331.25	1413.70	432	25.13	17.19
35000	1329.75	1400.30	420	20.63	20.36
35200	1328.25	1393.70	454	20.25	22.42
35400	1326.00	1391.45	382	18.00	21.22
35600	1325.25	1400.90	360	16.88	21.33
35800	1321.50	1395.45	358	12.75	28.08
36000	1320.75	1395.55	352	10.50	33.52
36200	1320.75	1395.55	385	11.25	34.22
36400	1320.75	1390.45	400	11.25	35.56
36600	1326.75	1396.45	396	16.50	24.00
36800	1329.75	1393.50	527	21.38	24.65
37000	1331.25	1394.15	596	25.88	23.03
37200	1334.25	1392.90	608	26.25	23.16
37400	1332.75	1392.25	676	22.50	30.04
37600	1332.75	1393.95	658	19.50	33.74
37800	1332.75	1392.25	558	18.00	31.00
38000	1329.00	1394.45	557	24.00	23.21
38200	1331.25	1393.30	390	15.75	24.76
38400	1329.00	1391.05	416	20.25	20.54
38600	1329.00	1387.65	416	22.50	18.49
38800	1329.75	1387.55	401	24.38	16.45
39000	1328.25	1383.50	402	24.75	16.24
39200	1326.75	1383.70	352	18.38	19.16
39400	1326.75	1390.50	355	17.25	20.58
39600	1326.75	1393.90	327	18.38	17.80
39800	1331.25	1378.85	360	18.38	19.59

40000	1334.25	1389.50	545	28.13	19.38
40200	1335.75	1391.00	552	24.38	22.65
40400	1335.75	1390.15	498	23.25	21.42
40600	1338.00	1389.85	418	26.25	15.92
40800	1338.75	1392.30	359	25.50	14.08
41000	1340.25	1395.50	409	24.00	17.04
41200	1338.75	1394.00	452	22.88	19.76
41400	1338.75	1392.30	374	25.88	14.45
41600	1335.75	1393.55	438	22.50	19.47
41800	1338.75	1392.30	449	22.13	20.29
42000	1338.75	1396.55	483	24.00	20.13
42200	1338.75	1393.15	477	23.25	20.52
42400	1341.00	1397.10	386	21.75	17.75
42600	1341.75	1392.75	386	23.25	16.60
42800	1341.75	1391.90	421	24.38	17.27
43000	1341.75	1389.35	459	24.75	18.55
43200	1341.00	1392.00	420	22.50	18.67
43400	1344.75	1394.90	422	22.88	18.45
43600	1344.75	1400.00	403	19.88	20.28
43800	1347.00	1404.80	451	21.38	21.10
44000	1350.00	1410.35	463	24.75	18.71

APPENDIX A2

The isochron maps presented in this appendix are the original maps, of which simplified interpretations are presented in Chapter 4. The interpreted isochron maps show most clearly the thicknesses and distribution of the architectural elements within the upper growth sequence of the Aga Fold.

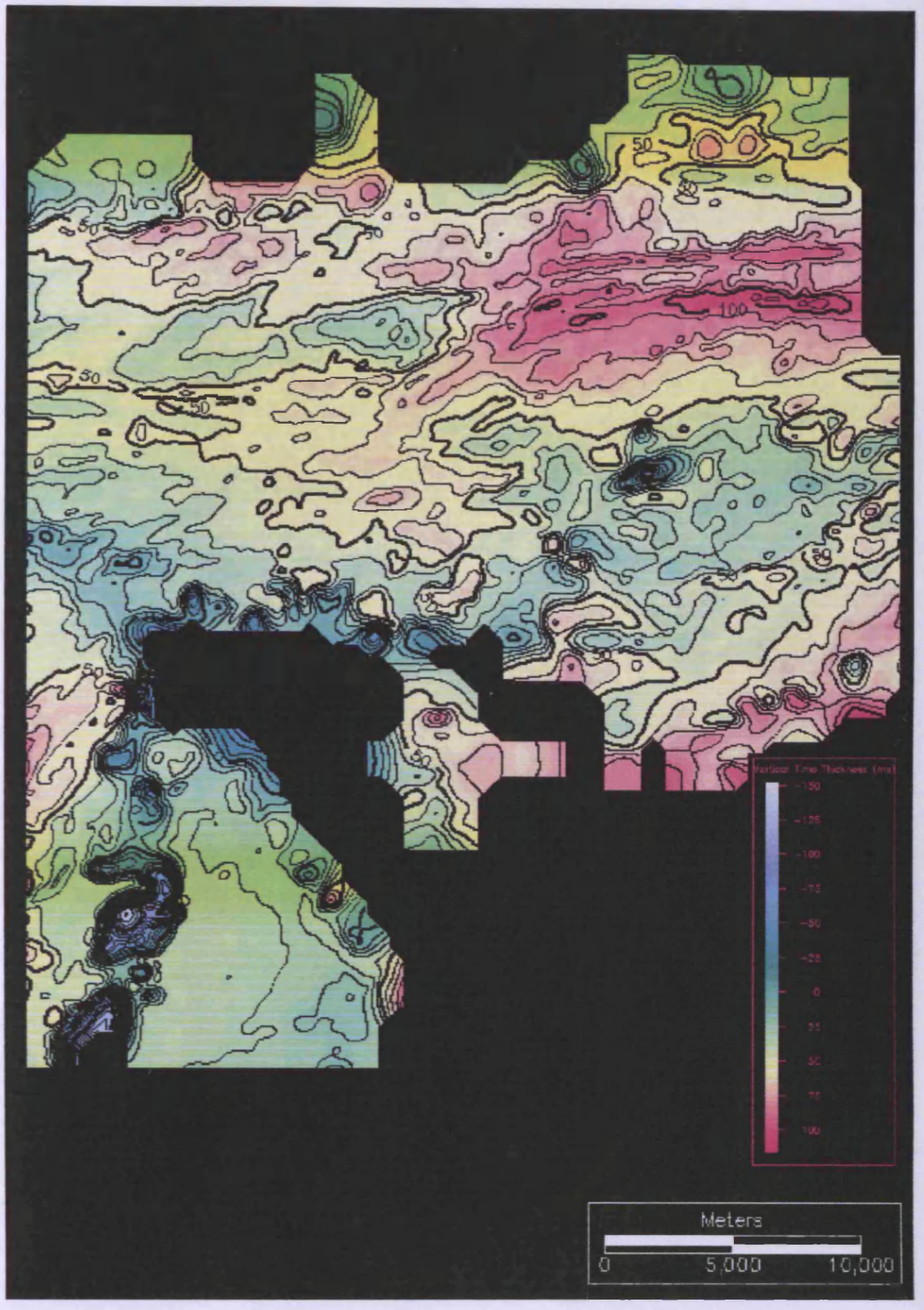

Fig. A2.1: Isochron map of MTD3.

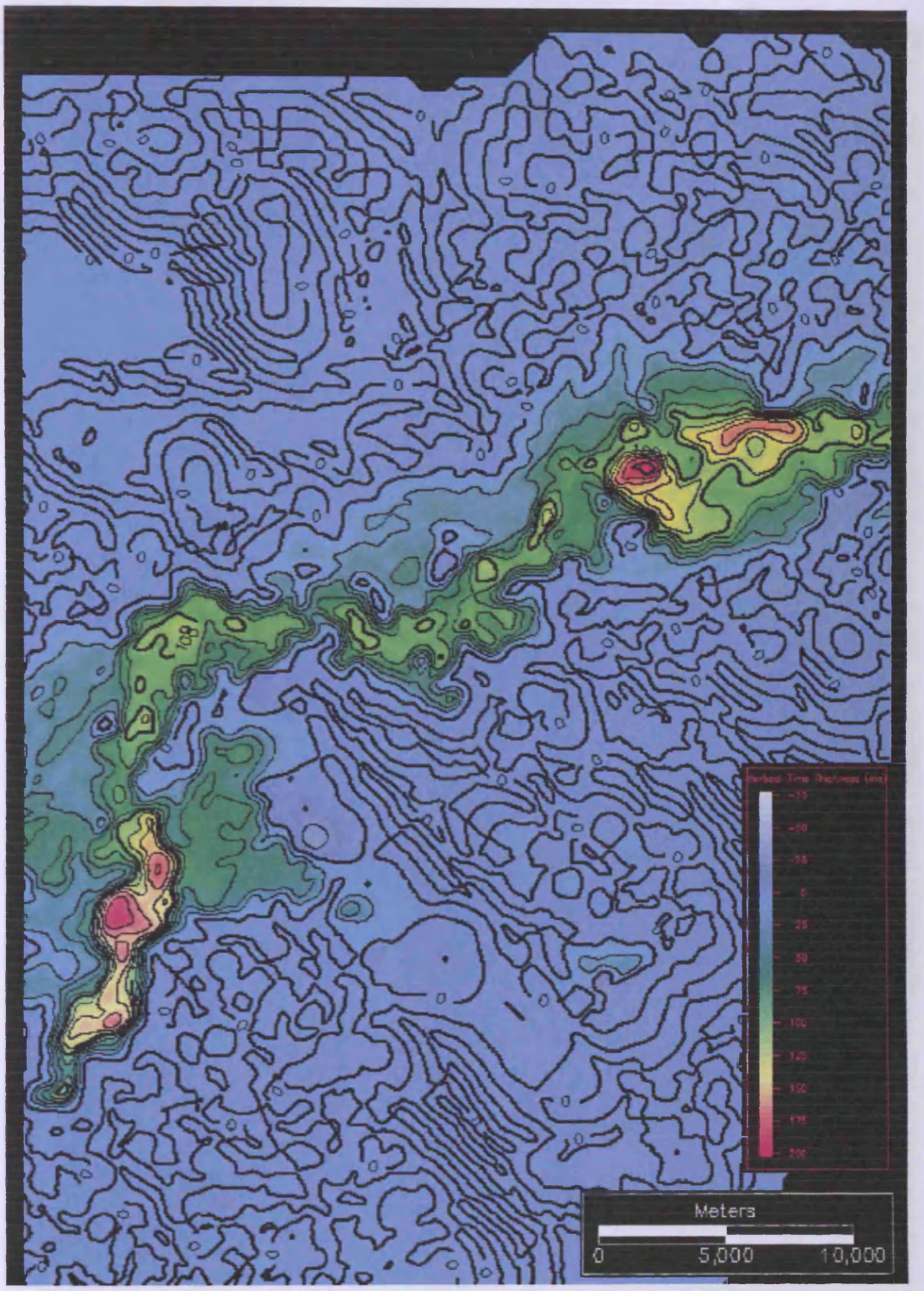

Fig. A2.2: Isochron map of CLS3.

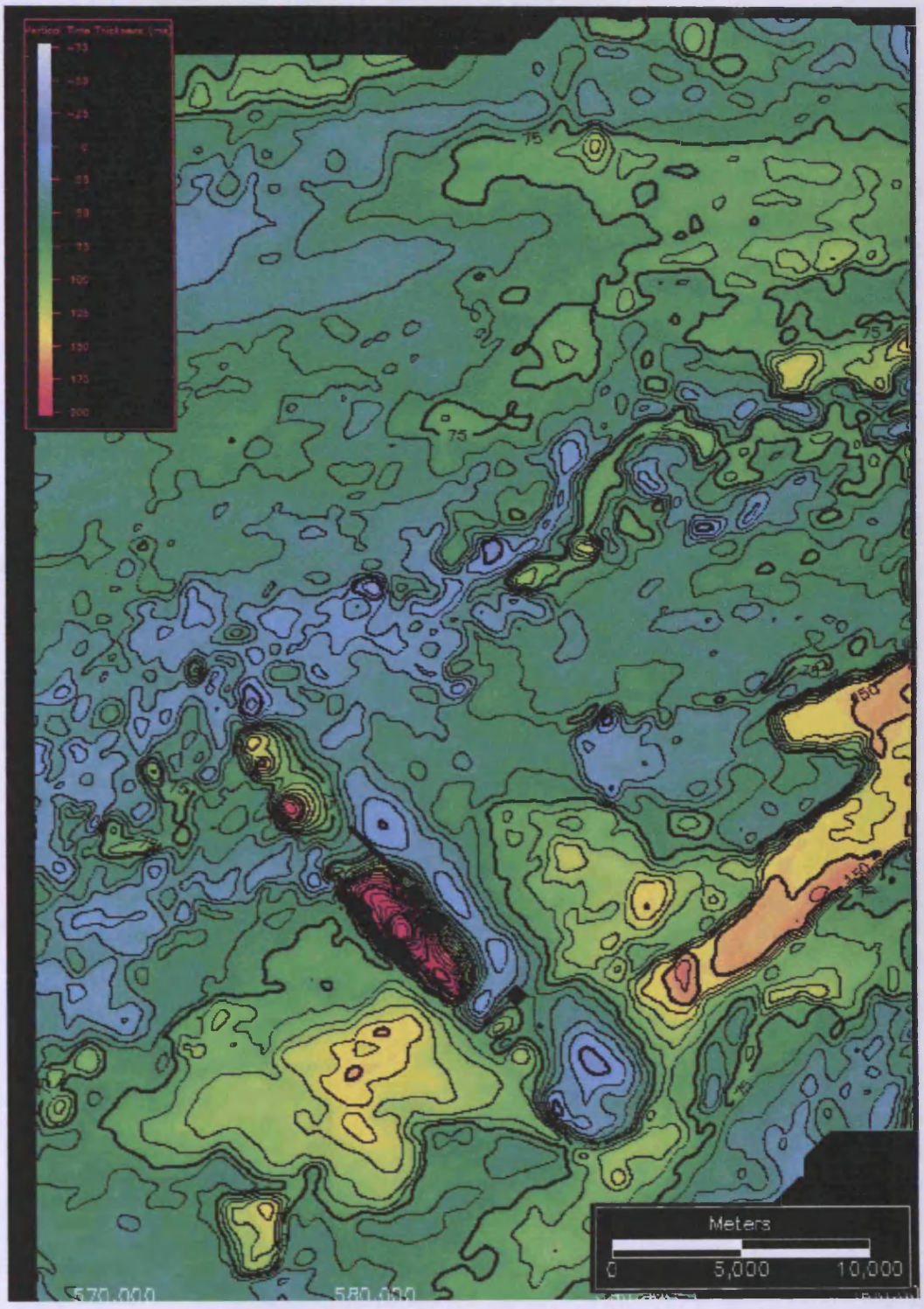

Fig. A2.3: Isochron map of MTD2.

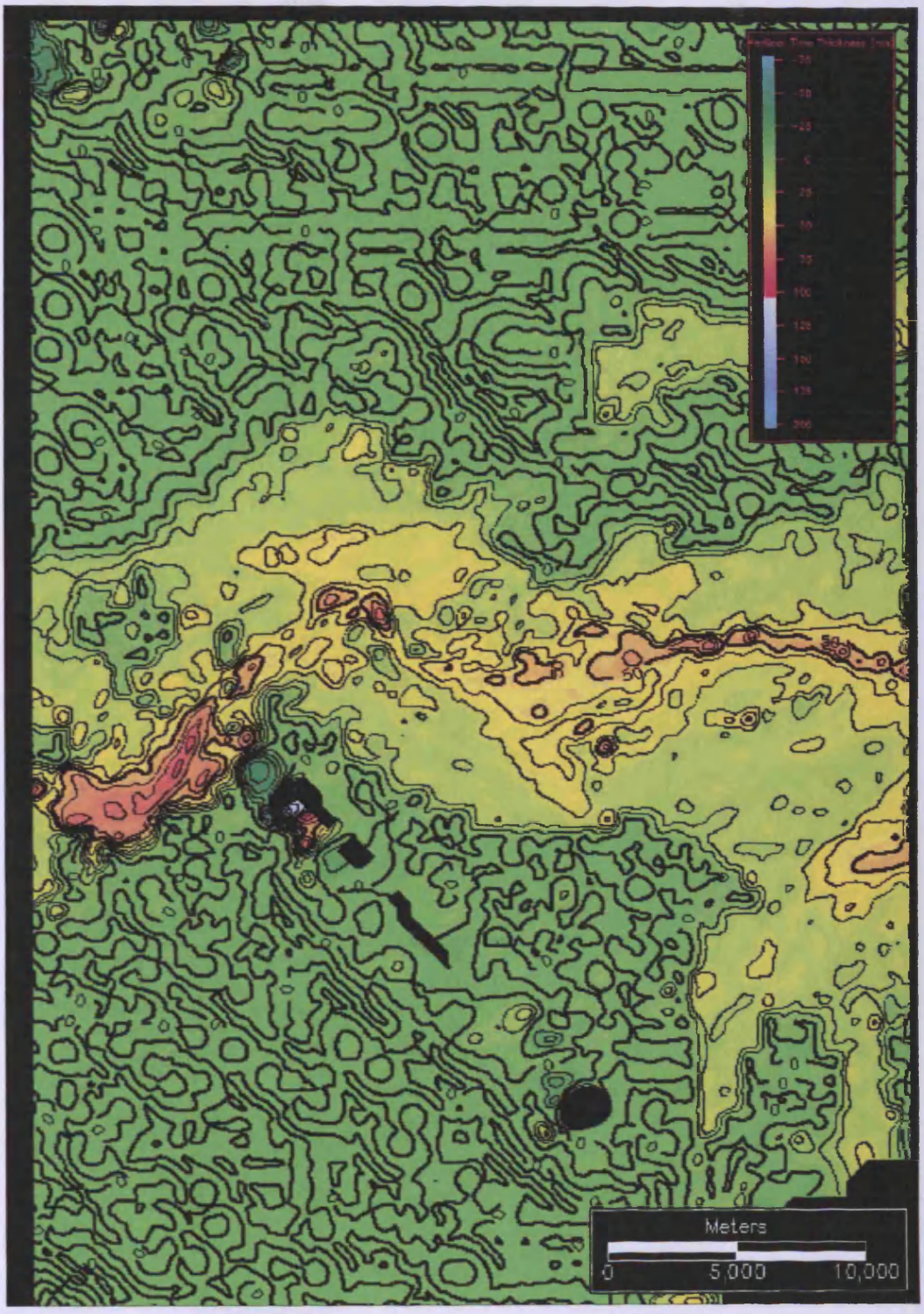

Fig. A2.4: Isochron map of CLS2.

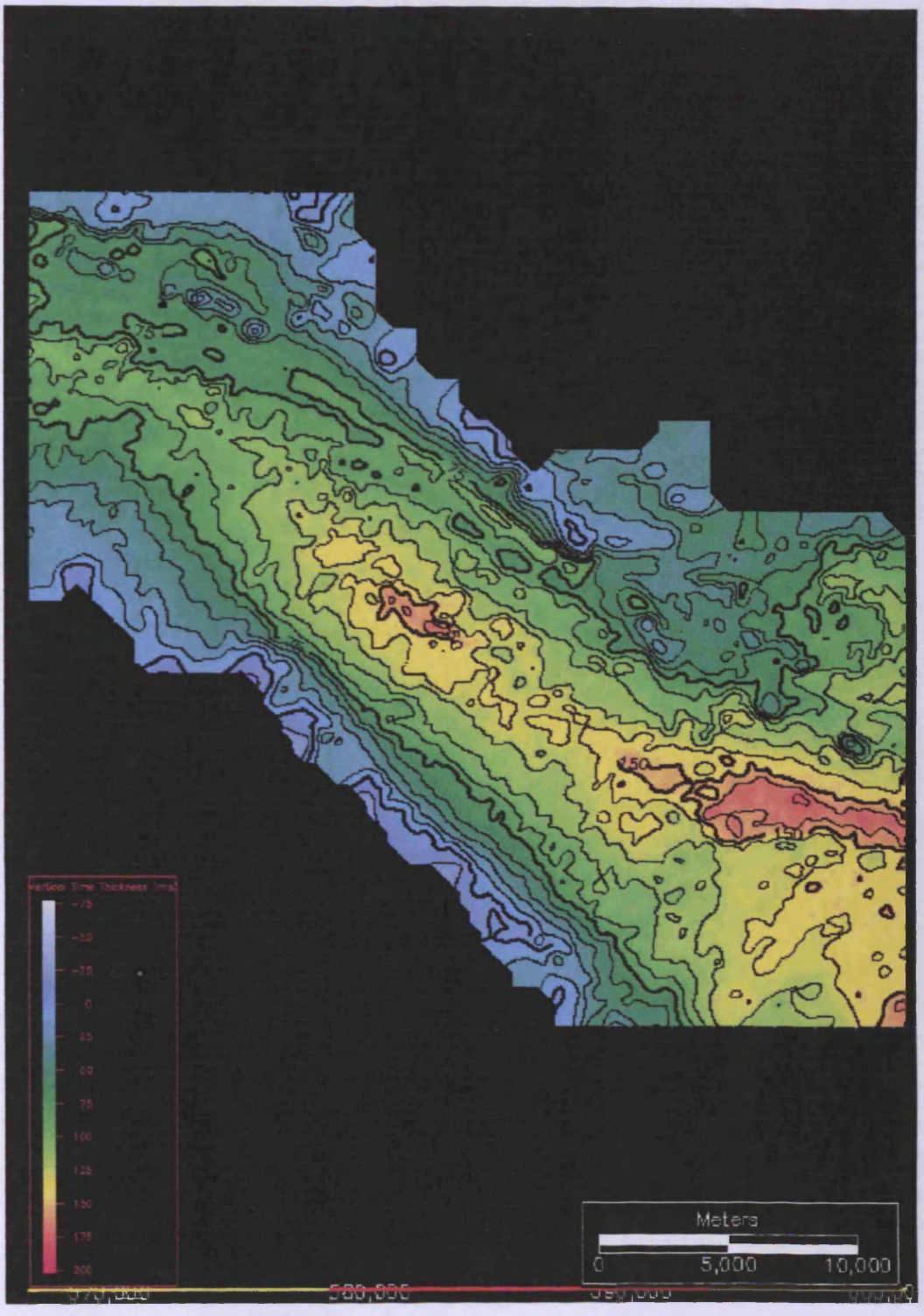

Fig. A2.5: Isochron map of MTD1.

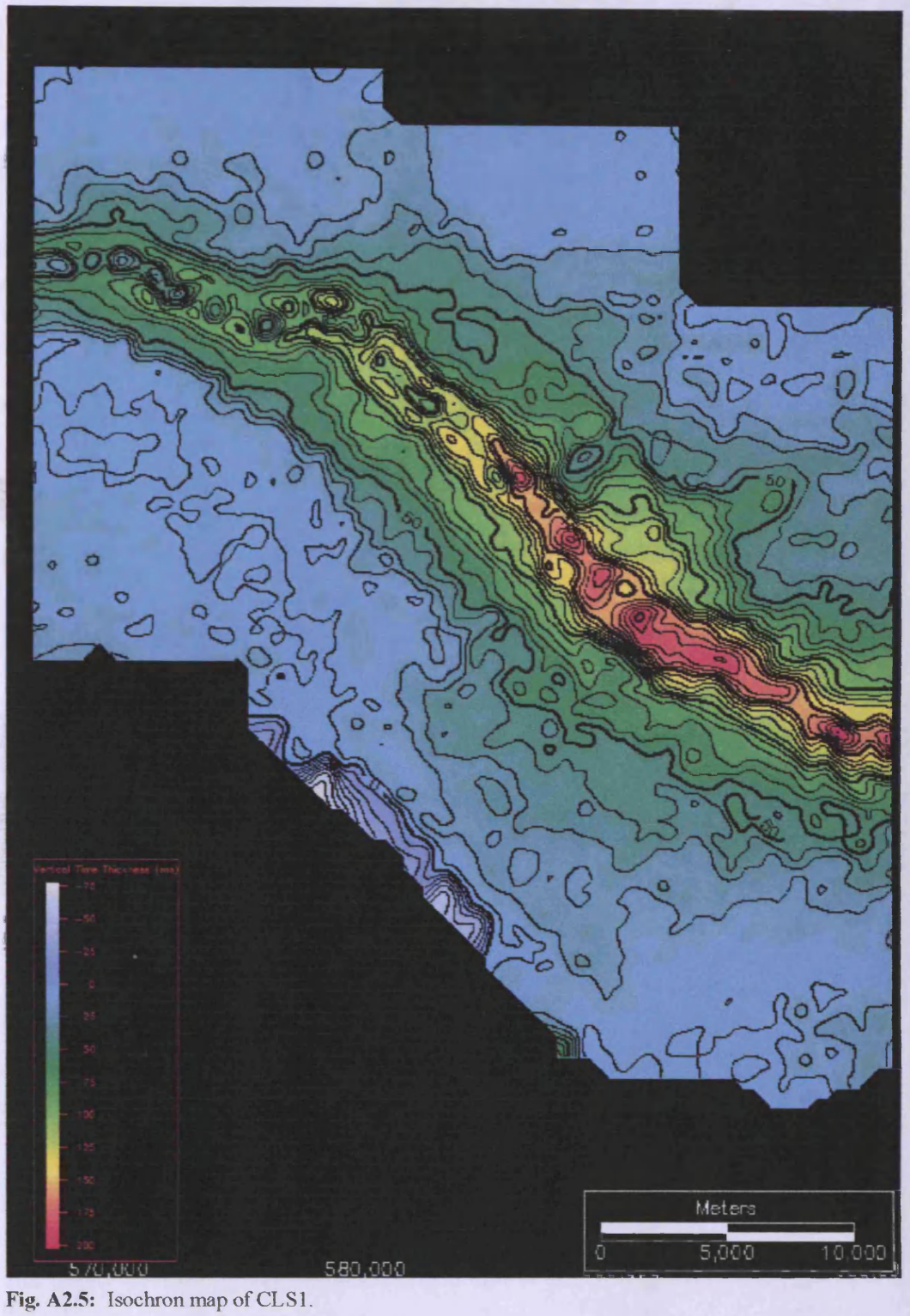

Fig. A2.5: Isochron map of CLS1.

APPENDIX A3

The tables in this appendix present the results from measurements taken of fold structural relief and growth sequence expansion factor presented in Chapter 5.

Table A3.1: Measurements from fold 1. LGS and UGS refer to Lower and Upper Growth Sequences respectively. $T_{footwall}$ and T_{crest} refer to stratigraphic thicknesses measured at the footwall and over the fold crest.

Distance/m	LGS Tfootwall/m	UGS Tfootall/m	Tcrest:LGS/m	Tcrest:UGS/m	LGS Growth Ratio	UGS Growth Ratio
0	106	134	34	64	3.12	2.09
100	124	132	42	48	2.95	2.75
200	108	138	72	28	1.50	4.93
300	102	146	40	62	2.55	2.35
400	102	136	46	64	2.22	2.13
500	98	132	52	60	1.88	2.20
600	106	126	60	56	1.77	2.25
700	106	132	68	56	1.56	2.36
800	106	132	70	58	1.51	2.28
900	112	128	80	60	1.40	2.13
1000	116	126	72	90	1.61	1.40
1100	116	126	84	104	1.38	1.21
1200	118	126	98	98	1.20	1.29
1300	116	132	100	104	1.16	1.27
1400	120	132	100	110	1.20	1.20
1500	118	130	100	116	1.18	1.12
1600	118	134	102	110	1.16	1.22
1700	126	128	104	110	1.21	1.16
1800	124	128	108	108	1.15	1.19
1900	130	126	106	112	1.23	1.13
2000	130	130	110	106	1.18	1.23
2100	130	128	116	108	1.12	1.19
2200	132	126	112	110	1.18	1.15
2300	128	130	112	108	1.14	1.20
2400	132	124	118	102	1.12	1.22
2500	136	122	116	102	1.17	1.20
2600	138	120	118	100	1.17	1.20
2700	136	120	116	102	1.17	1.18
2800	130	126	106	104	1.23	1.21
2900	132	124	100	98	1.32	1.27
3000	134	124	96	94	1.40	1.32
3100	130	124	90	92	1.44	1.35
3200	132	120	84	90	1.57	1.33
3300	130	122	78	94	1.67	1.30
3400	130	126	78	92	1.67	1.37
3500	128	124	80	92	1.60	1.35
3600	124	126	80	96	1.55	1.31
3700	124	122	84	94	1.48	1.30
3800	126	116	92	100	1.37	1.16

Table A3.2: Measurements from fold 2. LGS and UGS refer to Lower and Upper Growth Sequences respectively. $T_{footwall}$ and T_{crest} refer to stratigraphic thicknesses measured at the footwall and over the fold crest.

Distance/m	LGS Tfootwall/m	UGS Tfootwall/m	Tcrest:LGS/m	Tcrest:UGS/m	LGS Growth Ratio	UGS Growth Ratio
0	120	138	38	120	3.16	1.15
100	126	146	42	110	3.00	1.33
200	130	152	44	100	2.95	1.52
300	134	158	48	100	2.79	1.58
400	136	160	56	100	2.43	1.60
500	138	164	58	100	2.38	1.64
600	138	156	68	104	2.03	1.50
700	142	140	70	102	2.03	1.37
800	142	138	70	98	2.03	1.41
900	140	146	70	100	2.00	1.46
1000	144	146	70	98	2.06	1.49
1100	146	146	66	94	2.21	1.55
1200	148	146	72	90	2.06	1.62
1300	150	148	76	86	1.97	1.72
1400	148	146	74	86	2.00	1.70
1500	150	150	76	74	1.97	2.03
1600	150	152	72	78	2.08	1.95
1700	146	146	68	78	2.15	1.87
1800	144	148	74	76	1.95	1.95
1900	148	142	76	76	1.95	1.87
2000	150	142	78	74	1.92	1.92
2100	154	140	72	66	2.14	2.12
2200	152	144	74	62	2.05	2.32
2300	148	146	72	50	2.06	2.92
2400	148	148	72	46	2.06	3.22
2500	148	142	74	36	2.00	3.94
2600	146	142	74	34	1.97	4.18
2700	150	140	74	32	2.03	4.38
2800	150	136	74	36	2.03	3.78
2900	156	130	84	28	1.86	4.64
3000	158	122	90	28	1.76	4.36
3100	158	120	92	40	1.72	3.00
3200	158	116	100	30	1.58	3.87
3300	150	126	76	30	1.97	4.20
3400	150	122	82	30	1.83	4.07
3500	168	114	92	38	1.83	3.00
3600	174	102	98	36	1.78	2.83
3700	166	104	80	36	2.08	2.89
3800	160	110	50	60	3.20	1.83
3900	160	108	44	60	3.64	1.80
4000	160	106	40	58	4.00	1.83
4100	156	106	36	56	4.33	1.89
4200	152	114	28	56	5.43	2.04
4300	150	110	36	54	4.17	2.04
4400	150	112	38	52	3.95	2.15
4500	146	116	36	52	4.06	2.23
4600	148	112	38	50	3.89	2.24
4700	154	108	40	50	3.85	2.16
4800	150	110	46	50	3.26	2.20
4900	150	108	42	48	3.57	2.25
5000	152	108	46	48	3.30	2.25
5100	154	110	50	54	3.08	2.04
5200	160	100	56	58	2.86	1.72
5300	152	104	64	60	2.38	1.73

5400	146	108	78	62	1.87	1.74
5500	142	100	88	60	1.61	1.67
5600	136	102	88	84	1.55	1.21